Università di Pisa

School of Graduate Studies "G. Galilei"

PhD Thesis in Chemical Sciences

Monomer and polymer indole-derived systems having NLO properties for very high optical gain photorefractive materials. The role of the electrostatic interactions.

Francesco Greco

Supervisor: Referee:

Prof. Arturo Colligiani   Prof. Vincenzo Schettino

Local Supervisor:

Prof. Giacomo Ruggeri

Pisa, December 2008

Contents

General object of the research

Object of the present research is the study of some indole-based photorefractive (PR) materials. Novel indole-based NLO chromophores have been synthesized and their photoconductive (PC) and PR behaviour have been investigated when employed both alone (as low molecular weight glass forming multifunctional PR moieties) as well as in blends with a PC indolyl polymer, namely poly-(*N*-vinyl-2,3-dimethylindole). The aim was to get more insight in the onset of PR effect and to evaluate various contributions to it related to intermolecular interactions occurring among the components of a PR material. The introduction of increasing contents of polymer counterpart in PR blends containing the novel NLO chromophores permitted to follow these interactions in their onset and the establishment of new supramolecular arrangements, expected to be responsible for dramatic changes of electrooptic properties. In this way, it has been also possible to look for the proper formulation in order to take advantage of such interactions for the achievement of the best PC and PR performances. The joint analysis of the results of PC, PR and thermal (DSC) behaviour of the investigated materials revealed itself as particularly useful, due to the complexity of the many processes occurring simultaneously in organic PR materials. A careful comparison with numerous theoretical treatments permitted to rationalize the obtained results and to put in evidence the prominent role played by intermolecular interactions. On the other hand, the obtaining of long-term phase stability of amorphous PR materials, desirable for their practical use in a number of applications, was also a challenge. Many PR materials described in the past, indeed, although having good photorefractive properties, showed the undesirable drawback of fast recrystallization of one or more of their molecular components, leading to opacization of films and to the rapid loss of PR properties. Such aspect has been faced during this research obtaining indefinitely stable materials. As concerns PR, very large values of the photorefractive optical gain Γ (a main PR figure of merit) have been achieved in many cases, classifying the materials object of this research among the most efficient PR materials.

1 Introduction

The photorefractive (PR) effect refers to spatial modulation of the index of refraction under non-uniform illumination via space-charge-field formation and electrooptic nonlinearity[1,2]. The effect arises when charge carriers, photogenerated by a spatially modulated light intensity in a photoconductive material, separate by drift and/or diffusion processes and become trapped to produce a non-uniform space-charge distribution. The resulting internal space-charge electric field then modulates the refractive index to create a phase grating, or hologram, which can diffract a light beam. Because such an hologram can typically be erased by uniform optical illumination, PR holograms are dynamic, that is, they may be erased and rewritten many times. This last is one of many properties that distinguish PR materials from other mechanisms for hologram formation.

The PR effect has been observed and discovered for the first time in 1967 by a research group operating at Bell Telephone Laboratories[3]. They referred to it as a "detrimental effect" for the optics of nonlinear devices based upon $LiNbO_3$ or $LiTaO_3$ crystals. Prosecuting that initial observation, many other research groups devoted themselves to the understanding of this effect. The challenge was twofold: on one side the need for a deeper and more comprehensive understanding of the principles and mechanisms ruling the effect and for a theoretical modelling; on the other side, or complementary to this, the work for the ideation and realization of new materials and devices, pushed also by new technological demands. During the years, since that first discovery, photorefractive effect has been observed in many other materials, the research in this field focussing mainly on inorganic crystalline materials, e.g. ferroelectrics ($LiNbO_3$, $BaTiO_3$, KNO_3, $Sr_xBa_{1-x}NbO_3$), sillenites ($Bi_{12}SiO_{20}$), semiconductors (InP, GaAs, CdTe, multiple-quantum-wells semiconductors)[4]. Inorganic crystalline materials, however, have several intrinsic drawbacks, concerning for example their processability, their expensiveness, their poor flexibility; all these reasons limited the spread of such materials in technological applications. One of the main problems is represented by the difficulties and cost relative to the growth of high purity grade crystals (a primary requirement for optical applications).

It was only at the beginning of '90 that the discovery of the PR effect in organic crystals[5,6], and then in amorphous and polymeric materials[7,8], paved the way to the study of organic PR materials[2]. The main interest in this effect, besides the one aroused for the understanding of the complexity of phenomena related to it, lies in the potential use of

photorefractive materials as novel reversible recording media in many applications in the field of holography. Many of such applications has been proposed and realized, e.g. phase correlation, optical amplification, high density optical memory storage[9,10,11,12,13].

1.1 The Photorefractive (PR) effect

As already briefly mentioned, the PR effect is based on the redistribution of electric charges (electrons or holes) photogenerated by a non-uniform pattern of light impinging on a material; this gives rise to a spatially variable internal electric field E which, mainly through the electrooptic effect (EO), modulates the refractive index of the medium. It deals effectively with the creation of an optical diffraction grating in materials possessing simultaneously electrooptic (non linear optics), photogeneration and photoconductivity properties.

The PR effect has been treated by Kukhtarev in his theory describing its mechanism in crystalline inorganic materials[14]. We use this theory in order to describe the effect; further specifications will be made in the following, including the successive modifications to the original theory, necessary to expand its application to molecular organic materials.

In the frame of Kukhtarev model, the PR material can be seen as a crystal containing only one typology of charge carrier (electrons e-), and two different typologies of so-called impurities, i.e. donors (D) and acceptors (A). D and A normally lie inside the forbidden band of the crystal, viz between valence band and conduction band. Optical excitations may permit the electrons to "hop" from non-ionized donors towards the conduction band, where they are free to move owing to diffusion (caused by charge density gradients) or drift (which is the case if an electric field is applied), until they recombine elsewhere with ionized donors.

Considering a crystal such as the one described so far, two laser beams are directed symmetrically on it, with incidence angles ±θ with respect to sample normal incidence; their propagation inside the material can be described by means of two plane electromagnetic travelling waves

$$E_1 = E_{10}e^{j\varphi_1}e^{-j\vec{k_1}\cdot\vec{r}}$$

$$E_2 = E_{20}e^{j\varphi_2}e^{-j\vec{k_2}\cdot\vec{r}} \quad , \tag{1.1}$$

being E_1 beam 1 electric field, E_2 beam 2 electric field, E_{10} and E_{20} their respective amplitudes, φ_1 and φ_2 their respective phases and $\vec{k_1}$, $\vec{k_2}$ being the wave vectors indicating the directions in which they are propagating.
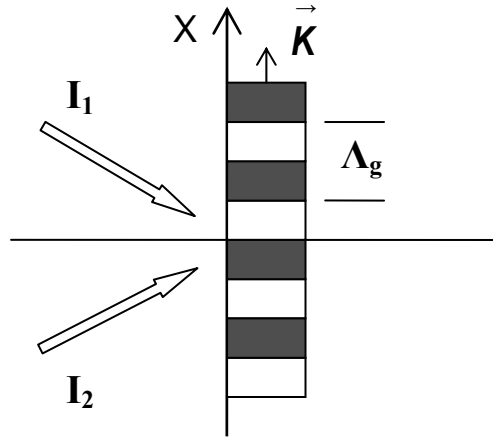
Figure 1.1 Schematic drawing displaying the process of writing of an hologram by means of the interference of two coherent laser beams of intensities I_1 and I_2. Interference pattern (represented by dark and light planes) is formed, having periodicity Λ_g. K is the grating wavevector (s. text).

These two intersecting coherent beams of light produce a standing-wave interference pattern, i.e. a time-independent but spatially modulated intensity pattern (*interference pattern*) described by the squared modulus of the electric field

$$I = \left| E_1 + E_2 \right|^2 = E_{10}^2 + E_{20}^2 + 2E_{10}E_{20}\cos\left(\vec{K}\cdot\vec{r} + \varphi_2 - \varphi_1\right) \qquad (1.2)$$

$$\vec{K} = \vec{k}_1 - \vec{k}_2 \qquad .$$

$\overrightarrow{K}$ is called the grating wavevector.

Considering the system in a proper reference frame, s. Figure 1.1 and after some simple operations, it is possible to write down an analytical expression for the interference pattern in a more useful and immediately comprehensible way, i.e.

$$I(x) = I_0\left[1 + m\cos\left(\frac{2\pi x}{\Lambda_g}\right)\right] \qquad (1.3)$$

in which $I_0 = I_1 + I_2$ is the total incident intensity of light, *m* is called fringes visibility, Λ_g is the spatial wavelength or *periodicity* of the interference pattern. They are, respectively, defined as

5

$$m = 2\frac{\left(I_1 I_2\right)^{1/2}}{\left(I_1 + I_2\right)} \tag{1.4}$$

$$\Lambda_g = \frac{\lambda_0}{2n\sin\theta} \; , \tag{1.5}$$

in which λ_0 is the optical wavelength of the incident radiation in the vacuum, n is the index of refraction of the material, $\theta = \theta_2 - \theta_1$ with $\theta_{1,2}$ the internal angles of incidence of the two writing beams relative to the sample normal. For visible light ($380 < \lambda_0 < 750$ nm) the spatial periodicity Λ_g can typically vary in the range from 0.1 up to 20-30 μm, depending on the angle between the beams. The grating wavevector $\vec{K}$ lies along the normal direction with respect to the light and dark planes; its magnitude is given by $K = 2\pi / \Lambda_g$. In Figure 1.2 (a) the optical intensity following a sinusoidal pattern is shown, being x the direction of the grating wavevector $\vec{K}$.

As we have previously mentioned, photoconductivity (PC) behaviour is a primary requirement for a material to show photorefractive effect. A PC material is an insulating one in the dark while it becomes a conductor under the exposure to light. Making an interference pattern, as the one described so far, to impinge upon a PC material gives rise to a spatially non-uniform excitation of couples electrons-ionized donors (holes), and, therefore, to the generation (photo-generation) of mobile charge carriers. Their density is proportional to the incident light intensity[15]; sites corresponding to the maxima of intensity of the interference pattern are the ones in which mobile electrical charge carriers photogeneration is maximum. The electrons (negative charge) or holes (positive charge) can therefore migrate from their original positions leaving behind fixed charges of opposite sign, through two different mechanisms: *diffusion* or *drift*. Diffusion is mainly related to charge density gradients inside the material and play a minor role in photorefractive materials. When an external electric field is applied the main charge transport mechanism is due to *drift*, i.e. photogenerated electric charges move under the effect of the electric field. The conductivity mechanism and the sign of the charge carrier (electrons or holes) depend on the nature of the material. It is important to remark here that charge mobility in a material is typically different for different kinds of charge carrier, i.e. one charge carrier is more mobile than the other one. If it would not be the case and both of them would possess the same value of mobility, the resulting charge distribution would be neutral, not giving rise to an internal electric field. For this reason, here and in the following of this study it has been referred only to one type of "charge carrier" (the

more mobile one), actually considering the other type as fixed. In organic amorphous materials charge migration is typically schematized by a *hopping* mechanism: the charge carrier moves by "jumping" from one molecular site to the other. This kind of migration process is limited and regulated by the presence of the so-called *traps*, i.e. molecular sites in which, by means of modified local potentials, charge carriers can live in a lower energy state. Indeed, traps are sites in which the mobile charges are blocked and excluded from the transport process for some time[16]. Traps in crystalline materials have been identified as ionic impurities, vacancies or defects in the crystal lattice. On the contrary, in organic amorphous photorefractive materials their nature has not yet been fully understood in detail, but it is surely related to the value of the ionization potential ip of the molecular species involved.
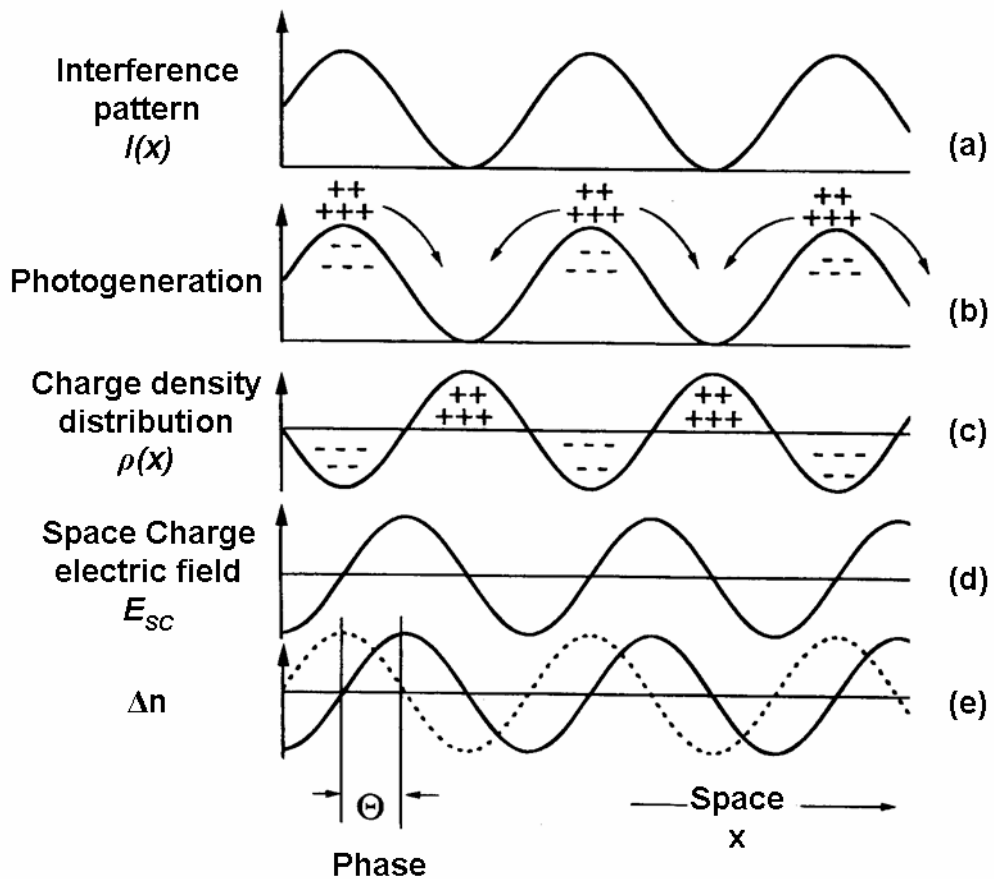
Figure 1.2 Schematic drawing summarizing the phenomena occurring in the formation of a PR grating. Space relationships between the incident light interference pattern, the resulting charge distribution, Space Charge Field E_{sc} and the refractive index modulation are displayed. The non-local nature of PR grating is reflected by the phase angle Θ.

Going back to the subject of the mechanisms involved in the illumination by an interference pattern of a PR material, the global effect is therefore represented by a migration

of free charges from "bright" regions towards "darker" regions, where charge mobility (and hence, conductivity) is lower and charges can be trapped. The distances typically covered in such migration process are in the order of few micrometers. This migration will result in a non-uniform charge density distribution $\rho(x)$, s. Figure 1.2 (c), that will give rise in turn to an internal electric field sinusoidally varying in space and called the Space Charge Field $E_{SC}(x)$, Figure 1.2 (d).

The equation that relates the charge distribution $\rho(x)$ with the gradient of $E_{SC}(x)$ is known as the Poisson equation

$$\frac{dE_{sc}(x)}{dx} = \frac{4\pi\rho(x)}{\varepsilon} \quad , \tag{1.6}$$

being ε the static dielectric constant of the material. Because of Poisson equation E_{SC} has maxima in correspondence of $\rho(x) = 0$, that is between positive and negative charges centers, thus resulting in a phase shift $\Theta = \pi/2$ (displacement) between the internal field E_{SC} and the charge distribution.

Kukhtarev[14] in his theoretical treatment of the PR effect in crystalline inorganic materials gave an extremely accurate derivation of the space charge field. In the frame of this model, the amplitude of the electric field created by a sinusoidal interference pattern is given by the following expression

$$E_{sc} = \left| E_{sc} \right| \exp(j\Theta)$$

$$\left| E_{sc} \right| = m \left(\frac{E_0{}^2 + E_D{}^2}{\left(1 + \frac{E_D}{E_q}\right)^2 + \left(\frac{E_0}{E_q}\right)^2} \right)^{1/2} \tag{1.7}$$

in which E_0 is the component of the applied static electric field along the pattern wave vector $\vec{K}$, while E_D, known as the *diffusion field,* is defined as

$$E_D = \frac{Kk_BT}{e} \quad . \tag{1.8}$$

$K = 2\pi / \Lambda_g$ is the wave vector of the interference pattern, k_B the Boltzmann constant, T the temperature, e the elementary charge, and E_q is the so-called *trap limited field* that is defined as

$$E_q = \frac{eN_T}{K\varepsilon\varepsilon_0} \qquad ; \tag{1.9}$$

ε is the static dielectric constant, ε_0 the static dielectric permittivity in the vacuum and N_T represents the numeral density of traps. Spatial phase shift Θ between the electric field E_{SC} and the incident light intensity pattern in the same Kukhtarev's description results to be

$$\Theta = \mathrm{arctg}\left[\frac{E_D}{E_0}\left(1 + \frac{E_D}{E_q} + \frac{E_0^{\,2}}{E_D E_q}\right)\right] \qquad . \tag{1.10}$$

If transport occurs only via diffusion, this phase shift is equal to $\pi/2$. Otherwise, Θ value depends on the relative forces of drift and diffusion processes. It is important to remark that, as a peculiar feature, PR effect produces only non-local gratings, that is gratings in which $\Theta \neq 0$.

The space charge field E_{SC} , Eq. (1.7), gives rise to the modulation $\Delta n(x)$ of the local refractive index inside the material, through the *Pockels Effect* or other non-linear optics (NLO) related effects

$$\Delta n(x) = -\frac{1}{2}n^3 r_{eff} E_{SC} \tag{1.11}$$

where n is the refractive index of the material and r_{eff} is the effective electrooptic parameter; it is actually a combination of different elements of the electrooptic tensor and it depends on the symmetry and mutual orientations of the NLO molecular moieties inside the material. The elements of the electrooptic tensor are related to the components of the second-order non linear susceptibility, of $\chi_{IJK}^{(2)}(-\omega;\, 0,\, \omega)$ type, i.e. those relative to interactions of an optical field (ω pulsation) with a static dc electric field (pulsation $\omega=0$)[17,18]. The sinusoidally varying refractive index modulation described by the Eq. (1.11) is actually a lattice; under the usual Bragg's conditions this lattice is able to diffract light along certain, defined directions.

The phase shift Θ between *I(x)* and *Δn(x)*, Figure 1.2, gives rise to an asymmetric energy transfer (*Asymmetric Two-Beam Coupling* or *2BC*), an effect that is peculiarly ascribed to the PR effect: one of the two incident beams (beam 2: "signal beam") gains energy at the expense of the other beam (beam 1: "pump beam"). Coupling of these two beams can occur because both of them fulfill Bragg's conditions for the lattice created by themselves. It could be said that the beams are "self-diffracted" by the lattice they have generated through their interaction with the PR material.

Such a mechanism applies to all holographic recording phenomena, including those producing local gratings ($\Theta = 0$) like, for instance, those related to effects as photochromism or photoisomerizations, or those related to thermal, chemical, electronic nonlinearities[2,19]. In all these effects transmitted light of one beam is dephased by $\pi/2$ in respect to other beam's diffracted light. After the transmission through the material, both waves ($I_{1,trans}$ and $I_{2,diffr}$, $I_{2,trans}$ and $I_{1,diffr}$, respectively) interfere each other identically in both directions. This is not the case for non-local gratings ($\Theta \neq 0$), like those produced by photorefractive effect: phase relationships existing between transmitted and diffracted parts are such that interference is constructive for one beam (signal beam increases) and destructive for the other beam (pump beam decreases). Phase shift is therefore a specific feature for photorefractive effect[8,20,21]. This feature is responsible for the energy transfer between the two beams. A strict treatment about the propagation of electromagnetic radiation at optical frequencies in a photorefractive material leads to the following equation[9]

$$E = E_0 \exp\left[\frac{\Gamma}{2}\left(\sin\Theta + j\cos\Theta\right)x\right] \quad .$$
(1.12)

Eq. (1.12) relates E, amplitude of the electric field associated with a beam at the exit from the material, to E_0, the value of the electric field of the same beam prior to the entrance. It actually describes the effect exerted on amplitude (and hence, on energy) by the photorefractive material. In Eq. (1.12) Γ appears, the photorefractive optical gain, whose dimensions are [cm^{-1}]. It is defined as follows

$$\Gamma = \frac{4\pi}{\lambda}\left(\hat{e}_1 \cdot \hat{e}_2^*\right)\Delta n \sin\Theta \quad ,$$
(1.13)

where $\hat{e}_i$ are polarization unit vectors of the two beams. From (1.13) it is clear that the highest obtainable energy transfer can occur fulfilling the requirement $\Theta = \pi/2$. Moreover, the sign of

10

Γ stands for the direction of energy transfer, viz. which beam gains energy ($\Gamma > 0$), and which looses it ($\Gamma < 0$). Actually, the experimentally determined quantity is the power of light, and not the amplitude of the electric field associated to a light beam. For this reason it is more useful to express the energy transfer between the two beams in terms of the intensity of light transmitted by the material. Resolution of the wave equation for the total field given by the sum of the two beams leads to the following expressions of the intensity of transmitted light for each beam, as a function of the distance z covered through the sample[22]

$$I_1(z) = \frac{I_1(0)b(1+b)\exp(-\alpha z)}{b + \exp(\Gamma z)} \tag{1.14}$$

$$I_2(z) = \frac{I_2(0)(1+b)\exp(-\alpha z)}{1 + b\exp(-\Gamma z)} \quad , \tag{1.15}$$

in which $b = I_2(0) / I_1(0)$ is the ratio of beams intensities at the entrance of the material, and α is the optical loss factor due to absorption.

Energy transfer between the two beams in an *Asymmetric Two Beam Coupling* (2BC) experiment can be helpfully characterized by the *beam coupling ratio* γ_0; it is defined[21] as the ratio between the intensities of transmitted signal beam in the presence of the other beam (PR effect "ON") and in the absence of the other beam (uniform irradiation, PR effect "OFF").

$$\gamma_0 = \frac{I_2(I_1 \neq 0)}{I_2(I_1 = 0)} \quad . \tag{1.16}$$

Beam coupling ratio γ_0 is related to photorefractive optical gain Γ through the relations

$$\gamma_0 = \frac{(1+b)\exp(\Gamma l)}{b + \exp(\Gamma l)} \quad ; \quad \Gamma = \frac{1}{l}[\ln(b\gamma_0) - \ln(1+b-\gamma_0)] \quad , \tag{1.17}$$

being l the length of the optical path of the beam inside the PR material.

1.2 Non Linear Optics (NLO) principles

An electric field $\vec{E}(\vec{r},t)$ in a linear, not dispersive, homogeneous and isotropic dielectric medium gives the medium a net polarization $\vec{P}$. A direct proportionality

relationship exists between the polarization $\vec{P}$ and the value of the applied electric field for such kind of medium; $\vec{P}$ and $\vec{E}$ are parallel vectors and the following relation holds

$$\vec{P}(\vec{r},t) = \chi^{(1)}\vec{E}(\vec{r},t) \qquad , \qquad (1.18)$$

where $\chi^{(1)}$ is defined as the linear susceptibility. If the electric field is that associated with an optical radiation, the response of the medium can be as well described in terms of its refractive index n, a quantity related to the linear susceptibility dependent on the angular frequency ω of the incident optical radiation

$$n(\omega) = \left(1 + 4\pi\chi^{(1)}(\omega)\right)^{1/2} \quad . \qquad (1.19)$$

A radiation propagating as plane wave through a linear medium is described by the equation

$$E = E_0 \cos(kz - \omega t) = \frac{1}{2}\left[E_0 e^{j(\omega t - kz)} + c.c.\right] \qquad , \qquad (1.20)$$

with c.c. conjugated complex; it is important to notice that in Eq. (1.20) the refractive index n, the wave vector $k = \dfrac{n\omega}{c}$ are all quantities independent by E.

The frame is different for anisotropic media; this is also the case for electrooptic and photorefractive organic materials in which the anisotropy is caused by the re-orientation of non-centrosymmetrical units having permanent electric dipole moment (edm) under the effect of a poling electric field. In this kind of media the polarization $\vec{P}$ is no longer necessarily parallel to the electric field, the components of $\vec{P}$ and $\vec{E}$ being related by tensorial quantities, instead of scalar proportionality factors. The component P_i along the i direction is therefore related to the electric field components along all the three directions in space. The polarization in an anisotropic medium can therefore be described by an expression like

$$P_i = \sum_j \chi_{ij} E_j \qquad \Leftrightarrow \qquad \begin{aligned} P_x &= \chi_{11}E_x + \chi_{12}E_y + \chi_{13}E_z \\ P_y &= \chi_{21}E_x + \chi_{22}E_y + \chi_{23}E_z \\ P_z &= \chi_{31}E_x + \chi_{32}E_y + \chi_{33}E_z \end{aligned} \quad . \qquad (1.21)$$

The susceptibility turns out to be a rank 2 tensor defined by 9 (that is, 3^2) terms χ_{ij}

$$\ddot{\chi} = \begin{pmatrix} \chi_{11} & \chi_{12} & \chi_{13} \\ \chi_{21} & \chi_{22} & \chi_{23} \\ \chi_{31} & \chi_{32} & \chi_{33} \end{pmatrix} \qquad . \qquad (1.22)$$

If the light-matter interaction is non-resonant (i.e. the material is transparent and has no absorption) the susceptibility tensor is a real and symmetric one, i.e. $\chi_{ij} = \chi_{ji}$ and it has only six independent elements. The magnitude of the tensor elements depends on the choice of the X, Y, Z axes relative to the symmetry axis of the anisotropic medium.

The linear dielectric approximation (viz., the response of a material to an applied optical field is simply proportional to the amplitude of the electric field and the susceptibility is independent by the value of the field) results to be valid as long as the field amplitude is low with respect to the internal atomic or molecular electric fields. When a laser light is applied this assumption can cease to be valid because the intensity of the optical field can be such that the response of the material becomes a non-linear one. The polarization for a non-linear dielectric medium is defined by additional contributions at higher orders in the electric field (squared, cubic, etc...) with respect to (1.18), that represents the first-order expression. A more general expression of the polarization for non linear media is

$$P(E) = \chi^{(1)}E + \chi^{(2)}EE + \chi^{(3)}EEE + ... = \chi E \qquad . \qquad (1.23)$$

The non-linear electric field dependence can be resumed in a new expression for the dielectric susceptibility χ; it depends on the applied electric field and is defined as

$$\chi(E) = \chi^{(1)} + \chi^{(2)}E + \chi^{(3)}EE + ... \qquad . \qquad (1.24)$$

where $\chi^{(1)}$ is the linear susceptibility, $\chi^{(2)}$ is the second-order susceptibility, $\chi^{(3)}$ is the third-order susceptibility, and so on. These corrections at the second and third order to the polarization are responsible for many NLO processes like, for instance, second-harmonic generation (SHG) or the dependence of the refractive index of the material on the incident light intensity. In order to visualize more clearly the origin of these effects, we must reconsider the propagation of a plane wave through a non-linear medium. In such a medium a travelling plane wave

13

$$E = E_0 \cos(kz - \omega t) = E_0 \cos\alpha \qquad (1.25)$$

will produce a polarization

$$P = \chi^{(1)} E_0 \cos\alpha + \chi^{(2)} E_0^2 \cos^2\alpha + \chi^{(3)} E_0^3 \cos^3\alpha =$$
$$= \chi^{(1)} E_0 \cos\alpha + \frac{1}{2}\chi^{(2)} E_0^2 \left(\cos 2\alpha + 1\right) + \chi^{(3)} E_0^3 \left(\frac{3}{4}\cos\alpha + \frac{1}{4}\cos 3\alpha\right) \qquad . \qquad (1.26)$$

Equation (1.26) clearly shows the harmonics generation (multiple frequencies components: 2α, 3α); the second-harmonic is related to $\chi^{(2)}$, and the third harmonic to $\chi^{(3)}$. Moreover, $\chi^{(3)}$ brings an additional term at the same frequency α of the incident radiation, taking into account the dependence of the refractive index on the intensity. Second-harmonic generation (SHG) and third-harmonic generation (THG), together with some other effects (e.g. two-photon absorption, 2PA), are known as non-linear optics (NLO) processes, field of an intense research activity during the last decades[23,24].

Generally speaking, all the materials could exhibit at various extent NLO properties at the third-order (and, generically, odd-order NLO properties), while second-order (and, generically, even-order) NLO properties are prerogatives to materials fulfilling certain symmetry requirements; only non-centrosymmetrical materials -that is those who lack inversion symmetry- can exhibit second-order NLO effects[17,25]. As already mentioned, Eq. (1.22), optical properties of anisotropic and non-centrosymmetrical media are described by means of tensorial quantities.

For a NLO process, nth order non-linear polarization deals with the interaction of n electric field vectors. It could happen that many different electric fields are simultaneously present at different frequencies ω_n ; such systems are described by means of the following relations

$$\vec{E}(\vec{r},t) = \sum_n \vec{E}(\omega_n)\exp(-j\omega_n t) + c.c.$$
$$\vec{P}(\vec{r},t) = \sum_n \vec{P}(\omega_n)\exp(-j\omega_n t) + c.c \qquad . \qquad (1.27)$$

In dispersive materials the direct proportionality between polarization and electric field, though not valid in time domain, is still valid in that of frequency, so that[26]

$$P(\omega) = \chi(\omega)E(\omega) \qquad\qquad (1.28)$$

and (1.28) describes dispersive non-linear media, in frequency domain.

Let us now take into consideration in greater detail the second-order contribution to the polarization; indeed, it will turn out to be the more useful and important one for the study of photorefractive organic materials.

A general expression for the non-linear second-order polarization is given by

$$P_i(\omega_n + \omega_m) = D\sum_{jk} \chi_{ijk}^{(2)}(\omega_n + \omega_m; \omega_n, \omega_m)E_j(\omega_n)E_k(\omega_m) \qquad\qquad (1.29)$$

with i,j,k referring to the cartesian components and D being the so-called *degeneration factor*, relating to the different distinct possible permutations of frequencies ω_n and ω_m. Every second-order non linear polarization component is therefore described by a sum of 9 different terms, so that the tensor $\ddot{\chi}^{(2)}$ has 27 elements. Fortunately, this tensor often possesses symmetry properties that permit to remarkably reduce the number of independent elements. Due to the intrinsic permutation symmetry, tensor elements are reduced to 18: tensor elements $\chi^{(2)}_{ijk}$ can be expressed in contracted form $\chi^{(2)}_{il}$ with only two indices but where the first index i takes the values 1,2 or 3, corresponding to the three Carthesian coordinates, and the second index l varies between 1 and 6. The values of l refer to the six different combinations of the indices j and k with the following convention:

l:	1	2	3	4	5	6
j,k:	1,1	2,2	3,3	2,3 or 3,2	1,3 or 3,1	1,2 or 2,1

Using this new convention,[17] susceptibility is described by means of a 3x6 tensor of 18 elements $\chi^{(2)}_{il}$.

When photorefractive polymer materials are considered, for instance, and their dipolar molecular units are poled by an externally applied electric field, second-order susceptibility tensor further reduces to only two independent elements, as follows[17,18]

$$\ddot{\chi}^{(2)} = \begin{pmatrix} 0 & 0 & 0 & 0 & \chi_{31}^{(2)} & 0 \\ 0 & 0 & 0 & \chi_{31}^{(2)} & 0 & 0 \\ \chi_{31}^{(2)} & \chi_{31}^{(2)} & \chi_{33}^{(2)} & 0 & 0 & 0 \end{pmatrix}, \qquad\qquad (1.30)$$

thanks to symmetry properties and making use of Group Theory.

Writing down the polarization in a different manner permits to better understand the effects related to second-order non-linearity:

$$\vec{P}(\omega_3) = \vec{\chi}(\omega_3; \omega_1, \omega_2)\vec{E}(\omega_1)\vec{E}(\omega_2)$$ (1.31)

with $\omega_3 = \omega_1 + \omega_2$.

A particular case is that in which $\omega_1 = 0$, namely when one of the involved electric fields is a d.c. one or its frequency is very low in comparison with optical frequencies; therefore, $\omega_3 = \omega_2 = \omega$ and it brings to

$$\vec{P}(\omega) = \vec{\chi}(\omega; 0, \omega)\vec{E}(0)\vec{E}(\omega)$$. (1.32)

This process is referred to as *linear electrooptic effect* (LEO), or more often as *Pockels Effect*, bearing the name of its discoverer. Though the input optical frequency ω is not modified by the interaction with the material, amplitude and phase of the transmitted light depend through a linear proportionality on the value of the applied d.c. electric field *E(0)*. The capability to manipulate the phase of an electromagnetic wave via the variation of the refractive index of a material is the fundament of the operation in many optical devices relying on NLO effects[17,18,21,25].

The description made up to now used an expansion of electric susceptibility in power series of the total electric field. In electrooptics it is often more useful to deal with the refractive index n(E) as a function of the static electric field, $E(\omega = 0) = E_0$; in this new notation it is possible to expand the refractive index by a Taylor series around $E_0 = 0$, obtaining:

$$n(E_0) = n(E_0 = 0) + \frac{dn}{dE_0}\bigg|_{E_0=0} E_0 + \frac{1}{2}\frac{d^2n}{dE_0^2}\bigg|_{E_0=0} E_0^2$$. (1.33)

Eq. (1.33) is usually written down as

$$n(E_0) = n(E_0 = 0) - \frac{1}{2} n^3 r E_0 - \frac{1}{2} n^3 s E_0^{\,2}$$

$$r = -\frac{2}{n^3} \left. \frac{dn}{dE_0} \right|_{E_0=0}$$

$$s = -\frac{1}{n^3} \left. \frac{d^2 n}{dE_0^{\,2}} \right|_{E_0=0}$$

(1.34)

The two quantities r and s are adopted as electrooptic (EO) parameters and they are called, respectively, *linear EO coefficient* and *squared EO coefficient*.

In an anisotropic medium the refractive index is represented by means of an *ellipsoid* describing light propagation along different axes; r and s are no longer scalar quantities but tensors. In (1.34) the *Pockels effect* is defined by the first term (term linear in E_0), while *Kerr effect* is related to the second one (squared in E_0). It is possible to show how the elements of the linear EO coefficient r_{ij} are related to the elements of second-order NLO susceptibility $\chi_{ij}^{(2)}$ according to the equation

$$r_{ij} = -\frac{8\pi}{n^4} \chi_{ij}^{(2)}$$

(1.35)

In analogy with susceptibility, Group Theory and symmetry properties permit to drastically reduce the number of independent terms of $\overleftrightarrow{r}$ tensor. It is represented by the matrix:

$$\overleftrightarrow{r} = \begin{pmatrix} 0 & 0 & r_{13} \\ 0 & 0 & r_{13} \\ 0 & 0 & r_{33} \\ 0 & r_{13} & 0 \\ r_{13} & 0 & 0 \\ 0 & 0 & 0 \end{pmatrix}$$

(1.36)

1.3 Connections between molecular and "in bulk" NLO properties

Up to now, in our description of non-linear phenomena we have dealt with "macroscopic" or bulk NLO properties, neglecting the microscopic world of molecules and

atoms that constitute the materials. Indeed, molecules (or atoms) and their "microscopic" properties are responsible for the bulk effects experimentally observed. Microscopic NLO properties can be correlated with macroscopic ones taking into account different factors like, for instance, mutual orientations and distances between different molecules, mean orientation, evaluation of local fields actually affecting the molecules in bulk that are different from the externally applied electric fields, mutual polarizations operated by nuclei and electrons on neighbour molecules (cooperative supramolecular effects). Second-order NLO effects in organic molecular materials result from strong intramolecular donor-acceptor interactions. As common features, such molecules are highly polarized (i.e. they own a permanent electric dipole moment μ) and/or polarizable systems; necessarily, due to symmetry requirements, they are non-centrosymmetrical. Their typical molecular structure is elongated: a "π-bridge", that is an extended region of conjugated π electrons, substituted at the opposite extremes by functional groups or atoms characterized by very different electron affinities (different substituents are referred to as electron *donor* and *acceptors*), s. Figure 1.3. Delocalization of π-electrons along the molecular principal axis (they can roughly be visualized as rod-like molecules) is obtained through the use of conjugated chemical structures as benzene, stilbene, azobenzene, heterocycles, polyenes, biphenyls, poly-phenylene-vinylene chains, etc. An increase of the electron density at the electron acceptor substituted molecular extreme (A) is correspondingly associated with a lowering at the opposite extreme (D) substituted by an electron-donor. On these grounds such molecules are usually called *push-pull* molecules or *push-pull* NLO chromophores.
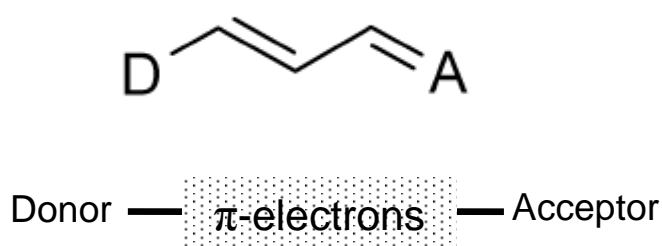
Figure 1.3 Drawing schematizing the typical molecular structure of a *push-pull* NLO chromophore. An electron acceptor and an electron donor are substituted at the opposite extremes of an elongated structure of π-conjugated electrons.

NLO chromophores own a permanent μ in their ground state. Further, NLO chromophores are characterized by a more or less pronounced anisotropy Δα defined as the difference between the polarizability $\alpha_{\parallel}$ along the molecular axis and the polarizability $\alpha_{\perp}$

along directions perpendicular to it. As in macroscopic treatment, it is possible to analogously define proper microscopic quantities describing the polarization, and non-linear higher order additional contributions. Concerning molecular moieties, under the condition of non-resonating excitation (i.e. making the simplifying assumption that no absorption of light by molecule is present at the operating wavelength), the application of an electric field E produces a microscopic polarization p (in order to distinguish it from P, the macroscopic polarization). It can be written down as

$$p_i = \mu_i + \sum_j \alpha_{ij} E_j + R^{(2)} \sum_{jk} \beta_{ijk} E_j E_k + R^{(3)} \sum_{jkl} \gamma_{ijkl} E_j E_k E_l + \dots \qquad (1.37)$$

i, j, k, l being the cartesian coordinates in the molecular frame of reference; α_{ij}, β_{ijk}, γ_{ijkl} are tensor elements; E_j, E_k, E_l are electric field components; $\vec{\alpha}$ is the *linear polarizability* tensor - microscopic equivalent to $\chi^{(1)}$-; $\vec{\beta}$ is the *first hyperpolarizability* tensor -microscopic equivalent to $\chi^{(2)}$-; $\vec{\gamma}$ is the *second hyperpolarizability* tensor -microscopic equivalent to $\chi^{(3)}$-; $R^{(n)}$ are *degeneration factors*, similar to those D factors valid in the macroscopic treatment, s. (1.29), concerning the typology of NLO processes and the frequencies of fields involved in the interactions.

In order to experimentally study macroscopic second-order NLO effects -those related to first hyperpolarizability β at molecular level- it is mandatory to impose a poling of molecular dipoles, that are otherwise randomly oriented in the bulk material. This is, for instance, the case for a NLO chromophore dissolved in an amorphous polymer matrix; poling is usually imposed by applying an external static electric field at temperatures well above T_g, the glass transition temperature of the material. In these conditions molecular units owning permanent electric dipoles (like NLO chromophores) can move and reorient themselves along the direction of the applied electric field. Poling of NLO chromophores, whether they are free or linked through covalent bonding to a macromolecular chain, is a fundamental process in organic photorefractive materials. The orientation degree of the molecular active units is the most important parameter that relates the microscopic NLO properties to the bulk effect.

Various models exist concerning this molecular re-orientation mechanism[18]. The simplest one, known as *Oriented Gas Model*, assumes a Maxwell-Boltzmann orientational distribution for dipoles and considers material's response as the sum of individual molecular responses. Electrostatic interactions among the molecules are totally neglected. In spite of the various simplifying assumptions adopted in this model, it provides an approximately good calculation of relations between microscopic factors and macroscopic properties. Avoiding a

more detailed description of the model, whose features can be found elsewhere[17,18], we present here the results only. For a poling electric field E_p applied along the direction of Z axis (macroscopic frame of reference) the change in linear susceptibility between a poled sample and a non-poled one (random oriented) turns out to be

$$\Delta\chi_{ZZ}^{(1)} = \frac{2}{45} N F^{(1)} \left(\alpha_{\parallel} - \alpha_{\perp}\right) \left(\frac{\mu}{k_B T}\right)^2 E_p^{\,2}$$

$$\Delta\chi_{XX}^{(1)} = -\frac{1}{2} \Delta\chi_{ZZ}^{(1)}$$

(1.38)

and the second-order susceptibility becomes

$$\chi_{ZZZ}^{(2)} = N F^{(2)} \frac{\mu E_p}{5 k_B T} \beta_{zzz}$$

$$\chi_{ZXX}^{(2)} = \frac{\chi_{ZZZ}^{(2)}}{3}$$

. (1.39)

Z and X are, respectively, parallel and perpendicular directions with respect to the applied electric field in the macroscopic frame of reference; N is the numeral density of NLO chromophores; μ is their permanent edm in ground state; $F^{(1)}$ and $F^{(2)}$ are local field correction factors taking the screening effect of the medium into account.

1.4 Orientational contribution to photorefractive effect

It is important to notice that, besides the second-order effects involved with β (LEO), s. Eqs. (1.32) and (1.39), other contributions exist due to linear polarizability α, s. (1.38). NLO chromophores, indeed, because of their elongated structure, show different linear responses to optical fields directed along directions that are parallel or perpendicular to the molecular principal axis, i.e. their linear polarizabilities components are $\alpha_{\parallel} \neq \alpha_{\perp}$. This peculiar feature permits to a poled sample of NLO chromophores, reoriented under the effect of an applied electric field, to exhibit birefringence. In merely electrooptic PR polymers, in which an electric d.c. field is not capable to reorient NLO units (as, for instance, when glass transition temperature $T_g > T_{rt}$, the so-called "hard" materials), this mechanism leads to a spatially uniform permanent birefringence contribution. It plays a minor role in the

modulation of refractive index due to EO effect. PR effect is said therefore to be "merely" electrooptic, i.e. due to the Pockels effect.

On the other hand, when NLO chromophores can reorient in a poling field, that is the case of polymeric photorefractive materials with $T_g < T_{rt}$ (the so-called "soft" materials) another contribution arises. The poling field acting on the dipoles is the one given by the superposition of the externally applied d.c. electric field E_{ext} and the modulated space charge field E_{SC} (s. Sect. 1.1); the effect is to produce inside the material a spatially modulated birefringence, whose additional contribution to the global PR effect is very important and, often, predominant. This additional contribution has been discovered and recognized some years after the first observation of PR effect in organic materials and scientific community commonly refers to it as *orientational contribution* or *birefringence contribution* to photorefractive effect[27]. It is important to notice that this enhancement is one of the main differences existing between the behaviour of organic and inorganic photorefractive materials.
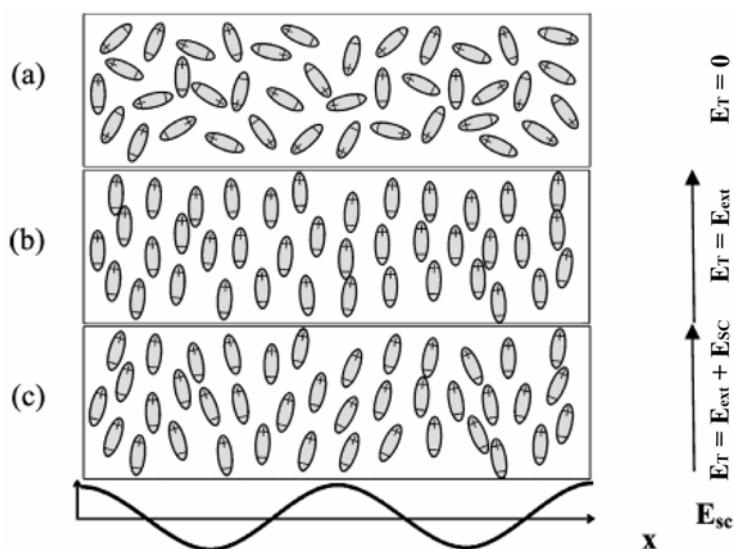
Figure 1.4 Dipolar NLO chromophores reorientation in the total electric field E_T. a) no electric field is applied; b) d.c. external electric field E_{ext} is applied; c) spatially modulated space charge field E_{SC} is added.

The orientational or birefringence contribution is strictly correlated to the capability of NLO chromophores to align along the total (local) electric field E_T, and hence to their mobility in the amorphous phase of the material. Figure 1.4 qualitatively displays the different alignment of dipolar NLO chromophores for different kinds of E_T. From this point of view, glass transition temperature T_g plays a fundamental role in determining the extent of the PR effect in organic amorphous materials; T_g, indeed, rules the dynamics of the poling process,

together with other features involved with charge transport and in general with all the viscoelastic properties of the materials, to be discussed later (s. Sect. 1.6.1 and Sect. 2).

In the model so far used in order to describe the PR effect, refractive index modulation Δn is caused by the space charge field E_{SC} through EO effect (1.11). In organic materials birefringence contribution can lead to a significant enhancement of PR effect which is related to space charge field in a different manner[27]. It is worth to notice that the poling field acting on the edms of NLO chromophores in a PR material is the *total* electric field E_T given by the sum of two different electric fields: E_{ext}, the externally applied d.c. electric field (static, uniform in space), and E_{SC}, the space charge field induced in the material by the interference pattern (modulated in space) (s. Figure 1.4). These two fields add together in the resulting E_T field that changes both its amplitude and direction over the grating axis (X axis in Figure 1.4), due to the modulation of E_{SC}, whose amplitude varies amidst its extremes $+\left| E_{SC} \right|$ and $-\left| E_{SC} \right|$. The presence of such a field is responsible for a space periodic reorientation of NLO chromophores, as illustrated in Figure 1.4 and Figure 1.5. Reorientation dynamics in low-T_g materials is therefore a fundamental aspect for the comprehension of PR materials and is the topic of extensive studies[28,29]. In addition, it has been noticed that the global writing speed of a PR grating in an organic material is mainly influenced by the chromophores mobility[30]. Indeed, molecular reorientation times can vary from picoseconds (e.g., in liquids), up to extremely long times of the order of years (as observed, for instance, in very high T_g polymers in which a high temperature, $T > T_g$, poling has been made under the effect of an externally applied electric field, followed by a rapid temperature quenching). Typical features related to reorientation times are material's viscosity, molecular dimensions and steric hindrances of NLO chromophores, intermolecular interactions.

The periodic reorientation of the anisotropic units responsible for the NLO effects gives origin to a corresponding periodic modulation of refractive index via a mechanism of orientational birefringence, s. Eq. (1.38).
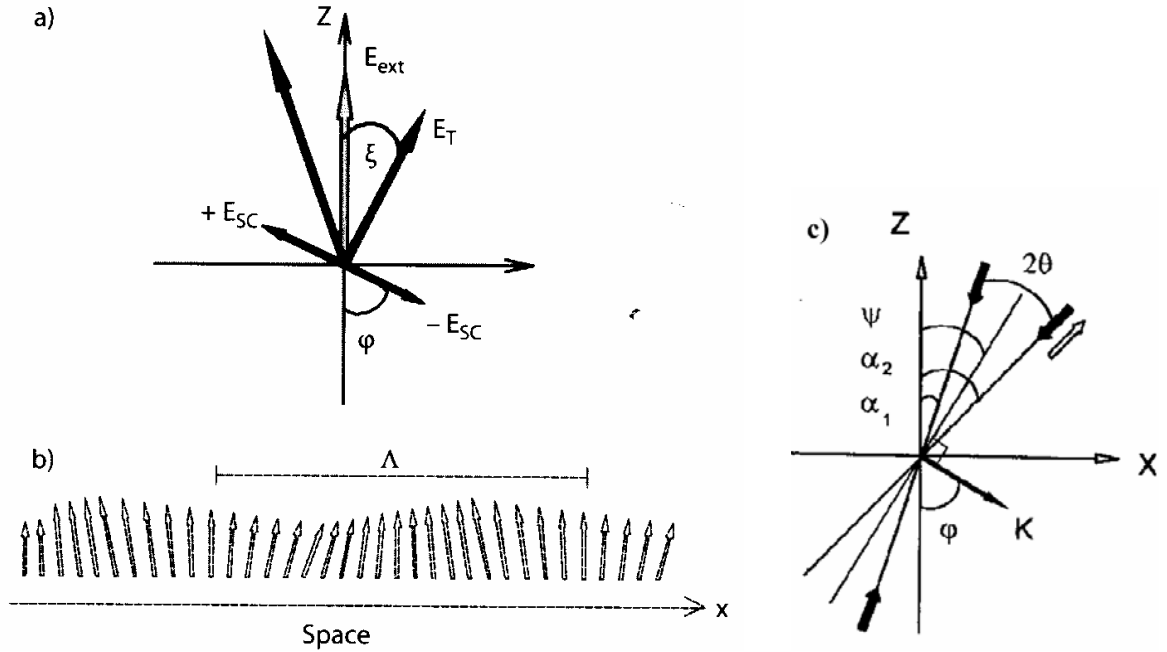
Figure 1.5 **a)** Poling total electric field E_T is the sum of d.c. external electric field, E_{ext}, and modulated space charge field, E_{SC}; **b)** periodic reorientation along x of NLO dipolar chromophores (dipoles are sketched as arrows) caused by the application of E_T; **c)** orientation of axes and definitions of angles in a common experimental geometry employed in 2BC or Degenerate Four-Wave Mixing (DFWM) techniques.

In this way, it is possible to recognize two different contributions to the total refractive index modulation Δn: an electrooptic contribution Δn_{EO}, related to second order NLO properties (β), and a birefringence contribution Δn_{BR}, related to edm μ and linear polarizability anisotropy $\Delta\alpha$. Making reference to the previous equations it is possible to sum up all these considerations and to deduce some general rules about molecular features that NLO chromophores must possess in order to exhibit the best PR properties. Here is a list of these requirements:

1) high value of first hyperpolarizability β, in order to maximize EO effect, Eq. (1.39);

2) high value of permanent edm μ, in order to obtain an efficient chromophores reorientation through the moment of the forces exerted on them by an electric field; an high value of μ is desirable also because of the μ^2 dependence of birefringence contribution, Eq. (1.38);

3) high value of linear polarizability anisotropy $\Delta\alpha$, in order to maximize birefringence contribution.

Given the resulting squared dependence on total electric field E_T of both contributions Δn_{EO} and Δn_{BR}, s. Eqs. (1.38) and (1.39), Wortmann *et al.* interpreted more correctly the

23

refractive index modulation in organic PR materials as a *Kerr* effect; otherwise, as concerns inorganic materials, a *Pockels* effect is recognized[31,32]. Coherently with this interpretation and with the observed peculiar behaviour of organic amorphous materials, the same group of researchers have subsequently defined a proper molecular figure of merit, F^{Kerr}, to be used for push-pull NLO chromophores. It quantitatively describes and measures the previously listed requirements. Kerr figure of merit is defined as[33]:

$$F^{Kerr} = \frac{1}{M}\left[9\mu\beta + \frac{2\mu^2\Delta\alpha}{k_B T} \right]$$ (1.40)

in which M is the molecular weight of the NLO chromophore, and k_B is the Boltzmann constant. In the simplest case, that is when NLO chromophores can be considered as "one-dimensional" push-pull moieties, the polarizabilities figuring in (1.40) can be approximated as follows[33]:

$$\Delta\alpha = \frac{2\mu_{eg}^2 \lambda_{eg}}{hc} \quad ,$$ (1.41)

$$\beta_0 = \frac{6\mu_{eg}^2 \Delta\mu \lambda_{eg}^2}{(hc)^2} \quad ,$$ (1.42)

with μ_{eg} transition dipole moment, λ_{eg} transition wavelength and $\Delta\mu$ variation of the edm between the ground state (g) and the excited state (e) in a simple two levels scheme, frequently employed in the modeling of such systems. Calculations made on typical NLO chromophores revealed that the main contribution to PR response is given by the term dependent on $\Delta\alpha$ (birefringence contribution up to > 75%), while β-dependent term has poorer relevance (< 25%)[31,33]. It is important to notice that, at low concentration of NLO moieties in the PR material, a good correlation exists between the isolated chromophore figure of merit F^{Kerr} and the bulk refractive index modulation Δn. This correlation ceases to remain valid at higher concentrations; actually it has been evidenced in some kinds of chromophores the onset of strong intermolecular interactions (like, for instance, the phenomenon of aggregation in head-to-tail dimers arrangement leading to a neat reduction of the total edm for dimer) that cause the deviation from the behaviour expected on the basis of molecular figure of merit[33,34,35]. This aspect has not yet been sufficiently explained and is currently the field of extensive studies.

The derivation of analytical expressions that describe the bulk electrooptic and birefringence contributions when poling field is the modulated total electric field E_T, is more complicated than in "traditional" purely electrooptic case. While details of such derivation are extensively described elsewhere[17], we report here the obtainable expressions for the different contributions of the refractive index modulation. For the birefringence (BR) contribution:

$$\Delta n_p^{BR} = \frac{2\pi}{n} B E_{ext} |E_{SC}| \left[2\cos\varphi \sin\alpha_1 \sin\alpha_2 - \cos\varphi \cos\alpha_1 \cos\alpha_2 + \frac{3}{2} \sin\varphi \sin(\alpha_1 + \alpha_2) \right] \quad , \quad (1.43)$$

being

$$B = \frac{2}{45} N(\alpha_{\parallel} - \alpha_{\perp}) \left(\frac{\mu}{k_B T} \right)^2 \quad . \quad (1.44)$$

For the electrooptic (EO) contribution:

$$\Delta n_p^{EO} = \frac{8\pi}{n} C E_{ext} |E_{SC}| \left[\cos\varphi \cos\alpha_1 \cos\alpha_2 + 3\cos\varphi \sin\alpha_1 \sin\alpha_2 + \sin\varphi \sin(\alpha_1 + \alpha_2) \right], \quad (1.45)$$

being

$$C = \frac{N\beta\mu}{15 k_B T} \quad . \quad (1.46)$$

In the previous equations, $\varphi = (90° - \Psi)$ is the angle between the interference pattern wave vector $\vec{K}$ and the normal direction to sample surface; Ψ is the tilt angle between sample normal and beams bisector; α_1 and α_2 are the incidence angles of beam 1 and 2 with respect to normal incidence, respectively. These angles are visualized in Figure 1.5 c) that schematizes the geometrical arrangement commonly employed in 2BC or Degenerate Four-Wave Mixing (DFWM) techniques, frequently used to test and study PR materials[2,36]. Details on 2BC and on the experimental setup adopted in the present research are given in the following (s. Sects. 3.6 and 3.7). The $\vec{E}_{ext}$ field component aligned along the grating wave vector $\vec{K}$ results to be $E_0 = E_{ext}\cos\varphi$; it is important to stress the fact that this component must be diverse from zero in order to permit the photogenerated charges to migrate over $\vec{K}$ direction and to give rise to

the periodic distribution of charges responsible for space charge field E_{SC}. The relations described so far are valid for p polarized beams, i.e. light beams whose electric field lies in a direction parallel to the plane of incidence (the plane made by the radiation propagation direction and a vector normal to the plane of a reflecting surface). Similar relations can be derived for s-polarized beams (even if, in that case, pump and signal beams invert themselves). Some studies have also been conducted in order to verify beams inversion and geometrical relations[1,2].

1.5 *Photoconductivity* (PC)

In order to have PR effect a material must be able to conduct charges, as briefly discussed in the introduction. This capability is obtained making use of photoconductors (PC); in organic PR materials several different types of materials can be used: photoconductive polymers (e.g., PVK, PSX, PPV), low molecular weight glass forming photoconductive molecules, insulating polymer matrices (e.g., polycarbonates, PS, PMMA, polysiloxane) doped with photoconductive monomers (PC monomers are dissolved in inert polymer matrices) or functionalized polymers having pendant groups with charge transport properties. All of them are unipolar photoconductors, that is, conduction takes place involving only one kind of charges (holes or electrons). The large majority of organic PR materials are hole-transporting photoconductors; for this reason in the following we refer only to hole transport. Nevertheless, it is important to remind that some electron transporting and bipolar organic PC materials have been discovered and studied[37,38,39]. The primary requirement for a PC material is photosensitivity; it means that a phenomenon is present through which charge generation under illumination of the material occurs. Several ways exist to introduce photosensitivity in an organic material; the more exploited one is the addition of species acting as photosensitizer agents whose role is to assist charge photogeneration. The choice of a particular photosensitizer is imposed by the nature of the moieties (molecular species or functional groups, grafted units, repetitive units of a macromolecular chain) designed as charge transport agent in the material and by the desired wavelength sensitivity. Dealing with wavelength sensitivity it is important to remark that, in order to fully exploit the sensitizer agent in the operating wavelength range, sensitizer moiety must exhibit the smaller bandgap (i.e. gap between ground and excited states; it is responsible for the absorption of light and, hence, for photogeneration) among the different components of the photorefractive material. On the other hand, absorption by other components must be avoided in order to minimize the

26

production of different photochromic gratings. At the same time, optical absorption by the sensitizer must be limited, in order to achieve a neat optical gain.

Several classes of organic molecules have been studied and utilized as sensitizers (e.g. squaraines, phtalocyanines, thiapyrylium salts, perylene dyes, transition metal complexes)[40,41,42,43]. Other approaches tried to use inorganic agents, like CdS or CdSe semiconductor quantum dots, as sensitizers in order to give hybrid inorganic-organic composites or nanocomposites[44,45,46,47].

The most common class of photosensitizers, indeed, is represented by charge transfer complexes (CTC)[48] formed by the interaction between electron-donor moieties responsible for conduction of holes (e.g., electron-rich molecules or polymers, like poly-(*N*-vinylcarbazole) PVK extensively studied and applied[49]), and electron-acceptor ones (e.g., molecular species as 2,4,7-trinitro-9-fluorenone TNF, or (2,4,7-trinitro-9-fluorenylidene)malononitrile TNFM, Table 1.1). Besides nitro-derivatives, other photosensitizers have been tested and employed: cyano-derivatives, halogenated compounds, fullerene C_{60}[50,51,52,53].

The intermolecular interaction between the donor *D* and the acceptor *A*, through the formation of a CTC, results in new absorption bands in the visible or near infrared regions; these bands do not appear in the absorption spectra of both single isolated molecules. The relative ease of formation of such complexes is primarily due to the low ionization potentials ip of electron rich moieties (e.g., the planar carbazole unit).

The mechanism of photogeneration operating in such systems is based on the optical excitation of a CTC; it is usefully schematized (s. Figure 1.6, right) as a three-steps process in a model called *coupled charges recombination model:*

1. optical excitation of CTC by incident radiation
2. electron transfer from a not-complexed donor species to the excited CTC
3. dissociation of the electron-hole pair and migration through transport molecules.

A fundamental role in such a frame is played by the energy stabilization of HOMO level (Highest Occupied Molecular Orbital) of the CTC, with respect to HOMO of the not-complexed donor. This stabilization energy is equal to complexation enthalpy ΔH_c,(s. Figure 1.6, left) whose value is in turn related to the ip of the donor. Molecules whose ip is low are indeed better electron-donors; it means, therefore, that they link more strongly the acceptors to create a CTC. The lower is the value of ip, the higher will be complexation enthalpy. These two quantities rule the rate of the process described in step 2, that is the transfer of an electron

from a donor molecule to an excited CTC. Marcus theory[54] predicts for the rate constant K_{ET} of the electron transfer reaction:

$$K_{ET} = K_0 \exp(-b\Delta R) \exp\left(-\frac{(\Delta H_c - \lambda)^2}{4\lambda k_B T}\right)$$

(1.47)

with K_0 and b constants; λ is a parameter called reorganization energy, ΔR is the distance between reaction centers.

The absorption of a photon by the CTC causes the generation of an electron-hole pair (*Frenkel's exciton)*; it is necessary to separate this pair so that free charges may rise. This separation process is competing with the corresponding *recombination*: because of the low values of dielectric permittivity in organic materials, Coulomb interactions between electron and hole are poorly screened, attraction thus leading to charges recombination. This process strongly influences the generation of free charges capable to participate in the transport, thus resulting in a diminished photogeneration efficiency. Quantum efficiency for the photogeneration process η (*photogeneration efficiency)* is defined as the ratio between the number of photogenerated charges (N_{PC}) and the number of absorbed photons (N_{AP}):

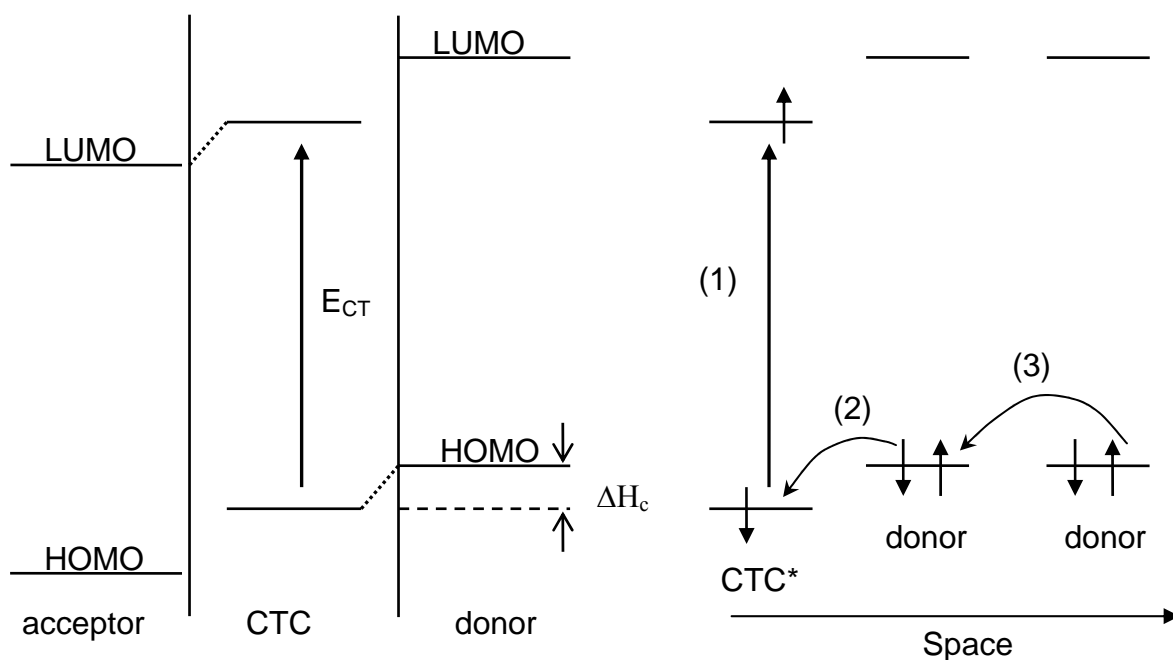$$\eta = \frac{N_{PC}}{N_{AP}} \qquad .$$

(1.48)

Figure 1.6 To the left, scheme displaying the energetic levels of acceptor and donor molecules and the corresponding levels of the CTC formed by the complexation of these two species. Only a simplified representation of the resulting HOMO and LUMO levels of CTC is displayed for clarity, even if more levels are formed, resulting in HOMO2, LUMO2, etc. levels of the CTC. The gap existing between HOMO levels of donor and CTC represents the stabilization energy, or complexation enthalpy, ΔH_c. To the right, the three steps of photogeneration mechanism by a CTC through its excitation at energy E_{CT} and migration of charges from neighbour donor molecules (s. text).

Photogeneration and recombination of charges are usually described by means of a kinetic model[55] schematized in Figure 1.7. During the first stage an absorption of light ($E = h\nu$) occurs by the CTC (DA) formed between an electron donor D and an electron-acceptor A. This event causes DA to change in $D^+ A^-$, the excited state; the rate of this process is regulated by the k_1 constant. The excited state might eventually decay to ground state with rate k_2 or the charges may separate each other via the jump of a hole (or of an electron) towards an A species (or, respectively, D species), thus forming a separated charges state $D^+....A^-$, this process being regulated by the k_3 constant. This is a reversible process: the CTC excited state (D^+A^-) can be obtained again via coupled recombination (k_4). The complete separation of electron-hole pairs into free charges occurs only when they can efficiently escape their mutual coulomb attraction field: it happens only when an electric field of proper magnitude is externally applied to the sample. The constant regulating this process, $k_5(E)$, is

therefore electric field dependent. Charge generation actually can increase under the application of an electric field capable to separate charges; in this way quantum efficiency for charge generation is strongly dependent on applied electric field, increasing as it increases. The dependence of photogeneration efficiency by parameters as temperature T and applied electric field has been described in the frame of a model developed by Onsager[56], and subsequently by more complex theories by Noolandi and Hong[50,57]; trends derived by this models show good agreement with experimental data.
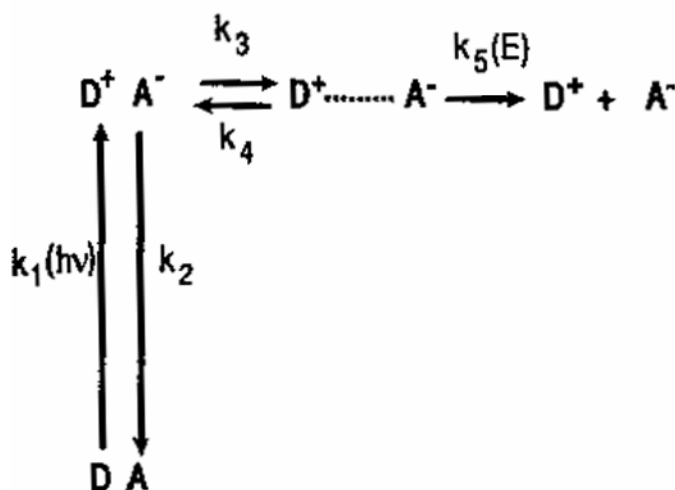

Figure 1.7 Kinetic scheme describing the process of charge generation in
a CTC formed by a donor (D) and an acceptor (A) moieties (s. text).

In inorganic materials (crystalline solids) conduction takes place through a transport mechanism based on the band structure of electronic levels, due to periodicity of crystal lattices. In that case "extended" electronic states are involved (states expanding over the entire lattice) and microscopic mobility of charges μ_0 is determined by band structure and scattering phenomena due to lattice vibrations (phonons). On the contrary, when organic amorphous material are considered PC is described by means of a *hopping* mechanism[16,58]. In this process, charges are said to be exchanged (or to "jump") among neighbour sites, namely molecular species or functional groups in polymeric chains. It is thus the case of "localized states". In this frame, holes are therefore cationic radicals -molecules or functional groups positively charged-, while electrons are the corresponding anionic radicals. Transport mechanism could be seen as a series of reversible redox reactions, driven by the applied electric field, in which neutral functional groups or molecules repeatedly transfer an electron to the nearest neighbour radical cation in the direction of the applied electric field. Charge migration involves ionic species (radical cations in the case of hole transport); nevertheless

hopping is not considered an ionic mechanism because matter transport is not involved (ions don't move). In this description it is assumed that energy distribution of various discrete hopping sites is narrow, that is, the activation energy required for a free charge to jump from one site to the other is approximately the same for all sites. An estimate made by Bässler *et al.*[59] calculated a mean width of ≈ 0.1 eV for such distribution.

In guest-host systems (s. Sect. 1.6.1) like polymers doped with molecular species, charge transport is a very complex process, its full description remaining a challenge because of the multiplicity of features influencing holes mobility. Energetic disorder degree, dipole moments of the host matrix and guest molecule/s, are only some of the many features taken into consideration in the literature[60]. A Gaussian Disorder Model (GDM) was introduced in order to describe the hopping mechanism[16,58,59,60,61,62]. In this GDM frame it has been shown that the edm of the active donor group, together with edms of other species involved in PC, cannot be ignored. The interactions of the migrating charges (holes) with the edms inside the material leads to the Poole-Frenkel-like equation for the mobility m:

$$m(E) \;=\; m(0) \, \exp\!\left(SE^{1/2}\right) \tag{1.49}$$

as a function of the square root of the applied electric field E [63]. In a semilogarithmic representation, m(0) is the intercept at E = 0 and S represents the slope of the linear function when $E^{1/2}$ is reported on the abscissa. A high value of m(0) has been put in relation, in the frame of the GDM[61], to a low value of the energetic disorder due to the dispersive interactions of the migrating charges with the donor D molecules. Such a disorder relates to the density of the states (DOS) whose width increases with the disorder. The slope S too is sensitive to the energetic disorder; it has been also related to the geometrical disorder connected to random distribution of the intermolecular distances and orientations among hopping sites. As a general remark, high S values are found for systems characterized by high disorder.

In this quite complex frame it is necessary to consider another important aspect, playing a major role in PC and PR: the presence of *traps*. Traps are known to be sites in which charges can be blocked for some time, thus limiting or hampering charge migration; they are hopping sites differing from the huge majority of sites: their activation energy, necessary to release charges, is larger than the average value of activation energy of the distribution. In a hole transport photoconductor, traps can be molecular moieties or functional groups in a polymer whose ip is lower with respect to ip of hopping species. Migrating holes (which are the mobile charges in the vast majority of organic PR materials) can incur and be trapped in various different trap sites: molecular impurities accidentally present in the

material, defective sites of a macromolecular chain (e.g. the terminating extremes of a polymer chain), NLO chromophore or photosensitizer molecules. A trap can be seen, in general, as a point site of the material where a migrating hole can be favourably stabilized in energy. In the previously cited GDM treatment it has been found that the probability of formation of a trap is higher where the width of DOS is larger, i.e., when the previously considered disorder is larger[16,64]. The precise nature of such trap sites is not yet fully understood and is still object of extensive studies[2]; nevertheless, traps are known to play a fundamental role in the development of efficient PR materials. Indeed, it is on these traps that part of the migrating charges stops to give rise to the charge lattice generating the space charge field E_{SC}. Reminding the relations reported in Sect. 1.1, it is important to stress that traps strongly influence E_q field (trap-limited field; Eq. (1.9)), as well as the PR grating phase shift Θ and charge mobility. Some detailed studies have been devoted to the understanding of the influence of traps on response dynamics of PR organic materials[65]. Different and increasing amounts of a molecule B having lower ip were added to a reference photoconductor A of known ip; in such study B acted as a trap for transport via B species. It has been observed that, after an initial remarkable increase due to a minimal addition of traps B, the subsequent addition of B caused a progressive decrease of response times, eventually restoring values similar to those of the original material (material A without traps). This behaviour has been explained as follows. In the absence of traps, charge transport proceeds through hopping among photoconductive sites (A-type). The addition of small quantities of traps B causes the blocking of migrating charges in these sites (B) for some time; this phenomenon is thus reflected in a reduced charge mobility. When larger traps concentrations are reached, the mean distance between traps decreases, eventually becoming comparable or lower than the distance between photoconductive (A-type) sites; conduction takes place now through hopping among B sites. This kind of phenomenon is called percolation.

1.6 Different categories of organic photorefractive materials

Organic materials have been taken into consideration in order to obtain efficient PR materials, alternatively to crystalline inorganic materials, due to their favourable chemical and physical properties. Indeed, low values of dielectric permittivity ε and high values of electrooptic coefficients -two mandatory requirements for efficient PR materials- are generally common parameters for organic materials. A specific figure of merit Q has been defined[21] in order to estimate the –at least potential- PR behaviour of the various materials.

The figure of merit is $Q = \dfrac{n^3 r}{\varepsilon}$ in which n is the refractive index of the material and r is the linear EO coefficient, Eq. (1.34). A comparison among values of Q obtainable for both organic and inorganic materials[21] clearly showed that organic materials are potentially preferable in spite of their generally lower refractive indexes. It is important to add to these general considerations what we have already described about the orientational enhancement effect, remarking its exclusive speci   city in organic materials (s. Section 1.4). Finally, it is worth to refer here also about the relative ease of synthesis, the huge capability to modulate properties by means of variations of functional groups in order to meet desired performances, the lower costs involved with organic materials. Many different approaches, from the first discovery of PR effect in organic crystals[5] and polymers[7], have been tested with the aim to obtain efficient organic materials. The following sections (1.6) briefly mention some of the various proposed approaches; the aim is to give the reader an overview of the state of art in this field. Materials are described and grouped in various categories[66,67] following closely the different approaches used to combine in a material the various necessary functionalities for the onset of PR effect.

1.6.1 Guest-host photorefractive materials

In the *guest-host* approach, low molecular weight molecules individually bearing the necessary functionalities are added to a polymer matrix. Polymer matrix itself may or not carry out some of the required functions. Polymer can be "inert", meaning that it does not actively contribute to the carrying out of the electrooptic properties (PC or NLO properties); in this particular case, it plays only the role of a matrix in which the active components of the blend are mixed and dispersed in glass (amorphous) phase. With this purpose, many different polymers have been employed like, for instance, *poly*-methyl-methacrylates (PMMA)[31] and *poly*-carbonates. The use of different polymers in combination with different NLO chromophores at various concentrations permits the "tuning" of materials parameters for the achievement of the best results. A drawback of these systems is the possible phase segregation of one or more components of the blends. NLO chromophores and PC monomers usually employed are indeed crystalline materials; their blends with amorphous polymers can give rise to metastable glass phases, useful in PR applications. Nevertheless, after periods ranging from some minutes to months, monomer species tend to aggregate and recrystallize in the polymer matrix, thus leading to the loss of transparency of films and the lack of PR properties. The extent of this phenomenon depends on the concentration of monomers in PR

blends. In such a way, concentration of monomers is forcedly limited with a detriment of PR properties. In the attempt to partially avoid segregation phenomena, many multi-functional PR chromophores have been synthesized and studied: molecules bearing simultaneously the various necessary functionalities; one example is given by triphenylamines class (TPA)[68]. Nevertheless, the choice to employ an inert polymer matrix is unfavourable because only a fraction of the active volume of a film actually participates in PR effect, the remainder being an inert polymer filler.

A diverse and more attractive strategy is to make use, in blends formulation, of polymers having NLO properties; groups bearing NLO functionality can be present in the main chain of macromolecules (repetitive units) or grafted as pendant groups. An example of this kind of approach is given by the first ever reported polymer PR material[7]: the NLO epoxy polymer bisA-NPDA (bisphenol A-diglycidyl ether 4-nitro-1,2-phenylenediamine), s. Figure 1.8. It was obtained by cross-linking reaction of bisphenol-A diglycidyl ether with 4-nitro-1,2-phenylenediamine (NPDA): the main chain groups NPDA supplied NLO properties and photosensitivity. The epoxy polymer was subsequently doped with a 30% amount of DEH (diethylaminobenzaldehyde-diphenylhydrazone), a low molecular weight component responsible for charge transport (s. Figure 1.8). Reduced PR performances, due to the low mobility of NLO units covalently linked in the main chain, have been reported for this blend, like for others based on similar approaches[69].

bisA-NPDA

DEH

Figure 1.8 Molecular species involved in the formulation of the first reported polymeric PR material. Epoxy resin bisA-NPDA acted as charge photogeneration agent and NLO species, while monomer DEH acted as charge transporting agent[7].

Other studies have been conducted making use of PC polymers. Such alternative way revealed itself as the most promising to achieve the best PR performances and for this reason a very large number of examples of such kind of blends exists. The most employed PC host polymer is poly-(*N*-vinylcarbazole) PVK, due to its excellent photoconductivity; it has been employed in the formulation of a very large number of blends, together with numerous NLO chromophores and sensitizing agents[20,66,70]. One of the possible examples of PVK based blend, and probably one of the most cited in literature as a reference[71] because of the obtained good PR results, is that of a blend containing:

<u>PVK</u> as photoconductive polymer;

<u>DMNPAA</u>, namely 2,5-dimethyl-(4-*p*-nitrophenylazo)anisole, as NLO chromophore;

<u>ECZ</u>, namely *N*-ethyl carbazole, as plasticizer agent (reducing T_g of the blend);

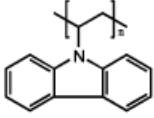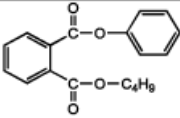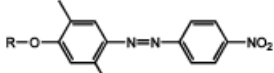<u>TNF</u>, namely 2,4,7-trinitro-9-fluorenone, as photosensitizer.
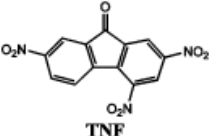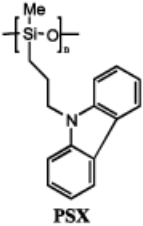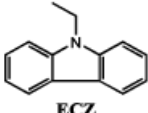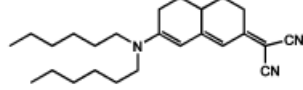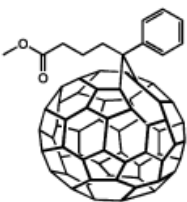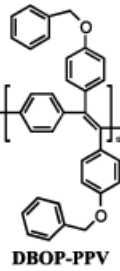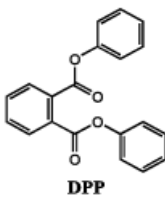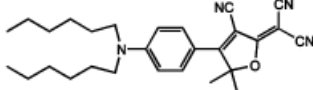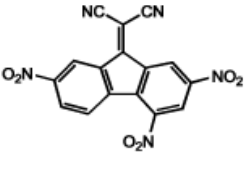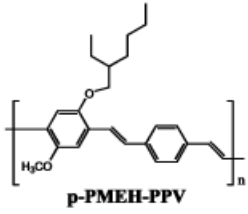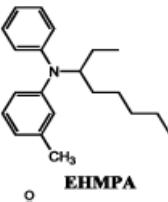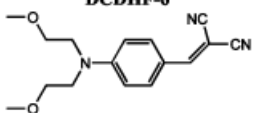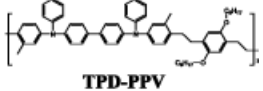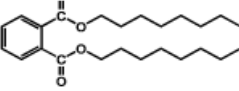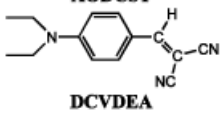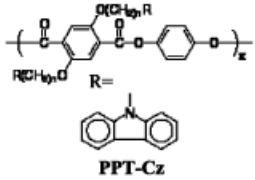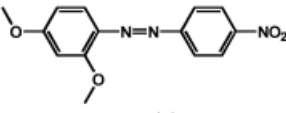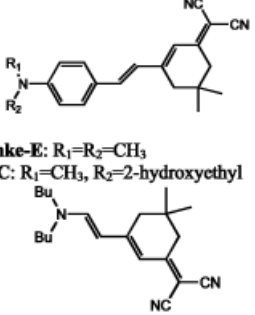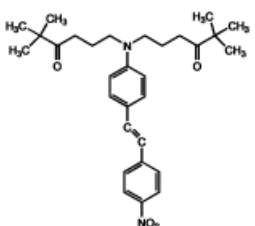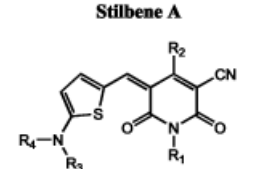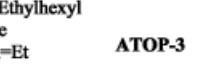
The use of plasticizer monomer species is mandatory in PVK blends due to the high value of its glass transition temperature, $T_g \approx 220°C$. Usually, like in the case of ECZ, plasticizer species lowering the value of T_g in PR blends are photoconductors themselves, in order to avoid "inert" volumes in the blends. Nevertheless, other "inert" plasticizer agents have been tested in PVK blends like, for instance, dibutylphtalate (DBP) or dibenzylphtalate (BBP); they were used only to obtain $T_g < T_{rt}$ in order to permit the orientational enhancement effect[66]. The employed sensitizer, TNF, is responsible for the formation of a CTC with PVK carbazole repetitive units; it is one of the most used sensitizers, together with TNFM and buckminsterfullerene C_{60}[72,73,74]; it is usually added in content of $\approx$ 1 wt.%.

DMNPAA content can vary in the range of $\approx$ 30 – 50 wt.% and 2BC measurements performed on blends containing 50 wt. % of DMNPAA made possible to appreciate their good PR properties[20]. On the other hand, these blends showed the drawback of recrystallization and phase segregation with obvious detrimental effects on the PR efficiency. Many other different PC polymers have been studied[67,75,76,77,78,79] for their employment as hosts in PR blends: derivatives of poly-(*p*-phenylene-vinylene) (PPV), poly-(fluorenes) (e.g. TFB), polysiloxanes containing pendant carbazole units connected with the main chain through alkyl spacers. Guest-host systems can achieve good PR properties in term of photorefractive optical gain Γ and of response times. Generally speaking, their gain Γ increases as the content of NLO species increases, and/or at the decreasing of T_g[80].

It is important to notice that all these blends suffer the yet described drawback of phase segregation and recrystallization of NLO chromophore in the host PC polymer matrix. The already recalled segregation effect is primarily due to the fact that highly polar moieties like NLO push-pull molecules are dissolved in apolar, or slightly polar polymer matrices; this results in a very poor compatibility, especially in those blends at high contents of NLO chromophore that are necessary to obtain high values of Γ. This results in a dramatic shortening of the shelf lifetime of devices based on such materials, e.g. the electrooptic cells usually employed in a 2BC experiment, therefore preventing their practical use in optical devices and applications. Some efforts have been devoted in the past with the aim to obtain stable glass phases of blends containing PVK. Several different approaches have been tested like, for instance, the employment of an eutectic mixture of isomers of the NLO chromophore[81], that actually reduces the onset of recrystallization. Unfortunately, this strategy does not eliminate this detrimental effect.

An approach that was successful in producing stable glass phases PR materials with unconditionally long shelf lifetime is the one reported some years ago by our group[71]. The higher and more diverse values of edm of indole and some of its methyl derivatives led to the prevision that polymer derivatives containing these moieties could permit a better solubilization of highly polar NLO molecules (e.g., DMNPAA). A preliminary study on the synthesis and PC properties of a series of poly-(*N*-vinylindole)-derivatives focussed the attention on two particular polymers, namely poly-(*N*-vinylindole) PVI and poly-(2,3-dimethyl-*N*-vinylindole) (PVDMI), whose photoconductivities are comparable to that of PVK[82,83,84,85]. In a comparative study[71] of DMNPAA blends with PVK, PVI, PVDMI, it was shown that PVDMI could replace PVK in blends formulation, without significant loss in PR properties, and to produce stable glass phases without hint of recrystallization for very long times, even in the case of high content of DMNPAA. In some of the studied blends recrystallization does not occur at all, their shelf lifetime becoming indefinitely long. A complete description of such indole-based materials, strongly related to the object of the present research, is given in Sect. 2.1.

Table 1.1 Chemical structures of sensitizers, photoconductors, plasticizers and NLO chromophores employed in the formulation of PR polymer composites

Photosensitizers	Polymers	Plasticizers	NLO Chromophores

1.6.2 Totally functionalized polymers

A possible method to improve the shelf lifetime of PR films and devices is to provide the total functionalization of a given polymer in order to include in it all the necessary PR functionalities. These functionalities can be present in the main chain of the macromolecule as well to be grafted on it like pendant groups. In this way NLO moieties are often covalently linked to a PC macromolecular chain. Several different examples of PR materials based on this approach are present in the literature[86,87,88,89,90,91,92].

This approach completely eliminates problems arising from phase segregation and recrystallization but it has very often the intrinsic drawback to give functionalized polymers whose glass transition temperature T_g is very high, namely $T_g > T_{rt}$ thus reducing the role that reorientational contribution could play. A way to overcome this limitation has been proposed by operating a *pre-poling* of dipolar species; samples are heated at temperatures $T > T_g$, then a poling electric field is applied until the sample has recovered room temperature in order to avoid relaxation of dipoles orientation. Apart from experimental complexity deriving from the need of such a pre-poling, nevertheless the PR optical gains obtainable with such systems are still poor and time response of materials are typically too slow. In Figure 1.9 we report some examples of fully functionalized polymers proposed for PR applications.
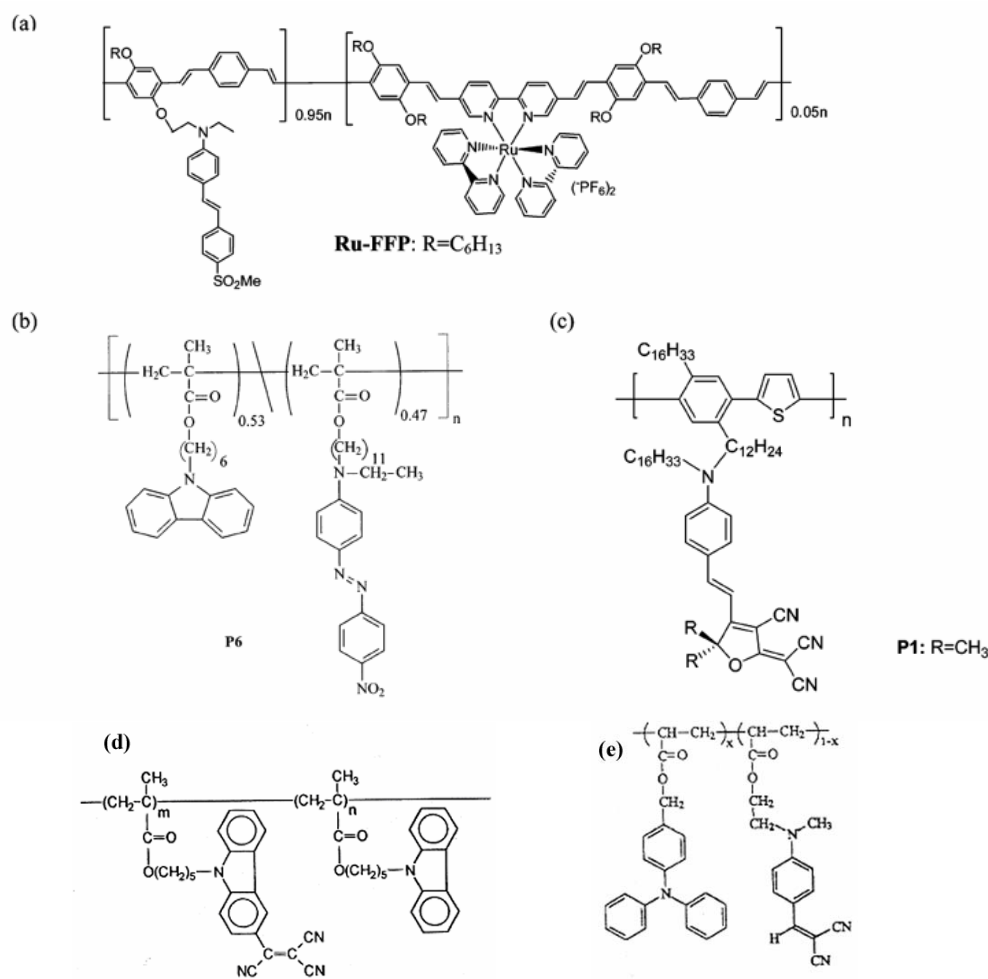
Figure 1.9 Molecular structures of some examples of fully functionalized PR polymers. a) Fully functionalized PR polymer containing ruthenium complex (Ru-FFP). b) Fully functionalized PR polymethacrylate (P6). c) Fully functionalized PR polymer containing DCDHF as NLO chromophore (P1). d) and e) poly-methacrylates functionalized with different pendant groups bearing EO and PC functionalities.

1.6.3 Low molecular weight organic glass formers (LMWG)

The doping of an organic material to achieve the necessary functionalities, as explained in previous chapters, has been obtained in polymer composite materials by using different dopant agents, each bearing one or more functionalities. One of the main reasons of using polymer matrices is to easily obtain an amorphous material, namely a blend in which molecular units can be easily reoriented. Obviously, as it has been already put in evidence while speaking about host-guest system, such systems suffer the main drawback of phase segregation and recrystallization of the different species. This is particularly true when different blend components are used only in view of their properties (e.g., good photoconductivity, high values of electrooptic parameters, and so on), but they are not properly tailored to be also chemically compatible and stable when used together. Aware of

39

these problems, some groups more recently proposed a different approach to the study of new organic PR materials. They focussed their efforts on the study of low molecular weight glass formers (LMWG) organic molecules. The goal is to obtain molecular species containing all the necessary functionalities and that are able to be stable in glass phase without recrystallizing. In this frame the tunability achievable with polymer composite materials is maybe reduced; but tunability of properties relating to PR effect can be foreseen from a synthetic point of view, that is in the design of new species and modifications of the glass former molecules. This new concept considers to compute in advance the properties (edm, α, β, ip) of target molecules together with some knowledge about relations between molecular structure and properties[33]. Good predictions can also be made, but with some not negligible exceptions as we have been able to appreciate[93], on structure-property relations concerning thermal behaviour and glass phase formation in particular. Typically, glass forming is favoured by hampering the crystallization process; very often this could be done by means of steric hindrance using, for example, large voluminous asymmetric alkyl groups (e.g. 2-ethylhexyl chain). The very large number of degrees of freedom of such alkyl chain (and so, the many different conformations it can assume) causes the reduction of probability for these molecules to approach themselves in a regular and specific asset to give rise to a crystal lattice. It is important to notice that other features like, for instance, electronic density on molecules, edm, asymmetrical substitutions, dimers formation, can equally influence electrostatic and dipolar interactions, therefore modifying phase stability.

One of the first examples of the approach based on LMWG, sometimes called *monolithic* approach (for the use of only one multifunctional component), can be found in papers referring to PR effect in functionalized carbazole trimers[94]. One of the main advantages of LMWG is the obtainable very high density of NLO species (nominally 100%); inert volumes are thus reduced. The overcoming of problems concerning mixing, phase segregation, recrystallization is also at least partially allowed. A particular care has to be devoted to glass transition temperature T_g of these materials. It must be carefully studied and tailored in order to achieve the best degree of reorientation at room temperature under the poling effect of an electric field. Glass phase stability has to be considered with equal care in order to have long shelf lifetime. It is important to notice that the birefringence contribution to PR effect could be of extraordinary importance in LMWG. Sometimes, NLO chromophores having very low values of hyperpolarizability β ($\beta \approx 0$) but very high values of edm and $\Delta\alpha$ are taken into consideration, these two latter terms being extremely more important than the first one. The selection of molecular species meeting simultaneously the many different demands is a real challenge; nevertheless several LMWG materials have been proposed

40

during the past years[13,34,37,95,96,97,98,99,100,101]. General considerations concerning the selection of molecular species can be made on the basis of the yet described parameters summarized in the Kerr Figure of merit, F_{Kerr} (s. Eq. 1.40)[33]. The PR behaviour of molecular glasses can be very good in terms of steady state performances (optical gain, diffraction efficiency) even at low values of the applied d.c. electric field. However, in several cases slow dynamics have been observed. This last feature has been related to long times of reorientation in the electric field caused by the strong dipolar interactions existing among the dipolar species. These interactions can also in some cases lead to the detrimental phenomenon of dipolar aggregation, in which dimers having $\mu = 0$ are formed by the coupling of two NLO chromophores in head-to-tail arrangement. Evidence of this dimers formation have been reported elsewhere[33,34,102]. The parameter mostly responsible for the PR behaviour in molecular glasses turned out to be the glass transition temperature T_g through the relative temperature $T_r = T_g - T_{rt}$, being T_{rt} room temperature. The relative temperature T_r strongly controls all the processes involved in PR effect, and its influence on both steady state and dynamic PR performances (s. Sect. 1.8) has been extensively studied during the last years[29,103,104,105].

1.6.4 Liquid crystals

Liquid crystals (LC) containing PR functionalities attracted much attention because of their potential capability to show PR effect at very low values of applied electric field, a feature of great interest for their applications in devices[106]. Generally speaking, indeed, LC can be easily oriented under the application of electric field of the order of few V/μm. Furthermore, they intrinsically have strong optical orientational behaviour, that is they usually behave as birefringent materials possessing very high values of first order polarizability anisotropy $\Delta\alpha$. When dealing with LC in PR materials it is possible to distinguish two different classes of materials: those employing LC as photorefractive materials themselves or in mixtures[107,108,109,110,111,112] and those consisting of polymer/LC dispersions[113,114,115,116]

Starting to consider the first class, the first ever reported case of PR effect in LCs makes reference to a well known and employed nematic LC, namely pentylcyanobiphenyl 5CB and other nematic liquid crystals[107]. They were employed together with varying amounts of photoionisable dyes, such as rhodamine R6G, Methyl Red, etc., that were responsible for charge photogeneration. It is important to remark that in these cases free charges were photogenerated ions that non-uniformly diffused in the material. The refractive index

modulation was obtained due to reorientation of the highly anisotropic nematic LC molecules in the space charge field and therefore PR effect in such materials lacks the electrooptic contribution. Subsequently, PR effect has been discovered also in chiral smectic and ferroelectric LC phases in which, at least in principle, electrooptic effect is possible[117,118,119,120]. Sometimes LCs can be doped with amounts of donor and acceptor molecules (e.g., perylene as donor, various imides as acceptor) in order to increase the efficiency of the charge photogeneration process[108]; similar improvements in PR performances have been tested using carbon nanotubes or fullerenes[121]. The best obtained results -in terms of stability, high values of PR optical gain and diffraction efficiencies obtainable at very low values of the applied electric field- turned out to be those related to materials in which LCs are used together with relatively small amounts of polymers. To this purpose, well known PC polymers have been employed as well as more unusual systems as, for instance, mixtures of nematic LCs in combination to side-chain LC polymers (SCLP), obtaining very good performances (PR optical gain up to 600 cm^{-1} for applied electric field E < 1 V/μm)[122]. Other approaches focussed on the particular behaviour of multilayer cells in which LCs were deposed over photoconductive substrates such as PR crystals or thin PC polymer films (e.g. PVK)[123].

A second class of LC having PR behaviour is that of polymer dispersed LCs (PDLCs)[106,124]. The high concentration tends to give rise to a phase separation for mixtures containing polymer and LC molecules. The phase separation leads to the formation of small LC droplets, thus producing a dispersion inside the photoconductive polymer matrix. Many different polymers have been employed as photoconductive matrix, while the molecules of LC inside the droplets can be very easily reoriented under the application of an electric field, resulting in high orientational contributions. Nevertheless PDLC materials suffer by scattering due to droplets and by very slow time response[125].

1.7 Optoelectronic applications

The many and different potential applications proposed for PR organic materials have determined the large development of this field, both in the continue search for new materials and in the ideation of new arrangements and devices based on them. The interest on PR organic materials aroused also for their easy processability, comparing to inorganic crystals. Indeed, one of the reasons of such interest derived from the possibility to have materials with good PR performance employing relatively cheap, flexible, conventional processing technologies as, for instance, injection molding. On the other hand, it is possible to "tune"

42

materials properties exploiting the huge number of functionalities that can be introduced by synthetic routes or by changes in blends composition.

Applications have been realized in various fields: image processing (optical phase conjugation, optical correlation, amplification, filtering, imaging through scattering media in the NIR, medical imaging), data storage (holography), non destructive remote testing (laser-based ultrasound sensing, LBU, dynamic holographic interferometry, DHI); applications have also been proposed for security, military, navigation[9,10,11,12,13].

The already described 2BC technique immediately suggests a first application of PR materials in the field of image amplification. Indeed it enables to transfer energy from one pump beam to a signal beam. The extent of amplification varies with 2BC gain coefficient Γ and with the interaction length in the sample L; referring to same conventions and notations used in Eqs. 1.13-17 in Sect.1.1 and assuming $I_1 / I_2 \gg 1$ (1,2 refer to pump and signal beams, respectively), a simplified expression for transmitted intensity of signal beam I_2 can be used

$$I_2 = I_{2,0} \exp(\Gamma L) \qquad . \qquad\qquad\qquad (1.50)$$

If an object is put in signal beam path, its image transmitted by a PR sample will be amplified at the expense of pump beam and can be recorded, e.g. by a common CCD camera. Image and, in general, light amplification has been realized with numerous organic PR materials at different operating wavelengths.

Optical phase conjugation (OPC)[126] is one of the most interesting and useful effects occurring in NLO materials. It has been demonstrated and extensively studied in PR organic materials. Among the several applications of OPC we recall here optical interferometry, beam cleanup, phase locking of lasers, transmission of undistorted images through atmosphere or optical fibers. A particularly important application of organic PR materials has been realized in the development of the self-pumped phase conjugator for which a material exhibiting very high 2BC gain is needed[127]. Films of polymer composites based on PVK placed between two mirrors have been successfully employed in this application[10].

By using the four wave mixing geometry (DFWM) PR materials can be employed in the development of optical correlators. The image correlation is based on the recognition of target objects through the comparison (correlation) of its image with stored images in a database. The aim is to develop exclusively optical systems for object detection and recognition. Applications have been proposed and demonstrated for optical correlation in military, security, navigation, space, aeromotive fields and many other ones can be foreseen.

Citing only some examples, retinal and fingerprints recognition, documents and credit cards security devices are some of the possible applications[128]. Organic PR polymer composites and PR nematic liquid crystals have been proposed for these applications[129,130].

Other image processing applications have been studied in PR organic materials both in DFWM and 2BC geometries as, for instance, edge enhancement (a process that, depending on relative intensities of pump and signal beams, permits to record either the image of an object or an edge enhanced one, i.e. only edges of the object are visualized)[9,12] or novelty filtering (only objects moving with a speed faster than PR response can be detected and visualized)[131].

Medical imaging diagnostic methods are nowadays widely developed exploiting X-rays, magnetic resonance, ultrasound techniques. The potential hazards for health of such techniques and their sometimes poor resolution demand for alternative techniques. One interesting chance can be offered by the good transparency of biological tissues in the near infrared region, between about 700-900 nm. Indeed, when dealing with biological tissues, transmitted optical radiation is made of several contributions due to refractive index inhomogeneities that lead to scattering. Together with ballistic light (light transmitted through the sample without experiencing scattering) there is also the so-called *snake* light (weakly scattered transmitted light and collinear to ballistic one) and the diffuse light (heavily scattered light coming from different directions at different times). Obviously diffuse light restricts the obtainable resolution, reduces signal to noise ratio, and complicates the way to extract useful information by optical transmission. PR materials have been proposed in various holographic techniques as potentially useful materials in order to record images (holograms) that allow to extract only the ballistic light from the background scattering. Some applications have been demonstrated employing PR polymer composites in a so-called Time Gated Holographic Imaging (TGHI) technique[132] using short-pulse or continuous-wave mode lasers or even laser diodes in the NIR wavelength region[133].

Holographic data storage is one of the most promising fields of application for organic PR materials. Indeed, in two-dimensional holographic storage, PR grating created by a non-uniform light intensity pattern by the interaction of two coherent laser beams (*reference* beam and *object* beam, containing the data to be stored) with a PR material, is a hologram, i.e. it contains all information about phase and intensity of object beam[134]. The hologram can be successively retrieved (object beam is created, restoring the virtual image of the object) by shining the reference beam at the proper incidence angle on the material, that is the angle used in the hologram writing process. In such a way, data can be efficiently recorded and it is possible to read them successively, as many times as the stability of hologram and material

44

can permit. It is also possible to change reference beam angle in order to store several different data pages in the same volume, in what is called angle multiplexing. Analogous multiple storage can be provided by wavelength or phase multiplexing. Obviously this capabilities extraordinarily increase the density of storable data per unit volume. An increasing interest towards PR materials has therefore aroused by the possible applications of them as highly efficient, high density holographic storage media. During the years several organic materials have been employed in such applications and their performances have been improved steadily. One of the major requirements for materials in holographic data storage is a slow dark grating decay in order to ensure long time storage of the data; this property could be achieved in materials exhibiting low dark currents, very slow chromophore relaxation, presence of deep traps. As a drawback, these properties could lead also to slow recording time (in the order of seconds) that should be avoided in real applications.

1.8 The role of T_g and the importance of intermolecular interactions in PR organic materials

The interest for a detailed calorimetric analysis of the thermal behaviour of glass phases in polymer blends has aroused in this study by two main reasons. First, there is the obvious need to properly characterize the obtained PR materials in terms of an estimate of their T_g, phase stability and shelf lifetime. Besides this reason, calorimetric analysis can be in general a powerful tool when more and more detailed insight is needed to study the nature and intensity of interactions among the different components of the blends. Indeed, it is rational to think that the highly polar moieties, constituting both polymer repetitive units and NLO species in PR blends, undergo strong dipolar interactions, that are of enormous importance in the setting of PR effect. As it has been already described in the previous sections (e.g. s. Sect.1.4, Sect. 1.6.1 and Sect. 1.6.3), some of the most important PR parameters are strongly related to T_g: extent of NLO chromophores reorientation in an applied electric field, number of *deep traps*, photoconductivity, time response, free volume available for the orientation of dipolar species. The concept of free volume is a particular important one. The free volume is associated with the space between molecules in a sample: a difference in volume for a glass and a melt could be estimated. The difference in volume between a glass and the extrapolation of the melt curve (i.e. in a volume vs. temperature graph) is called the free volume. The extent of this free volume, in which chromophores can reorient themselves under the effect of applied electric fields, is important in PR materials because of the birefringence contribution. Indeed, when dealing with PR "soft materials" $(T_g < T_{rt})$[1,2,28,80], the birefringence

contribution[27] (s. Sect. 1.4) plays a predominant role, influenced by interactions among dipolar species. The importance of T_g in PR materials has been sometimes put in evidence[29,80,135] and some considerations have been made about the role of interactions among highly dipolar species[33]. On this last feature, the already cited case (s. Sect. 1.4) of phenomena of aggregation of dipolar species in head-to-tail dimers arrangement (strong interactions) has been initially investigated[33,34,35]. Nevertheless, an investigation about the onset of supramolecular arrangements of NLO species and the role played by interactions (comprising those whose intensity could be considered weak or moderate) still lacks, particularly for PR materials. Some theoretical calculations have been accomplished on clusters of dipoles (mimicking the behaviour of NLO push-pull molecules) and evidenced rapid changes in their EO properties in dependence of interactions, mutual orientations, distances[136,137]. Interestingly, some specific arrangements (clusters) give rise to sharp enhancement of properties such as polarizability α, hyperpolarizability β, electric dipole moment μ. Figure 1.10, reported from reference[136], clearly shows the foreseen possible variations of the electrooptic parameters depending on the concentration of the NLO molecules (dipoles) and the considered typology of the dipole clusters. Similar enhancement effects (sometimes they are referred to as "cooperative" or "collaborative" effects) were also experimentally evidenced in different optical systems (e.g. TPA in organic dyes)[138]. On these bases the interest was raised about the understanding of such mechanisms and of their role in establishing the final PR behaviour of organic materials.

Several thermodynamic treatments revealed to be useful in this study in order to understand the mechanisms influencing the thermal behaviour of glass phases of miscible polymer blends; the same treatments are able to predict T_g as a function of blends composition. In the following, these treatments are summarized and employed to evidence the features that are more strictly of interest for the present study.
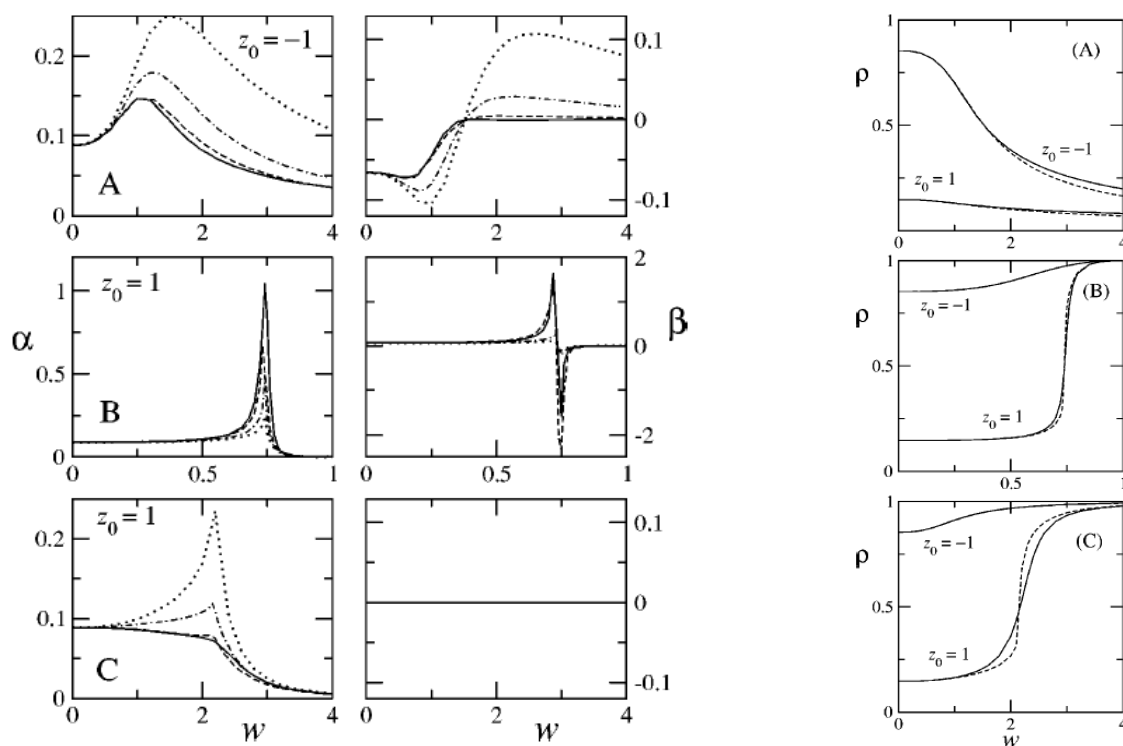
Figure 1.10 Foreseen trends of some of the electrooptic parameters for the various types of the considered dipole clusters. Dipoles are treated in a simple two-levels scheme (neutral and zwitterionic states). A is the side by side head-to-tail type, B is the linear head-to-tail type and C is the side by side head-to-head type. ρ represents the ionicity of the NLO molecule and it is proportional to the value of the edm. w is a parameter inversely proportional to the intermolecular distance. $z_0 = 1$ refers to a dipole with neutral g.s., while $z_0 = -1$ to a dipole with ionic g.s., $2z_0$ being defined as the energy gap between the two neutral and zwitterionic states[136,137].

1.8.1 Thermodynamics of miscible binary polymer blends

Starting from the basis of the general Free Volume Theory[139] -in which glass transition temperature is seen as an iso-free volume state[140], i.e. glass transition occurs at a fixed value of free volume or, equivalently, all the compounds have exactly the same value of free volume at T_g- many different models have been developed in the past, dealing with the thermal behaviour of both polymer/polymer (some of this models apply also for copolymers) and polymer/monomer miscible binary blends. Binary blends of amorphous polymers are said to be homogeneous when they have a single glass transition temperature over the full range of composition; i.e. they are miscible at all relative concentrations and a unique glass phase is formed. On the contrary, immiscible blends -even for a limited range of composition- tend to form two different phases thus having two different glass transition temperatures, corresponding to those of the pure components. In practice, the polymer blends miscibility is often studied by means of the measured T_g values. For a homogeneous system, the trend of T_g

47

as a function of blend composition has in general a continuous monotonous behaviour, each blend having a T_g value that is intermediate between the pure components T_g values. Many different models have been proposed with the aim to predict the T_g of a miscible blend from the knowledge of some pure components properties. The simplest model is based on an additivity rule, i.e. a simple weighted average, which predict a linear behaviour for T_g vs. composition curves[140]

$$T_g = w_1 T_{g1} + w_2 T_{g2} \qquad (1.51)$$

being T_g the glass transition temperature of the blend, T_{g1}, T_{g2} the pure components glass transition temperatures and w_1, w_2 are the respective weight fractions. Experimental data for a variety of binary miscible blends have shown both positive and negative deviations from this simple prediction, s. Figure 1.11. Some "S-shaped" curves have been found as well. Positive deviations are involved in strong specific intermolecular interactions in blends like, for instance, those related to hydrogen bonding, formation of electron donor-acceptor complexes, transition metal complexes, ionic interactions[141,142,143,144]. On the other hand, very weak or weak interactions are known to be related to negative deviations of the trends from the additivity rule. The difference between experimental T_g values from theoretically predicted ones is often considered as a semi-quantitative estimate of the force and number of the interactions between the components of the blend [144,145,146,147,148,149,150].
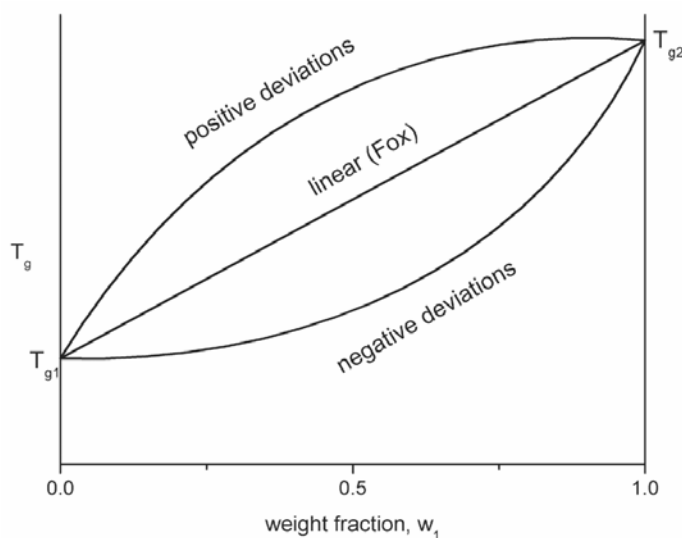

Figure 1.11 Trends of T_g for binary miscible blends. Linear trend by a simple additivity rule (Fox[140], s. Eq. (1.51)), positive and negative deviations.

Many studies have been attempted in order to correctly predict such deviations from linearity; some of them predict the deviations by classic thermodynamical arguments trying to explain the role of interactions; some others only get some useful empirical rule[151] in order to fit the data by using adjustable parameters whose physical meaning still lacks.

A first attempt developed by Gordon and Taylor[152] resulted in the well known and widely used Gordon-Taylor (GT) equation:

$$T_g = (w_1 T_{g1} + K w_2 T_{g2})/(w_1 + K w_2) \qquad (1.52)$$

being $T_{g2} > T_{g1}$. The K parameter of GT equation was considered, at the beginning, as a pure fitting parameter; subsequently, several efforts have been devoted to extract some general rule starting from different thermodynamic considerations; T_g vs. composition relations based on additivity of the specific volumes[152] or on continuity at T_g of thermodynamic functions[153] resulted in GT-like equations in which different meanings are attributed to K parameter, this latter becoming specific for each model. Models with two different K_1 and K_2 parameters have also been proposed[154]. Various approaches led to different definitions of K parameter; as an example, $K = (\rho_1 \Delta \alpha_2)/(\rho_2 \Delta \alpha_1)$ for additivity of specific volumes or continuity of the thermodynamic volume functions at T_g; $K = \Delta C_{p2} / \Delta C_{p1}$ for continuity of enthalpy at T_g. This last expression keeps its validity also for continuity of entropy, even if it appears in a logarithmic form of (1.52). In these relations, ρ_i are the densities, $\Delta \alpha_i$ and ΔC_{pi} are the increment of the expansion coefficients α and of the heat capacities C_p at T_g, respectively.

Couchman derived very useful equations by means of classic thermodynamics considerations; this treatment together with its subsequent developments, turned out to be particularly useful in order to extract some useful and meaningful quantities from T_g vs. composition curves. Couchman, in the original treatment of his theory[153,155,156,157,158] deals with "regular" solutions, i.e. those in which specific interactions are absent. A second initial simplifying assumption was to consider that the glass phase entropy of mixing might be equal to that of an ideal solution, that is mixing is a random process and it is only pushed by the achievement of the maximum disorder. Thus, mixing entropy for a given composition is simply combinatorial and it is a continuous function at T_g. Such a situation, in practice, is only occurring when strong and/or specific interactions are absent ("regular" solutions) and only dispersion forces are active among non-polar components of the blend. The increment of entropy due to mixing, ΔS_m, is therefore approximately equal to ideal (combinatorial) mixing entropy, which is phase-independent, i.e. it depends only on composition (and not on the

physical state of the blend, glass or liquid phase). For this reason, at T_g, ΔS_m is a continuous function, that is, for $T = T_g$

$$\Delta S^l_m = \Delta S^g_m \qquad . \qquad (1.53)$$

The superscripts l,g refer to liquid and glass phase, respectively. This last relationship could be seen as the condition of absence of interactions in Couchman model. If S^l e S^g are the entropy of liquid and glass phase, respectively (expressed in J·mol^{-1}·K^{-1}), for a polymer binary blend having a weight fraction w_1 of component 1, at $T = T_g$ the following relation holds

$$S^l (T_g, w_1) = S^g (T_g, w_1) \qquad , \qquad (1.54)$$

and the entropy of each phase can be written:

$$S^l (T, w_1) = w_1 S_1^l(T) + w_2 S_2^l(T) + \Delta S^l_m \qquad (1.55)$$

$$S^g (T, w_1) = w_1 S_1^g(T) + w_2 S_2^g(T) + \Delta S^g_m \qquad . \qquad (1.56)$$

From some integral relations derived from Eqs. (1.55) and (1.56)[148] and assuming various different functional dependences over T of the specific heat, $\Delta C_{pi}(T)$, various formulations of the Couchman-Karasz equation are obtained, predicting T_g values of the binary blends. The most known and used formulation assumes the specific heat to be constant over T, $\Delta C_{pi} = \Delta C_{pi}(T_{gi})$, and it is written as

$$\ln T_g = (w_1 \Delta C_{p1} \ln T_{g1} + w_2 \Delta C_{p2} \ln T_{g2}) / (w_1 \Delta C_{p1} + w_2 \Delta C_{p2}) \qquad . \qquad (1.57)$$

Another, more realistic, functional dependence for the specific heat change of pure components on temperature have been proposed, $\Delta C_{pi} = const./T = \Delta C_{pi}(T_{gi})T_{gi}/T_g$; using this expression one obtains an alternative equation:

$$T_g = (w_1 \Delta C_{p1} T_{g1} + w_2 \Delta C_{p2} T_{g2}) / (w_1 \Delta C_{p1} + w_2 \Delta C_{p2}) \qquad . \qquad (1.58)$$

Eqs. (1.57) and (1.58) are currently called Couchman-Karasz equations. Both equations improve the fitting quality of experimental data in many cases by predicting negative deviations from the additivity rule; nevertheless, they are not able to satisfactorily

50

predict the actual trends when some specific interactions are present. This remark forces to relax the hypothesis (1.53) of the continuity of ΔS_m at T_g. In real systems, indeed, non-weak interactions are often present and interactions existing in blends differ in general from those existing in pure components. The number and strength of such interactions are obviously temperature dependent; moreover, they can't be considered as independent of the physical state of the blend. It was Couchman himself that extended his theory starting from the forsaking of (1.53) hypothesis. In some following papers[158,159] he tried to take into consideration these important interactions and the contributions coming from the non-random mixing. He therefore developed a theory based on a twofold treatment: from one side based on entropic considerations, and from another side on enthalpic ones.

These two (entropic and enthalpic) treatments are not fully alternative themselves; they must be considered as complementary and both adopted in order to appreciate the role played by specific interactions in determining the peculiar behaviour of non regular and non-athermal blends (athermal blends are those ideal blends for which $\Delta H^l_m = \Delta H^g_m$, that expresses the absence of interactions in the enthalpic treatment).

Assuming the existence of specific interactions in blends, and therefore considering (1.53) as a false condition, some additional terms must be introduced in the simple equations (1.57) and (1.58). Some authors have tried to discuss the T_g vs. composition curves on the basis of these considerations, further extending the resulting equations to more and more general cases of various kinds of interactions. The aim has also been to obtain some useful parameters which give a quantitative measure of such interactions. In particular, Righetti et al.[148,149,150], dealing with both enthalpic and entropic treatments reported some useful equations including the effects of specific interactions. The parameters employed in the analytical expressions as a measure of the effect of specific interactions are the so-called "in excess" quantities described by the differences $(\Delta S^l_m - \Delta S^g_m)$ and $(\Delta H^l_m - \Delta H^g_m)$. They appear in the following two expressions derived for the entropic and enthalpic approaches, respectively[149]:

$$T_g = (w_1 \Delta Cp_1 T_{g1} + w_2 \Delta Cp_2 T_{g2}) \, / \, (w_1 \Delta Cp_1 + w_2 \Delta Cp_2 + (\Delta S^l_m - \Delta S^g_m)) \qquad (1.59)$$

$$\ln T_g = (w_1 \Delta Cp_1 T_{g1} \ln T_{g1} + w_2 \Delta Cp_2 T_{g2} \ln T_{g2} - (\Delta H^l_m - \Delta H^g_m)) \, / \, (w_1 \Delta Cp_1 T_{g1} + w_2 \Delta Cp_2 T_{g2}) \,.$$
$$(1.60)$$

It is therefore possible, through Eqs. (1.59) and (1.60), to obtain the values of the two "in excess" quantities $(\Delta S^l_m - \Delta S^g_m)$ and $(\Delta H^l_m - \Delta H^g_m)$ from the experimental T_g data of the studied blends. Such quantities have been put in relationship with the entity of interactions in

various kinds of polymer blends and their validity has been proved in systems in which strong or weak interactions exist[150,160]. In practice, one keeps the product w_1w_2 as the independent variable; the new quantities Q_s, Q_h, are defined as

$$(\Delta S^l_m - \Delta S^g_m) = Q_s\, w_1w_2 \qquad (1.61)$$

$$(\Delta H^l_m - \Delta H^g_m) = Q_h\, w_1w_2 \qquad , \qquad (1.62)$$

whose physical meaning is related to the strength of the intermolecular interactions[159]. Q_s and Q_h are then obtained from experimental T_g data and using Eqs. (1.59) and (1.60). The comparison of such calculated values with analogous ones reported for various systems in the literature can be a proper way in order to recognize and describe interactions in polymer blends.

Concluding the overview about the different theoretical approaches to this theme, it is important to cite the one by Lu and Weiss[143,144]. They extended Couchman's theory[158] including a term involving the Flory-Huggins parameter χ (a measure of the intermolecular interactions in binary systems)[161] which, in turn, is related to other thermodynamical quantities such as ΔH_m defined as the enthalpy of mixing; χ can be calculated from other independent measurements, like, for instance, from melting point depression data. In this way, when χ is known from other measurements, Lu and Weiss theory can be applied to predict T_g; alternatively, when T_g data are available as a function of composition, the theory can be used to calculate χ. Because of the important role played by enthalpic interactions in determining the phase behaviour of polymer blends, and considering the relation existing between enthalpy of mixing ΔH_m and χ[144,161], i.e.

$$\Delta H_m\,(T) = \chi\, RT\, w_1w_2 \qquad , \qquad (1.63)$$

R being the gas universal constant, Lu and Weiss adopted Couchman's enthalpic approach to start the development of their own theory. Finally, the general equation proposed by Lu and Weiss is the following

$$T_g = [(w_1T_{g1} + Kw_2T_{g2}) / (w_1 + Kw_2)] + Aw_1w_2 / [(w_1 + Kw_2)(w_1 + bw_2)(w_1 + cw_2)^2] \quad (1.64)$$

with

$$A = -\chi\, R(T_{g1} - T_{g2})c / M_1\Delta Cp_1 \qquad (1.65)$$

$$K = (\Delta Cp_2 - w_1 \delta C_p^l) / (\Delta Cp_1 - w_2 \delta C_p^g) \qquad (1.66)$$

$$c = \rho_1 / \rho_2$$

$$b = M_2 / M_1 \quad ,$$

ρ_i being the density of i component, M_i being the molar mass per chain segment (repetitive unit) for i component; δC_p is the specific heat change due to the mixing process which is usually negative for a miscible blend, and it is defined by an approximate law for the specific heat of a blend Cp_m (m, stands for mixing) as $Cp_m = x_1 Cp_1 + x_2 Cp_2 + x_1 x_2 \delta C_p$ [162]. Through Eq. (1.64), knowing T_g experimental values for the blend, it is possible to calculate the Flory-Huggins parameter χ. Authors consider three different cases in which (1.64) assumes simplified forms, describing different kinds of interactions: a first case of very weak or no specific interactions, a second one of relatively weak specific interactions and a third one relating to strong specific interactions.

In the first case (no specific interactions), Eq. (1.64) reduces to Couchman's equation in the case of random mixing (a GT equation, s. (1.52) in which $K = \Delta Cp_2 / \Delta Cp_1$); in this frame negative deviations are predicted from the linear trend (s. Figure 1.11) and $\chi = 0$, obviously.

When dealing with second (reatively weak interactions) and third (strong interactions) cases, another simplifying assumption is helpful in order to visualize the prediction of (1.64). The parameter K, Eq. (1.66), is indeed a complicate function, containing various quantities; it can be re-written down in an alternative way as:

$$K = (\Delta Cp_2 / \Delta Cp_1)(1 + w_1 \delta C_p^l / \Delta Cp_2 + w_1 \delta C_p^g / \Delta Cp_1 \qquad , \qquad (1.67)$$

being δC_p always very small (and usually negative) with respect of ΔCp_i, it could be neglected in a first approximation. In such way (1.67) reduces again to the usual $K = \Delta Cp_2 / \Delta Cp_1$ (Couchman's theory). With this minor simplification Eq. (1.64) predicts negative deviations from the linear trend of T_g vs. composition in the second case (relatively weak interactions); Flory-Huggins parameter χ results to be $\chi < 0$ with relatively small values ($0 < \chi < -3$ or -4). On the contrary, positive deviations are predicted for blends in which strong specific interactions exist (the third case; e.g. hydrogen bonding, complex formation) with values of $\chi \ll 0$. Generally speaking, Eq. (1.64) proposed by Lu and Weiss satisfactorily fits T_g data of various systems and represents a good method to inspect interactions in polymer blends.

2 Indole-based PR materials

2.1 Why the indole group in polymers for PR materials

The present research has focussed on PR materials based on indole and indolyl derivatives. Some researchers[82,83,84,85] carried out studies in the group active at the Department of Chemistry and Industrial Chemistry of the University of Pisa led by Prof. Colligiani, concerning the synthesis and the characterization of polymer derivatives of indole and their detailed study as photoconductive materials. In particular, various methyl and dimethyl indolyl vinyl polymers were tested together with some polysiloxane derivatives.
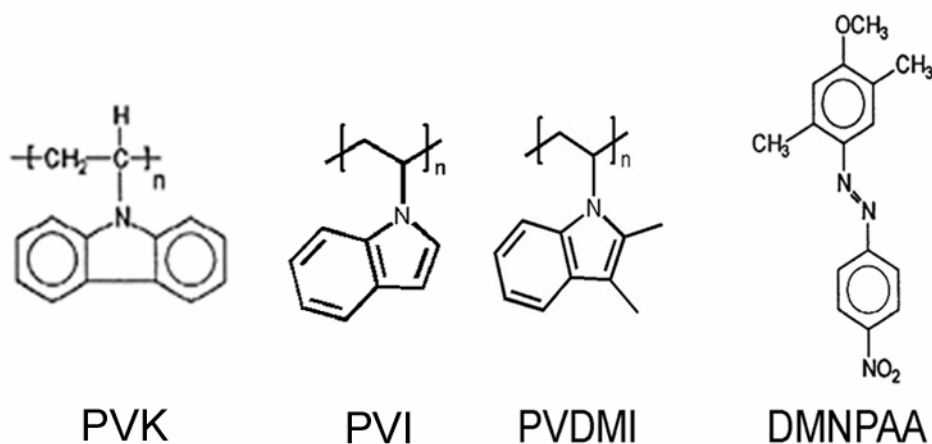
Figure 2.1 Molecular structures of PVK, indolyl polymers PVI and PVDMI, NLO chromophore DMNPAA employed in some previous researches (s. text).

In the starting idea, the indole group was considered as a valid substitute of the carbazole moiety. Indeed, poly-(N-vinylcarbazole) (PVK) has been extensively studied and employed in PC and PR materials (s. Sect. 1.6.1) due to its excellent photoconductivity properties, as well as other carbazole-containing polymers. Nevertheless, as it has been briefly mentioned in the previous sections, in spite of the good results[20] carbazole-based materials suffer from some drawbacks that can limit their technical applications. These drawbacks concern the very high glass transition temperature T_g of the related polymers, the poor availability on the chemical market of properly substituted derivatives and the carbazole high molecular symmetry that gives it a relatively small edm μ. The high $T_g \approx 220°C$ of PVK demands the use of large quantities of plasticizers in order to obtain materials having sufficiently low T_g values. The low value of T_g is very important to allow film formation without the need of using very high temperatures on samples. Large quantities of plasticizers can negatively affect the electrooptic

behaviour of the resulting materials (reducing active species concentration) or cause poor control due to mechanism of percolation affecting the overall photoconductivity (s. Sect. 1.5).

The influence of the substituents introduced on the carbazole ring was expected to be important both on the ionization potential ip and the value of edm, μ. As it has been described in Sect. 1.5, these latter parameters play a fundamental role in determining the photoconductive response. Unfortunately, only very few carbazole derivatives are available in the chemical market, and they are often expensive and difficult to synthesize or modify. The poor availability of the carbazole group to be modified in its electronic and morphological characteristics constitutes a factor limiting the potential tunability of materials. Moreover, most PR materials adopt the guest/host approach described in Sect. 1.6.1; they are indeed mixtures of several low and high molecular weight components whose reciprocal compatibility must be properly assured in order to avoid problems relating to phase segregation. We recall here the already described example of blends containing DMNPAA and PVK (s. Sect. 1.6.1). Such aspects influence dramatically the shelf lifetime of the electrooptic cells. The compatibility among different components in a blend is related to their respective edm and to the free volume available. On the basis of these arguments the indole moiety and a series of its available methyl derivatives were taken into consideration[83]. Indeed, many and interesting indole derivatives can be purchased on the chemical market. The electronic nature of the different available substituents on the indole ring such as, for instance, -CH$_3$, -CHO, -OH, -NH2, -NO2, -CN, -OCH$_3$ and many others, can determine, together with the resulting edm values, the electron donor behaviour that is typical of the indolyl moiety.

The values of edm μ, together with those of ionization potential ip, were computed[82,85] for the *N*-ethyl derivatives of each molecule of the studied series of different indolyl derivatives; *N*-ethyl derivatives were taken as model compounds of the corresponding poly-*N*-vinyl derivatives. Some of the values of μ and ip, computed using a semi-empirical MOPAC-7 program in that research[85], are listed in Table 2.1 together with those relative to carbazole K and to *N*-ethylcarbazole NEK, for comparison purpose. Very few edm and ip values can be found in the literature[163,164,165] and often the experimental ones are strongly dependent on the employed experimental method and material. Nevertheless, calculated values were sufficiently well consistent with the experimental ones; experimental ip values of indole and carbazole, for instance, have been reported to amount to 7.76 eV and 7.57 eV, respectively, to be compared with the computed 7.85 eV and 7.65 eV values, as displayed in Table 2.1.

Table 2.1 Computed electric dipole moments (edm) and ionization potentials (ip) for some indole and carbazole derivatives[85]. *N*-ethyl derivatives are taken as model compounds in order to evaluate the values for the corresponding poly-(*N*-vinyl-derivative). I = indole, K = carbazole, M = methyl, E = ethyl, N = substituted heterocyclic nitrogen, See *Glossary*.

Compound	edm (Debye)	ip (eV)
I	2.09	7.85
NEI	2.49	8.22
NE2MI	2.57	8.17
NE3MI	2.34	8.07
NE23MI	2.47	8.02
NE4MI	2.31	8.14
NE5MI	2.34	8.15
NE6MI	2.40	8.16
NE7MI	2.64	8.10
K	1.59	7.65
NEK	1.65	7.65

Poly-(2,3-dimethyl-1-vinylindole) (PVDMI) was chosen as the indolyl derivative characterized by the lowest ionization potential ip = 8.02 eV, as computed for its model compound NE23MI (Table 2.1). This value of ip, even if higher than that of PVK, ip = 7.65 eV, gave PVDMI photoconductivity characteristics just slightly lower than PVK; therefore, it was assumed as a promising behaviour for significant photorefractivity. On the other hand, the evaluated values of the edm μ of all indolyl derivatives (mean value, μ = 2.45 D) were higher than that of the carbazolyl group, μ = 1.65 D, thus predicting a possible better electrostatic compatibility between the components of PR blends when a chromophore having an high value of μ is employed.

Moreover, all poly-(*N*-vinylindoles) (PVIs) were characterized by T_g values quite lower than that of PVK[83]. Giving some examples, poly-(*N*-vinylindole) PVI has a value of T_g = 172.8°C while PVDMI has a value of T_g = 181°C. Lower T_g values were desirable in order to reduce the concentration of employed plasticizer in PC or PR blends.

On the basis of these considerations, PVI series polymers were tested as PC materials in blends with a 1 wt.% TNFM sensitizer (in order to allow CTC formation) and with various

concentrations of plasticizers; PC measurements were constantly compared with those of similar PVK-based blends[84]. The experimental results could be explained on the basis of the calculated ip and edm values. The value of ip being lower for carbazole than for indole group, the lower photoconductivity of all the PVIs with respect to PVK could be in part explained. Interestingly, the PVDMI improved photoconductivity was also rationalized as a consequence of the presence of two methyl groups in positions 2 and 3 of the indole ring. Indeed, their hyperconjugative effect increases the electronic density on the rings of the heteroaromatic moiety, thus lowering the ip value with respect to that of the unsubstituted or monosubstituted indole. This brings to an increase of photoconductivity up to values just slightly lower or comparable to those of PVK. These considerations were also sustained by measured spectral features of the CTC bands appearing in the UV-Vis absorption spectra of different polymers complexed with the sensitizer TNFM[84]. On the other hand, the larger edm values of the indole moiety and of its methyl derivatives with respect to that of carbazole could also contribute to the lower photoconductivity of the former polymers. Species having high values of edm are known to have lower photoconductivity because of the effect that edm has on the hopping mechanism between active sites[60] (s. Sect. 1.5). As concerns the other parameter that could directly affect photoconductivity, that is the distance between active hopping sites , it should be very similar in PVK and in PVIs due to the common backbone structure and the same length of the direct C–N linkage between the backbone and the side chain moieties (s. Figure 2.1). Therefore it was not considered responsible for the found differences in PC.

All measurements confirmed with clear evidence that the general behaviour of PVDMI is more similar to that of PVK than that of PVI and its methyl derivatives. The similarity of behaviour of PVK and PVDMI as concerns photoconductivity made the latter to become the candidate for a test as PR material, when using it in blend with DMNPAA (s. Figure 2.1), a NLO chromophore extensively employed in PR materials formulation.

A comparative study of both the time stability (shelf lifetime of the electrooptic cells) and PR extent of similar blends containing DMNPAA, in PVK and PVDMI, respectively, was made[71] by means of a 2BC experiment. The results clearly showed that DMNPAA was more compatible with PVDMI than with PVK[71]. The obtained glass films of PVDMI-based blends were characterized by abundantly longer shelf lifetimes; in some cases, depending on composition, PVDMI based cells remained indefinitely stable and transparent.. So, it has been confirmed that DMNPAA with a value of edm $\mu = 6.43$ D (as computed by the MOPAC7 software, s. Table 4.1), is more compatible with indole-based polymers (average edm value $\mu = 2.45$ D) rather than with carbazole-based ones (edm value $\mu = 1.65$ D). Other factors such

as the free volume (s. Sect. 1.8) could also be more favourable to accommodate DMNPAA due to the intrinsically asymmetric nature of the indolyl structure.

On the other hand, PVDMI-based PR blends showed values of the PR optical gain Γ_2 just a little lower than those of similar PVK blends[71]. The possibility that an indolyl-based polymer can replace the traditionally used PVK in building up PR materials was therefore successfully verified.

The results of this research were carefully discussed and the importance of glass transition temperature T_g in determining the PC and PR behaviour of blends as well as their time stability, emerged as one of the most important factors. Indeed, when dealing with PR "soft materials", that is blends having T_g values lower than room temperature $T_{rt} = 22.0°C$[1,2,28,80], the birefringence contribution[27] (s. Sect. 1.4) plays a predominant role. The molecular reorientation process in the applied electric field is controlled by the free volume available for the dipolar species to be oriented. The value of the free volume magnitude is related to T_g. In the cited works the role of T_g, and hence of $T_r = T_g - T_{rt}$, has been carefully evaluated. A strong correlation with T_r for PC and PR data of the blends has been clearly put in evidence, confirming some observations previously made for other systems[29,80,135].

Another important result was to put in evidence the role played by electrostatic interactions among the NLO molecules. In these polarized and polarizable organic molecules, a distinct separation of negative and positive charges on their linear geometry gives rise to their very high value of edm (s. *push-pull* molecules, Sect. 1.3). Because of this high edm values, homologous interactions can often prevail on similar interactions acting between the chromophores and the repetitive units of the polymer, thus leading to phase segregation and recrystallization of NLO species; this is the case for PVK-DMNPAA blends. On the contrary, PVDMI (with its high edm associated to dimethylindole pendant groups) revealed itself as a favourable polymer matrix in which to dissolve a NLO chromophore, as a consequence of the stronger interactions with the polymer matrix. These experimental evidences led to the conclusion that, in order to fully exploit the potential PR behaviour of a material, a careful tailoring of both polymer and NLO-chromophore properties is necessary. Moreover, interactions among different species must be taken into consideration to think out a proper combination of a chromophore and of a polymer matrix in the planning of a supramolecular arrangement.

2.2 Aim of the research

The excellent results obtained in the described studies led to the conclusion that PVK can be replaced by indolyl polymers in the formulation of PR materials. A further and maybe more important conclusion suggested that a great attention must be given to the interactions existing among the various components of the PR blends. Compatibility is indeed not only a mandatory demand for the realization of long-lasting, reliable materials to be used in practical applications, but it can also actually affect the extent of PR responses. On these bases a different original approach has been thought out aiming at the realization of indole-based PR materials in which compatibility between the polymer substrate and the NLO molecules could be optimized. Making the hypothesis that the presence of equal chemical groups in the components of the blends had to increase the compatibility, the interest was aroused on the design of novel indolyl NLO chromophores; their use in combination with indolyl polymers could give real supramolecular systems in which the intermolecular interactions can overcome the interactions among the monomers. Moreover, although monolithic systems (s. Sect. 1.6.3) have been less extensively studied, in the last years some low molecular weight glass forming moieties have been tested as PR materials and they gave good results as, for instance, with a series of merocyanine dyes[33,34,97]. The original object of this research has been first of all the design and selection of various LMWG species that could be supposed to behave as multifunctional PR materials, that is molecules having all the necessary properties (CTC formation capability, photoconductivity, NLO properties, glass forming ability) for PR effect (s. Sect. 1.1). The introduction on a similar indole-based molecular skeleton of various functional groups with different electronic or steric effects was decided in order to study their influence on PR responses as well as on glass phase formation and stability. We selected a class of *push-pull* molecules (s. Sect. 1.3) to be synthesized and studied also on the basis of theoretical calculations of the relevant parameters (ip, edm, polarizability α, first hyperpolarizability β, F^{Kerr}; s. Eq. (1.40), Sect. 1.4); such calculations will be presented in Sect. 4.1. The series comprised five different species, namely NPEMI, NPEMI-A, NPEMI-E, MeO-NPEI-E, NO_2-NPEI-E (s. *Glossary* and Sect. 3.3). A complete characterization of the series has been planned as concerns their optical, spectroscopic, calorimetric behaviour. Their CTC formation capability with TNFM has also been verified by means of UV-vis absorption spectroscopy. Glass phase formation and stability have been studied for the 5 species of the series by DSC measurements. A polymer counterpart in which to dissolve the novel NLO-chromophores was also selected in order to study their compatibility in a polymer matrix and to get more insight in the intermolecular interactions occurring in PR blends. For the reasons

60

yet described in the preceding sections, the polymer of choice has been PVDMI. The aim was to prepare and study, both from an electrooptic point of view (PC and PR behaviours) and from a calorimetric point of view, blends of this polymer with high content of the novel NLO species, i. e. for compositions ranging from 50 to 100 wt.% in NLO moiety. It is important to remark here the originality of this approach. Monolithic LMWG indeed have been studied up to now chiefly as neat materials; on the other hand, blends of PC polymers with NLO chromophores have been composed with concentration of the latter not higher than 50 wt.% due to the already described drawbacks related to poor compatibility. The novel approach could permit to study a not yet explored concentration range in which, being NLO species the main component, polymer counterpart is no more forming a matrix in which the NLO monomer is dispersed; polymer chains more likely could be visualized as "spacers" between NLO active molecules. The high content of NLO chromophore could permit the achievement of very high values of the PR optical gain Γ. A particular behaviour could be expected both for PC and PR in such materials. Indeed, comparing the results obtained for the neat LMWG material (100 wt.% of NLO species) with those for increasing content of polymer PVDMI, it could be possible to follow and study the influence on the electrooptical behaviour of the interactions between different components of the blends. A careful calorimetric analysis of PR blends, on the whole concentration range, has been accomplished in order to put in evidence the onset and to evaluate the extent of the intermolecular interactions. The obtained results have been investigated at the light of many theoretical treatments in order to extract useful thermodynamical parameters concerning interactions. The joint analysis of the obtained results for PC, PR and DSC measurements has been necessary in order to rationalize the obtained data by taking into account collaborative phenomena due to particular supramolecular arrangements of the active species in the materials. This approach revealed itself as particularly useful because of the complexity of effects occurring simultaneously and often influencing themselves reciprocally. Finally, Spectroscopic Ellipsometry technique has been employed for NPEMI-E based PR blends in order to get more insight in the refractive index variation confirming the chromophore reorientation in an electric field.

3 Materials and Methods

3.1 Reagents and solvents

Diethyl ether (Carlo Erba RPE, 99,8%): the commercial solvent has been purified at reflux and stored over $LiAlH_4$ under inert Ar atmosphere.

Ethanol absolute (Carlo Erba RPE, 99,8%): the commercial solvent has been employed without further purification.

Toluene (Baker, >99,5 %): the commercial solvent has been dried over Na, distilled and stored under inert atmosphere of Ar.

Tetrahydrofuran (THF) (Baker, >99%): the commercial solvent has been dried over Na and $LiAlH_4$, distilled and stored under inert atmosphere of Ar.

n-Hexane (Carlo Erba, >95%): the commercial solvent has been employed without further purification.

Chloroform (Carlo Erba RPE, 99%): the commercial solvent has been employed without further purification.

Dichloromethane (Carlo Erba RS, 99,8%): the commercial solvent has been employed without further purification.

Piperidine (Aldrich, 99%): the commercial reagent has been distilled under inert Ar atmosphere (b.p. 106°C at 760 mmHg) and stored under inert Ar atmosphere at T = - 20°C.

Potassium *ter*-Butoxide (Aldrich, 95%): the commercial reagent has been dried at T = 130° C under reduced pressure for eight hours.

2,3-Dimethylindole (Aldrich, > 97%): the commercial reagent has been employed without further purification.

2-Methylindole-3-carboxaldehyde (Aldrich, 97%): the commercial reagent has been employed without further purification.

5-methoxyindole-3-carboxaldehyde (Aldrich, 99%): the commercial reagent has been employed without further purification.

5-nitroindole-3-carboxaldehyde (SynChem, 97%): the commercial reagent has been employed without further purification.

4-Nitrophenylacetic acid (Acros, 99%): the commercial reagent has been employed without further purification.

18–Crown-6 Ether (Aldrich, 99%): the commercial reagent has been employed without further purification.

3-Chloropropene (allyl chloride) (Fluka, 99%): the commercial reagent has been distilled under inert Ar atmosphere (b.p. 44°C at 760 mmHg) and stored under Ar at T = -20°C.

1-Bromine-2-ethylhexane (2-ethylhexylbromide) (Aldrich, 95%): the commercial reagent has been distilled under inert Ar atmosphere (b.p. 76°C at 760 mmHg) and stored under Ar at T = -20°C over molecular sieves (zeolites 4-A).

2,4,7-Trinitrofluorenylidenemalononitrile (TNFM) (Acros, 98%): the commercial reagent has been employed without further purification.

Boron trifluoride diethyl etherate (BF$_3$.Et$_2$O): (Aldrich, 97%) the commercial reagent has been employed without further purification.

3.2 Methods and instrumentation for characterization

Nuclear magnetic resonance spectroscopy (^{1}H, ^{13}C NMR)

NMR spectra have been recorded with a Varian Gemini 200 spectrometer operating at 200 MHz for ^{1}H and 50,3 MHz for ^{13}C. All the spectra have been recorded at room temperature on solutions of samples in CDCl$_3$ or DMSO-d_6. Chemical shifts are reported in ppm units.

Infrared absorption spectroscopy (FT-IR)

FT-IR spectra have been recorded with a Perkin-Elmer 1600 spectrometer, controlled by a PC. Spectral data have been treated with a IR Data Manager Perkin Elmer software. Spectra of solid products have been performed over pellets of powdered samples dispersed in dry KBr powder. When treating liquid or glass forming products, spectra were recorded over a thin film of sample deposed by evaporation of a chloroform or dichloromethane solution over the polished surface of a KBr window.

Ultraviolet-visible absorption spectroscopy (UV-Vis)

UV-Vis spectra were recorded with a Jasco Uvidec 510 spectrophotometer, on quartz cuvettes 1 cm large, containing sample solutions in dichloromethane (ACS spectrophotometric grade, $\geq$ 99.5%, Aldrich). Solutions of pure samples for characterization had concentrations c $\approx$ 6·10^{-5} M. UV-Vis spectra were recorded also for solutions of mixtures 1/1 (mol/mol) of NLO Chromophore/TNFM for the chromophores NPEMI, NPEMI-E, NPEMI-A, MeO-NPEI-E, NO$_2$-NPEI-E, in order to study the CTC formation with TNFM. In this latter case, very concentrated dichloromethane solutions were employed, i.e. c $\approx$ 10^{-2} M, after 1 hour long stirring of the prepared solutions. All the spectra were recorded over the spectral range 250 < λ < 900 nm. Spectra deconvolutions and spectral data were obtained with the aid of the Origin 7.0 software (OriginLab Corp.).

3.3 Syntheses

3.3.1 Synthesis of 3-[2-(4-nitrophenyl)ethenyl]-2-methylindole (NPEMI)

Under Ar atmosphere, 16,00 g (0,100 mol) of 2-methylindole-3-carboxaldehyde (ALD) and 19,65 g (0,108 mol) of 4-nitrophenylacetic acid, were dissolved in 360 ml of absolute ethanol in a 1l three-necks flask. The solution was stirred for 30 min at T=60°C. During this time the reaction mixture turned its colour from yellow to brown.

Constantly under Ar flux and stirring, a solution of 20 ml (0,202 mol) of piperidine in 30 ml of absolute ethanol was added to the reaction mixture with a dropping funnel while the temperature was raised to T = 90°C. The colour turned red. The progress of the reaction was followed by FT-IR spectroscopy until the aldehydic and carboxylic C=O stretching bands disappeared from the spectra of periodic samples of the reaction mixture. The reaction was stopped after 40 hours. The crude solid product, a deep red powder, was recovered by evaporation of the solvent under reduced pressure, washing with water and drying under high vacuum. The product was purified by recrystallization from ethanol with a yield of 40% (m.p. 204°C). Spectroscopic characterization by ^{1}H-NMR, ^{13}C-NMR, FT-IR, UV-Vis techniques allowed to identify the purified product as 3-[2-(4-nitrophenyl)ethenyl]-2-methylindole (NPEMI).

^{1}H-NMR (δ, DMSO-d_6, 200 MHz) 2.57 (s, 3H, CH$_3$ indol.), 7.09 − 7.16 (m, 2H, indol.), 7.16 (d, 1H, J$_{trans}$ = 16.11 Hz), 7.32-7.36 (m, 1H, indol.), 7.74 (d, 1H, J$_{trans}$ = 16.48 Hz), 7.85 (d, 2H, benz., J = 9.16 Hz), 7.98 − 8.05 (m, 1H, indol.), 8.16 (d, 2H, benz., J = 9.16 Hz), 11.50 (bs, 1H, N-H).

^{13}C-NMR (δ, DMSO-d_6, 50.3 MHz) 11.76, 109.50, 111.05, 119.55, 119.94, 120.10, 121.31, 123.86, 125.71 (two superimposed lines), 127.53, 135.88, 139.21, 144.60, 146.40.
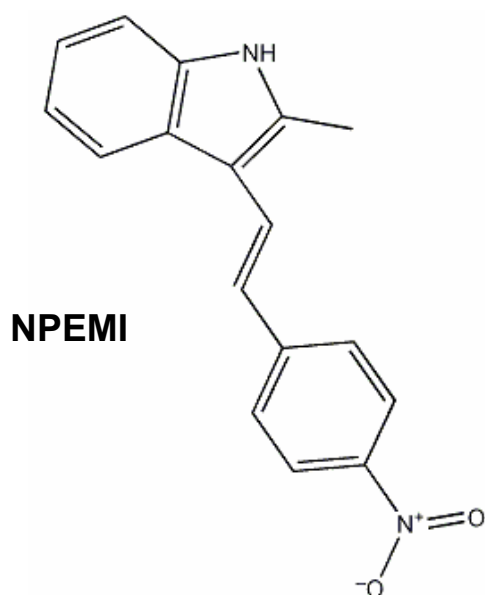
NPEMI

Figure 3.1 Molecular structure of 3-[2-(4-nitrophenyl)ethenyl]-2-methylindole (NPEMI).

3.3.2 Synthesis of 3-[2-(4-nitrophenyl)ethenyl]-1-allyl-2-methylindole (NPEMI-A)

In a 1l three-necks flask provided with reflux condenser and dropping funnel 4,78 g (17,2 mmol) of crystalline 3-[2-(4-nitrophenyl)ethenyl]-2-methylindole (NPEMI) were dissolved in a solvent mixture of 300 ml anhydrous toluene and 60 ml of tetrahydrofuran (THF), under Ar flux. Vigorously stirring with the aid of a magnetic stirrer, 1,96 g (34,9 mmol) of KOH in pellets and 0,480 g (1,82mmol) of 18-Crown-6 ether were added to the reaction mixture, whose colour immediately darkened, turning from brilliant red to dark red/brown.

The reaction mixture was maintained under stirring for 50 minutes; after this time a solution containing 2,80 ml of allyl chloride (d = 0,939 g/ml ; 34,34 mmol) in 8,2 ml of anhydrous toluene has been slowly added (15 min) to the reaction mixture with the aid of the dropping funnel under Ar flux. The flask containing the reaction mixture was then maintained under stirring at room temperature. The reaction progress was checked by FT-IR spectroscopy following the decrease of the intensity of the N-H stretching absorption band at $\nu = 3200$ cm^{-1}

in the spectra of periodic samples of the reaction mixture.

After nine days since the beginning (216 h), the solution assumed a black/greenish colour; it has been transferred in a separating funnel together with a dark solid formed on the bottom of the flask. Adding 300 ml of deionised water in the separating funnel and shaking it, three phases were formed: an organic (upper) brilliant red phase, a dark oily (intermediate)

67

interface, an aqueous (lower) red-orange phase. The upper phase was recovered and repeatedly washed in the separating funnel with a 5% HCl solution and then with deionised water, until the obtaining of neutral washing water. The resulting organic phase has been filtered on a Buckner funnel provided with filter paper and then dried over powdered Na_2SO_4 overnight. After a second filtration, in order to remove residual Na_2SO_4 powder, crude product has been recovered by evaporation of the solvent at reduced pressure in a rotary evaporator. The resulting product has been purified via recrystallization in absolute ethanol, lowering the temperature down to T = 4°C. The pure product (dark red crystalline solid) has been obtained with a yield of 60,2 %.

Melting point has been estimated to be m.p. = 108°C. The product has then been characterized through ^{1}H-NMR, ^{13}C-NMR, FT-IR, UV-Vis spectroscopies.

^{1}H-NMR (δ, CDCl$_3$, 200 MHz) 2.61 (s, 3H, CH$_3$ indol.), 4.81 (dt, 2H, J = 1.83, 4.40 Hz), 4,93 (dq, 1H, J = 1.83, 17.00 Hz), 5.24 (dq, 1H, J = 1.83, 10.70 Hz), 5.92 – 6.14 (m, 1H), 7.21 (d, 1H, J$_{trans}$ = 16.48 Hz), 7.30 – 7.37 (m, 3H, indol.), 7.59 (d, 1H, J$_{trans}$ = 16.11 Hz), 7.66 (d, 2H, benz., J = 8.79 Hz), 8.04 – 8.10 (m, 1H, indol.), 8.25 (d, 2H, benz., J = 8.79 Hz).

^{13}C-NMR (δ, CDCl$_3$, 50.3 MHz)   10.54, 45.47, 109.56, 110.56, 116.69, 119.85, 120.91, 121.97, 122.06, 124.19, 125.52, 125.61, 126.77, 132.44, 136.93, 138.39, 145.64, 146.06.
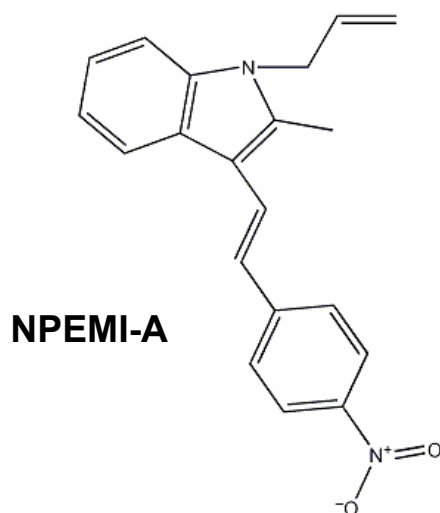

NPEMI-A

Figure 3.2 Molecular structure of 3-[2-(4-nitrophenyl)ethenyl]-1-allyl-2-methylindole (NPEMI-A).

3.3.3 Synthesis of 3-[2-(4-nitrophenyl)ethenyl]-1-(2-ethylhexyl)-2-methylindole (NPEMI-E)

In a 1l three-necks flask provided with magnetic stirring 4.70 g (16.9 mmol) of NPEMI were dissolved in 60 ml of anhydrous THF under a flux of Ar. After total solubilization, 300 ml of anhydrous toluene were introduced together with 1.91 g (34.0 mmol) of KOH pellets and 0.460 g (1.74 mmol) of 18-Crown-6 ether. The colour of the solution turned from red to deep green. After 30 min. stirring at room temperature, a solution containing 6.0 ml of 2-ethylhexyl bromide (6.52 g , 33.8 mmol) in 17.7 ml of toluene was dropped in the reaction mixture. The reaction progress was checked by FT-IR spectroscopy following the decrease of the intensity of the N-H stretching absorption band at $\nu = 3200$ cm^{-1} in the spectra of periodic samples of the reaction mixture, during 280 hours.

Filtration of the reaction mixture with a Büchner funnel allowed to recover a large amount of unreacted NPEMI. The filtered solution was repeatedly washed with a 5 % solution of HCl in water and successively with water, until neutral washing water was obtained. The organic phase was dried over Na$_2$SO$_4$ and then the solvent was removed by 3 hours high vacuum treatment. Possible residual 2-ethylhexyl bromide was removed by washing with hexane on a Büchner funnel. The obtained crude deep red product, dried under high vacuum, when examined by FT-IR, ^{1}H-NMR and TLC chromatography resulted to contain appreciable amount of unreacted NPEMI together with the desired NPEMI-E. The difficulty in obtaining pure NPEMI-E arises, as we will see by DSC measurements, from its poor tendency to crystallize giving preferably a glass material. Anyway, by using a silica gel chromatography column eluted by a 1/1 hexane-chloroform mixture, NPEMI-E was separated from NPEMI as a viscous glass product; the yield was of only 14%. The pure product begun to slowly crystallize after some months at room temperature.

^{1}**H-NMR** (δ, CDCl$_3$, 200 MHz) 0.87 – 0.99 (m, 6H), 1.24 – 1.49 (m, 8H), 1.83 – 2.07 (m, 1H), 2.60 (s, 3H, CH$_3$ indol.), 4.03 (d, 2H, J = 7.69 Hz), 7.17 (d, 1H, J$_{trans}$ = 16.12 Hz), 7.23 – 7.32 (m, 2H, indol.), 7.32 – 7.39 (m, 1H, indol.), 7.56 (d, 1H, J$_{trans}$ = 16.11 Hz), 7.64 (d, 2H, benz., J = 8.79 Hz), 7.99 – 8.06 (m, 1H, indol.), 8.25 (d, 2H, benz., J = 8.79 Hz).

^{13}**C-NMR** (δ, CDCl$_3$, 50.3 MHz) 10.90, 11.14, 13.97, 23.00, 24.12, 28.75, 30.80, 40.01, 47.78, 110.00, 110.29, 119.76, 120.68, 121.59, 121.76, 124.19, 125.43, 125.58, 126.96, 137.35, 139.80, 145.50, 146.16.

3.3.4 Second NPEMI-E synthetic route

First Stage - Synthesis of 1-(2-ethylhexyl)-2-methylindole 3-carboxaldehyde (ALD-E)

In a 250 ml three-necks flask equipped with a dropping funnel and water reflux condenser, 1,17 g (4,43 mmol) of 18-Crown-6 ether and 70 ml of anhydrous diethyl ether were introduced under inert nitrogen atmosphere. The solution was stirred with the aid of a magnetic stirrer until complete dissolution of the crown ether. 5,62 g (50 mmol) of dry powdered Potassium *ter*-butoxide were then introduced in the reaction vessel and remained in suspension, being insoluble in diethyl ether. Successively, 6,52 g (41 mmol) of 2-methylindole-3-carboxaldehyde (ALD) were added, together with 70 ml of diethyl ether and 170 ml of THF. This last addition resulted to be necessary in order to completely dissolve the indolyl reagent that is not very soluble in diethyl ether only. The resulting mixture appeared as a dark brown suspension.

Stirring has been maintained for ten minutes in the reaction mixture and then a solution containing 9,270 g (8,536 ml; 48 mmol) of 2-Ethylhexyl-bromide in 30 ml of diethyl ether was slowly added with the aid of a dropping funnel; colour and temperature of the reaction mixture were not altered by this addition. The introduction of all the reagents have been made under nitrogen flux. The reaction mixture was then heated and maintained at reflux (T = 54°C) under continuous stirring. The progress of reaction was monitored through TLC chromatography and FT-IR spectroscopy over periodic samples of the reaction mixture. The progressive disappearing in the FT-IR spectra of the absorption band at $\nu = 3200$ cm^{-1} relative to the N-H stretching of indolyl reagent, was a hint of the selective alkylation on the indole ring nitrogen.

After 10 hours since the start of the reaction, the flask has been slowly cooled down to room temperature and stirring was stopped. The reaction mixture was washed two times with deionised water in a separating funnel and the obtained acqueous phase was extracted two times with diethyl ether. The organic solutions obtained in the washing procedures were then collected together and dried over anhydrous powdered Na_2SO_4 overnight. The ether solution of a dark red colour was then recovered by filtration on a buckner funnel provided with filter paper. A TLC plate and the FT-IR spectrum of a sample of this solution evidenced the presence of the desired product (1-(2-ethylhexyl)-2-methylindole; ALD-E) as well as that of a not negligible quantity of not reacted ALD. The latter being very poorly soluble in diethyl ether, the solution was concentrated by means of partial evaporation of the solvent at reduced

pressure. The concentrated solution was then cooled down to T = -10°C for some hours; during this time a pale yellow solid appeared on the bottom of the flask containing the ether solution. The solid (that was recognized as the not reacted aldehyde by means of TLC chromatography and FT-IR spectroscopy) was then removed with the aid of a buckner funnel provided with paper filter. The crude product was recovered by evaporation of the solvent at reduced pressure; it had the appearance of a ropy very viscous liquid of light-red colour. The residual solvent was removed at high vacuum pressure for 8 hours. The crude product, whose weight was determined to be 8,9233 g resulted to contain, by ^{1}H-NMR spectroscopy analysis, a 13% in mol impurity of ALD. Therefore, it has been obtained 8,20 g of 1-(2-ethylhexyl)-2-methylindole-3-carboxaldehyde ALD-E (30,25 mmol), corresponding to a yield of 74%.

The product was characterized by means of ^{1}H-NMR, ^{13}C-NMR, FT-IR, UV-Vis spectroscopy.

^{1}H-NMR (δ, DMSO-d_6, 200 MHz) 0.79 (t, 3H, J = 7.33 Hz), 0.83 (t, 3H, J = 7.33 Hz), 1.21 (m, 8H), 1.87 (m, 1H), 2.70 (s, 3H, CH$_3$ indol.), 4.09 (d, 2H, J = 7.70 Hz, CH$_2$-N), 7.14 - 7.26 (m, 2H), 7.48 (d, 1H, J = 6.22 Hz), 8.10 (d, 1H, J = 6.22 Hz), 10,09 (s, 1H, CHO).

^{13}C-NMR (δ, DMSO-d_6, 50.3 MHz) 10.25, 10.60, 13.71, 22.37, 23.45, 27.96, 29.99, 39.05, 46.88, 110.57, 113.53, 119.99, 122.11, 122.58, 125.03, 136.69, 148.83, 184.27.

Second Stage - Synthesis of 3-[2-(4-nitrophenyl)ethenyl]-1-(2-ethylhexyl)-2-methylindole (NPEMI-E).

In a 500 ml three-necks flask provided with thermometer, reflux condenser, dropping funnel, magnetic stirrer, 8,095 g (29,85 mmol) of 1-(2-ethylhexyl)-2-methylindole-3-carboxaldehyde (ALD-E) were introduced under Ar flux, together with 50 ml of absolute ethanol. Under stirring 5,824 (32,15 mmol) of 4-nitrophenylacetic acid were added to the reaction mixture and it was heated up to a temperature of T= 60°C. The reaction mixture had a bright red colour and appeared well transparent. Maintaining temperature at T= 60°C and continuously stirring, a solution of 6 ml (5,17 g, 60,7 mmol) of piperidine in 11 ml of absolute ethanol was added with the aid of a dropping funnel. The addition of piperidine led to a rapid darkening of reaction mixture, whose colour became dark red. After a final addition of a volume of 125 ml of absolute ethanol, the solution was then set to reflux (T = 78°C) and maintained under vigorous stirring. The reaction progress was checked by TLC chromatography and FT-IR spectroscopy on periodic samples of the reaction mixture, during 48 hours.

Solvent removal at reduced pressure and T = 65°C permitted to recover a red viscous liquid that was then redissolved in chloroform. The resulting solution was washed repeatedly with deionised water in a separating funnel and successively transferred in a flask over powdered anhydrous Na_2SO_4, to remove residual water for eight hours. Filtration using a Buckner funnel and successive solvent removal at reduced pressure permitted to recover a bright red glassy solid. The crude product was then heated up to T = 110°C (temperature at which it has been sufficiently softened) and exposed to high vacuum under stirring for three hours in order to remove residual chloroform. Some preliminary FT-IR and ^{1}H-NMR spectra and TLC plates revealed the presence of the desired product NPEMI-E as well as that of other by-products like, e.g. not reacted aldehyde ALD-E. Products were separated by means of silica gel column chromatography, using as eluting mixture a *n*-Heptane/ Ethyl Acetate 4/1 in volume mixture. NPEMI-E was recovered as a red ropy glass material and then the residual solvent was removed at high vacuum pressure for 10 hours at T = 90°C. The product was stored under inert Ar atmosphere and, as long as it was stored at T = -20°C, it did not showed any tendency to crystallize for periods of months.

NMR, UV-Vis, FT-IR spectra and DSC measurements did not reveal hints of impurities. Nevertheless, high dark current was measured in electrooptic cells of samples of this product by means of carefully performed photoconductivity measurements; this led to consider it as impure. A good purity grade is indeed a mandatory feature for PR applications; another purification step was therefore necessary. The second purification was performed by silica gel column chromatography using a Chloroform/Hexane ½ in volume eluting mixture. The eluted fractions relative to NPEMI- E was recovered, concentrated at reduced pressure, residual volatiles were removed at high vacuum pressure for 6 hours at room temperature. Because of the high viscosity of the obtained product, a successive treatment at high vacuum pressure at T = 80°C has been necessary in order to remove solvent traces. The obtained NPEMI-E was stored under inert Ar atmosphere and at T = -20°C; the glass product showed the tendency to crystallize after periods of some months.

The pure product was recovered with a 33% yield and characterized by means of ^{1}H-NMR, ^{13}C-NMR, FT-IR, UV-Vis spectroscopy.

Obtained spectroscopic data are in good accordance with those previously reported for NPEMI-E obtained through a different synthetic route (s. Sect. 3.3.3).

¹H-NMR (δ, CDCl$_3$, 200 MHz) 0.87 – 0.99 (m, 6H), 1.24 – 1.49 (m, 8H), 1.83 – 2.07 (m, 1H), 2.60 (s, 3H, CH$_3$ indol.), 4.03 (d, 2H, J = 7.69 Hz), 7.17 (d, 1H, J$_{trans}$ = 16.12 Hz), 7.23 – 7.32 (m, 2H, indol.), 7.32 – 7.39 (m, 1H, indol.), 7.56 (d, 1H, J$_{trans}$ = 16.11 Hz), 7.64 (d, 2H, benz., J = 8.79 Hz), 7.99 – 8.06 (m, 1H, indol.), 8.25 (d, 2H, benz., J = 8.79 Hz).

¹³C-NMR (δ, CDCl$_3$, 50.3 MHz) 10.90, 11.14, 13.97, 23.00, 24.12, 28.75, 30.80, 40.01, 47.78, 110.00, 110.29, 119.76, 120.68, 121.59, 121.76, 124.19, 125.43, 125.58, 126.96, 137.35, 139.80, 145.50, 146.16.
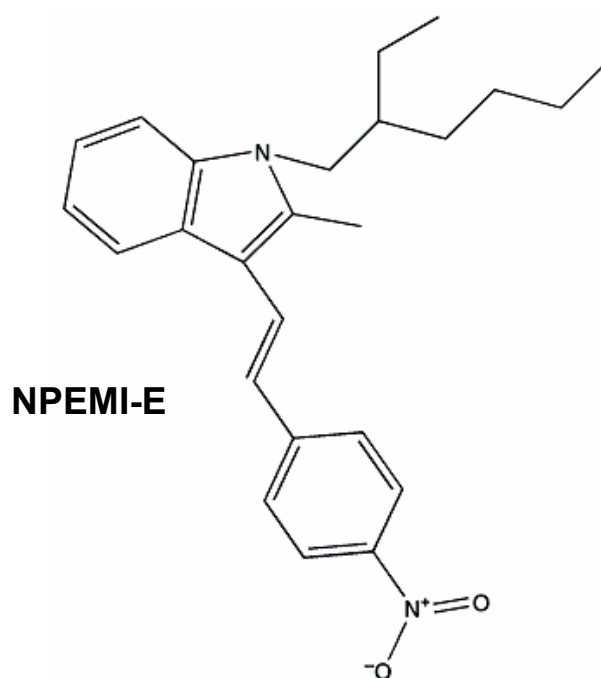

NPEMI-E

Figure 3.3 Molecular structure of 3-[2-(4-nitrophenyl)ethenyl]-1-(2-ethylhexyl)-2-methylindole (NPEMI-E).

3.3.5 Synthesis of 1-(2-ethylhexyl)-5-methoxyindole 3-carboxaldehyde (MeO-ALD-E)

In a 250 ml three-necks flask equipped with a dropping funnel and water reflux condenser, 0.452 g (1.71 mmol) of 18-Crown-6 ether and 3.00 g (17.12 mmol) of 5-methoxyindole-3-carboxaldehyde (MeO-ALD) were introduced, together with 100 ml of anhydrous THF under inert nitrogen atmosphere. The solution was stirred with the aid of a magnetic stirrer until complete dissolution of the products. The resulting solution appeared as light yellow and clear.

2.240 g (20 mmol) of dry powdered Potassium *ter*-butoxide were then introduced in the reaction vessel causing a rapid darkening of the solution whose colour became dark; the

solution became turbid because some of the added Potassium *ter*-butoxide remained in suspension.

Stirring has been maintained for ten minutes in the reaction mixture and then a solution containing 3.860 g (3.55 ml; 20 mmol) of 2-ethylhexyl-bromide in 20 ml of anhydrous THF was slowly added with the aid of a dropping funnel; colour of the reaction mixture was altered by this last addition, turning pink. The introduction of all the reagents have been made under nitrogen flux. The reaction mixture was then heated and maintained at reflux (T = 67°C) under continuous stirring. After 2,5 hours the colour of the reaction mixture has turned pale yellow, although remaining turbid. The progress of reaction was monitored through TLC chromatography and FT-IR spectroscopy over periodic samples of the reaction mixture. The progressive disappearing in the FT-IR spectra of the absorption band at $\nu = 3100$ cm^{-1} relative to the N-H stretching of indolyl reagent, was an hint of the selective alkylation on the indole ring nitrogen.

After 4 hours since the start of the reaction, the flask has been slowly cooled down to room temperature and stirring was stopped. The reaction mixture consisted of a clear pale yellow THF solution over a white solid (probably, KBR formed during the reaction and not reacted Potassium *ter*-butoxide) that was removed by means of filtration over a Buckner funnel. The solution was washed two times with deionised water in a separating funnel. Being THF soluble in water, 150 ml of diethyl ether were added to recover the organic phase. The obtained aqueous phase was successively extracted two times with diethyl ether (Et$_2$O). The Et$_2$O solutions obtained in the washing procedures were then collected together and dried over anhydrous powdered Na$_2$SO$_4$ overnight. The solution of a yellow-brown colour was then recovered by filtration on a buckner funnel provided with filter paper. A TLC plate and the FT-IR spectrum of a sample of this solution evidenced the exclusive presence of the desired product (1-(2-ethylhexyl)-2-methylindole; ALD-E). No hint was found of not reacted MeO-ALD product. The desired product was recovered by evaporation of the solvent at reduced pressure, obtaining a brown viscous liquid. The residual solvent was removed at high vacuum pressure for 8 hours.

4.64 g (16 mmol) of the desired product 1-(2-ethylhexyl)-5-methoxyindole-3-carboxaldehyde MeO-ALD-E were obtained, corresponding to a yield of 95%.

The product was characterized by means of ^{1}H-NMR, ^{13}C-NMR, FT-IR, UV-Vis spectroscopy.

¹H-NMR (δ, DMSO-d_6, 200 MHz) 0.71-0.92 (m, 6H), 1.05-1.35 (m, 8H), 1.87 (m, 1H), 3.79 (s, 3H, OCH$_3$), 4.12 (d, 2H, J = 7.44 Hz, CH$_2$-N), 6.92 (dd, 1H, J = 8.97 Hz), 7.48 (d, 1H, J = 8.97 Hz), 7.61 (d, 1H, J = 2.20 Hz), 8.24 (s, 1H), 9.87 (s, 1H, CHO).

¹³C-NMR (δ, DMSO-d_6, 50.3 MHz) 10.67, 14.12, 22.37, 23.52, 27.93, 30.10, 39.02, 46.93, 111.09, 112.34, 121.37, 122.11, 122.58, 125.03, 136.69, 148.83, 155.07, 184.27.

3.3.6 Synthesis of 3-[2-(4-nitrophenyl)ethenyl]-1-(2-ethylhexyl)-5-methoxyindole (MeO-NPEI-E).

In a 250 ml three-necks flask provided with thermometer, reflux condenser, dropping funnel, magnetic stirrer, 4.430 g (15.34 mmol) of 1-(2-ethylhexyl)-5-methoxyindole-3-carboxaldehyde MeO-ALD-E were introduced under Ar flux, together with 65 ml of absolute ethanol. Under stirring 3.060 g (16.87 mmol) of 4-nitrophenylacetic acid were added to the reaction mixture and it was heated up to a temperature of T= 60°C. The reaction mixture had a bright red colour and appeared well transparent. Maintaining temperature at T= 60°C and continuously stirring, a solution of 3.0 ml (2.610 g, 30.68 mmol) of piperidine in 8.0 ml of absolute ethanol was added with the aid of a dropping funnel. The addition of piperidine led to a rapid darkening of reaction mixture, whose colour became dark orange. The solution was then set to reflux (T = 79°C) and maintained under vigorous stirring. The reaction progress was checked by TLC chromatography and FT-IR spectroscopy on periodic samples of the reaction mixture, during 22 hours.

Solvent removal at reduced pressure and T = 65°C permitted to recover a red viscous liquid that was then redissolved in 100 ml of chloroform. The resulting solution was washed repeatedly with deionised water in a separating funnel and successively transferred in a flask over powdered anhydrous Na$_2$SO$_4$, to remove residual water overnight. Filtration using a Buckner funnel and successive solvent removal at reduced pressure permitted to recover a bright red glassy solid. The crude product was then heated up to T = 70°C (temperature at which it has been sufficiently softened) and exposed to high vacuum under stirring for three hours in order to remove residual chloroform. Some preliminary FT-IR and TLC plates revealed the presence of the desired product MeO-NPEI-E as well as that of other by-products like, e.g. not reacted aldehyde MeO-ALD-E. Products were separated by means of silica gel column chromatography, using as eluting mixture a *n*-Heptane/ Ethyl Acetate 4/1 in volume mixture. MeO-NPEI-E was recovered as a red ropy glass material and then the residual solvent was removed at high vacuum pressure for 10 hours at T = 80°C. The product was

stored under inert Ar atmosphere and, as long as it was stored at T = -20°C, it did not showed any tendency to crystallize. Anyway, it rapidly crystallizes when stored at room temperature.

NMR, UV-Vis, FT-IR spectra and DSC measurements did not reveal hints of impurities.

The product 3-[2-(4-nitrophenyl)ethenyl]-1-(2-ethylhexyl)-5-methoxyindole (MeO-NPEI-E) was recovered with a 39 % yield and characterized by means of ^{1}H-NMR, ^{13}C-NMR, FT-IR, UV-Vis spectroscopy.

^{1}H-NMR (δ, CDCl$_3$, 200 MHz) 0.87 – 0.99 (m, 6H), 1.20 – 1.48 (m, 8H), 1.83 – 2.03 (m, 1H), 3.95 (s, 3H, O-CH$_3$), 4.00 (d, 2H, J = 7.89 Hz), 6.95 (m, 1H indol.) ,7.08 (d, 1H, J$_{trans}$ = 16.32 Hz), 7.24 – 7.34 (m, 2H, indol.), 7.42 (d, 1H, indol.), 7.48 (d, 1H, J$_{trans}$ = 16.32 Hz), 7.60 (d, 2H, benz., J = 8.90 Hz), 8.25 (d, 2H, benz., J = 8.90 Hz).

^{13}C-NMR (δ, CDCl$_3$, 50.3 MHz) 10.71, 14.21, 23.14,   24.10, 28.79, 30.78, 40.07 50.89, 56.20, 102.83, 111.09, 112.34, 112.99, 121.37, 124.33, 125.69, 126.65, 126.95, 130.52, 132.88, 145.80, 155.06.
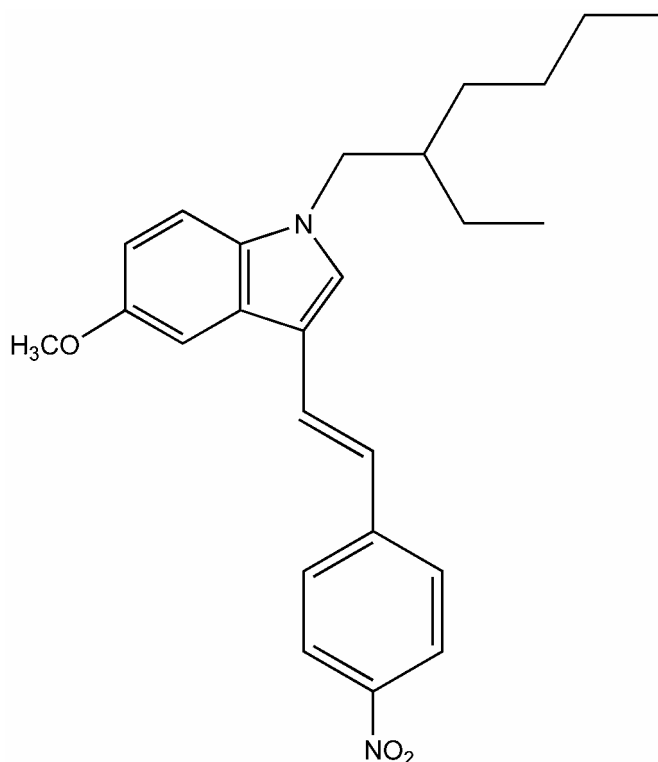

Figure 3.4 Molecular structure of 3-[2-(4-nitrophenyl)ethenyl]-1-(2-ethylhexyl)-5-methoxyindole (MeO-NPEI-E).

3.3.7 Synthesis of 1-(2-ethylhexyl)-5-nitroindole 3-carboxaldehyde (NO$_2$-ALD-E).

In a 250 ml three-necks flask equipped with a dropping funnel and water reflux condenser, 0.463 g (1.75 mmol) of 18-Crown-6 ether and 3.330 g (17.52 mmol) of 5-nitroindole-3-carboxaldehyde (NO$_2$-ALD) were introduced, together with 80 ml of anhydrous THF and 20 ml of anhydrous DMSO under inert nitrogen atmosphere. The addition of DMSO to THF was due to the poor solubility of the reagent NO$_2$-ALD in THF only. The solution was stirred with the aid of a magnetic stirrer until complete dissolution of the products. The resulting solution appeared as light yellow and clear.

2.240 g (20 mmol) of dry powdered Potassium *ter*-butoxide were then introduced in the reaction vessel causing a rapid darkening of the solution whose colour became dark red; the solution became turbid because some of the added Potassium *ter*-butoxide remained in suspension.

Stirring was maintained for ten minutes in the reaction mixture and then a solution containing 3.860 g (3.55 ml; 20 mmol) of 2-ethylhexyl-bromide in 15 ml of anhydrous DMSO was slowly added with the aid of a dropping funnel; the colour of the reaction mixture was altered by this last addition, turning pink. The introduction of all the reagents have been made under nitrogen flux. The reaction mixture was then heated and maintained at reflux (T = 74°C) under continuous stirring. During the successive 4 hours the colour of the reaction mixture has not turned and remained turbid The progress of reaction was monitored through TLC chromatography and FT-IR spectroscopy over periodic samples of the reaction mixture. The progressive partial disappearing in the FT-IR spectra of the absorption band at $\nu = 3100$ cm^{-1} relative to the N-H stretching of indolyl reagent, was an hint of the selective alkylation on the indole ring nitrogen. TLC and FT-IR spectra showed the presence of both the desired product and a not small quantity of the reagent NO$_2$-ALD. Nevertheless, after 4,5 hours since the start of the reaction, the flask has been slowly cooled down to room temperature and stirring was stopped. The reaction mixture consisted of a clear pale yellow solution over a white solid that was removed by means of filtration over a Buckner funnel. The solution was washed two times with deionised water in a separating funnel. The reaction mixture was washed two times with deionised water in a separating funnel; being DMSO and THF soluble in water, 50 ml of diethyl ether were added to recover organic phase. During the washing with water a yellow powder separated, insoluble in both aqueous and organic phases: it has been identified as the unreacted reagent NO$_2$-ALD, and thus separated from the crude product by filtration. The organic phase (solutions in Et$_2$O) obtained in the washing procedures was then

collected in a vessel and dried over anhydrous powdered Na_2SO_4 overnight. The ether solution of a dark red colour was then recovered by filtration on a buckner funnel provided with filter paper. A TLC plate and the FT-IR spectrum of a sample of this solution evidenced the presence of the desired product (1-(2-ethylhexyl)-5-nitroindole 3-carboxaldehyde; NO_2-ALD-E) as well as that of a residual quantity of not reacted NO_2-ALD. The desired product was recovered by means of crystallization from concentrated solution in diethyl ether, obtaining a finely powdered yellow solid. TLC and FT-IR permitted to appreciate the good purity grade and the almost complete recovery of all the formed product.

NO_2-ALD-E was obtained in 2.90 g giving a yield of 55 %.

The product was characterized by means of ^{1}H-NMR, ^{13}C-NMR, FT-IR, UV-Vis spectroscopy.

^{1}H-NMR (δ, DMSO-d_6, 200 MHz) 0.75-0.90 (m, 6H), 1.07-1.31 (m, 8H), 1.90 (m, 1H), 4.25 (d, 2H, J = 7.47 Hz, CH_2-N), 7.84 (d, 1H, J = 8.97 Hz), 8.18 (dd, 1H, J = 8.97 Hz), 8.61 (s, 1H), 8.94 (d, 1H, J = 2.3 Hz), 10,00 (s, 1H, CHO).

^{13}C-NMR (δ, DMSO-d_6, 50.3 MHz) 10.82, 14.21, 23.15, 24.18, 28.82, 30.83, 40.42, 51.24, 110.32, 116.01, 118.36, 124.43, 126.37, 131.86, 144.69, 146.55, 183.84.

3.3.8 Synthesis of 3-[2-(4-nitrophenyl)ethenyl]-1-(2-ethylhexyl)-5-nitroindole (NO_2-NPEI-E).

In a 250 ml three-necks flask provided with thermometer, reflux condenser, dropping funnel, magnetic stirrer, 2.720 g (9 mmol) of 1-(2-ethylhexyl)-5-nitroindole -3-carboxaldehyde (NO_2-ALD-E) were introduced under Ar flux, together with 50 ml of absolute ethanol. An initial heating is necessary in order to solubilize this reagent. Under stirring 1.790 g (10 mmol) of 4-nitrophenylacetic acid were added to the reaction mixture and it was heated up to a temperature of T= 60°C. The reaction mixture had a bright red colour and appeared well transparent. Maintaining temperature at T= 60°C and continuously stirring, a solution containing 1.8 ml (1.53 g, 18 mmol) of piperidine in 4 ml of absolute ethanol was added with the aid of a dropping funnel. The addition of piperidine led to a rapid darkening of reaction mixture, whose colour became dark orange. The solution was then set to reflux (T = 78°C) and maintained under vigorous stirring. The reaction progress was checked by TLC chromatography and FT-IR spectroscopy following the decrease of the intensity of the

absorption band at $\nu = 1667$ cm^{-1} (associated to aldehydic C=0) in the spectra of periodic samples of the reaction mixture, during 17 hours.

After 17 hours the reaction has been stopped and the reaction mixture has been cooled down to room temperature. A red crystalline solid is present in the reaction mixture. It has been removed and separately recovered by filtration of reaction mixture. The crystalline solid has been then redissolved in chloroform and washed two times with deionised water in a separating funnel; the solution was successively transferred in a flask over powdered anhydrous Na_2SO_4, to remove residual water overnight. Filtration using a Buckner funnel and successive solvent removal at reduced pressure permitted to recover a bright red crystalline powder. It has been identified as the desired product 3-[2-(4-nitrophenyl)ethenyl]-1-(2-ethylhexyl)-5-nitroindole (NO$_2$-NPEI-E) by means of FT-IR, 1H-NMR spectroscopy. Anyway, the rest of reaction mixture still contained a large quantity of desired product. After a first recrystallization in diethyl ether in order to separate a large part of the unreacted NO$_2$-ALD-E, the product has been purified by means of silica gel column chromatography, employing a 4/1 in volume Chloroform/n-Heptane solution as eluting mixture. Solvent removal from the eluted fractions at reduced pressure and at high vacuum pressure for 5 hours permitted to recover a brown-red crystalline solid. The desired product has been obtained in 0.550 g giving a yield of 15 %.

The pure product was characterized by means of ^{1}H-NMR, ^{13}C-NMR, FT-IR, UV-Vis spectroscopy.

^{1}H-NMR (δ, CDCl$_3$, 200 MHz) 0.80 – 0.99 (m, 6H), 1.20 – 1.45 (m, 8H), 1.93 (m, 1H), 4.08 (d, 2H, J = 7.36 Hz), 7.17 (d, 1H, J$_{trans}$ = 16.53 Hz), 7.25 – 7.53 (m, 3H, indol.), 7.64 (d, 2H, benz., J = 8.87 Hz), 8.16 – 8.27 (m, 3H), 8.91 (d, 1H, J = 2.17 Hz).

^{13}C-NMR (δ, CDCl$_3$, 50.3 MHz) 10.82, 14.21, 23.15, 24.18, 28.82, 30.83, 40.42, 51.24, 110.32, 116.01, 117.55, 118.36, 124.43, 124.55, 124.73, 125.53, 126.37, 131.86, 140.35, 142.40, 144.69, 146.55.
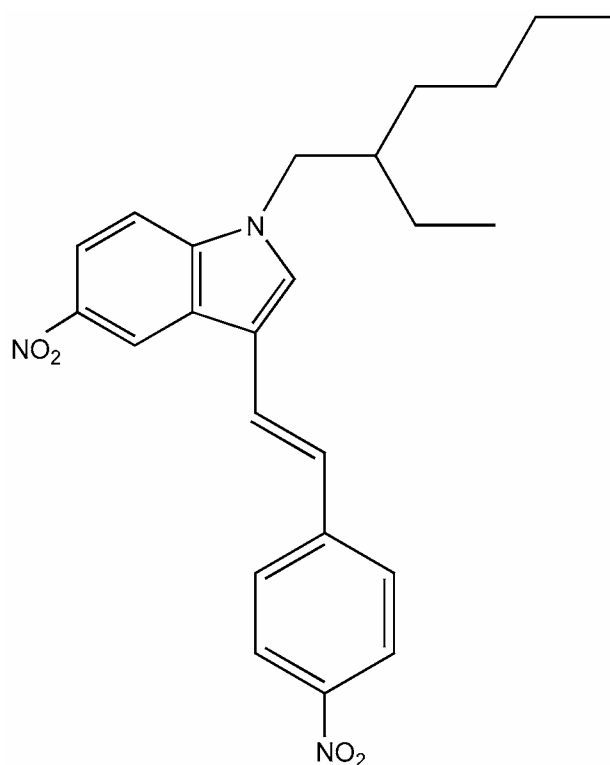
Figure 3.5 Molecular structure of 3-[2-(4-nitrophenyl)ethenyl]-1-(2-ethylhexyl)-5-nitroindole (NO2-NPEI-E).

3.3.9 Synthesis of 2,3-dimethyl-N-vinylindole (DMVI)

Synthesis of monomer 2,3-dimethyl-N-vinylindole (DMVI) was accomplished through vinylation of the K salt of 2,3-dimethylindole using acetylene at high pressure and temperature[166,167].

Metallic K was introduced in the reactor in catalytic quantity to form the potassium salt together with liquid 2,3-dimethylindole. The stainless steel high pressure resistant reactor was then charged at the total pressure of 60 atm with a gas mixture containing 10 atm of acetylene and 50 atm of nitrogen. The reaction was then started introducing the reactor in an oil bath at T = 160°C and maintaining the mechanical agitation. After 6 hours reactor was cooled down to room temperature, in excess pressure was discharged and then a second filling was made with the same mixture (60 atm; 50 atm nitrogen, 10 atm acetylene). Reactor was maintained at T = 160°C and in agitation for successive 6 hours. The crude product was recovered from the reactor and transferred in a Claysen distiller in order to be purified. The pure product was obtained by distillation at reduced pressure (b.p. 87°C; 0,3 mm Hg) with a yield of 75%.

The product was characterized by means of ^{1}H-NMR, ^{13}C-NMR, UV-Vis, FT-IR spectroscopies and stored under Ar atmosphere at T = -20°C.

80

3.3.10 Polymerization of 2,3-dimethyl-1-vinylindole

In a 250 ml flask 14,2 g (83 mmol) of 2,3-dimethyl-1-vinylindole and 110 ml of anhydrous dichloromethane were introduced under inert Ar atmosphere. The reaction mixture was maintained under vigorous stirring by means of a magnetic stirrer and cooled down to T = -40°C with the aid of a bath of liquid nitrogen and methanol. At this temperature 0,7 ml of $BF_3.Et_2O$ were added. Solution colour turned form yellow to bright red.

After 1 hour reaction progress was stopped by addition of cool (T = -40°C) ammoniacal methanol. The reaction flask was then removed from the cool bath and left at room temperature maintaining the stirring. When reaction mixture reached room temperature it was transferred in a separating funnel and washed with deionised water until the obtaining of neutral washing water. The organic phase was then purified from residual water over powdered anhydrous Na_2SO_4 overnight.

After the subsequent filtration, the solvent was removed at reduced pressure and the polymer was recovered by a double precipitation in methanol. The obtained polymer was then filtered and dried under high vacuum pressure for eight hours.

The desired polymer was obtained with a yield of 67% and characterized by means of FT-IR, 13C-NMR spectroscopies. Gel permeation chromatography (GPC) permitted to estimate a molecular weight Mw = 30338 (Mn = 11421).

3.4 Preparation of photorefractive blends

Photorefractive blends investigated in this research were composite materials: a polymer, a NLO chromophore, a photosensitizer were employed, in the typical guest-host approach (s. Sect. 1.6.1). Two different materials series have been prepared in order to comparatively study the PC and PR behaviour of similar blends of the two different NLO chromophores NPEMI-E and NPEMI-A. In Figure 3.6 the molecular structures of the different species constituting the blends are displayed. The composition and names assigned to the blends are summarized in Table 3.1 and Table 3.2 for NPEMI-E and NPEMI-A blends, respectively. It is important to notice that, for blends of both NLO chromophores, PR and PC measurements were conducted only on some selected compositions: blends at 50, 75, 80, 85, 90, 95, 99 wt.% of NPEMI-E (or –A). Only such blends, indeed, had sufficiently low T_g

values, comparable or lower than room temperature; for this reason they were expected to show a birefringence contribution that enhances PR optical gain (s. Sect. 1.4). The other blends were just employed in the DSC calorimetric analysis (s. Sect. 4.3.2), their PR optical gain being expected to be very low (as it was successfully verified).

Table 3.1 Composition of the studied blends based on NPEMI-E.

Blend name	Composition (wt.%)			T_g (°C)	T_r (°C)
	PVDMI	NPEMI-E	TNFM		
PVD99	99	-	1	198.5	176.5
NPE5	94	5	1	176.5	154.5
NPE10	89	10	1	154.9	132.9
NPE20	79	20	1	116.7	94.7
NPE30	69	30	1	86.3	64.3
NPE40	59	40	1	59.4	37.4
NPE50	49	50	1	43.0	21.0
NPE60	39	60	1	29.4	7.4
NPE70	29	70	1	19.5	-2.5
NPE75	24	75	1	15.4	-6.6
NPE80	19	80	1	11.8	-10.2
NPE85	14	85	1	8.2	-13.8
NPE90	9	90	1	4.6	-17.4
NPE95	4	95	1	0.5	-21.5
NPE99	-	99	1	-2.6	-24.6

Table 3.2 Composition of the studied blends based on NPEMI-A.

Blend name	Composition (wt.%)			T_g (°C)	T_r (°C)
	PVDMI	NPEMI-A	TNFM		
PVD99	99	-	1	198.5	176.5
NPA10	89	10	1	150.3	128.3
NPA20	79	20	1	111.2	89.2
NPA30	69	30	1	88.0	66.0
NPA40	59	40	1	67.6	45.6
NPA50	49	50	1	49.9	27.9
NPA60	39	60	1	39.0	17.0
NPA70	29	70	1	33.1	11.1
NPA75	24	75	1	29.3	7.3
NPA80	19	80	1	26.7	4.7
NPA85	14	85	1	23.9	1.9
NPA90	9	90	1	22.0	0.0
NPA95	4	95	1	19.8	-2.2
NPA99	-	99	1	18.4	-3.6

Due to the availability of NPEMI-E and NPEMI-A to give stable glass amorphous phases, whose T_g values are lower than room temperature (T_g (NPEMI-E) = -2.6°C; T_g (NPEMI-A) = 18.4°C), these two NLO chromophores acted themselves as plasticizers for the blends. There was no need therefore to add a plasticizer monomer species in blends composition; such plasticizer agents are used in organic PR materials containing crystalline NLO species, in order to obtain glass phases and reduce T_g values of the blends.

Blends have been prepared in solution, dissolving the exact necessary quantities of the components in dichloromethane and mixing the obtained solutions. A precaution was observed to take the photosensitizer TNFM solution as the last to be added in order to avoid competition between different species to be complexed by TNFM in the formation of the charge-transfer complex (CTC) responsible for the photosensitivity of the blends. The solutions, once containing all the components, have been left under vigorous stirring for 2 hours and then filtered with the aid of Teflon membrane microporous filters (pores diameter d = 0.22 µm) in order to remove macro and micro mechanical impurities (e.g. dust or hairs). A

particular accuracy in cleaning and removing all mechanical impurities from flasks and tools used to manipulate the blends was taken because of the known tendency of such impurities to favour dielectric breakdown in cells when high voltage is applied. Moreover, they act as scattering center for light incident on samples, worsening their transparency and homogeneity. After the filtration the solvent was removed under reduced pressure (20 mm Hg) and under high vacuum for 6 hours. Another treatment has been performed in order to completely remove every trace of residual volatile impurity responsible for the formation of micro-bubbles in the subsequent process of cells preparation. Blends were heated up to temperatures well higher than their own T_g and m.p. of NLO chromophores (s. Sect. 4.3.2; typically, T was set around 120-150°C) under inert Ar atmosphere. Once blend was sufficiently softened and temperature had been stabilized it was exposed to high vacuum for 1-2 minutes, during which sometimes bubbles were formed, and then atmospheric pressure was recovered. The process was repeated two times without changing the temperature. At the end of the second cycle a rapid temperature quenching was performed on the blend: by maintaining high vacuum, the flask was rapidly dipped in a bath of water at room temperature. Only when blend temperature had reached room temperature, and the material had therefore hardened, atmospheric pressure was restored. This process permitted to obtain glass materials free of volatile impurities or crystalline nuclei.

The obtained blends were stored under inert Ar atmosphere at T = -20°C to slow down or prevent eventual crystallization/segregation of NLO chromophore from polymer matrix, even if this process effectively occurred at room temperature only in NPEMI-A blends containing very high amounts of chromophore (> 90 wt.%) and with times longer than one month.
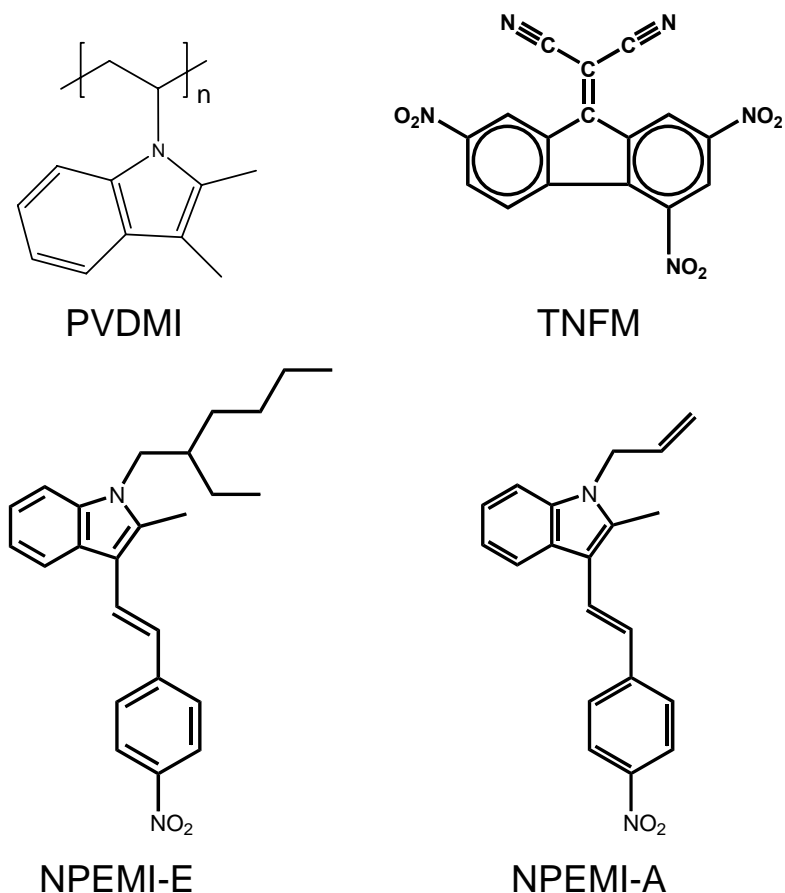
Figure 3.6 Molecular structures of species employed in the formulation of photorefractive blends.

3.5 Preparation of electrooptic cells for photorefractive measurements

The present study of PR properties by means of the 2BC technique required the use of electrooptic cells in which thickness-controlled amorphous films of the materials under study were formed. The electrooptic cell permitted the application of very large electric field E (up to $E = 10^6$ V/cm) in the active zone of the film, i.e. the zone in which light intensity pattern is formed by the interference of the two laser beams. As we have already evidenced in previous sections, electric field plays a fundamental role in determining PR properties of organic materials: it enhances photogeneration efficiency of free charge carriers, increases photoconductivity, permits the reorientation of molecular dipoles (through birefringence contribution, s. Sect. 1.4). Moreover, cells permit to safely handle the samples and protect films from air or moisture and from mechanical damages. A particular care has been therefore devoted in the design and preparation of cells. Figure 3.7 A) and B) display some schematic drawings of the design of cells.

A)

ITO trace

B)

Spacer microspheres
t = 22.8 μm

PR blend
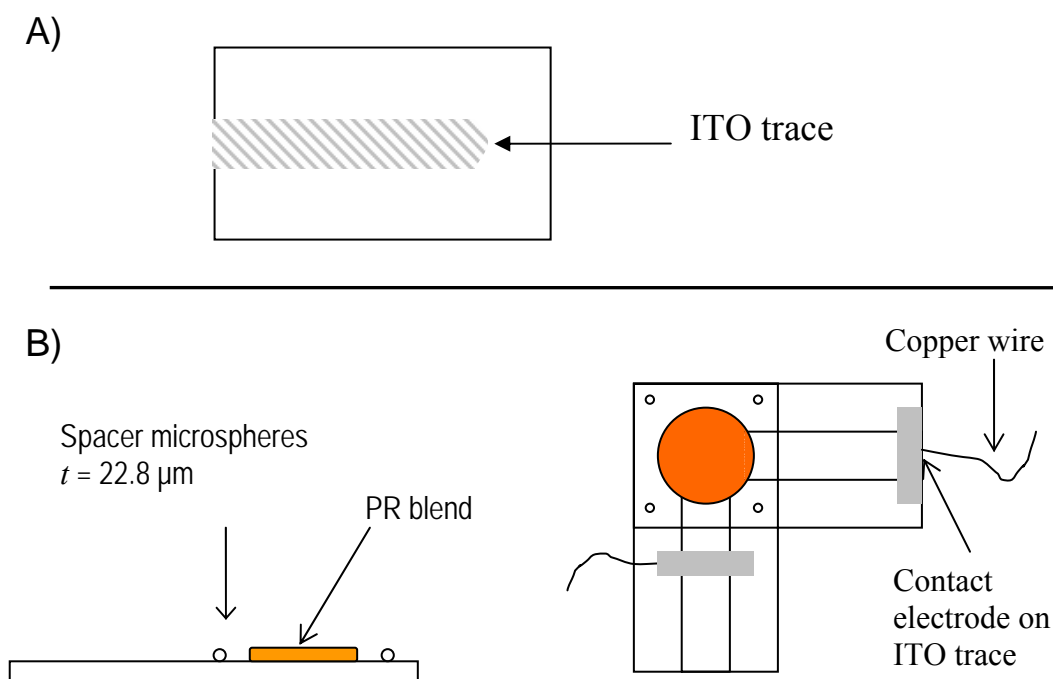
Copper wire

Contact
electrode on
ITO trace

Figure 3.7 **A)** ITO-covered glass sheet (30 x 15 mm) employed in electrooptic cell for photorefractive measurements. **B)** Schematic drawing displaying the design of the electrooptic cells.

Cells were prepared employing ITO-covered glass sheets (AET Technologies[®], France) whose dimensions were 30 x 15 mm. ITO (Indium Tin Oxide, a transparent electric conductor) layer originally covered the entire area of one surface of the glass sheets. The ITO layer has been successively shaped in the form of a strip, as displayed in Figure 3.7 A), in order to obtain two electrodes for the application of the electric field only in the central area of the cell (active zone). The shaping of ITO layer has been obtained by masking with adhesive tape the area to maintain covered with ITO and dipping the glass sheets in a HCl solution at room temperature for 10 minutes. Successive washing with water, removal of the adhesive tape, washing in acetone and ether (removal of adhesive glue), drying under high vacuum for 6 hours permitted to obtain clean shaped ITO strips. Before its employment in the preparation of the cells, each glass sheet was carefully observed with a binocular microscope in order to reject those sheets that have been badly shaped or damaged by hydrochloric acid and to sweep mechanical impurities as dust, paper fragments, hairs.

As concerns the preparation of amorphous films of the blend at a controlled thickness, it has been complied with the following procedure. The necessary quantity of blend (of the order of few mg) was placed on the upper face of a glass sheet (the one covered with shaped

86

ITO layer) at the center of the internal extreme of the ITO strip (s. Figure 3.7 B). In the surroundings of the blend fragment –but outside the ITO trace– glass microspheres (Whithehouse Scientific Ltd., UK) were placed to act as spacers; their mean diameter was $t = 22.81 \pm 0.78$ μm. Because of the small dimensions of the microspheres and of their tendency to aggregate it was quite impossible to manipulate them individually. With the aid of the microscope and of a thin copper wire they were placed on the surface as small clusters. These spacer clusters were placed at the four corners of the area which had to be superimposed by the second glass sheet having the ITO strip on the lower face. Successively the glass sheets were transferred on a copper "shaper" that helped in the correct geometrical positioning of the glass sheets and permitted the necessary rapid heating/cooling processes. The copper shaper containing the first glass sheet was then placed on a heating plate together with a brass cube and a second glass sheet whose ITO-covered side was facing down, in contact with the plate surface. The heating plate was covered with a removable glass cover in order to achieve the formation of a controlled temperature environment as well as to permit to follow the operation with the microscope placed over it. The heating plate was then set at the desired temperature to cause the softening of the blend, depending on the blend composition. For the blends under study, heating process was made at temperatures in the range $90 < T < 120$ °C. After some minutes the second glass sheet was laid over the first one and orthogonally to it, its ITO-covered side facing down; the second sheet is pushed in order to "squeeze" the soft sample and to reach the thickness imposed by the spacers. The brass cube was placed over the two superimposed glass sheets and copper shaper in order to prevent their relative displacement before the hardening of the material. The shaper was then quickly transferred over a large piece of copper, operating the rapid temperature quenching to room temperature necessary to favour the formation of an amorphous film.

Electrical connections for the obtained electrooptic cell were provided by soldering with indium two thin copper wires at the extreme portions of ITO traces.

3.6 AsymmetricTwo-Beam Coupling (2BC) measurements apparatus

An Asymmetric Two-Beam Coupling (2BC) experiment has been set up in order to measure PR properties of the materials under study. The optical setup (s. Figure 3.12 A)) was mounted on a vibration damping optical table (Newport Corp., Irvine, CA, USA). All the optical components of the circuit were supported on rigid holders fixed on the optical table.

The 2BC setup employed a solid state laser diode (AlGaInP Laser Diode - ML1413R, Mitsubishi, Japan –supplied by Schäfter + Kirchoff, Gmbh, Hamburg, Germany) working in the single transverse mode, with an emission wavelength λ_{LD} = 685 nm, comprising also collimation optics.

Technical optical and electric characteristics of the laser diode are summarized in Table 3.3.

Table 3.3 Electric/optical features of the employed laser diode (ML1413R, Mitsubishi) at T = 25°C.

Parameter		min	typical	max	units
Threshold current	I_{th}	-	35	60	mA
Operating current (P$_0$ = 50 mW)	I_{op}	-	95	140	mA
Operating voltage	V_{op}	2.0	2.7	3.0	V
Emission wavelength	λ_{LD}	670	685	700	nm

Power supply and control of laser diode were provided by a laser diode controller (LDC 500 Thorlabs, Inc., Newton, NJ, USA) that permitted to control and change the emission conditions. In the present study laser diode was employed in continuous-wave mode (CW) and at constant emission power.

Careful adjustment was performed using an optical powermeter (Pocket Power – Melles Griot, France) that permitted to correctly relate supplied operating current I_{op} to emission power of the laser diode P$_o$. The following relation holds

$$P_0(\text{mW}) = 0.802 I_{op}(\text{mA}) - 28.42 \qquad . \tag{3.1}$$

In Table 3.4 typical operating values are reported for both operating current and emission power of the employed laser diode.

Table 3.4 Typical operating values of P_0 and I_{op} of the employed laser diode.

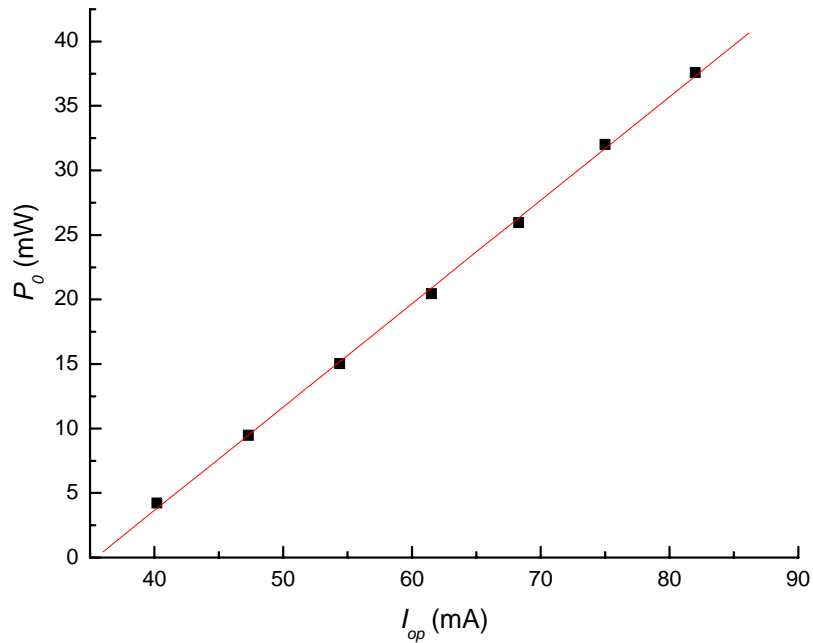| I_{op} (mA)	P_0 (mW)
40.2	4.21
47.3	9.47
54.4	15.02
61.5	20.44
68.3	25.95
75.0	31.70
82.0	37.59

Figure 3.8 Adjustment of emission power P_0 of the laser diode as a function of the supplied operating current I_{op}. Linear fit of the experimental data is displayed as a continuous line and is relative to Eq. (3.1).

A special care in the setup of this experimental arrangement has been devoted to the temperature stabilization of the laser diode and of the entire optical apparatus. As concerns laser diode, temperature stabilization is fundamental in order to permit it to operate in a single emission mode. Variations in temperature of the order of few tenth of degree cause the laser to "jump" from an operating mode to another, changing emitted frequency and mode. Another important factor is represented by the polarization ratio of the diode, defined as $P_{||}/P_{\perp}$, in which $P_{||}$ is the power of the radiation emitted with polarization along a direction parallel to

the optical table plane, while P⊥ is the power relative to radiation emitted with polarization along a direction orthogonal to the optical table plane. Polarization ratio is strongly dependent on temperature and supply current. Polarization ratio increases as I_{op} increases; when operating with an I_{op} = 75 mA (corresponding to an emitted power P_0 = 31.7 mW), polarization ratio is of the order of P∥/P⊥ ≈ 1200, that is, emitted laser light is well defined as a linear polarized radiation. In the present study it was decided to work with the two laser beams incident on the sample each having a power of about 1 mW. Nevertheless, in order to keep an high value of polarization ratio, laser diode was employed with an operating current I_{op} = 75.0 mA. Laser beam intensity has been attenuated with a neutral filter (D43813, Edmund Optics, Inc., Barrington, NJ, USA) placed at the output of laser diode. The neutral filter had a transmittance T = 10%, so that the output power was P = 3.17 mW). In order to test the invariance of the photorefractive measurements on incident laser beam power, some measurements have been performed on the same cell without using a filter ($P = P_0$ = 31.7 mW) or alternatively using a neutral filter having a transmittance T = 1% ($P = 0,01 \, P_0$ = 0.317 mW). It has been correctly verified that identical values of the PR optical gain can be obtained both for high or low power conditions.

The temperature stabilization of the laser diode has been provided introducing it in a copper piece which was in thermal contact with one surface of a circular ring Peltier cell. Peltier cell worked by means of an homemade thermoelectric controller driven by a thermistor plugged in the copper piece. A thermocouple was also plugged in the copper piece in order to monitor its temperature with a digital multimeter. The homemade thermoelectric controller assured a thermal stabilization of the laser diode of the order of 10^{-2} °C. The thermal exchange of the Peltier cell with the environment to dissipate the heat generated by the laser diode was provided with a water flux cooling circuit. It was realized with a copper pipe coil inside the copper piece. The choice for a water cooling instead of air cooling (employment of a fan or heatsink) was made in order to avoid the establishment of air fluxes in the measurements area, these last being a potential source of instability for other optical components of the 2BC setup (e.g., mirrors, detectors). This is especially true for the electrooptic cell containing the sample, that revealed itself as extremely sensitive to such kind of perturbations. With the aim to prevent that incoming environmental light (solar, artificial) could alter the measurements, the table containing the electrooptic circuit has been enclosed in a box, provided with a frontal door. The internal walls of the box has been covered with an opaque black paint in order to reduce undesired noise due to reflections and parasitic light. The laser diode block (comprising copper piece, Peltier cell, cooling pipes, electrical mountings) is mounted on a

circular holder that permits the rotation on one axis of the laser diode in order to select polarization direction.

An anamorphotic beam expander was placed at the exit of the laser diode (ABE P-AN1600U GFO Gerhard Franck Optronick, Gmbh, Drakenburg, Germany; s. Figure 3.12 A). The beam expander provided to transform the elliptical section of the beam in a circular one having a diameter of 3 mm.

Beam coming from ABE enters a neutral cubic beamsplitter (BS014, ThorLabs; BS in Figure 3.12 A) with transmission/reflection fixed ratio equal to 1 (50/50) that splits the original beam in a reflected (beam 1) and a transmitted beam (beam 2) of nominally equal power. Measurements performed during the adjustment of setup permitted to appreciate a difference between the power of the two beams, their ratio being experimentally determined as $P_1/P_2 \approx 3/4$.

Beams 1 and 2 are directed to two circular flat mirrors (D32,107 Edmund Scientific ThorLabs; M1 and M2 in Figure 3.12 A) mounted on holders with micrometer control screws on two movement axes that permitted the relative orientation and the superposition of the two beams on the active zone of the sample cell. Along the beam path of both beams, between the mirrors M1, M2 and the cell, two shutters (mod. 846HP, Newport Corp., USA) were placed, driven by an electric controller placed outside the measurement apparatus box. Shutters permitted to individually interrupt the incidence of beams on the sample, making it possible to choose among different conditions of incident light: both beams ON ($P_1^{IN} \neq 0$; $P_2^{IN} \neq 0$; $P_{1,2 \text{ ON}}$ in the following); beam 1 ON, beam 2 OFF ($P_1^{IN} \neq 0$; $P_2^{IN} = 0$; $P_{1\text{ON,2OFF}}$ in the following), and viceversa; both beams OFF ($P_1^{IN} = 0$; $P_2^{IN} = 0$; $P_{1,2\text{OFF}}$).

The electrooptic cell was mounted on a sample holder realized in PTFE (polytetrafluoroethylene) to ensure electrical isolation; the cell was fixed with a screw that blocks the glass sheet of the cell in the sample holder. The sample holder was mounted on a graduated rotating base (ThorLabs) that permitted to select the desired angle between the cell and the beams incidence directions; it is defined as the tilt angle Ψ in a 2BC experiment (see below). The choice of the tilt angle affects both intensity and sign of the power transfer in a 2BC experiment, determining which one of the two beams is the "signal" beam -the one gaining in power due to PR effect- and which one is the "pump" beam –the one loosing its power due to PR effect. Preliminary measurements were accomplished varying the value of the tilt angle. It was verified the inversion of roles for beams (pump/signal) when changing the angle from Ψ to $-\Psi$ and the vanishing of PR effect when $\Psi = 0$ (symmetric configuration). In this research a standard tilt angle was chosen, $\Psi = +40°$, that remained fixed for all the performed measurements. If **n** is the normal direction respect to cell surface

(s. Figure 3.9), beams incidence angles were $\alpha_1 = 33°$ and $\alpha_2 = 47°$. The internal angle between the two incident laser beams was $2\theta = 14°$. The experimental geometry and angles are displayed in Figure 3.9. In this experimental geometry beam 1 assumed the role of pump beam, while beam 2 that of signal beam.

In order to apply the external electric field E on the sample, the electrooptic cell was connected in series in the circuit displayed in Figure 3.12 B. The two extremes of the copper wires were put in series with an high voltage generator (mod. ER15R20, Glassman High Voltage, Inc., USA) and a series of 10 resistors, each one of resistance $R = 10M\Omega$. This $100M\Omega$ total resistance was used to safely protect measurement apparatus against damages caused by drastic electrical breakdowns eventually occurring in the cell. When a breakdown occurs, indeed, the resistance of the cell (whose original values in intact cells is of the order of 10^{12} - $10^{15}\Omega$) quickly drops to very low values, current flowing in the circuit proportionally growing. Thus, $R = 100M\Omega$ was a negligible value when an intact cell was connected in series, but it could limit the current in case of breakdown of the cell. A digital multimeter was connected in parallel to one of the ten $R = 10M\Omega$ resistors in order to measure the voltage V_{R2} across $R_2 = 5M\Omega$, the resulting resistance for the parallel of resistance R and the internal resistance $R_{mult} = 10\ M\Omega$ of the digital multimeter. The photocurrent flowing in the cell was measured through V_{R2} values by using the Ohm's law.

Beams 1 and 2 transmitted by the cell were directed on two flat circular mirrors (ThorLabs; M11, M22 in Figure 3.12 A) and reflected towards the detectors.
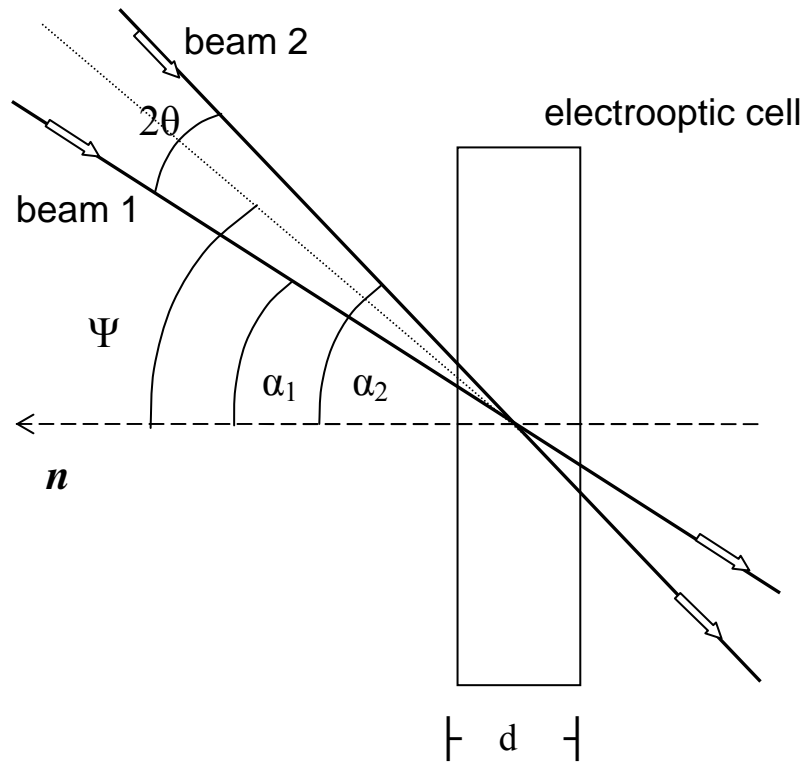
Figure 3.9 Experimental geometry of 2BC experiment. Angles of incidence of laser beams on sample electrooptic cell.

The employed detectors (DET1, DET2 in Figure 3.12 A) were two silicon photodiodes having a detection surface $S = 100$ mm^2 (Edmund Optics). Negative output voltages of photodiodes (OUT 1, OUT 2 in Figure 3.12 A), whose values were proportional to laser beams power incident on them, were connected to the inverting input channels of a low-frequency amplifier circuit (a.c.). The scheme of the homemade two stage amplifier circuit is displayed in Figure 3.10. Each amplifying stage has a fixed gain factor of 10. Amplifier circuit comprises 5 outputs, connectable to the inputs of a two channels oscilloscope (PM 3217 50 MHz, Philips). Amplifier circuit first stage outputs A_1 and A_2 provided positive voltages, while second stage ones, B_1 and B_2, provided negative voltages. Output A_1- A_2 provided the algebraic sum of signal A_1 (inverting input) and signal A_2 (not inverting input). Outputs A_1, A_2 were employed for the measurement of the laser beams power in absence of photorefractive effect, that is, before the application of an electric field to the sample (($P_1(E=0);P_2(E=0)$).
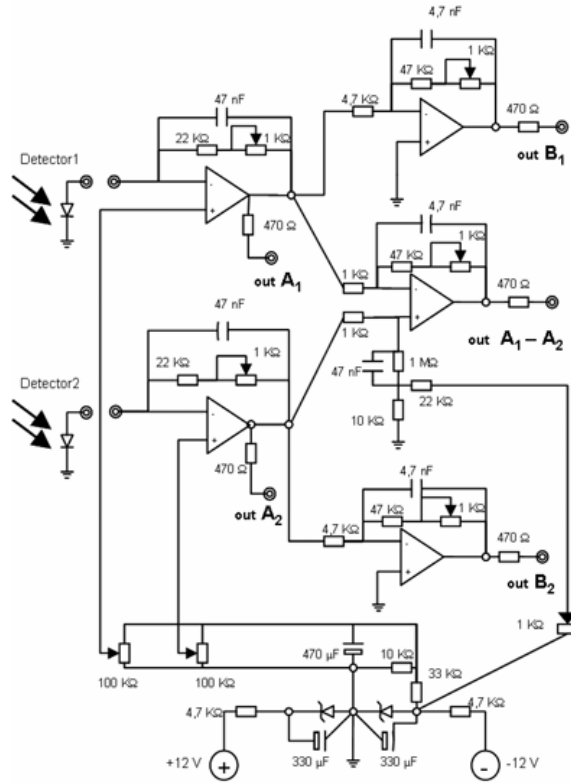
Figure 3.10 Schematic drawing of the homemade low-frequency amplifier circuit.

Signals A_1 and A_2 were indeed related to the power of laser beams incident on detectors, P_1^{DET} and P_2^{DET}; these were in turn related to beams power transmitted by the cell, P_1^{OUT} and P_2^{OUT}, if one takes into account the losses due to circuit components (mirrors, discontinuity surfaces of detectors). Such loss factor has been calculated for the experimental geometry employed in this research during the setup adjustment, obtaining the relations

$$P_1^{DET}(mW) = 0.92\, P_1^{OUT}(mW) \tag{3.2}$$

$$P_2^{DET}(mW) = 0.92\, P_2^{OUT}(mW) \qquad , \tag{3.3}$$

that is, beams transmitted by the sample cell suffered for an 8% loss of power before to arrive to detectors active surface.

Figure 3.11 displays detection apparatus adjustment data together with a linear fit representing the following calculated relations:

$$P_1^{DET}(mW) = \frac{A_1(mV)}{2189.9} \tag{3.4}$$

$$P_2^{DET}(mW) = \frac{A_2(mV)}{2236.2} \qquad . \tag{3.5}$$

94

At very low power of the incident laser beams, the values of $A_{1,2}$ were found to be correlated to $P_{1,2}$ as it is shown in the insert of Figure 3.11.
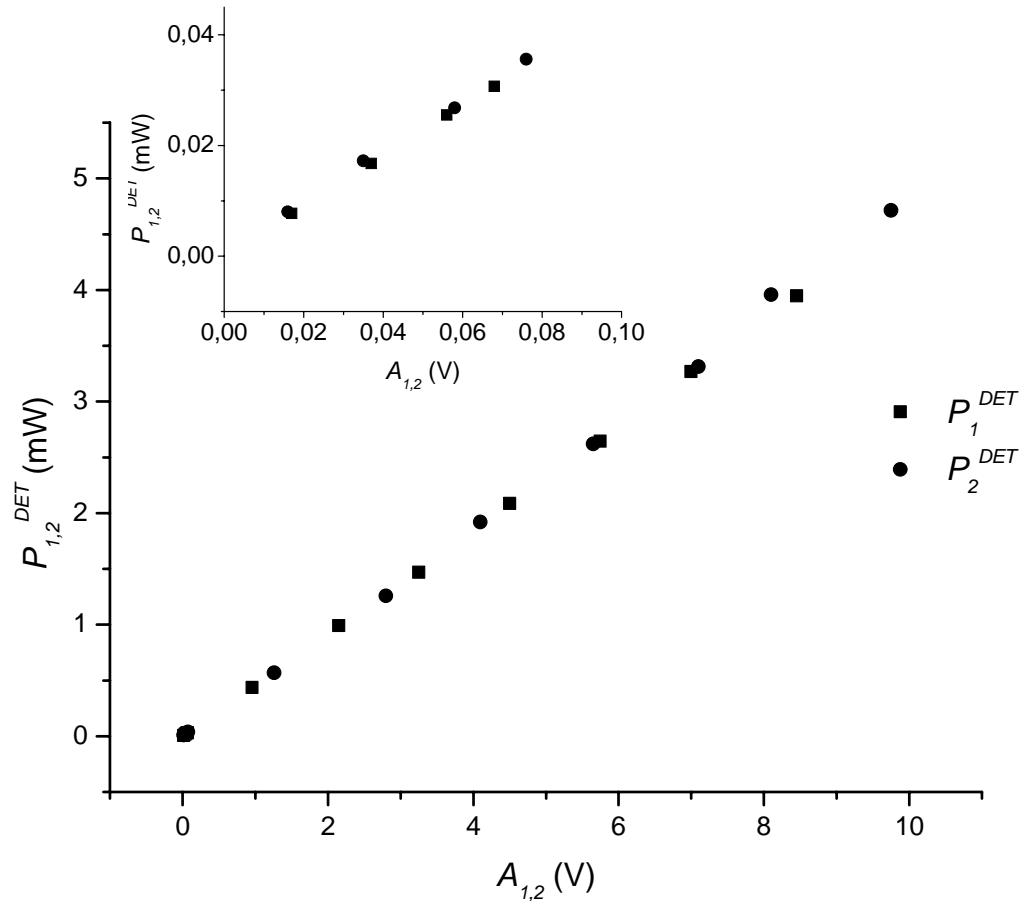

Figure 3.11 Detection apparatus adjustment data. Output voltages (first stage of a.c.) A_1 and A_2 as functions of incident beam power at detectors, P_1^{DET} and P_2^{DET}. In the insert, details of the adjustment data at low power regimen are displayed.

Amplifier circuit second stage outputs (amplified by a factor 10 with respect to A_1 and A_2 inputs) were employed for the effective measurement of signal variations due to PR effect. In such way, it was possible to measure very small signal variations and therefore to accurately evaluate the extent of the PR effect. Finally, output $A_1 - A_2$ could be helpful to evidence power transfer from pump beam to signal beam because of the choice made to use two beams of similar intensity. Indeed, when PR effect is absent, no power transfer is active and $A_1 - A_2 \approx 0$. When power transfer increases, due to the PR effect onset, $A_1 \neq A_2$ and $| A_1 - A_2|$ proportionally increases.

Measurements registration could be accomplished by means of a paper recorder (PM 8271, XYt Recorder, Philips) connected in parallel with an input channel of the oscilloscope.
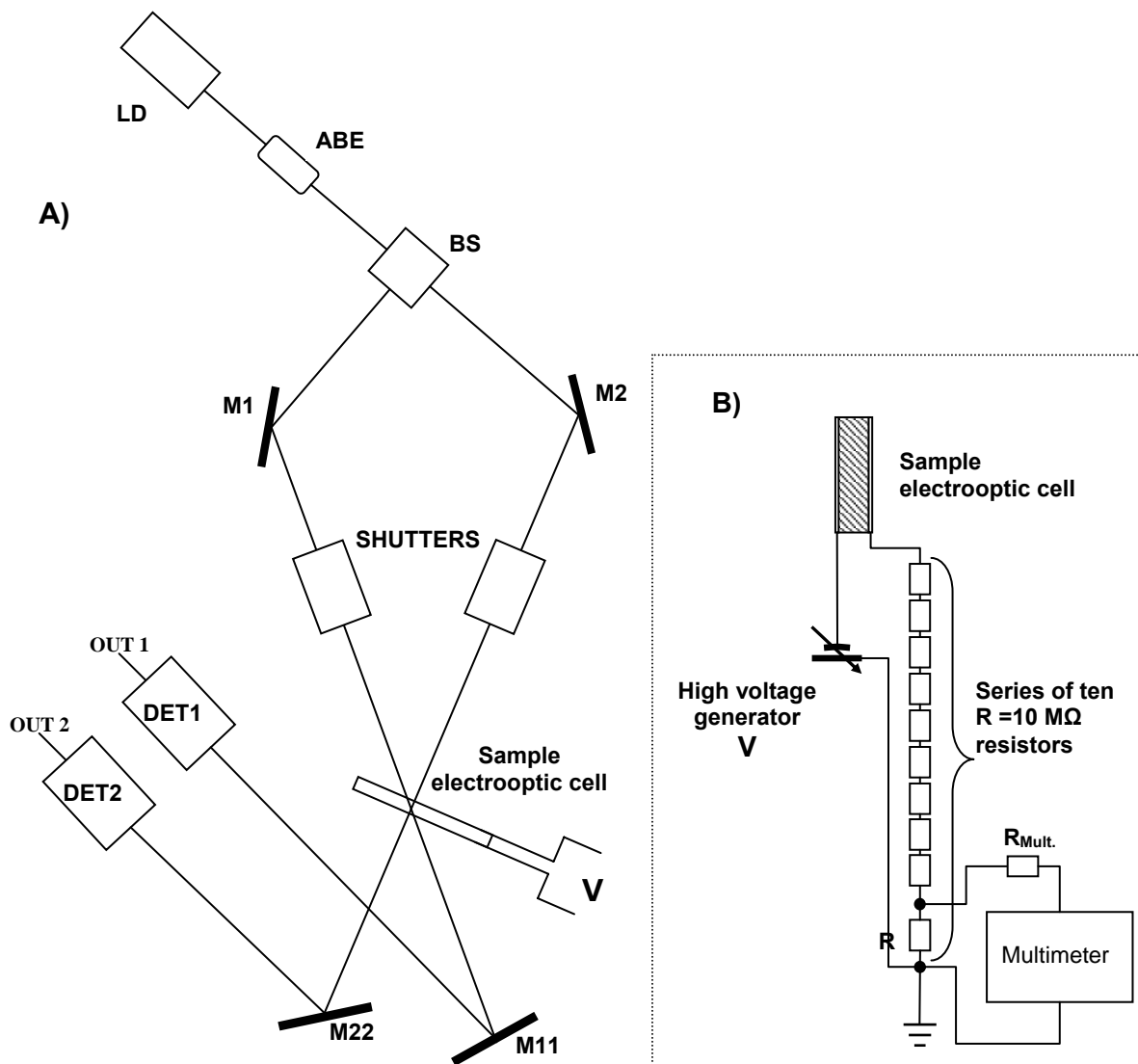
Figure 3.12 **A)** Schematic drawing of the 2BC experimental apparatus, s. text for description of components; **B)** Insert displaying the electrical circuit used to apply voltage across the cell and for photoconductivity measurements.

3.7 Measurement methods in the 2BC experiment

Photorefractivity measurements with 2BC experiment were performed employing a laser beam power P_0 = 31.7 mW. The use of a neutral filter with transmittance T = 10% (s. Sect. 3.6) reduced the emitted power, so that the beams arriving on the cell have power P_1^{IN}= 0.9 mW and P_2^{IN} = 1.2 mW. These values should be considered as average values; actual and accurate power measurements of incident radiation P_1^{IN} and P_2^{IN} have been performed for each cell individually. Indeed, the fine adjustment of the experimental setup, necessary for each cell in order to correctly position the beams in the active zone of the sample, caused some minor variations on incident beam power.

The following experimental procedure was followed for all the samples. A first measurement of transmitted power P_1^{OUT} and P_2^{OUT} was accomplished when no electric field was applied on the sample (E = 0). Photogenerated charges were not able to actively migrate and to cause the onset of the space charge field E_{SC}, responsible for PR effect; under these conditions, no power transfer is active between the beams. This measurement permitted to estimate the value of the absorbance A of the electrooptic cell in the employed experimental geometry, and then α [cm^{-1}], defined as absorbance coefficient per length unity of beam path in a medium:

$$A = \alpha l = \ln\left(\frac{I^{IN}}{I^{OUT}}\right) = \ln\left(\frac{P^{IN}}{P^{OUT}}\right) \quad , \tag{3.6}$$

with l [cm] being beam path length in the medium. It is important to take account for the effect of α in order to correctly put in evidence a net optical gain due to PR effect (s. Sect. 1.1).

Energy transfer occurring in a 2BC experiment due to PR effect is measured by means of beam coupling ratio γ_0 defined[20] (s. Sect. 1.1) as the ratio of signal beam intensity transmitted by a PR material in presence of pump beam, $I_2(I_1 \neq 0)$, over the same intensity in absence of pump beam, $I_2(I_1 = 0)$:

$$\gamma_0 = \frac{I_2(I_1 \neq 0)}{I_2(I_1 = 0)} = \frac{P_2^{OUT}\left(P_1^{IN} \neq 0\right)}{P_2^{OUT}\left(P_1^{IN} = 0\right)} \quad . \tag{3.7}$$

In the current research the measurement of $P_2^{OUT}\left(P_1^{IN}\neq0\right)$ and $P_2^{OUT}\left(P_1^{IN}=0\right)$ were accomplished by measuring the variations ΔB_1 and ΔB_2, occurring when one of the two beams was alternatively turned on or off, of the output signals B_1 and B_2 of the second stage of the a.c. described in the preceding section. Measurements of ΔB_1 and ΔB_2 have been related to variations in transmitted power ΔP_1^{OUT} and ΔP_2^{OUT}, by means of the relations (3.2), (3.3) and (3.4), (3.5). We recall here that, in the employed experimental geometry, beam 1 acted as pump beam and beam 2 as signal beam: negative ΔP_1^{OUT} and positive ΔP_2^{OUT} values were therefore expected for the onset of a PR effect. The experimental procedure consisted in applying both beams for some minutes without applying the electric field on the PR film. Then, by means of the shutter, one of the beams, e.g. beam 1, was interrupted and the variation ΔB_2^0 of signal B_2 was measured (0 superscript indicating the condition of E = 0). After some minutes, the beam 1 was switched on again; the same procedure was then repeated measuring variations on beam 1 following the interruption of beam 2. Variations ΔB_1^0 and ΔB_2^0 were always very small or negligible. They were not related to PR effect, occurring at E = 0, and therefore had to be considered as "disturbance" effects (due, possibly, to spurious reflections, or other instrumental disturbance sources) to be subtracted in the true PR measurements.

Maintaining the application of both beams on the cell, high voltage generator is turned on and voltage V is applied at the electrodes of the cell starting from very low values of V. Applied voltage values depended on sample thickness that was fixed for all the cells at t = 22.8 μm, the microsphere spacers diameter. Voltages to be applied were chosen in order to record measurements at applied electric field E values starting from E = 0 V/μm up to values of the order of E = 90 V/μm, with steps of about 5 V/μm each. For each value of the applied electric field the same experimental procedure was used. Some minutes were elapsed since the application of a new value of E with both beams turned on, in order to permit the onset and stabilization of the photogenerated charges lattice. Then, beam 1 was interrupted by a shutter (P_1^{IN} = 0; $P_2^{IN}\neq$ 0); ΔB_2 variation of beam 2 is measured due to the vanishing of photorefractive effect in condition of uniform illumination (only one beam is present). Interference pattern is then restored switching on again beam 1 and PR effect is then recovered (beam 2 gained in power at the expense of beam 1). The same procedure was repeated for beam 1, turning off beam 2 ($P_1^{IN}\neq$ 0; P_2^{IN} = 0) and measuring the related ΔB_1 variation. Having restored illumination by both beams, applied electric field E was changed to the subsequent value and so on. Applied electric field E was increased, when possible, up to the maximum value of E = 90 V/μm. Indeed, sometimes cells experienced electric breakdown

at lower values of E. When an electrical breakdown occurred, the cell was usually irreversibly damaged; microspots of damaged blend acted, indeed, as low resistance channels through which current preferentially flowed, making cells unserviceable. As an example of output signals variations, in Figure 3.13 the variation ΔB_1 of signal B_1 due to some cycles of alternatively switching on and off of beam 2 is displayed.
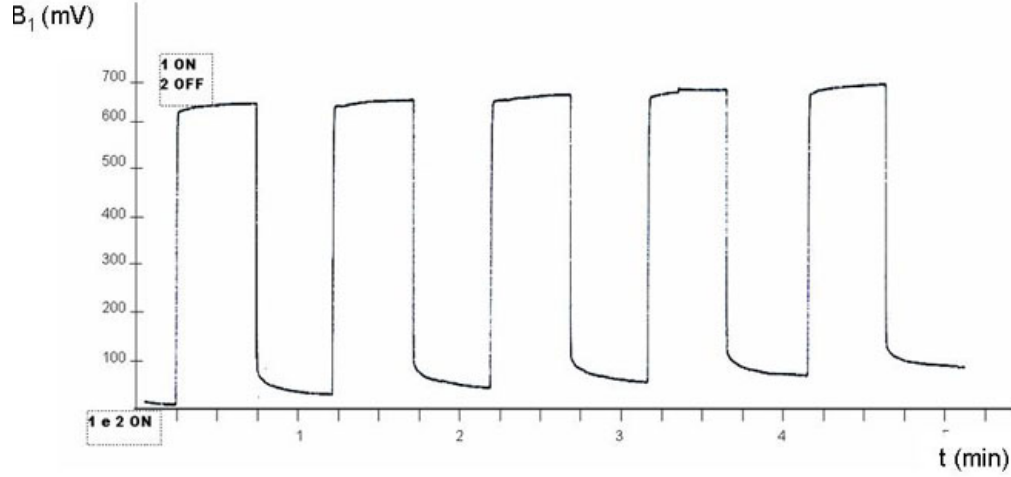

Figure 3.13 Output signal B_1 related to beam 1 (pump beam) intensity. Effect of imposing alternate cycles of switching beam 2 on (1,2 ON) and off (1 ON, 2 OFF).

The values ΔB_1 and ΔB_2 obtained for each value of the applied electric field were corrected from disturbance effects subtracting the described ΔB_1^0 and ΔB_2^0 values; relations (3.2), (3.3) and (3.4), (3.5) permitted finally to calculate the corresponding variations in transmitted power due to PR effect, ΔP_1^{OUT} and ΔP_2^{OUT}.

For each beam, at each applied electric field value, it was therefore possible to obtain the values $P_1^{OUT}(P_2 \neq 0)$ and $P_2^{OUT}(P_1 \neq 0)$, that is, beams power affected by PR energy transfer. It was simply made by adding the variations (with signs) to the P_1^{OUT} and P_2^{OUT} measured at E = 0:

$$
\begin{aligned}
P_1^{OUT}(P_2^{IN} \neq 0) &= P_1^{OUT} + \Delta P_1^{OUT} \\
P_2^{OUT}(P_1^{IN} \neq 0) &= P_2^{OUT} + \Delta P_2^{OUT}
\end{aligned}
\qquad (3.8)
$$

Beam coupling ratio (3.7) was obtained for each beam at each applied electric field value through the formulae:

$$\text{(beam 1)} \quad \gamma_0^1 = \frac{P_1^{OUT}(P_2^{IN} \neq 0)}{P_1^{OUT}(P_2^{IN} = 0)} \tag{3.9}$$

$$\text{(beam 2)} \quad \gamma_0^2 = \frac{P_2^{OUT}(P_1^{IN} \neq 0)}{P_2^{OUT}(P_1^{IN} = 0)} \quad . \tag{3.10}$$

Beam coupling ratio γ_0 is related to PR optical gain Γ through the following relations (s. Sect. 1.1):

$$\gamma_0 = \frac{(1+b)\exp(\Gamma l)}{b + \exp(\Gamma l)}; \quad \Gamma = \frac{1}{l}\left[\ln(b\gamma_0) - \ln(1 + b - \gamma_0)\right] \quad , \tag{3.11}$$

with

$$b = \frac{I_2(0)}{I_1(0)} \tag{3.12}$$

being defined as the ratio of the incident beams intensities and l is the beam path length inside the sample. Experimentally, b was calculated as the ratio of incident beams powers:

$$b = \frac{P_2^{IN}}{P_1^{IN}} \quad . \tag{3.13}$$

Photorefractive optical gains Γ_1 and Γ_2 for corresponding beams were calculated by using (3.11); Γ_1 values were, obviously, negative, indicating the loss of optical power experienced by pump beam, while Γ_2 values were positive, indicating power gain of signal beam caused by PR effect. It is important to notice here that Γ_1 and Γ_2 values are equal in modulus when other effects or mechanisms are not present, as, for instance, power losses due to beams diffracted at higher orders by the charge lattice or other minor effects[168,169]. Energy transfer efficiency, indeed, is often affected by imperfections so that Γ_2 values can be slightly lower in modulus than Γ_1 ones. Furthermore, because of the tilted geometry employed in a 2BC experiment ($\Psi \neq 0$, tilt angle between normal incidence direction to cell and beams paths bisector), and because of the many discontinuity surfaces between media at different refractive index n encountered by beams traversing the cells (interfaces air/glass/ITO/sample blend/ITO/glass/air), many reflections are produced. Some of them, those occurring before

the entrance in the PR material, cause only a minor (often negligible) power loss; other reflections cause multiple reflections inside the material. These last reflected beams inevitably interact each other and with incident radiation and could possibly cause the onset of many different competing patterns, thus giving origin to diffracted beams on different optical paths. These rather complicated mechanisms have been sometimes taken in consideration and reported as a source of power loss for signal beam[169]. Nevertheless, all these detrimental effects are frequently of minor importance if compared to PR effect due to principal interference pattern and thus they are safely negligible in the vast majority of cases.

Calculations made on photorefractive data in order to obtain photorefractive optical gains Γ_1 and Γ_2, their analyses and plotting were performed using an Origin 7.0 software (OriginLab, USA).

3.8 Photoconductivity measurements

PC measurements were accomplished by using the same experimental apparatus employed for 2BC PR measurements and on the same electrooptic sample cells. The current flowing in the circuit of Section 3.6 and displayed in Figure 3.12 B) was obtained from the value of the voltage measured on a known resistor of resistance R = 10MΩ put in series with the cell. The measured current was made up of a dark current contribution, i_{dark} (referring to the current flowing in the cell and circuit in the absence of incident radiation on sample), and a photocurrent, i_{ph} due to migration of photogenerated charges under the applied electric field (s. Sect. 1.5). In PC materials dark current should be very low, so that they act as insulators in the dark and as conductors or semiconductors under light irradiation at proper wavelength. Usually i_{ph}/i_{dark} ratios of 10-100 or more are expected for good photoconductive materials, especially in PR applications where current flows in the dark have to be avoided in order to achieve non-volatile holograms. Such condition for current ratio was met for all the blends in the present research. In one case, as reported in Section 3.3 when describing NPEMI-E purification procedures, insufficiently purified samples of NPEMI-E were tested whose dark current values resulted to be abnormally high. This was correctly ascribed to impurities existing in the blend. Measurements performed on samples after a further purification restored normal dark current values.

If dark current is negligible with respect to photocurrent, this last could be obtained by V_{R2} voltage measurements (s. Section 3.6) through the relation:

$$i_{ph} = \frac{V_{R2}}{R_2} \quad . \tag{3.14}$$

Values of photocurrent reported in this research refer to i_{ph} values measured under illumination by only the beam 2 in the already described geometry of 2BC experiment. All measurements have been performed on the same range and with the same values of the applied electric field E used in 2BC optical gain measurements.

Being d = 3 mm the diameter of circular section of beams, the surface of sample irradiated by laser light is found to be S = 7.07 10^{-2} cm^2. From this value it is possible to calculate another important figure, the photoconductivity σ defined as

$$\sigma = \frac{i_{ph}}{ES} \quad . \tag{3.15}$$

Photoconductivity σ has dimensions [Ω^{-1} cm^{-1}], when other quantities are expressed as E [V/cm], S [cm^2], i_{ph} [A] and it is commonly used as a parameter to compare different photoconductive materials.

Data of PC measurements were analysed and plotted with an Origin 7.0 software.

3.9 Calorimetric analysis (DSC)

Calorimetric analysis was accomplished with a Perkin Elmer DSC7-type Differential Scanning Calorimeter controlled by an interface TAC-7/DX Perkin-Elmer driven by Pyris Software Version 3.52. The instrument was equipped with a liquid nitrogen variable temperature controller that enabled measurements with block thermal stabilization down to T = -70°C Measurements were performed under atmosphere of nitrogen, used also as purge gas. High purity grade Indium and cyclohexane were the standards for precise temperature determinations (error of 0.1°C).

Samples of average weight of ~ 5 mg were introduced in Al sample holders cells. For each thermal scan a *blank* thermogram was recorded on an empty cell, using the same experimental conditions, in order to be subtracted from sample thermograms. The obtained thermograms permitted the evaluation for each sample of the quantities: melting point, T_m; recrystallization temperature on heating, T_{cryst}; glass transition temperature, T_g; specific heat change associated to T_g, ΔC_p; glass transition width, ΔT, defined as the length of temperature

range in which T_g occurs ($\Delta T = T_{end} - T_{onset}$). T_g was measured as *fictive temperature*, that is temperature at which intersection between enthalpy curves of liquid and glass phases occurs. Analyses on thermograms and calculation of the quantities of interest were performed with the aid of an Origin 7.0 software (OriginLab Corp., Northampton, MA, USA).

3.10 Spectroscopic Ellipsometry measurements

Spectroscopic Ellipsometry (SE) measurements were performed with a mod. GES5E Spectroscopic Ellipsometer (SOPRA S.A., Bois-Colombes, France) equipped with a 1024 pixel CCD array in Multi Channel Measurement Mode, over the wavelength range 190 – 900 nm. Measurements were accomplished with rotating polarizer technique in reflection arrangement, using Xe lamp (Hamamatsu Inc., Japan) of intensity I $\approx$ 150 mW/cm^2 as light source. Polarizer rotation frequency was fixed at 6Hz, angle of incidence (AoI) of the light beam over samples was fixed at AoI = 60°, analyzer angle at A =45°; signal integration time was t = 2s. SE measurements were performed on ITO cells of mean thickness d $\approx$ 22.8 μm of the same geometry of those used in photorefractive 2BC measurements. Cells were mounted on a homemade sample holder; cell lied horizontally on a base, its upper side facing SE incident beam. Lower face of the cell was in thermal contact with the refrigerating side of an electronically controlled Peltier cell in order to stabilize temperature. All the measurements have been conducted at T = 23.0 °C. Cell was tightly fixed to Peltier cell with the aid of plastic clamps. High voltage was applied using calibrated power supply (high voltage generator) connected with the circuit of a reference resistor and cell in series. Applied voltage measurements were performed with a digital multimeter connected in parallel to the cell. SE data for each sample blend were collected for applied electric field from E = 0 V/μm up to E $\approx$ 30 V/μm. Refractive index n at λ $\approx$ 685 nm and E = 0 V/μm was calculated for each cell using SE data in the range 600< λ < 900 nm.

Δn at different values of applied electric field E, calculated as the difference $\Delta n(E) = n(E) - n(E=0)$, gave a measure of the variation of the refractive index at a particular value of E from its value when electric field is not applied.

Due to the complexity of arrangement in the multi-layered structure of employed cells, in order to obtain a complete description of refractive index in these blends it was necessary to define a complete set of couples n,e (refractive index, thickness) measured in various position. Different n_i, e_i are defined, subscripts referring to different positioning of the incident beam on the cell.

SE measurements were performed adhering to the following experimental procedure:

0) *SE measurement on Al foil*; for this substrate for which reflectivity R ≈ 1 is assumed, the measurement was performed in order to obtain an intensity background that takes into account the wavelength dependence of source light intensity. This measurement was performed prior to all other measurements.

Subsequently, on each cell we have performed four different types of measurements in different areas of the cell summarized as follows (s. Figure 3.14):

1) *SE measurement in "air gap" zone <u>outside</u> the blend, points 1,2*; reflection came out by the air layer between the two glass sheets; by measuring the distance between fringes of the interference pattern, assuming refractive index n=1 for air, it was possible to extract the sample thickness e_1 and e_2. Comparing these values, being known the distance between points 1 and 2, it was possible to obtain information about parallelism of glass sheets and therefore whether the thickness of the cell is uniform or not.

2) *SE measurement in "blend" zone, point 3*; reflection came out by blend layer between the two glass sheets; by measuring the distance between fringes of the interference pattern, assuming uniform sample thickness ($e_3 ≈ e_1$) , it was possible to extract refractive index $n_2 = n$ of the blend. Using a regression technique it was also possible to determine e_3 and compare how well the equivalence $e_3 ≈ e_1$ fitted with experimental data.

3) *SE measurement in "active" zone, point 4*; reflection came out by blend layer between the two ITO layers (thickness) covering the glass; by measuring the distance between fringes of the interference pattern, assuming uniform sample thickness ($e_4 ≈ e_1$) , it was possible to extract refractive index $n_2 = n$ for the blend. Using a regression technique it was also possible to determine e_3 and compare how well the equivalence $e_4 ≈ e_1$ fitted with experimental data.

The refractive index n measured with this procedure is then called n_0, indicating that its value is obtained without the application of an electric field, i.e. $n_0 = n(E=0)$, in order to distinguish n_0 from values n (*E*) obtained under the application of an electric field (s. following).

4) *SE measurement in "active" zone, point 4, E ≠ 0*; n is measured with the same procedure in the same point 4 of the active blend for increasing values of an externally applied electric field E. The change in the value of n with respect to n_0 (measured as described at the preceding step) is defined as $\Delta n = n\,(E) - n_0$.

The effect on refractive index n of blends due to the application of an electric field E was verified to be reversible, i.e. it vanishes when applied voltage is turned off, returning to the zero-field value n_0.
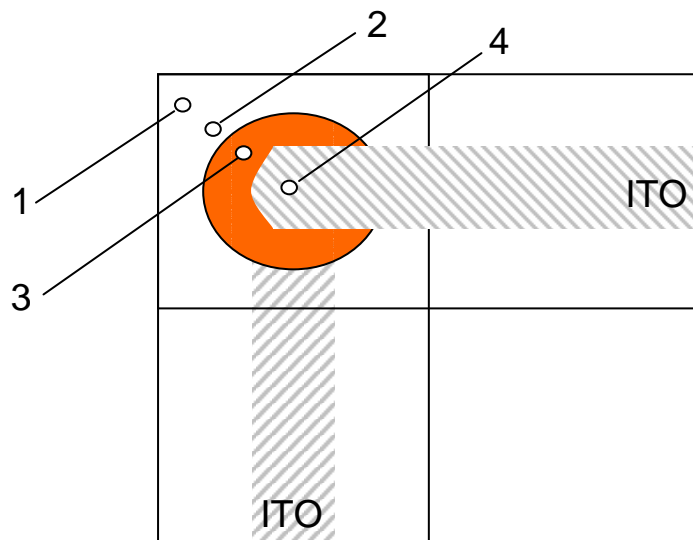
Figure 3.14 Schematic drawing of electrooptic cell displaying points 1-4 selected to perform SE measurements; points 1,2 – "air gap zone", thickness measurements; point 3 – "blend zone", refractive index n measurements; point 4 – "active zone", Δn vs. applied voltage V measurements.

4. Results and discussion

4.1 MOPAC-7 calculations of the relevant electrooptic parameters of the chromophores

The selection of the new class of molecules to be synthesized and studied in this research has been based on some theoretical predictions and on calculations of the relevant parameters for PR effect (s. also Sect. 2.2). Besides the already described compatibility considerations on the basis of chemical similarity of the indolyl structures and of the introduction of chemical groups described to prevent crystallization, a careful preliminary study on the molecular electrooptic parameters was performed. The aim was indeed twofold: on one side the molecules to be selected were demanded to act as efficient and compatible NLO-chromophores when used in blends with photoconductive PVDMI; on the other hand, their properties must permit their use as LMWG, that is they must own all the necessary properties to act themselves as PR materials, when used in the pure state. Some preliminary estimates on charge generation and photoconductive properties could be made on the basis of foreseen values of ionization potential ip. The optimization of NLO properties could be accomplished by taking into account some general rules[33] concerning the relevant molecular parameters: ground-state electrical dipole moment (edm) μ, linear polarizability α together with its anisotropy $\Delta\alpha$, first order hyperpolarizability β. When dealing with low-Tg organic materials ("soft" materials), the contribution of the orientational enhancement effect[27,31,32] (s. sect. 1.4) to PR effect, due to the reorientation of the NLO chromophores under the effect of the externally applied electric field, must be taken into account. The extent of this reorientation and of the resulting orientational enhancement to PR effect are described by the Kerr figure of merit F^{Kerr} (s. Eq. (1.40), Section 1.4,). F^{Kerr} is a function of the electrooptic parameters and it summarizes the requirements for an efficient PR NLO-chromophore. Theoretical calculations performed with MOPAC-7 software (J. J. P. Stewart, QCPE, Version 7; 1993) permitted to comparatively evaluate the properties of a series of indolyl derivatives[170]. On the basis of these calculations the choice was made to select the series of push-pull indolyl derivatives to be studied. Data obtained for these molecules are listed in Table 4.1, together with those referring to the frequently employed DMNPAA chromophore, reported for a useful comparison, and to those of the PC polymer PVDMI used for the PR blends. The term c^2 appearing in Table 4.1 is a parameter that specifies the extent of polarization of the polarizable π-system of the chromophore; it measures how much negative and positive charges are separated in push-pull molecules[34].

Table 4.1 Relevant electrooptic molecular parameters computed by MOPAC-7 software for NPEMI-R, MeO-NPEI-E, NO$_2$-NPEI-E, MeO-NPEMI, NO$_2$-NPEMI NLO chromophores series and PVDMI[170]. DMNPAA data are listed for comparison.

molecule	c^2	μ (10^{-30} C m)	$\Delta\alpha$ (10^{-40} C V^{-1} m^2)	β (10^{-50} C V^{-2} m^3)	F^{Kerr} (10^{-74} C^2 V^{-2} m^4 Kg^{-1} mol)	ip (eV)
DMNPAA[a]	0.16	21.4 (6.43 D)	22.0	56.0	0.20	7.54
NPEMI-R	0.32	27.4 (8.23 D)	74.32	7.82	0.39	7.76
MeO-NPEI-E	0.30	26.72 (7.43 D)	71.53	6.19	0.31	7.35
NO$_2$-NPEI-E	0.35	34.58 (10.37 D)	70.98	5.80	0.35	7.92
MeO-NPEMI[b]	0.32	25.41 (7.62 D)	75.10	5.79	0.34	7.29
NO$_2$-NPEMI[b]	0.34	36.92 (11.47 D)	75.40	6.01	0.37	7.82
PVDMI		8.22 (2.47 D)				8.02

a) Data reported for DMNPAA are from Table 1 of ref. 33, apart from ip values, that were computed by the MOPAC-7 software.
b) For these two molecules, in which the methyl group in 2-position is again present and the N-2-ethylhexyl is missing, only the reported computed data are available.

In Table 4.1 NPEMI-R refers to NPEMI molecule bearing a generic alkyl substituent on the 1-nitrogen atom of indole ring. Indeed, it has been found that only methyl substituent, with its peculiar electron releasing characteristics, can appreciably change π-conjugated electrons distribution. On the contrary, different alkyl substituents (e.g. ethyl, 2-ethylhexyl, allyl) give rise to very negligible changes in the relevant electric and electrooptic parameters; therefore NPEMI-R values are intended to be valid for NPEMI, as well as for NPEMI-A and NPEMI-E.

Coming now to a discussion of the obtained data, it is important to evidence that, as concerns the NPEMI-R series NLO chromophores, the calculated value of F^{Kerr} is about two times larger than that of DMNPAA. Recalling the definition of F^{Kerr} (s. Eq. (1.40), Sect. 1.4), it is clear that this result is due mainly to the stronger dipolar character of NPEMI-R dyes, feature reflected in the improved c^2 and edm values. An important contribution to the improvement of F^{Kerr} is also due to the three times larger value of $\Delta\alpha$, the linear polarizability

anisotropy. On the contrary, first hyperpolarizability β of NPEMI-R dyes is markedly reduced with respect to that of DMNPAA. This last parameter β is much less involved in orientational contribution (BR) than edm and $\Delta\alpha$; it is indeed mostly related to Pockels effect (EO contribution to PR effect). It is therefore rational to make a prevision for these molecules to act as PR materials primarily through BR contribution rather than through EO one ($\Delta n_{EO} < \Delta n_{BR}$), and it is possible to expect a strong dependence of their PR behaviour from factors influencing their orientational mobility (free volume, T_g, intermolecular interactions, collaborative phenomena).

The value of $c^2 = 0.32$, that specifies the extent of polarization of the polarizable π-system of the chromophore, places NPEMI-R in an intermediate position between the neutral ($c^2 = 0$) and the totally polarized (zwitterionic, $c^2 = 1$) electronic structures, with a good push-pull character. The value of c^2 for NPEMI-R is not so far from some of the c^2 values reported for merocyanine dyes in Table 1 of ref. [33]. The resulting value of F^{Kerr}, when compared with those of the already cited molecules[33] is not exceptionally high. Nevertheless it could be considered sufficiently high to give a good "orientational contribution" to the measured photorefractivity. As concerns PC, the particularly low value of the computed ip = 7.76 eV for NPEMI-R (ip = 7.65 eV was previously computed for N-ethylcarbazole[85], s. Sect. 2.1.), permits to expect good photocurrent values even for neat materials, i.e. without the addition of PVDMI as photoconductive polymer. Such value of ip is lower than that already reported for N-ethyl-2,3-dimethylindole (the model compound for PVDMI): an ionization potential ip = 8.02 eV was previously computed for it[85], s. sect. 2.1. It seems reasonable, therefore, as it has been verified (s. Sect. 4.4), to expect an increase in PC for blends more rich in NPEMI-E or NPEMI-A. As a concluding remark, the low value of ip could also have important consequences in the formation of the traps due to considerations related to GDM formalism[16,58,60,62] to be discussed when dealing with PC measurements results (s. Sect. 4.4).

Even if electrooptic parameters have been shown to be similar for all NPEMI-R molecules, leading to the consideration of a similar PR behaviour for differently substituted N-alkyl derivatives of NPEMI, other considerations have to be done in order to select NPEMI, NPEMI-E and NPEMI-A (s. Sect. 2.2).

The choice to introduce an asymmetric 2-etyhlhexyl group as alkyl substituent on the 1-nitrogen atom of the indole ring, obtaining NPEMI-E, was made on the basis of the often reported capability of such group to avoid chromophore crystallization. This behaviour seems to be originated by the disorder and the steric hindrance provoked by the quite long and asymmetric alkyl "tail"; it is able to assume numerous different conformations and probably could prevent chromophores from coming in contact in the proper orientation to crystallize

109

(this event leading to phase segregation, s. Sects. 1.6 and 2.1). The 2-ethylhexyl group should favour the formation of a glass state through its steric hindrance and conformational disorder. Moreover, 2-ethylhexyl chain could even go against the interactions with neighbour chromophore moieties. Indeed, it has been reported for many highly polar NLO species that they could give rise to aggregation phenomena: dimers in head-to-tail arrangement are formed, leading to strong reduction of edm and thus to reduction of NLO and PR performances. The 2-ethylhexyl chain is said to avoid all such drawbacks. Anyway, as it has been already verified[33], the 2-ethylhexyl group has not invariably this effect: sometimes the glass forming capability and the stability of glass-phase could not be simply related to its presence (s. Sects.4.3.1.4 and 4.3.1.5). A role is possibly played by the methyl group in the 2 position of indole ring, present in both NPEMI-E and NPEMI-A. As it will be described in Sect.4.3.1, they showed a very low tendency to crystallize. Moreover, it has been demonstrated[83,84,85] that the presence of methyl group in that position also increases the electron density on the indole ring. NPEMI-A, that maintains on the position 2 the methyl group but has on the indole nitrogen atom (position 1) a small allyl group in place of 2-ethylhexyl chain, shows a propensity to crystallize that is just a little higher than that of NPEMI-E. On the contrary, the two other different chromophores that we have synthesized, namely MeO-NPEI-E and NO_2-NPEI-E, both having the 2-ethylhexyl group on the indole nitrogen and the $-OCH_3$ or the $-NO_2$ group, respectively, on the position 5 but missing the methyl group on the position 2, have a lower tendency to remain in glass phase. From these results it can be possibly inferred that electronic contributions can be as much important as the steric ones.

NPEMI-A was selected to study its PR behaviour in comparison with that of NPEMI-E. The aim was to investigate the role of alkyl substituent on the 1-nitrogen atom of indole ring and of glass transition temperature T_g (these are indeed the only different features in NPEMI-E and NPEMI-A, the rest being identical) on interactions occurring inside PR blends. Moreover, a possible outlook could be the use of NPEMI-A as a pendant substituent in the functionalization of a poly-siloxane chain, due to the presence of an unsaturated alkenyl chain (allyl). A totally functionalized polymer could be realized in which phase-segregation phenomena could be totally excluded.

MeO-NPEI-E and NO_2-NPEI-E were selected in order to study the changes caused by the introduction of functional groups, having opposite electronic characteristics, in the same chemical site (position 5 of the indole ring) of a quite identical chemical structure. MeO functional group, indeed, is known to be a strong electron donor, while NO_2 group is a strong electron acceptor. Such groups dramatically influence charge distribution of π-conjugated

110

electrons, therefore changing edm and polarizability of the substituted compounds. Data of these parameters have been computed in order to have some quantitative predictions, and Table 4.1 reports values concerning MeO-NPEI-E and NO$_2$-NPEI-E. It is evident that, as expected, the presence of the methoxy group leads to a very strong and interesting lowering of the ionization potential ip even with respect to that of NPEMI-R. On the contrary, the nitro-group increases the value of ip and particularly that of edm. The other two molecules reported in Table 4.1 have been studied only by theoretical calculations, MeO-NPEMI and NO$_2$-NPEMI. Besides the methoxy and nitro group in position 5 of the indole ring, they have also the methyl group in position 2 as it happens for NPEMI-E but they are missing the alkyl groups on the 1 position (nitrogen atom). Their characteristics are very similar to those of the corresponding NPEI derivatives, with the value of ip further decreased for the methoxy-derivative. These modifications, in turn, are clearly responsible for the observed different thermal behaviours (due to the occurrence of different intermolecular interactions), s. Sects. 4.3.1.4 and 4.3.1.5, and for the shifted position of bands in UV-Vis absorption spectra of CTC formed with TNFM (s. Sect. 4.2).

4.2 Charge transfer complexes with TNFM. UV-Vis spectra

CTC formation among electron-donor moieties (carbazole or indole derivatives) and electron-acceptor ones had been extensively tested and reported[52,171]. Carbazole and its derivatives had shown to form 1:1 stoichiometric complexes when used with the well known electron-acceptor molecules TNF (2,4,7-trinitrofluorenone) or TNFM (2,4,7-trinitrofluorenylidenmalononitrile); these two species are among the most widely used photosensitizers in the formulation of PC and/or PR blends. Evidences for the formation of such charge transfer complexes can be obtained by the examination of UV-Vis spectra of equimolar mixtures of the two components (electron donor and acceptor moieties). The onset of a broad absorption band in the visible region, not present in the respective spectra of isolated compounds, is related to excitations of level HOMO or HOMO2 of CTC (s. Figure 1.6, Sect. 1.5). Such bands, found at higher values of wavelength respect to absorptions of single isolated compounds, make clear the presence of less energetic transitions. In some previous researches,[71,82,83,84,85] CTC formation with TNFM has been demonstrated in indolyl polymers. In these latter cases absorption bands onset has been evidenced in 500 – 700 nm region. It is important to remark that absorbance maximum values of these bands were extremely lower than those referring to absorptions from single isolated components. This is the reason why spectra must be recorded on very concentrated solutions (10^{-2} M in

111

dichloromethane, s. Sect. 3.2) in order to evidence CTC bands. Dichloromethane has been selected as a good solvent because its absorptions are negligible in all the wavelength range of interest and they become preponderant only at wavelengths $\lambda < 240$ nm. All spectra have therefore been recorded over the spectral range $250 < \lambda < 900$ nm.

Taking into account these previous studies, CTC formation has been investigated for NLO chromophores object of this study, complexed with TNFM. UV-Vis spectrum of TNFM in dichloromethane is displayed in Figure 4.1. UV-Vis spectra of 1:1 molar NLO chromophore/TNFM mixtures in dichloromethane solution are displayed in Figures 4.2 – 4.6. The onset of a broad absorption band has been verified in all cases; such band is absent in the spectra of single components.
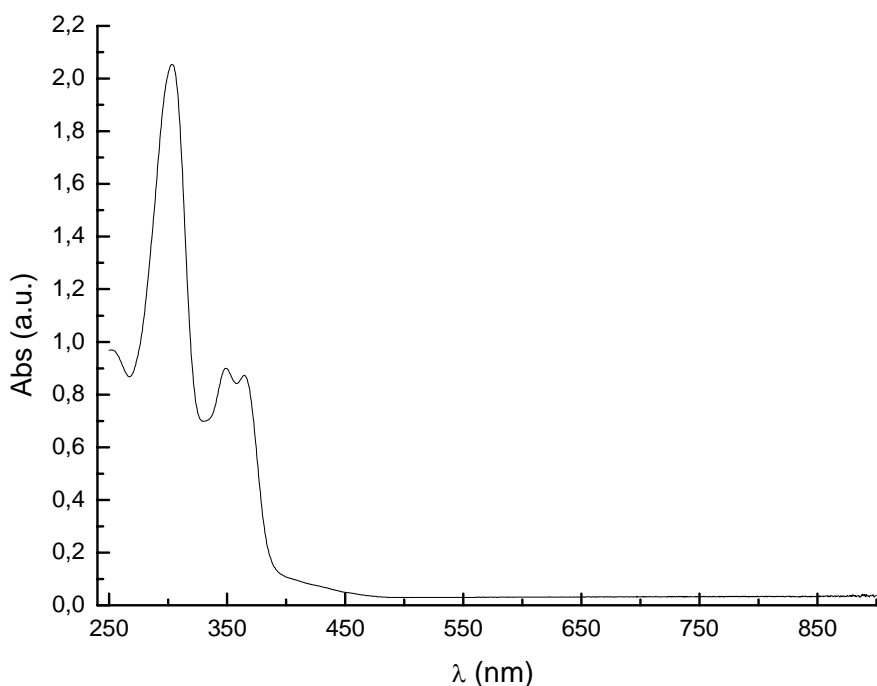
Figure 4.1 UV-Vis spectrum of 2,4,7-trinitrofluorenilidenmalononitrile (TNFM) in CH_2Cl_2.

All spectra underwent a band deconvolution process in order to distinguish CTC band from absorptions due to the NLO chromophore or the sensitizer (s. UV-vis spectra of isolated compounds, Sect. 6.3, and Figure 4.1). The band related to absorption by the CTC was found in all cases at larger wavelengths respect to what has been reported for CTC formed by indolyl polymers with TNFM[83,84]. In that case, indeed, the onset of two different asymmetrical absorption bands was observed[52] caused by two different transitions occurring in the CTC species: the first one, centered at larger wavelengths (lower energy transition), has been imputed to HOMO-LUMO transition and it is more intense; the second one, at lower wavelengths, has been imputed to a more energetical HOMO2-LUMO transition and is

112

characterized by a weaker intensity. In particular, as concerns PVDMI, the onset of two absorption bands respectively centered at λ_1 = 505 nm and λ_2 = 668 nm, was found. The value λ = 668 nm represents the larger value obtained for the complete series of variously methylated polymer indole derivatives[82,83,84]. The presence of two possible and distinct bands had been previously reported in the literature; a study investigating CTC formation among chloranil and 1-alkylcarbazole species tried to establish a relationship between the geometry of the formed complex with energy of permitted transitions[52]. In the case of asymmetric geometry, both transitions from HOMO and HOMO2 are allowed and detectable. On the other hand, when symmetric geometry is ascribable to the formed CTC complex, which is the case for carbazole monomer, only lower energy transition is favoured. Nevertheless, in the case of CTC of PVK, two absorption bands were found in its UV-Vis spectrum.

As concerns NLO chromophores object of this study, even if these compounds actually contain indole asymmetric units, nevertheless their CTC with TNFM showed the onset of a single absorption band in their UV-Vis spectra, i.e. the one at larger wavelength. As a second important feature, these bands appear to be very broad (bandwidth W, defined as full width at half maximum (FWHM), is W ≈ 300 nm), practically straying in the NIR. This last feature takes on a great importance because it can provide a good efficiency of CTC excitation at the emission wavelength of the laser diode employed in the 2BC measurements (λ_{LD} = 685 nm) and also in commercial applications. Due to the broadness of the main absorption band, a hypothesis could be done that the weaker absorption at lower wavelength related to HOMO2-LUMO transition, although not visible, could be totally covered by the main CTC absorption band and/or by the NLO chromophore absorptions.

It is important to remark that laser irradiation at λ_{LD} = 685 nm does not precisely correspond to absorption maximum for anyone of the investigated NLO chromophores. This feature obviously influences the number of photogenerated charges. Data of absorbance at λ = 685 nm have been gathered, s. Table 4.2, for the NLO chromophores together with those pertaining to PVDMI whose photoconductivity has been widely investigated[82,83]. Absorbance data turned out to be quite similar or even larger than those of PVDMI or other polymer photoconductors (PVI, PVK), making reasonable the expectation for a good PC behaviour (in particular as concerns photogeneration efficiency) of these novel species.
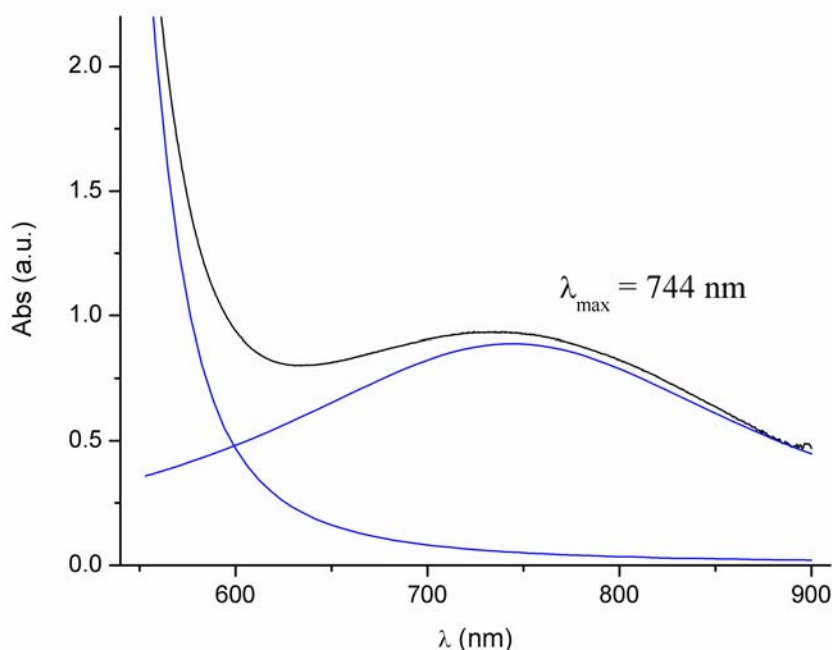
Figure 4.2 Magnified portion of the UV-Vis spectrum of 1:1 NPEMI/TNFM mixture in CH_2Cl_2, black line. Deconvoluted spectrum with the onset of CTC band centered at λ_{max} = 744 nm is displayed in blue.

Table 4.2 UV-Vis spectroscopic data obtained from deconvolution of spectra of CTC formed between TNFM and NLO molecules. Data are related to CTC absorption band (HOMO-LUMO transition of CTC).

molecule	λ_{max} (nm)	A [a] (a.u.)	W [b] (nm)	$A_{685\,nm}$ [c] (a.u.)
NPEMI	744	0.88	312	0.88
NPEMI-A	782	0.64	306	0.57
NPEMI-E	809	0.67	298	0.55
MeO-NPEI-E	778	0.79	319	0.59
NO$_2$-NPEI-E	638	0.86	205	0.73
PVDMI	668	0.31	316	0.28

a) A is the absorbance related to the maximum of CTC absorption band.
b) W is the FWHM bandwidth of the CTC absorption band.
c) $A_{685\,nm}$ is the value of absorbance at λ = 685 nm = λ_{LD}, the emission wavelength of the laser diode employed in 2BC measurements.

The displacement occurring in the absorption maximum position for CTC band of the studied series of NLO chromophores can be rationalized by means of some considerations. The diverse electronic distributions on the indole ring, caused by the different inductive and resonance effects of the various substituents, have been already described as one of the main

114

factors influencing ip of the molecule, s. Sect. 4.1. Ionization potential ip is indeed a fundamental parameter in determining the charge transfer between donor and acceptor molecules in a CTC, together with molecular geometry, distances between groups, respective orientation of TNFM and donor molecule.

From data of Table 4.2 it is evident that, when going from NPEMI to NPEMI-E, the value of λ_{max} increases towards higher wavelengths. This behaviour, together with the corresponding decrease of the bandwidth W, could indicate that NPEMI-E has the lowest value of the ionization potential ip. As it could be verified in Sect. 4.4, when discussing PC data, this forecast could have a beneficial effect on the photoconductivity of NPEMI-E as such and also on the photoconductivity of its blends. Similar considerations allowed in the past to foresee the highest photoconductivity of poly-(2,3-dimethyl-N-vinylindole) (PVDMI) among various methyl derivatives of poly-N-vinylindoles[82,83], s. Sect. 2.1.

Similar considerations can be done as concerns the two chromophores MeO-NPEI-E and NO$_2$-NPEI-E complexed with TNFM, s. Figure 4.5 and Figure 4.6. From data reported on Table 4.2 it is possible to verify that for the first one, MeO-NPEI-E, CTC band parameters are quite similar to those reported for NPEMI, NPEMI-A, NPEMI-E. Absorption band is centered at $\lambda = 778$ nm, a value comparable to those reported for NPEMI-A. Bandwidth is large and comparable to that related to NPEMI. The electron donor capability of MeO group on position 5 of indole ring could be therefore supposed to act similarly to the methyl group (with its well known inductive properties) present on position 2 of NPEMI-R chromophores. We recall here that NPEI species lack the methyl group on position 2 of indole ring. Charge distribution in the push-pull molecular structure is therefore not too much changed with respect to NPEMI. On the contrary, nitro-group present in NO$_2$-NPEI-E strongly influences π-conjugated electrons of the same indolyl unit. Its electron acceptor character provides a totally different electronic arrangement, reflected in the different spectral parameters found for CTC of this chromophore with TNFM. Indeed, CTC absorption band is found at a significantly lower value with respect to all other studied chromophores, i.e. $\lambda = 638$ nm. This low value, related to a more energetical transition in CTC, is connected with a larger value of its ip (ip = 7.92 eV, s. Table 4.1) that diminishes the electron donor character of the moiety. Bandwidth W = 205 nm also is significantly reduced with respect to mean value of W $\approx$ 300 nm reported for all other species. As it can be verified from the data reported in Table 6.1, also the second UV-Vis band at $\lambda_{2\ max}$, for the neat NLO molecules, shifts towards longer wavelengths when ip lowers, s. Table 4.1.
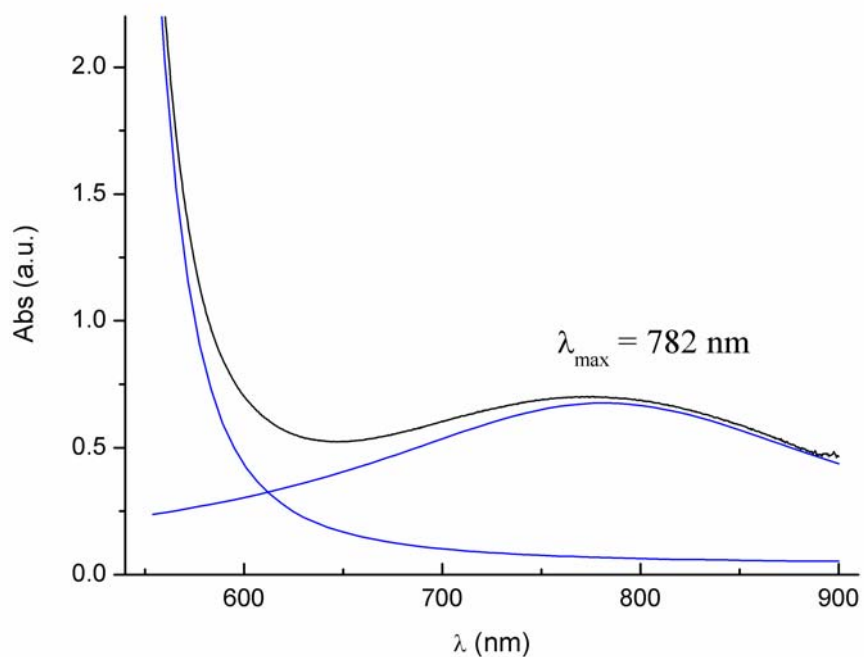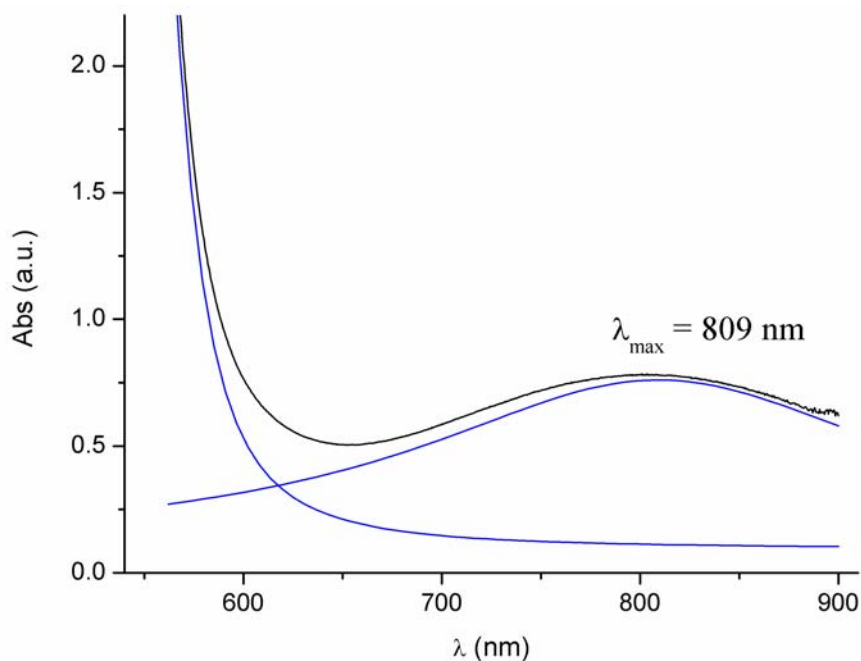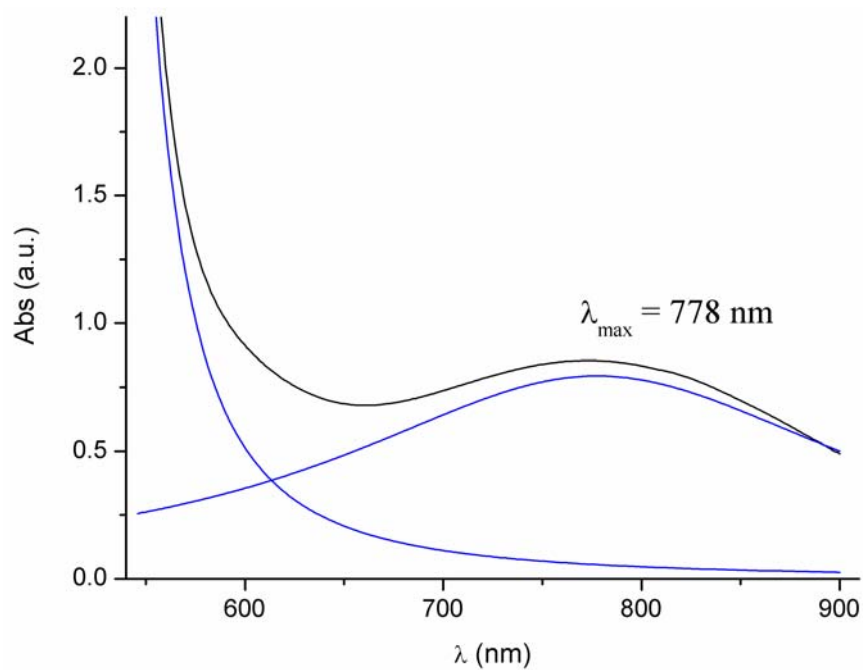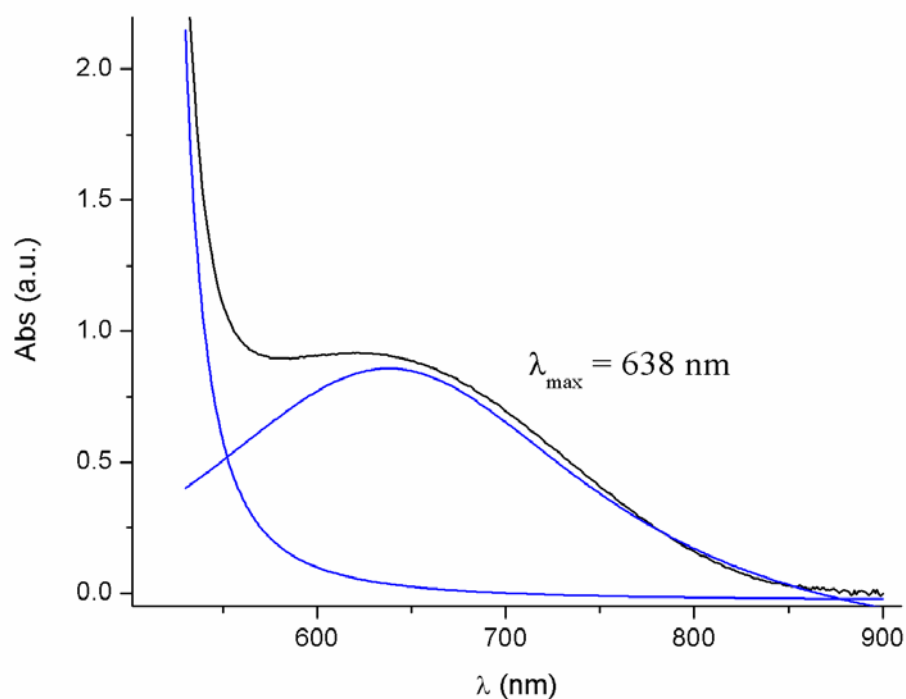
Figure 4.3 Magnified portion of the UV-Vis spectrum of 1:1 NPEMI-A/TNFM mixture in CH_2Cl_2, black line. Deconvoluted spectrum with the onset of the CTC band centered at λ_{max} = 782 nm is displayed in blue.

Figure 4.4 Magnified portion of the UV-Vis spectrum of 1:1 NPEMI-E/TNFM mixture in CH_2Cl_2, black line. Deconvoluted spectrum with the onset of CTC band centered at λ_{max} = 809 nm is displayed in blue.

Figure 4.5 Magnified portion of the UV-Vis spectrum of 1:1 MeO-NPEI-E/TNFM mixture in CH_2Cl_2, black line. Deconvoluted spectrum with the onset of CTC band centered at λ_{max} = 778 nm is displayed in blue.

Figure 4.6 Magnified portion of the UV-Vis spectrum of 1:1 NO$_2$-NPEI-E/TNFM mixture in CH_2Cl_2, black line. Deconvoluted spectrum with the onset of CTC band centered at λ_{max} = 638 nm is displayed in blue.

4.3 Calorimetric analysis (DSC)

Complete calorimetric analyses have been accomplished in this research by means of DSC technique (s. Sect. 3.9) both on neat NLO chromophores and on PR blends (PVDMI/NPEMI-A and PVDMI/NPEMI-E blends). The aims, as already remarked in Sects. 1.9 and 2.2, were to investigate the role of intermolecular interactions in PR materials and to properly characterize the thermal behaviour of the novel NLO chromophores and of their blends with PVDMI. The determination of glass transition temperature T_g for all the studied materials (together with other thermodynamic quantities related to glass transition, e.g. ΔC_p, T_r) can permit to rationalize the data of photorefractivity; such knowledge indeed is fundamental in order to describe the behaviour of PR materials in which chromophore reorientation and interactions among different species play a major role. PR blends with PVDMI selected for the present study have been specifically thought out in order to put in evidence such effects, operating in the "soft materials" regimen, that is, their glass transition temperatures have been planned to be $T_g \leq T_{rt}$. Moreover, the new NLO chromophores were specifically designed in order to act as LMWG (s. Sect. 2.2). Calorimetric analysis is essential to investigate their glass-phase behaviour: glass forming capability, slow-term and long-term recrystallization, shelf lifetime, etc.

As concerns glass transition, the typical onset of a T_g in a DSC thermogram (Heat capacity or Heat Flow vs. Temperature) is evidenced by a step-like level variation. The glass transition is a kinetic process (sometimes referred as a pseudo second-order phase transition) that can be very broad (its range covering up to tens of °C). It strongly depends on cooling/heating rate and in general on measurement conditions, differently from first order phase transitions which are sharp and related to a well defined latent heat. It is therefore useful to strictly adopt a proper experimental procedure in order to gather reproducible and comparable T_g data. Moreover, the application of consecutive heating and cooling scans at different rates in a proper series can permit to obtain useful informations. The precise experimental procedure and the temperature limits of the scans are specified in Sect. 4.3.1 and Sect. 4.3.2 for NLO chromophores and PR blends, respectively. In general, the first heating supplies information about the state of the material as it is obtained by its original preparation or by successive thermal treatments accomplished to eliminate volatile impurities (s. Sect. 3.4). The eventual presence of crystalline fractions can be evidenced during this first heating by the onset of a melting point (an endothermal peak in the DSC thermogram). The

successive cooling (first cooling, fast cooling) is a very rapid one (cooling rate ≈ 200°C/min), operating an efficient temperature quenching: this process is used in order to promote, if possible, the formation of a glass phase by preventing the system to reorganize itself in a crystal lattice. This occurrence can be verified in the successive heating (second heating) which is accomplished at the same rate of the first heating (in the present research all the heating rates were fixed at 10°C/min to permit an easy comparison) and on the same temperature range. A second cooling (slow cooling) is then applied on the sample at the same rate of heating: time is given to the sample in order to reorganize itself during the cooling. The third and last heating is successively applied; thermogram relative to this last scan can permit to evaluate the eventual differences respect to the second heating, due to kinetic reasons: complete or partial recrystallization can be evidenced or also the perduring presence of glass phase. Such last occurrence can establish the good glass forming capability of a material. Such a thermal cycle is summarized for clarity in the case of PVDMI/NPEMI-E blends in Figure 4.15, s. page. 130. Careful analysis of the data obtained in DSC measurements has been accomplished. Data have been studied in the light of various thermodynamic treatments (s. Sect. 1.8.1) in order to get more insight in intermolecular interactions occurring in PR materials. This analysis is presented together with experimental results in the following sections, separately for the case of NLO chromophores (s. Sect. 4.3.1) and for PR blends PVDMI/NPEMI-E and PVDMI/NPEMI-A (s. Sect. 4.3.2).

4.3.1 Thermal behaviour of NLO chromophores

Multifunctional NLO chromophores synthesized during this research, namely NPEMI, NPEMI-A, NPEMI-E, MeONPEI-E, NO_2-NPEI-E, have been characterized from the thermodynamic point of view by means of DSC technique. In this case, the aim was to obtain some information about glass-forming ability and stability. The properties of such moieties when glass phases are formed without the addition of plasticizer agents are important for their use both as LMWG PR materials and in blends with PVDMI. On the other hand, molecular structures of these compounds have been selected in order to prevent crystallization, especially with the introduction of alkyl substituents known to act in this way (e.g. 2-ethylhexyl chain in NPEMI-E). Moreover, intermolecular interactions among chromophores and their influence on glass transition can be studied by the inspection of the different thermal behaviour of NLO chromophores caused by changes in the choice of substituents.

The adopted thermal cycles are summarized as follows:

1. Heating from T= -45°C up to T_{max} at rate 10°C/min (*first heating*)
2. Cooling from T_{max} down to T = -45°C at rate ≈ 200°C/min (*fast cooling*)
3. Heating from T= -45°C up to T_{max} at rate 10°C/min (*second heating*)
4. Cooling from T_{max} down to T = -45°C at rate 10°C/min (*slow cooling*)
5. Heating from T= -45°C up to T_{max} at rate 10°C/min (*third heating*).

For the reasons already explained in the preceding section, T_{max} varied for the different NLO chromophores in dependence of their respective melting points (T_m), which have been previously approximately evaluated with a controlled temperature heating stage and a polarized light microscope. Such preliminary m.p. evaluation gave the results:

T_m (NPEMI) ≈ 190 – 205°C;
T_m (NPEMI-A) ≈ 120°C;
T_m (NPEMI-E) ≈ 75°C;
T_m (MeO-NPEI-E) ≈ 75°C;
T_m (NO$_2$-NPEI-E) ≈ 130-170°C.

T_{max} for each molecule was therefore fixed at T > T_m, typically at 15 - 20 °C higher than T_m.

T_g values being expected in the range -10 < T < 30 °C, lowest temperature limit was fixed at T = -45°C in order to be sure to record the entire glass transition, that can be sometimes a very broad process extending on a large temperature range. Relevant thermodynamic data of the NLO chromophores obtained in this analysis are summarized in Table 4.3. As a useful reference parameter, already described as playing a major role in PC and PR behaviour of organic materials[29], relative temperature T_r is also reported, defined as T_r = T_g - T_{rt}, being room temperature T_{rt} = 22.0°C.

120

Table 4.3 Relevant thermodynamical parameters of NLO chromophores obtained in DSC analysis.

molecule	T_g [a] (°C)	T_r [b] (°C)	ΔCp [c] (J/g °C)	$T_{cryst.}$ [d] (°C)	$T_{m.}$ [e] (°C)
NPEMI	-	-	-	170	204
NPEMI-A	18	- 4.0	0.334	-	122
NPEMI-E	-2.5	- 24.5	0.324	-	68
MeO-NPEI-E	- 9.6	- 31.6			80[*]
NO$_2$-NPEI-E	20[**]	-2.0		77	170[*]

a: glass transition temperature T_g measured on the DSC thermogram relative to second heating (successive to fast cooling).
b: relative temperature $T_r = T_g - T_{rt}$; room temperature is considered fixed at $T_{rt} = 22$°C.
c: specific heat change associated to glass transition.
d: T_{cryst} is defined as temperature at which recrystallization during heating occurs.
e: T_m is the melting temperature; it is observed only during the first heating for glass forming species.

*: for MeO-NPEI-E and NO$_2$-NPEI-E the value of T_m reported in Table refers to the higher T melting peak present in thermogram; a second peak relative to melting is present at $T_{m2} < T_m$ whose interpretation is given in the text, s. Sect. 4.3.1.4 and 4.3.1.5.
** glass transition occurs only after fast cooling (third heating).

4.3.1.1 NPEMI

DSC thermograms relative to the three heating scans on NPEMI sample have been merged in Figure 4.7. During the first heating (red line) no trace of glass transition appears, the one and only feature being a broad endothermal peak (melting) at $T_m = 204$°C. The sample did not undergo any thermal treatment after its preparation and purification by means of crystallization from ethanol, s. Sect. 3.3.1. It therefore appears as a 100% crystalline material. Glass phase was not formed even after the successive fast cooling because second heating (blue line) does not show any hint of step-like glass transition. However, during this second cycle, the onset of two new peaks occurred: a first endothermal one at $T_1 = 176$°C and an immediately successive exothermal one at $T_2 = 180$°C (s. insert in Figure 4.7). The successive endothermal melting process occurs at the previously recorded $T_m = 204$°C. It is important to remark that peaks at T_1 and T_2 cover identical associated areas. Moreover, this area is smaller than that associated to the main endothermal process of melting at $T = 204$°C, whose area is equal to that recorded on first heating, and thus referring to melting of all NPEMI sample. In the successive third heating (green line) the two small peaks are still

present, although their areas are a little increased and the peaks are found at slightly different temperatures, i.e. $T_1 \approx 179$ and $T_2 \approx 183°C$, respectively for endothermal and exothermal one (s. insert in Figure 4.7). The occurrence of these two peaks can be explained hypothesizing the existence of two different crystalline structures. The most stable one is that having $T_m = 204°C$ (crystal phase I). The other one, with $T_m = T_1 \approx 176°C$ (crystal phase II), must be considered a metastable phase, formed in a relatively fast cooling such that imposed on the sample during the DSC analysis. It is important to remark that this second crystalline phase is only formed for a small fraction of the sample, the majority of it crystallizing in the crystal phase 1 structure, having $T_m = 204°C$; this feature is clearly evidenced when comparing peak areas of the two melting processes. Therefore, the exothermal process occurring during the heating at T_2 and having an area identical to the endothermal one at T_1, can be seen as the process of recrystallization in the crystal phase I of the fraction melted at T_1 (only just after melting, indeed, molecules that were in crystal phase II are free to reorganize themselves and to crystallize in the more stable crystal structure I). Differences in the relative proportion of sample crystallizing in one or the other crystal phase are seen to be dependent on kinetics of heating/cooling.

Anyway, what is important to remark is the total absence of formation of glass phase both for fast or slow cooling. NPEMI must be considered as a crystalline solid and its use as neat LMWG is therefore prevented.
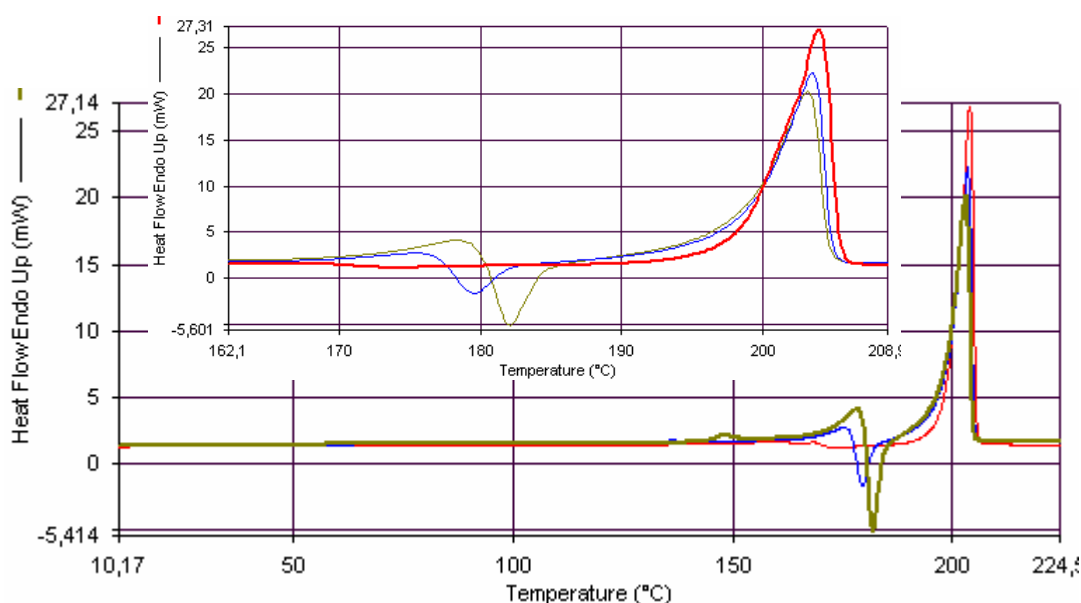
NPEMI

Figure 4.7 DSC thermograms of NPEMI displaying the three heating scans (s. text). The coexistence of two different crystal phases is better appreciated in the insert representing a magnified portion of the thermograms, displayed for clarity purposes.

4.3.1.2 NPEMI-A

DSC thermograms relative to the three heating scansions on NPEMI-A sample are reported in Figure 4.8. The only feature appearing on the thermogram of first heating (red line) is the peak associated to melting at $T_m = 122°C$, thus evidencing that NPEMI-A sample was totally crystalline, no fraction of it being amorphous after the recovery and purification procedures, s. Sect. 3.3.2. The successive temperature quenching (fast cooling) was indeed efficient in totally avoiding the formation of a crystal structure: during the second heating (blue line in Figure 4.8) a step-like level variation occurs related to glass transition at $T_g = 18°C$. An enlargement of the thermograms around glass transition temperature is provided in Figure 4.9. The absence of peaks related to melting at $T = T_m$ led to the conclusion that the overall sample formed a glass amorphous solid in the cooling. This occurrence is also repeated in the case of slow cooling (10°C/min rate): the third heating thermogram (green line) actually superimposed on the second one. NPEMI-A can therefore be considered as a good glass former material. In order to study the long-term stability of NPEMI-A glass phase, the same cell used in a first DSC analysis has been stored at $T = T_{rt}$ for 15 days. It is important to remark that, being $T_{rt} > T_g$, NPEMI-A molecules are relatively more free to reorganize themselves and to recrystallize in a crystal structure than at $T < T_g$ where system dynamics is "frozen" and such rearrangements take very long times. After 15 days a DSC scan, identical to the first one, was repeated (DSC thermograms are not displayed for conciseness) with the result that, during the first heating, both a glass transition ($T_g = 18°C$) and a weak melting peak ($T_m = 122°C$) occurred. The conclusion is that a 15-days time is enough to permit a partial recrystallization of NPEMI-A, even if a substantial fraction of the sample still exists in glass phase. This last observation could be made on the basis of a comparison of melting peak area (latent heat is an extensive property) recorded in the first and second analysis. The repetition of the same DSC analysis on the same sample after an additional month at $T = T_{rt}$ gave the result that a smaller fraction of NPEMI-A lasts in the glass phase. Therefore, NPEMI-A has a moderate tendency to give a stable glass phase as a neat material. It is also important to put in evidence that the measured $T_g = 18°C$ is a temperature not so distant from T_{rt}.

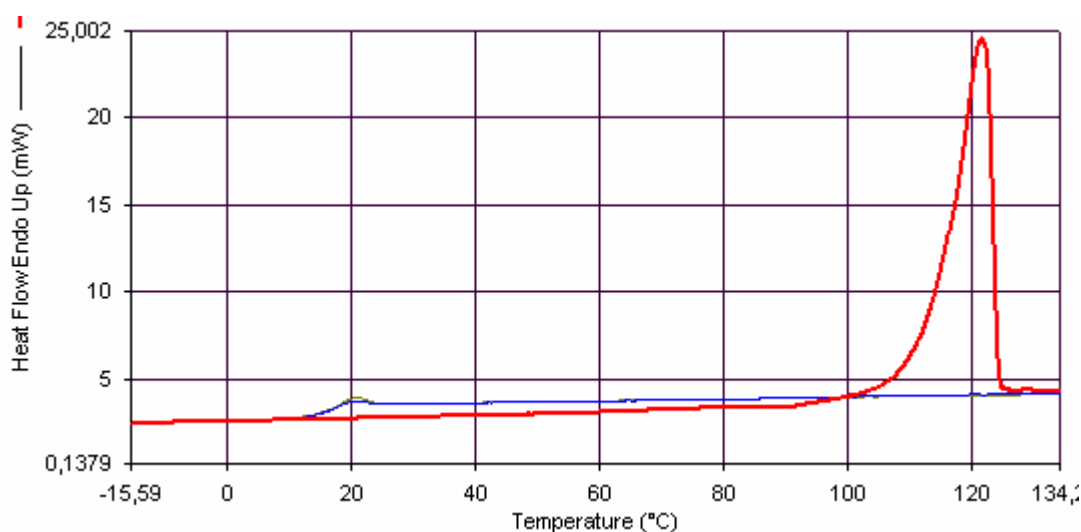Figure 4.8 DSC thermograms of NPEMI-A displaying the three heating scans (s. text).

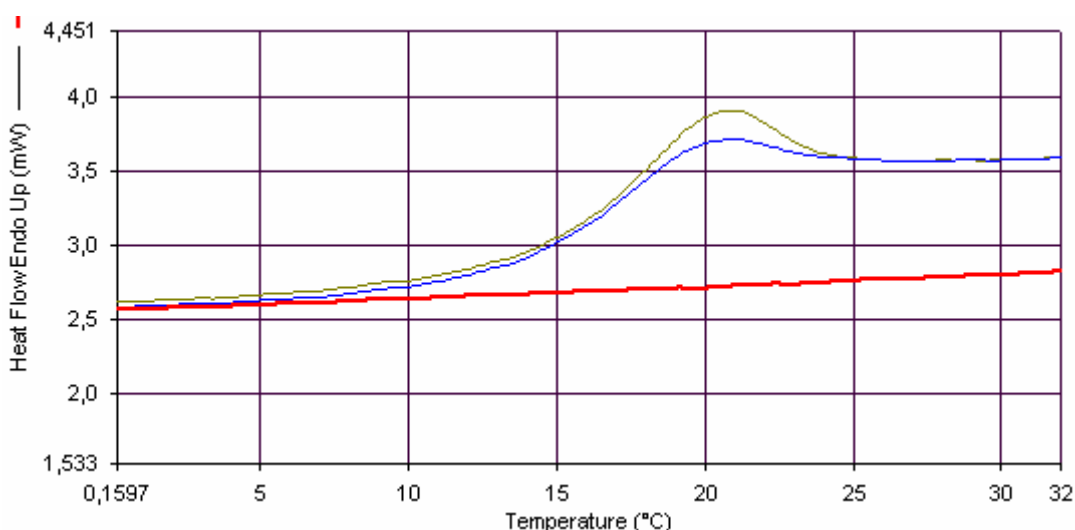Figure 4.9 Enlargement around Tg = 18°C of the DSC thermograms related to three heating scans performed on NPEMI-A sample.

4.3.1.3 NPEMI-E

DSC thermograms relative to the three heating scans on NPEMI-E sample are reported in Figure 4.10. The only phase transition occurring during the first heating (red line) is the melting at $T_m = 68°C$; this reveals the totally crystalline nature of the product as obtained by purification and recovery procedures, s. Sect. 3.3.3. Nevertheless, a rapid temperature quenching (fast cooling) permitted to obtain a totally amorphous glass material with $T_g = -2.5°C$, as evidenced in the second heating (blue line). DSC curves around T_g have been enlarged and displayed separately in Figure 4.11 for clarity. No hint of melting at $T = T_m$ has been evidenced, confirming that the overall sample did not crystallize during the cooling.

124

Totally similar considerations hold for the third heating (green line), after the slow cooling, thus evidencing the good glass-former properties of the neat product.

In a similar manner to what has been done for NPEMI-A, long-term stability of the glass phase of NPEMI-E was investigated. Similar scans performed after 15 days, and then after subsequent 30 days on the same sample, stored at controlled T_{rt}, revealed the exceptional stability of amorphous NPEMI-E. No hint of recrystallization was evidenced. A further verification was accomplished repeating the scans after subsequent 30 days: during this time the sample was allowed to follow night/day temperature variations of a room, being stored without any control of temperature. Such temperature oscillations are known to promote recrystallization processes. Nevertheless, NPEMI-E remained for a very long time in glass-phase. Actually, it has been verified that partial crystallization occurred in some samples stored at room temperature after many months.

The good glass forming properties, together with the low value of T_g = -2.5°C permit to consider this product for the study of its PR behaviour both alone (LMWG multifunctional PR material) as well as in blends with PVDMI. Its low T_g, indeed, permits to add PVDMI to neat NPEMI-E obtaining what are expected to be "soft" materials ($T_g < T_{rt}$; $T_r < 0$) and thus to follow the onset of PR and the influence of intermolecular interactions with the increasing of polymer counterpart. The condition of low T_g ($T_r \leq 0$) is very important in order to enhance PR effect (s. Sect. 1.4). On the other hand, the proved good stability of NPEMI-E glass phase can be expected to overcome the crystallization drawbacks described for PVK/DMNPAA systems; the possibility to have stable blends containing high content of NPEMI-E is moreover interesting in order to achieve high values of PR optical gain Γ, this property being obviously related to NLO species concentration.
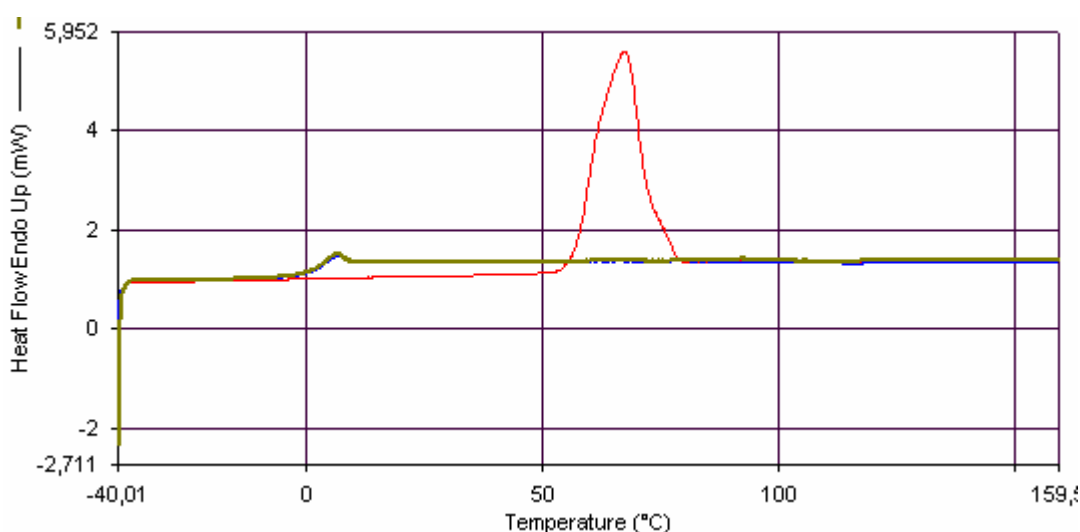

Figure 4.10 DSC thermograms of NPEMI-E displaying the three heating scans (s. text).
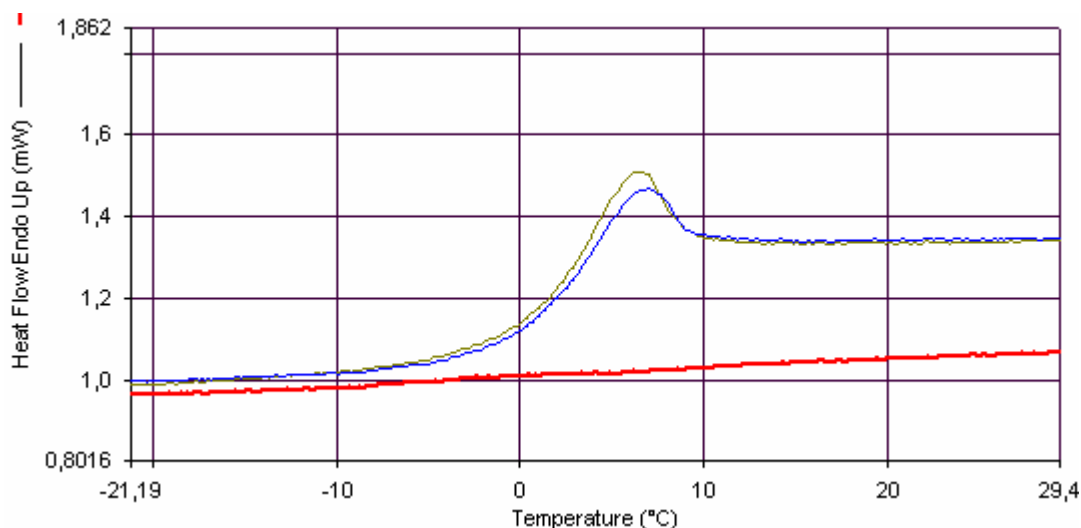
Figure 4.11 Enlargement around Tg = - 2°C of the DSC thermograms related to three heating scans performed on NPEMI-E sample.

4.3.1.4 MeO-NPEI-E

DSC thermograms relative to the three heating scans on MeO-NPEI-E sample are reported in Figure 4.12. During the first heating the only thermal process is represented by a broad asymmetric endothermal peak spanning on the interval 50 < T < 80°C. Melting point is taken at T_m = 80°C, revealing the totally crystalline nature of the product as obtained by purification and recovery procedures, s. Sect. 3.3.6. The asymmetric nature of the peak and its shoulder at $T_{m2} \approx 70$°C could be due to the coexistence of two different crystal phases in which pristine material is obtained, although only a minor part of the sample seems to exist in the crystal phase having melting point T_{m2}. The rapid temperature quenching (fast cooling) performed on the sample gives rise to a totally amorphous glass material with T_g = - 9.6°C, as evidenced in the second heating.   Moreover, also the slow cooling produces the same result, with third heating thermogram almost superimposing the second one. A totally similar T_g value is obtained in this third heating, namely Tg = - 9.9°C.   The good glass-former properties of MeO-NPEI-E have been therefore demonstrated.

As concerns melting point, T_m = 80°C, it is easy, from a comparison of the data reported in Table 4.3, to verify that similar thermal and glass-forming properties have been found for MeO-NPEI-E and NPEMI-E. It could be expected that electronic distributions of these two NLO chromophores are very similar too, due to the electron donor nature of MeO functional group in 5 position of the indole ring that could compensate the analogous nature of the missing methyl group in the position 2 of the indole ring. Anyway, as concerns long-

126

term stability of the obtained glass phase, the behaviour of MeO-NPEI-E is quite different with respect to that of NPEMI-E. MeO-NPEI-E, indeed, rapidly crystallizes when stored at room temperature in times of the order of one day. On the other hand, crystallization can be avoided when the sample is stored at T = -20°C immediately after the obtainment of glass-phase through temperature quenching of the melt.
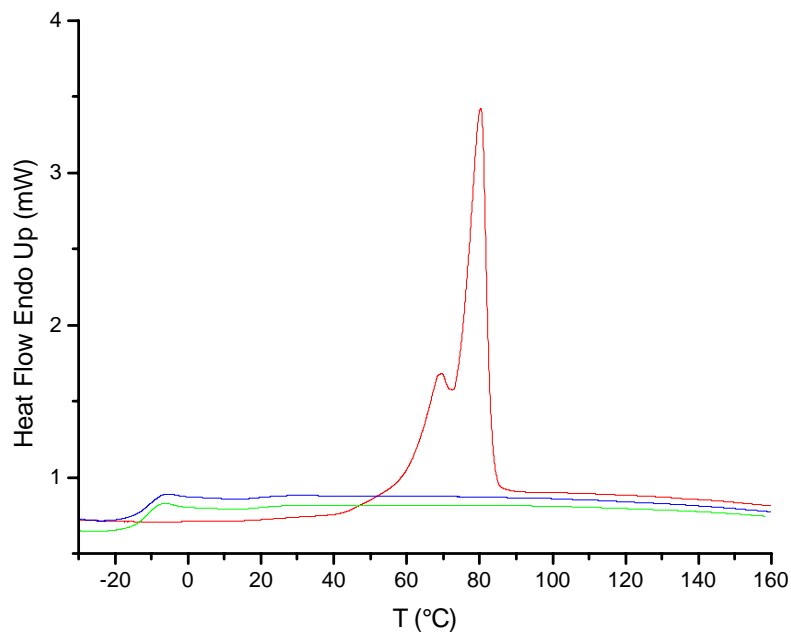

Figure 4.12 DSC thermograms of MeO-NPEI-E, displaying the three heating scans (s. text).

4.3.1.5 NO$_2$-NPEI-E

DSC thermograms relative to the three heating scans performed on NO$_2$-NPEI-E sample are reported in Figure 4.13. The only thermal process occurring during the first heating (red line) is the relatively sharp endothermal peak associated to melting. Melting point is taken at $T_m = 167$ °C. The red line in Figure 4.13 reveals the totally crystalline nature of the product as obtained by purification and recovery procedures, s. Sect. 3.3.8 and, differently to what described in the case of the methoxy-derivative, s. Sect.4.3.1.4, the overall NO$_2$-NPEI-E sample exists in the same crystal phase. A rapid temperature quenching (fast cooling) performed on the sample gives rise to a partially amorphous glass material with $T_g = 20$ °C, as evidenced in the second heating (blue line). Glass transition is better evidenced in Figure 4.14, blue line. Nevertheless, the fluid phase over T_g rapidly undergoes a recrystallization that begins at T = 50°C, as visible in Figure 4.14, blue line. The exothermal process in blue line, whose peak has been taken at $T_{cryst} = 77.0$ °C, is ascribable to such a recrystallization. It is probably due to the formation of crystal nuclei during the preceding cooling scan; once T > T$_g$

127

is reached, nuclei are able to grow obtaining a crystal phase. Interestingly, the sample partially crystallizes in a crystal phase different from that evidenced during the first heating scan. During the same second heating (blue line) a melting indeed occurs at $T_{m2} = 149°C$. This relatively small peak is immediately followed by an exothermal process (recrystallization) whose area is comparable to that of the preceding melting peak. Finally, melting at $T_m = 167°C$ occurs. The complicated trend is explained by the formation of two different crystal phases (the principal one characterized by $T_m = 167°C$, and a secondary one characterized by $T_{m2} = 149°C$). Sample is able to recrystallize in these two crystal phases during the second heating because of the formation of crystal nuclei during the fast cooling. The principal phase is perhaps the most stable one; it is indeed the only one present in the pristine material, stored at room temperature for several days before the measurements. Moreover, also the fraction of sample crystallized in the secondary phase tends to recrystallize at higher temperatures in the principal one: once the melting is completed at $T_{m2} = 149°C$, it rapidly crystallizes joining the rest of sample in the principal crystal phase. The overall sample finally melts at $T_m = 167°C$.

A slow cooling produces different results. The subsequent third heating thermogram (green line, Figure 4.13) indeed does not show evident trace of glass transition: the slow cooling allowed the overall sample to crystallize. What is perhaps more surprising is that melting for the overall sample occurs for the third heating at $T_{m2} = 149°C$. The formation of the secondary crystal phase seems to be favoured by a slow cooling. At the same time, it must be remarked that the described behaviour evidences a very poor glass-forming capability of the product NO_2-NPEI-E. Glass phase is formed only partially even when a fast cooling is provided. Moreover the observed recrystallization during heating seems to confirm a poor stability of the glass phase eventually formed, caused by the unavoidable onset of crystal nuclei. As it could be expected, the introduction of the nitro-group in position 5 of the indole ring to replace the methoxy-group present in MeO-NPEI-E causes a dramatic change in thermal properties (T_m, T_g, glass phase stability). The effect is ascribable to the completely different distributions of electrons on the π-conjugated structure of these two NLO chromophores: nitro-group, with its electron acceptor properties, reduces the electron density on indole ring, modifying also the edm of the molecule. Indeed, as it has been reported in Table 4.1, calculated edm of NO_2-NPEI-E is $\mu = 10.37$ Debye, well larger with respect to MeO-NPEI-E one, $\mu = 7.43$ Debye.
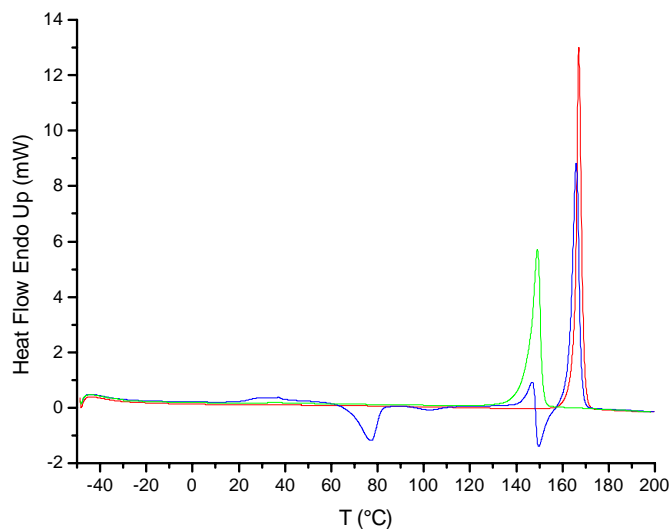
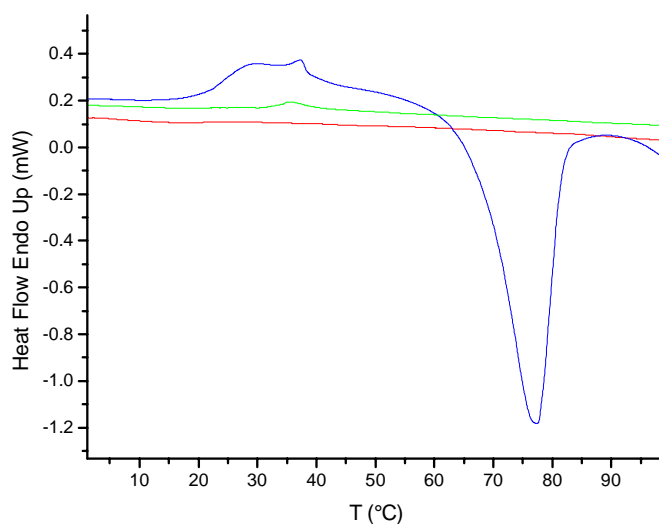Figure 4.13 DSC thermograms of NO$_2$-NPEI-E, displaying the three heating scans (s. text).

Figure 4.14 Enlargement around Tg = 20°C and T$_{cryst}$ = 77 °C of the DSC thermograms related to three heating scans performed on NO$_2$-NPEI-E sample.

4.3.2 Thermal behaviour of binary polymer blends

In order to make possible a comparison for the calorimetric results of all the investigated materials, a general common experimental procedure has been planned. All the calorimetric DSC measurements complied with the following thermal treatment:

1. Heating from T= -45°C up to T = 220°C at rate 10°C/min (*first heating*)
2. Cooling from T = 220°C down to T = -45°C at rate ≈ 200°C/min (*fast cooling*)
3. Heating from T= -45°C up to T = 220°C at rate 10°C/min (*second heating*)

129

4. Cooling from T = 220°C down to T = -45°C at rate 10°C/min (*slow cooling*)

5. Heating from T= -45°C up to T = 220°C at rate 10°C/min (*third heating*).

Thermal treatment is schematically summarized in Figure 4.15. The upper limit of scanned temperatures was set by the glass transition temperature of the employed polymer PVDMI, i. e. T_g = 198°C. Beyond this limit, indeed, the material is certainly fluid (all aging and segregation effects are erased) and the NLO chromophore is totally amorphous (eventual crystalline portions have melted and dissolved in a fluid matrix). The application of too high temperatures must be avoided in order to reduce the risk of irreversible changes in blend composition caused by degradation and/or vaporization of volatile components. The lower limit, T = - 45°C has been selected on the basis of the known values of T_g for NPEMI-E and NPEMI-A (s. Table 4.3), in order to reach with cooling the glass phase region for all the studied composition range.

Blends with PVDMI were studied over the whole composition range 0-100 wt.% of both the NLO chromophores NPEMI-E and NPEMI-A; their compositions are summarized in Table 4.4 and Table 4.5, respectively, together with the obtained relevant thermodynamic parameters. All the studied blends were prepared with the addition of the photosensitizer TNFM in 1 wt.% concentration.
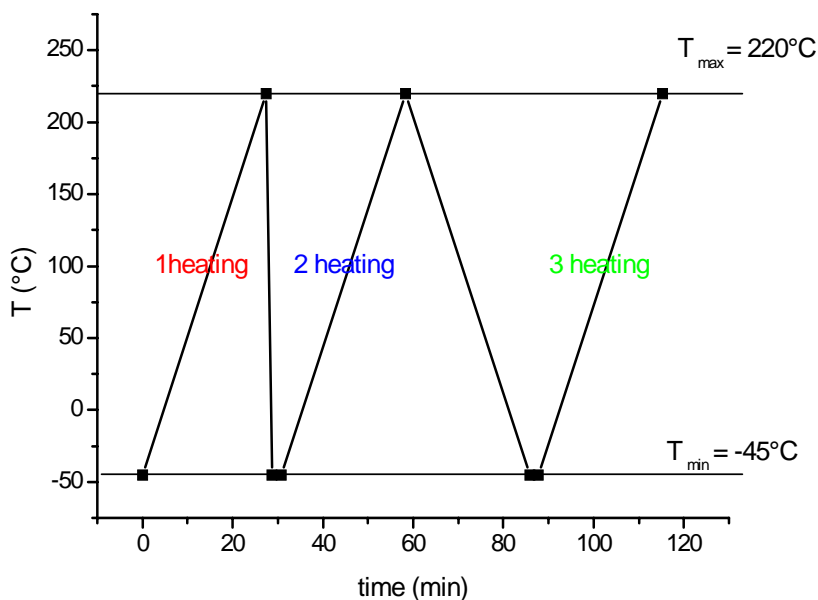

Figure 4.15 Scheme of thermal cycles applied to PVDMI/NPEMI-E blends samples in DSC analysis.

4.3.2.1 PVDMI/NPEMI-E blends (NPE)

Because NPEMI-E is soluble in PVDMI at any concentration (at room temperature, T_{rt}= 22°C), DSC measurements could be accomplished on the overall series of the blends: NPEMI- E content w_1, expressed as weight percent (wt.%), varied from w_1 = 0 (neat PVDMI) up to w_1 = 100 (neat NPEMI-E). The DSC thermograms of the complete series are not reported for conciseness. Table 4.4 reports the composition of the studied blends together with the measured values of the glass-transition temperature T_g and reduced temperature T_r. The trend of the measured T_g values as a function of the composition of the blends are reported in Figure 4.17, together with the results of various fitting procedures explained in the following.

None of the blends reported in Table 4.4 showed a hint of recrystallization. Only neat NPEMI-E, as we have elsewhere shown[105] (s. Sect. 4.3.1.3), poorly tends to crystallize in the bulk but after some months at r.t. and when it is extremely pure. As a thin film (for instance in the NPE99 cell, s. PR measurements in Sect. 4.5.2), it totally loses this tendency and the film lasts indefinitely perfectly transparent. NPE99 blend appears like a ropy red fluid but the viscosity of the blends increases quickly with the increase of the content of PVDMI, whose T_g = 198.5°C. For w_1 = 50 wt.%, the blend already behaves like a hard glass solid. This rapid variation of the viscosity as a function of T_g is not surprising. Some estimate could be made in order to evaluate viscosity behaviour and to distinguish the "soft-blend" regimen from the "hard" one. Being $w_1 \approx 65$ wt. % the composition at which $T_g = T_{rt} = 22.0°C$ ($T_r = 0°C$), s. trend in Figure 4.17, NPE65 is considered the "border" blend between the so-called "soft-blend", $T_g < T_{rt}$, and the "hard-blend" materials, $T_g > T_{rt}$. By applying the Williams-Landel-Ferry (WLF) law[139], we have found that the viscosity of NPE99 (T_g = -2.5°C, T_r = - 24.5°C) is about six orders of magnitude lower than its value for NPE65 (T_g = 22.0°C, T_r = 0), s. Figure 4.16.
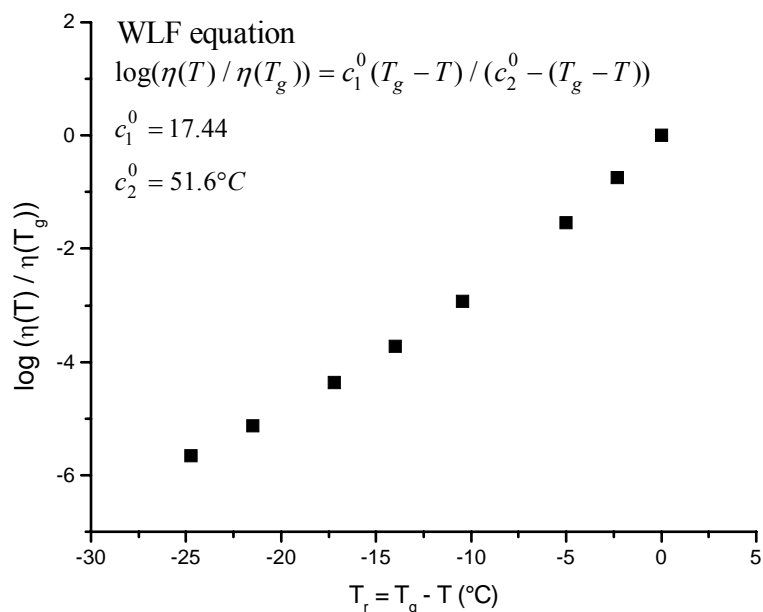
Figure 4.16 The trend of the viscosity of NPE blends as a function of T_r as computed by the WLF equation.

Besides T_g, other quantities related to glass transition have been obtained for each blend, namely ΔT and ΔCp, s. Table 4.4. ΔT is defined as the "width" of glass transition, that is, the range of temperatures in which the sample undergo transition from glass to amorphous fluid phase (s. Sect. 3.9). Its value can be related to the disorder of the blend. ΔCp is the heat capacity change associated with glass transition, measured as the difference in heat capacity between liquid phase ($T > T_g$) and glass phase ($T < T_g$), s. Sect. 3.9. The trends of the values of these quantities as a function of composition in NPE blends are displayed in Figure 4.18 and Figure 4.19, respectively. Such trends share some common features: both ΔT and ΔC_p increase from their values at $w_1 = 0$ (pure PVDMI) reaching a maximum for $w_1 \approx 40$ wt. % and then decrease, down to the values at $w_1 = 100\%$ (pure NPEMI-E). As concerns width ΔT, the obtained trend is related to disorder in blends: a sharp transition (small value of ΔT) is proper of a pure material. For intermediate compositions, disorder increases, the glass transition becomes larger and attains its largest value at about 40 wt.%. Actually, it is possible to verify that a neat monomer species (as NPEMI-E) has sharper glass transition than its blends with PVDMI, due to the intrinsic higher disorder of the macromolecular chain.

ΔC_p trend shows a trend similar to that of ΔT. The knowledge of ΔC_p values is fundamental in order to employ them in the various thermodynamic treatments, to be discussed in the following, used to extract information about intermolecular interactions.

Free Volume Theory[139,140], dealing with glass materials, describes the soft-blend materials as containing microvoids where a second molecular component of the blend can be allocated.
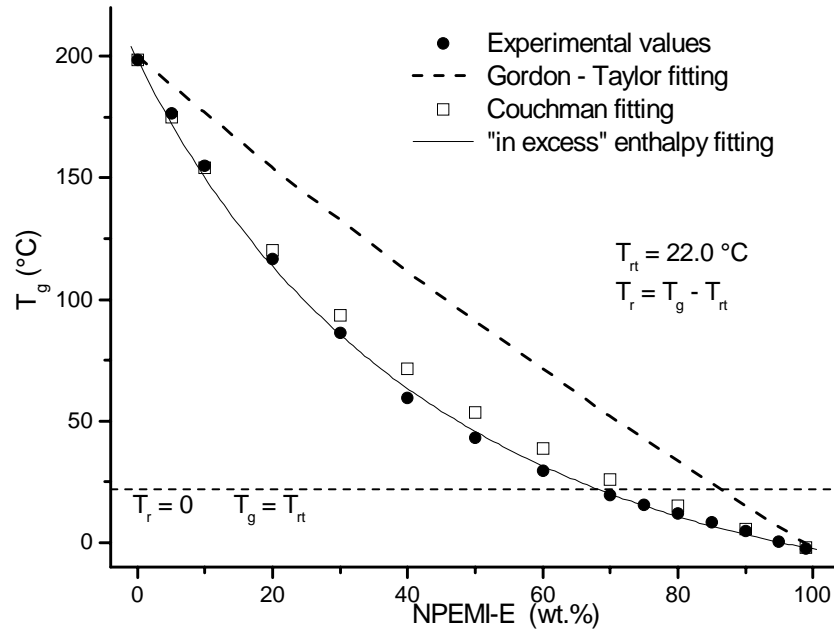

Figure 4.17 The dependence of the measured values of the glass transition temperature T_g (full circles) on the composition of the studied NPE blends. The results for various fitting procedures are also reported (s. text).

Depending on the volume of the microvoids and of the allocated molecule together with the value of its edm, a molecular reorientation can be possible under the influence of an external electric field E. In conclusion, the extent and the typology of the intermolecular interactions occurring in such binary blends can be considered of fundamental importance in planning and optimizing the behaviour of a photorefractive device. For these reasons, some detailed information about the intermolecular interactions and the possible consequences on the molecular reorientation have been gathered by means of a careful analysis.

The value of T_g of polymer binary miscible blends depends in principle on the Tg values of pure components and on the change of the thermodynamic state functions like ΔH (enthalpy), ΔS (entropy) and other ones (s. Sect. 1.8.1). Unfortunately, very often such kind of information is not available in the literature over the whole range of composition, due to the already evidenced segregation problems for PR blends. Our analysis, instead, has been made possible by the availability of the T_g data of Figure 4.17 and Table 4.4, spanning from $w_1 = 0$ to 100 wt.%

As a first step, the trend of the experimental T_g values reported in Figure 4.17 have been submitted to various fitting procedures in the light of some of the many elaborated thermodynamic approaches[140,162] (s. Sect. 1.8.1). Our first approach was based on the Gordon-Taylor (GT) equation[152], s. Eq. (1.52),

$$T_g = (w_1 T_{g1} + K w_2 T_{g2})/(w_1 + K w_2) \qquad (4.1)$$

that was derived from the Free Volume Theory. In Eq. (4.1) T_{g2} refers to the pure component having the highest glass transition temperature (in our case PVDMI, $T_{g2} = 198°C$) while $T_{g1} = -2.5°C$ concerns NPEMI-E; w_1 and w_2 are the respective weight percent (wt.%) content. A simple fitting of the experimental T_g values allows the determination of the K parameter. GT fit of experimental data is reported in Figure 4.17 as a broken line. Unfortunately, the derivation of the GT equation does not consider the possible existence of intermolecular interactions inside the blend and no thermodynamic information can be obtained from K that is merely a fitting parameter. Nevertheless, experimental deviations from GT fit trend can be correlated with the existence of specific interactions (s. Sect. 1.8.1). Negative deviations are typical of weak or moderate interactions while positive deviations seem to suggest strong or very strong interactions; by considering the trend of the experimental data, NPE blends are therefore classifiable as systems in which weak interactions are active. The further step in the analysis was to take into consideration the model proposed by Brekner, Schneider and Cantow (BSC)[154,172], s. Sect. 1.8.1. BSC treatment provides a mathematical expression, similar to GT equation, containing two new K parameters, namely K_1 and K_2. The authors claim that the value of K_1 should quantitatively express the extent of the interactions between homologous species whereas K_2 should pertain to those between heterologous ones. The fitting with BSC equation gave for the two parameters the values $K_1 = 0.327$ and $K_2 = -0.457$. Making reference to many other studied blends[154,172], the obtained values of K_1 and K_2 can be considered as relatively small and represent a system in which weak interactions are active; moreover, both chromophore/chromophore interactions and chromophore/indole groups of PVDMI ones can be considered as weak interactions. These results seem to justify the experimental remarks concerning the availability of NPEMI-E based blends to remain in the glass phase. This conclusion has also been sustained by the observed easy reorientation of the NPEMI-E molecules when an external poling electric field E is applied (s. PR measurements, Sect. 4.5). BSC fit is not reported in Figure 4.17 for conciseness and clarity of representation.

A more meaningful description of the blend formation and of the thermodynamic parameters controlling the mixing process has been obtained by Couchman et al.[153,155,159] and by Righetti et al.[148,149,150], as already described in Sect. 1.8.1. Analysis of T_g data of NPEMI-E based blends by means of the Couchman equations (s. Eqs. (1.57) and (1.58), Sect. 1.8.1) allowed the evaluation of some useful quantities. Fitting based on a Couchman equation (1.57) is reported in Figure 4.17 (open squares). If an improvement is evident in the fitting quality with respect to the GT equation, nevertheless the fitting is not satisfactory. The presence of interactions must be taken into consideration and some of the simplifying assumptions of the Couchman theory must be relaxed. A successive fitting procedure employed the approach described in Sect. 1.8.1, Eqs. (1.59), (1.60), (1.61), (1.62), as proposed by Righetti et al.[148,149,150], extending Couchman considerations. The "in excess" quantities (ΔS_m^l - ΔS_m^g) and (ΔH_m^l - ΔH_m^g) were extracted from the experimental T_g data of the studied blends. For a practical comparison of these results with those of other systems reported in literature, the quantities Q_s, Q_h were also obtained (s. Sect. 1.8.1), respectively referring to "in excess" entropy and enthalpy; they are independent from composition and defined in Eqs. (1.61), (1.62): their physical meaning is related to the strength of intermolecular interactions[159]. Such quantities have been estimated for NPE blends to amount to Q_s = 0.0618 J g^{-1} K^{-1} and Q_h = 33.0980 J g^{-1}. These values are comparable to those cited for polymer blends in which weak or moderate specific interactions exist among blends components. Moreover, the introduction of such values in Eqs. (1.59), (1.60) in order to predict T_g vs. composition trend, resulted in a optimized fitting of experimental T_g data. "In excess" enthalpy fitting (1.60) is displayed in Figure 4.17 as a continuous line.

A different reproduction of the variation of T_g as a function of w_1 could be obtained by using the treatment proposed by Lu and Weiss[143,144], s. Sect. 1.8.1. It allows to consider both weak and strong interactions leading to negative or positive deviations, respectively, starting from the linear mixing rule expressed by the GT equation. The Lu-Weiss treatment permits the evaluation of the enthalpy of mixing ΔH_m , s. Eqs. (1.63) and (1.64), considered as the most important parameter controlling the process. A negative value of ΔH_m (i.e. mixing process being exothermic) can only arise from the formation of specific interactions between the components of the blend. By means of a careful fitting of the overall trend of T_g values using Eq. (1.64) the Flory-Huggins interaction parameter χ[161] can be obtained, its value being in turn related to ΔH_m through Eq. (1.63). The largest value of χ resulted to amount to about - 3.5. The value of ΔH_m can correspondingly be evaluated[144,161] as $\Delta H_m \approx$ - 2.5 kJ·mol^{-1}. Once again, this result classifies NPE blends as characterized by weak dipole-dipole interactions.

The trend of Lu-Weiss fitting gave an optimized matching with experimental data; it is not displayed in Figure 4.17 for clarity but it is very similar to "in excess" enthalpy fitting (continuous line).

Table 4.4 Composition of the studied NPE blends, their glass transition temperature T_g, their reduced temperature ($T_r = T_g - T_{rt}$; $T_{rt} = 22.0°C$), glass transition width ΔT, heat capacity change associated to glass transition ΔC_p.

Blend	Composition[a]		T_g	T_r	ΔT	ΔC_p
	(wt.%)		(°C)	(°C)	(°C)	($J\,g^{-1}\,°C^{-1}$)
	PVDMI	NPEMI-E				
PVD99	99	-	198.5	176.5	12.31	0.235
NPE5	94	5	176.5	154.5	14.31	0.235
NPE10	89	10	154.9	132.9	17.60	0.256
NPE20	79	20	116.7	94.7	22.94	0.283
NPE30	69	30	86.3	64.3	30.67	0.365
NPE40	59	40	59.4	37.4	42.97	0.531
NPE50	49	50	43.0	21.0	22.06	0.375
NPE60	39	60	29.4	7.4	19.85	0.328
NPE70	29	70	19.5	-2.5	13.09	0.305
NPE75	24	75	15.4	-6.6		
NPE80	19	80	11.8	-10.2	14.21	0.320
NPE85	14	85	8.2	-13.8		
NPE90	9	90	4.6	-17.4	9.66	0.292
NPE95	4	95	0.5	-21.5		
NPE99	-	99	-2.5	-24.6	7.42	0.324

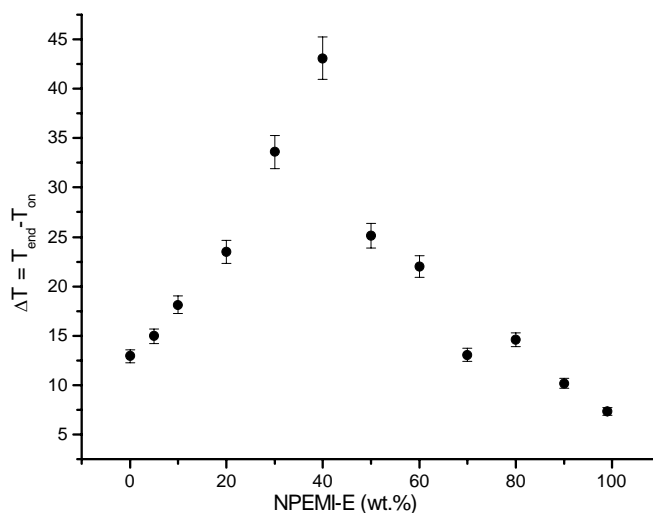a) TNFM photosensitizer is added to each blend in 1 wt% concentration.

Figure 4.18 Trend of glass transition width ΔT as a function of composition in NPE blends. Error bars are related to averaging over the three different scansions of DSC measurements.
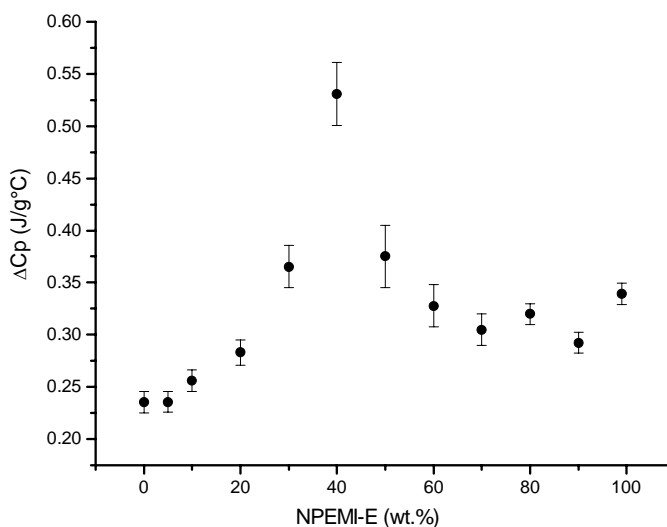

Figure 4.19 Trend of heat capacity change associated to T_g as a function of composition in NPE blends. Error bars are related to averaging over the three different scansions of DSC measurements.

4.3.2.2 PVDMI/NPEMI-A blends (NPA)

Similarly to NPEMI-E, NPEMI-A is soluble in PVDMI at any concentration (at room temperature, T_{rt}= 22°C). DSC measurements were accomplished on the overall series of blends: NPEMI-A content, expressed as weight percent w_1 (wt.%), varied from $w_1 = 0$ (neat

PVDMI) up to $w_1 = 100$ (neat NPEMI-A). The DSC thermograms of the overall series are not reported for conciseness. Table 4.5 reports the composition of the studied blends together with the measured values of the glass-transition temperature T_g and reduced temperature T_r. Trends of the measured T_g values as a function of the composition of the PVDMI/NPEMI-A blends (NPA blends) are reported in Figure 4.21, together with the results of the various fitting procedures explained in the following. Besides T_g, other quantities related to glass transition have been obtained for each blend, namely width of transition ΔT and change at T_g of the heat capacity ΔCp, s. Table 4.5. ΔT and ΔCp trends as a function of composition are rationalizable as already described for NPE blends (s. Sect. 4.3.2.1) and are reported in Figure 4.22 and Figure 4.23 respectively.

Some of the blends reported in Table 4.5, namely those with $w_1 > 70$ wt.% showed a hint of recrystallization after some months, when stored in bulk quantities. Interestingly, when such blends are used to form a thin film (for instance in the realization of the electrooptic cells employed in this research for PC and PR measurements, s. Sect. 4.5.2), they totally lose this tendency and the film lasts perfectly transparent. Chemical and/or electrostatic interactions with the walls of the cells could be considered as responsible of this stabilization of the blends.

NPA blends showed a thermodynamic behaviour similar to that of NPE blends. NPA99 blend is a material well harder than NPE99; its higher viscosity is at least qualitatively confirmed by its appearance, more similar to that of a rubbery solid than that of a ropy fluid. As for NPE series, viscosity of the blends increases quickly with the increase of the content of PVDMI, $T_g = 198.5°C$. The transition from "soft-blend" regimen to the "hard" one occurs for NPA blends at a concentration of NPEMI-A $w_1 = 90$ wt. % for which $T_g = T_{rt} = 22.0°C$ ($T_r = 0°C$), s. trend in Figure 4.21. A comparison with the corresponding NPE65 gives a first idea of the different calorimetric behaviour of these two series of PR materials. It is important to stress that such an increase in T_g (and hence T_r) values of blends will have deep implications in the PR behaviour (s. Sect. 4.5.2). NLO chromophores reorientation is indeed hampered or totally blocked in systems at high values of T_g with respect to room temperature. Figure 4.20 reports the trend of the viscosity as a function of T_r as obtained by using the Williams-Landel-Ferry equation (WLF)[139]. In this case, well differently with respect to NPE blends (s. Figure 4.16), the viscosity of NPA99 ($T_g = 18.4°C$, $T_r = - 3.6°C$) is only one order of magnitude lower than its value for NPA90 ($T_g = 22.0°C$, $T_r = 0$), s. Figure 4.20.

Some detailed information about the intermolecular interactions and the possible consequences on the molecular reorientation have been gathered for NPA blends by means of a calorimetric analysis equal to that already described for NPE blends; all the considerations

138

about the different thermodynamical approaches employed can be found in Sect. 1.8.1 and Sect. 4.3.2.1.

WLF equation

$$\log(\eta(T)/\eta(T_g)) = c_1^0 (T_g - T)/(c_2^0 - (T_g - T))$$
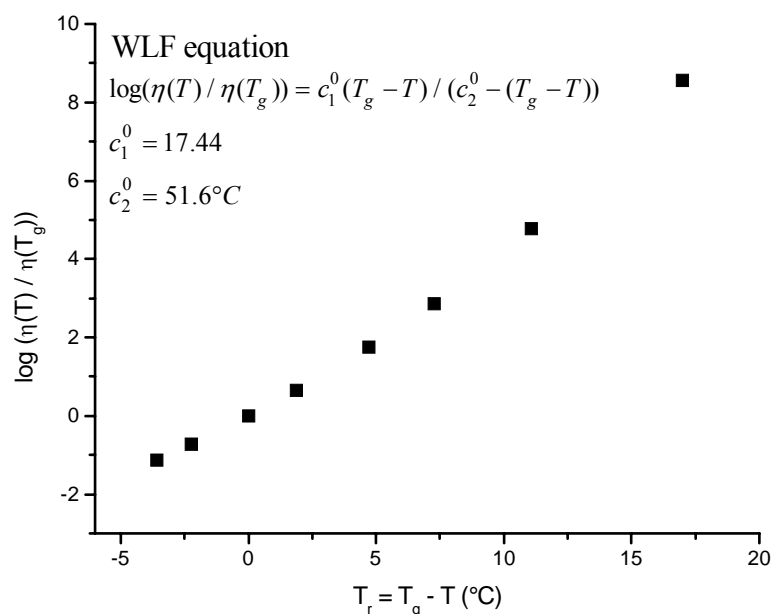
$c_1^0 = 17.44$

$c_2^0 = 51.6°C$

Figure 4.20 The trend of the viscosity of NPA blends as a function of T_r as computed by the WLF equation.

A GT fit, Eq. (4.1), of the experimental data is reported in Figure 4.21 as a broken line; the substitution in Eq. 4.1 of the values T_{g2} = 198.5°C (PVDMI) and T_{g1} = 18.4°C (NPEMI-A) and the use of experimental T_g values allowed the determination of the K parameter. As it has already been noticed, no thermodynamic information can be obtained from such a K, being it merely a fitting parameter. Experimental negative deviations from GT fit are observed inspecting Figure 4.21: they have been correlated with the existence of specific weak or moderate interactions (s. Sect. 1.8.1). A fitting based on a Couchman equation (1.57) is reported in Figure 4.21 (open squares). The fitting quality improved with respect to GT fit (broken line), as already observed in NPE blends, although not satisfactorily. The successive fitting procedure with Eqs. (1.59), (1.60), (1.61), (1.62)), proposed by Righetti et al.[148,149,150], takes into account the interactions occurring among the components of the blends, through the use of the "in excess" quantities (ΔS_m^l - ΔS_m^g) and (ΔH_m^l - ΔH_m^g). These quantities have been extracted from experimental T_g data of NPA blends, together with Q_s and Q_h (Eqs. (1.61) and (1.62), s. Sect. 1.8.1), respectively referring to "in excess" entropy and enthalpy, that contain information about the strength of intermolecular interactions[159]. The values Q_s = 0.0806 J g^{-1} K^{-1} and Q_h = 36.7300 J g^{-1} have been estimated for NPA blends, ascribable to weak or moderate specific interactions existing among blends components.

These Q_s and Q_h values are larger respect to those already reported for NPE blends; interactions existing in NPA blends are relatively stronger than that in NPE ones. A good prediction of T_g vs. composition trend is obtained through the introduction of such Q_s and Q_h values in Eqs. (1.59) and (1.60), the "in excess" enthalpy fitting is reported in Figure 4.21 as a continuous line

A different reproduction of the variation of T_g as a function of w_1 could be obtained by using the treatment proposed by Lu and Weiss[143,144] . The Lu-Weiss treatment permits the evaluation of the enthalpy of mixing ΔH_m and of Flory-Huggins interaction parameter χ[161] through Eqs. (1.63) and (1.64). By means of a careful fitting of the overall trend of T_g values of NPA blends, χ resulted to amount to about -4.5, while the value of ΔH_m can correspondingly be evaluated[144,161] as $\Delta H_m \approx$ - 3.2 kJ·mol^{-1}. This result classifies NPA blends as characterized by weak dipole-dipole interactions. Moreover, from a comparison with corresponding results obtained for NPE blend (χ = -3.5, $\Delta H_m \approx$ - 3.2 kJ·mol^{-1}, s. Sect. 4.3.2.1), it is possible to consider that interactions existing in NPA blends are stronger respect to those in NPE blends. This conclusion agrees with the prediction already made by "in excess" enthalpy and entropy treatment through the estimate of Q_s and Q_h values. The trend of Lu-Weiss fitting gave an optimized matching with experimental data; it is not displayed in Figure 4.21 for clarity, but it is very similar to in excess enthalpy fitting (continuous line).
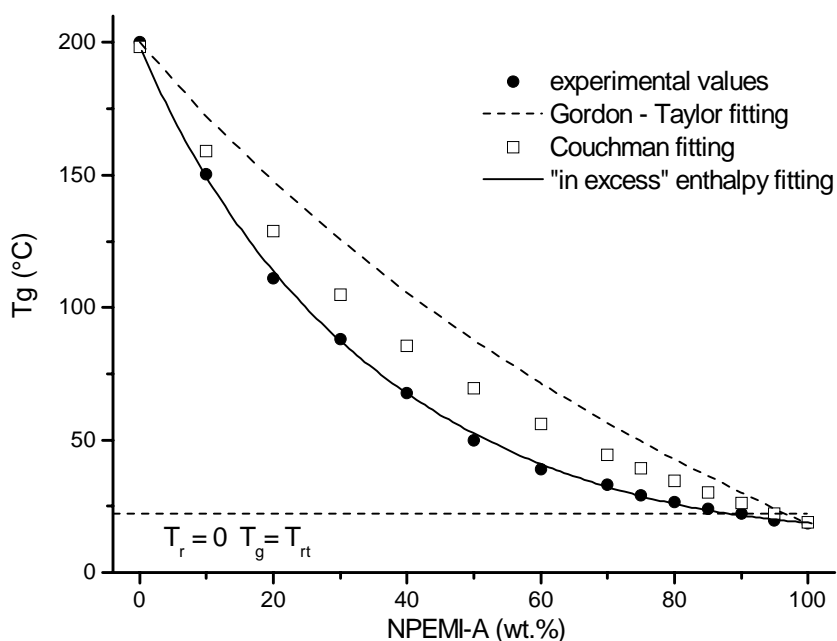

Figure 4.21 The dependence of the measured values of the glass transition temperature T_g (full circles) on the composition of the studied NPA blends. The results for various fitting procedures are also reported (s. text).

Table 4.5 Composition of the studied NPA blends, their glass transition temperature T_g, their reduced temperature ($T_r = T_g - T_{rt}$; $T_{rt} = 22.0°C$), glass transition width ΔT, heat capacity associated to glass transition ΔC_p.

Blend	Composition[a] (wt.%)		T_g (°C)	T_r (°C)	ΔT (°C)	ΔC_p (J g^{-1} °C^{-1})
	PVDMI	NPEMI-E				
PVD99	99	-	198.5	176.5	12.3	0.235
NPA10	94	5	150.3	128.3	17.5	0.265
NPA20	89	10	111.2	89.2	14.0	0.296
NPA30	79	20	88.0	66.0	21.4	0.329
NPA40	69	30	67.6	45.6	16.6	0.345
NPA50	59	40	49.9	27.9	35.1	0.394
NPA60	49	50	39.0	17.0	26.9	0.420
NPA70	39	60	33.1	11.1	18.1	0.447
NPA75	29	70	29.3	7.3	14.7	0.411
NPA80	24	75	26.7	4.7	12.2	0.382
NPA85	19	80	23.9	1.9	10.7	0.364
NPA90	14	85	22.0	0.0	7.7	0.356
NPA95	9	90	19.8	-2.2	5.1	0.335
NPA99	4	95	18.4	-3.6	3.2	0.334

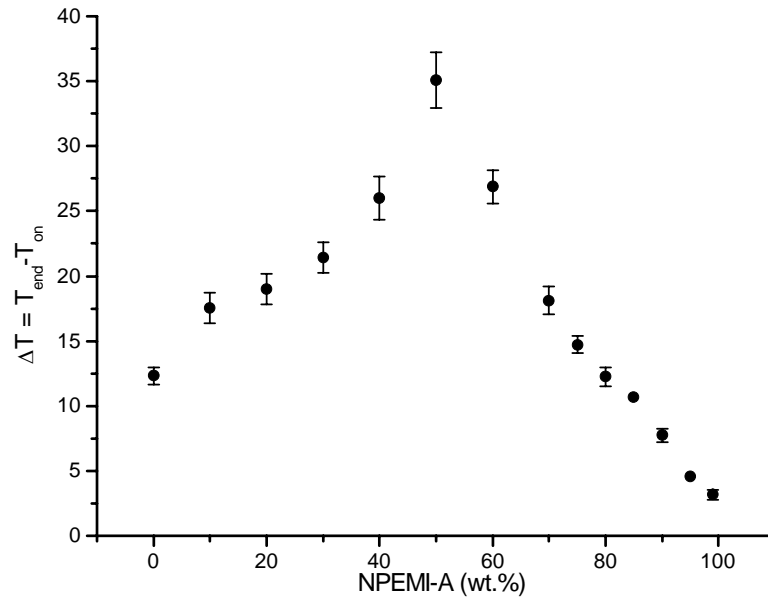a) TNFM photosensitizer is added to each blend in 1 wt% concentration.

Figure 4.22 Trend of glass transition width ΔT as a function of composition in NPA blends. Error bars are related to averaging over the three different scansions of DSC measurements.
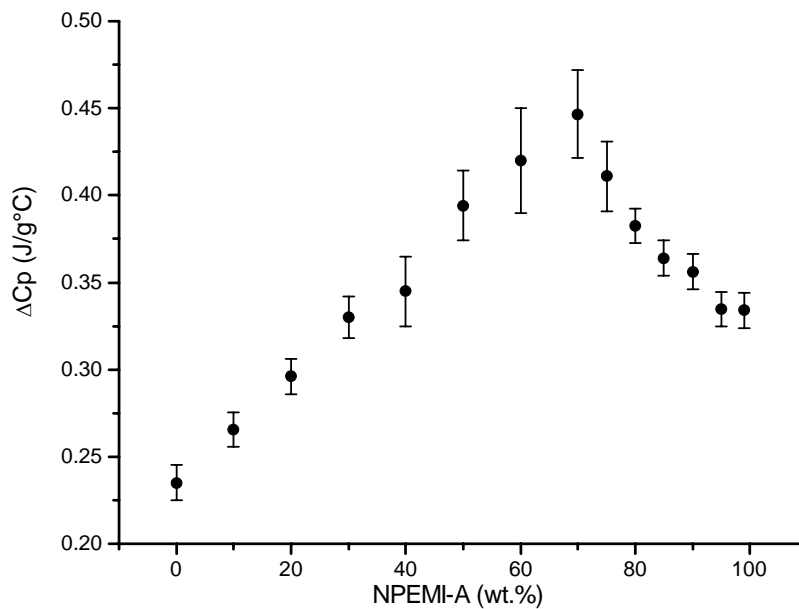

Figure 4.23 Trend of heat capacity change associated to T_g as a function of composition in NPA blends. Error bars are related to averaging over the three different scansions of DSC measurements

4.4 Photoconductivity measurements

Photoconductivity (PC) measurements were accomplished on blends of NPEMI-E and NPEMI-A with PVDMI. PC properties of both classes of materials were investigated in the $50 \leq w_1 \leq 100$ wt. % range of concentration of the NLO chromophores: exactly the same range of composition studied in PR measurements. Indeed, as already described in Sect. 3.8, PC and PR measurements were performed on the same electrooptic cells. Composition of the studied blends are listed in Table 4.6 and Table 4.7.

As a general remark concerning both NPEMI-E and NPEMI-A investigated blends, PC measurements evidenced the fundamental importance to use an extremely clean and chemically pure material. Chiefly with the fluid low-T_g samples, traces of mechanical impurities or micro droplets of residual solvents promoted the electric breakdown of the film also at low values of the applied electric field. On the other hand, traces of chemical impurities favoured the onset of a large dark current i_{dark} through the film (i.e. current measured when incident laser radiation is turned off, s. Sect. 3.8). When the necessary purity grade was not achieved, i_{dark} values comparable with the photocurrent i_{ph} (i.e. current measured when laser radiation is turned on) were recorded (s. also Sect. 3.8). It is well known that a high value of the conductivity contrast (i_{ph} / i_{dark}) is necessary in order to have a high value of the internal space charge field E_{SC} in PR effect[29,80]. Therefore, the minimization of effects due to impurities is mandatory in this research focussed on PR materials. As concerns NPEMI-E, only a double purification on chromatographic silica gel columns allowed to obtain a sample with satisfactory purity grade and whose dark current was equal to a hundredth of the value of the photocurrent ($i_{ph} / i_{dark} \approx 100$). In the following, results of PC measurements are discussed dealing with the values of photocurrent i_{ph} (s. Eq. (3.14), Sect. 3.8) measured at increasing values of the applied electric field from $E = 0$ up to $E = 90$ V/μm (Figure 4.25 and Figure 4.27). In Table 4.6 and Table 4.7 the measured values of i_{ph} are reported at the two reference values of E (E = 60 V/μm and E = 90 V/μm for NPE blends, E = 50 V/μm and E = 75 V/μm for NPA blends). Photocurrent is related to photoconductivity σ [Ω^{-1} cm^{-1}] through the relation $i_{ph} = \sigma ES$, Eq. (3.15), E [V/cm] being the applied electric field and S [cm^2] the area of the film lightened by the laser beam, whose diameter is equal to 3.0 mm.

4.4.1 PVDMI/NPEMI-E blends (NPE)

Table 4.6 reports the values of the photocurrent i_{ph} as measured at E=60V/μm and E=90V/μm on PVDMI/NPEMI-E blends (NPE blends). Figure 4.24 shows the trend of experimental i_{ph} values as a function of relative temperature T_r and of the composition of the blends (NPEMI-E wt.%). Composition of the investigated blends is reported in Table 4.4.

Table 4.6 Photocurrent i_{ph} of the studied NPE blends as measured at two values of the applied electric field, E = 60 V/μm and E = 90 V/μm.

Blend	i_{ph} (E = 60 V/μm) (A)	i_{ph} (E = 90 V/μm) (A)	T_r (°C)
NPE50	2.12 x 10^{-9}	8.42 x 10^{-9}	21.0
NPE75	1.68 x 10^{-8}	9.84 x 10^{-8}	-6.6
NPE80	2.66 x 10^{-8}	1.40 x 10^{-7}	-10.2
NPE85	3.30 x 10^{-8}	1.71 x 10^{-7}	-13.8
NPE90	3.40 x 10^{-8}	1.54 x 10^{-7}	-17.4
NPE95	3.56 x 10^{-8}	8.59 x 10^{-8}	-21.5
NPE99	8.52 x 10^{-8}	3.55 x 10^{-7}	-24.6

$i_{ph} = \sigma ES$. σ is photoconductivity, E is the applied electric field and S is the area of the film lightened by the laser beam, whose diameter is equal to 3.0 mm.

A discussion on the reported values and trend has been tried on the basis of the Gaussian Disorder Model (GDM) cited in Sect. 1.5 that describes the hopping migration of the photogenerated charges through the molecular lattice[16,58,60,61,62]. Photoconductivity results obtained previously in PVDMI containing blends were taken as reference for useful comparison.

Photocurrent measured in NPE50, the blend with the lowest content of NPEMI-E, is $i_{ph} \approx 10^{-9}$ A (at E = 60 V/μm); this value is about one order of magnitude lower compared to that ($i_{ph} \approx 10^{-8}$ A at E = 50 V/μm) found for a blend of PVDMI containing a 30 wt.% of the plasticizer N-methyilindole with a comparable value of T_g ($T_g \approx 35$°C)[85]. Because of the similarity of T_g values, this result can be justified by the effect of the large edm of the dissolved NPEMI-E, together with an expected increase of the distance R among the active sites of PVDMI. At this composition regime of relatively low content of NPEMI-E, indeed, it can be considered that hopping mechanism is primarily occurring through PVDMI units. The

144

effect of NPEMI-E can be therefore seen as the introduction of moieties acting as screens among hopping sites. The edm of NPEMI-E disturbs the process of migration, NPEMI-E does not being really involved in conductivity as an active site. Calculation by the MOPAC-7 software gave for NPEMI-E a value of edm μ = 8.23 D (s. Table 4.1), very much higher than the value computed for PVDMI edm μ = 2.47 D [84,85]. The effect of NPEMI-E on the lowering of the photoconductivity of PVDMI is the same previously found and reported for DMNPAA in blends of both PVDMI and PVK[71]. On the basis of the GDM treatment[16,58-62] the observed behaviour is related to an increase of the width of the DOS with the corresponding increase of the disorder of the sites whose electrostatic interactions condition the mobility of the migrating photogenerated charges.

As long as NPEMI-E content increases in NPE blends (s. Table 4.6) at the expense of polymer counterpart PVDMI, the photocurrent i_{ph} correspondingly grows. The continuous increase of PC is a clear evidence that NPEMI-E molecules (having electron donor properties) progressively replace PVDMI units, becoming charge carriers in the migration process. Two different types of charge carriers co-exist now at the same time in the system. This true percolation mechanism[173] (s. Sect. 1.5) from a system to another one is accounted for by the already discussed computed values of the ionization potential, Sect. 4.1. From Table 4.1, ip = 7.76 eV for NPEMI-E, a value lower than ip = 8.02 eV computed for PVDMI[85]. This lower value of ip determines the best PC properties attained by NPE99 blend (s. Table 4.6) notwithstanding the detrimental effect played on PC by the high edm value of NPEMI-E. In the frame of the GDM treatment, indeed, it is not only the value of edm of the donor molecules that conditions the dispersive interactions of the migrating charges. As reported in Sect. 1.5, the value of the charge mobility m, and hence of the photocurrent, depends also on the energetic and topological disorder of the dipolar chromophores with a corresponding variable width of the DOS[58,60,62].

When the content of NPEMI-E becomes higher than 80 wt.%, the trend of i_{ph} remarkably deviates from the usual linear dependence on the T_r value of the blend[29,71,80,135]. The sudden deviation, clearly visualized in Figure 4.24, is a negative one, that is i_{ph} lowers while the content of NPEMI-E increases. A minimum value is found for NPEMI-E content 90 < w_1 < 95 wt.%. The successive increase in i_{ph} does not restore the previous linear trend, so that i_{ph} for NPE99 blend (neat NPEMI-E) does not attain the value extrapolated by linear fit of low content blends (Figure 4.24, continuous line).
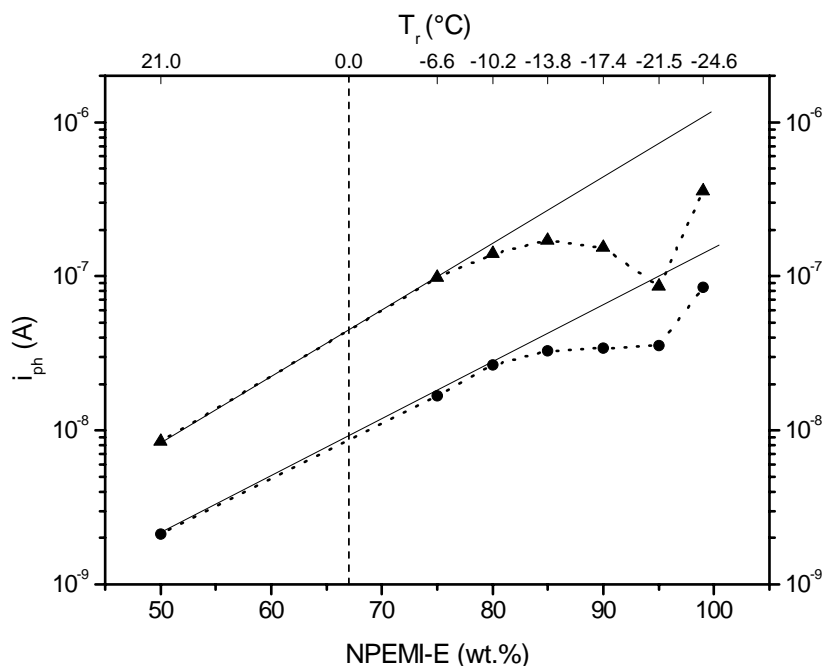
Figure 4.24 Trend of the measured photocurrent i_{ph} in NPE blends as a function of both the composition of the different blends (lower axis) and of the reduced temperature $T_r = T_g - T_{rt}$ (upper axis); full circles, values at E = 60 V/μm; full triangles, values at E = 90 V/μm. Dotted curves are guides for the eye.

In order to explain this unexpected and never previously recorded behaviour of i_{ph}, the same theoretical treatment of the "hopping" migration of photogenerated charges involving GDM used up to now has been considered. In the GDM frame, the value of i_{ph} chiefly depends on the values of ip and edm of the NLO chromophores (it is the edm seen by migrating charges). However, taking into account the high values of E (E = 60 and 90 V/μm) at which the variation of i_{ph} has been recorded, it seems to be reasonable to consider edm as the most important factor responsible for the rapid lowering of i_{ph}, ip playing a prominent role in the low electric field regime. The relatively sudden variation of photocurrent could be therefore related to a rapid increase of edm occurring in the material for some specific composition. Considering the graphs in Figure 4.24, the relative minimum of the trend of i_{ph} can be located at a $w_1 \approx 93$ wt.% content of NPEMI-E; a value of $i_{ph} \approx 8.0 \times 10^{-8}$ A at E = 90 V/μm corresponds to this concentration. The trend relative to measurements at E = 60 V/μm has a quite similar behaviour even if the minimum is less pronounced. The rapid increase of the edm value can be taken as an experimental evidence of what has been theoretically foreseen by Painelli et al.[136,137,174,175], s. Sect. 1.8. Clusters of dipoles, schematizing the highly polarized and polarizable push-pull molecules (s. sect. 1.3) were considered in a simple two-levels scheme. The two levels correspond to the two extreme electronic structures of the

dipole, namely the totally covalent (neutral charge distribution) and the totally ionic (zwitterionic) one. In the frame of this representation, the cited papers report rapid variations of the electrooptic molecular parameters (edm, first and second-order polarizabilities α and β) in clusters of dipoles in dependence of mutual distances and orientations. The behaviour of such clusters is therefore different depending on the different interactions among the dipoles. Clusters containing iso-orientated dipoles (parallel edm) or back to front dipoles (antiparallel edm) give a totally different response in terms of change of the electrooptic parameters. The possible variations were studied as a function of the intermolecular distances and hence of the concentration of dipoles. It has been found that for clusters of iso-orientated dipoles, as possibly are those present in our material under the effect of E, the rapid variation of the electrooptic parameters, and particularly the increase of edm, has a maximum at an intermolecular distance corresponding to a concentration of about 90-95 wt.% of the chromophores. On these bases, trends reported in Figure 4.24 find a good, at least qualitative, theoretical support to the lowering and to the position of the observed minimum of i_{ph}. Actually, due to the large concentration of NPEMI-E, the blend can be visualized as built by a large quantity of NPEMI-E with a very low amount of dispersed low-edm PVDMI molecules that control the electrostatic interactions inside the bulk. The good isoorientation of the NPEMI-E chromophores is made possible by the already discussed low values of T_g, as concerns the blends from NPE85 to NPE99. The corresponding large "free volume" allows the isoorientation of the NLO chromophores under the influence of the applied electric field E. The lowering of i_{ph} in Figure 4.24 should not be ascribed to some other usually invoked effects, namely, for instance, to the frequently cited formation of edm = 0 dimers arising from the coupling of back to front dipoles[33,34,35,102], s. Sect.1.4. If it were the case, i_{ph} should continuously lower when the concentration of NPEMI-E increases. The supramolecular phenomenon as described by Painelli et al. depends exclusively on the intermolecular distance and geometry.

Other evidences of the peculiar behaviour of the blends, due to the supramolecular effect discussed above, have been obtained in the study of the dependence of photocurrent i_{ph} on the value of the applied electric field E. The dependence on applied electric field of the mobility m of the migrating charges, interacting with the edms inside the material, is described by the already cited Poole-Frenkel-like equation (s. Sect. 1.5). We recall here Poole-Frenkel-like equation for clarity:

$$m(E) = m(0)\exp(SE^{1/2}) \qquad (4.2)$$

As it has been theoretically shown[176], when $E^{1/2}$ is reported on the abscissa in a semilogarithmic representation, the values of m(0) (the intercept of the trend at E = 0), and S, the slope of the linear part of the function, represent the energetic disorder of the interactions and the topological disorder of the random distribution of the interaction directions, respectively. Larger value of m(0) relates to a more energetically ordered system (a narrow width of the DOS), while a higher value of S represents a more geometrically disordered one. In Figure 4.25, trends of i_{ph} as a function of $E^{1/2}$ are reported in the typical semilogarithmic scale, in order to evidence a Poole-Frenkel-like behaviour. It is immediately evident from Figure 4.25 that the linear parts of the trends for NPE50 to NPE99 are nearly parallel; for the considerations made above, this result suggests a nearly constant topological order with the increase of the chromophore content. In the same time, the value of m(0) increases, indicating, as it could be expected, that the energetic order increases with the progressive replacement of PVDMI by NPEMI-E (i.e. DOS for NPE99 is narrower than for NPE50). The trends of NPE80 and NPE85, following these general rules without deviations, have been omitted in order to simplify the figure. However, and this is perhaps the most interesting point, the trends of NPE90 (full squares, dashed lines) and NPE95 (full triangles, dotted lines) blends appear to be "anomalous" respect to the overall blends series. Their slopes, particularly that of NPE95, are markedly less pronounced than those of all other blends; recalling the considerations made above, a low S is related to a more geometrically ordered system. The observed minimum of i_{ph} in Figure 4.24, when correlated to the "anomalous" trends of Figure 4.25, seems to effectively correspond to a more ordered system both in energy and geometry. It could be said that, in the frame of the Painelli's treatment proposed to explain the effect put in evidence in these measurements, the supramolecular effect of enhancement of electrooptic properties does not depend only on the chromophore concentration; it represents also a peculiarly ordered distribution of the intermolecular interactions that brings, for instance, to a larger value of edm.

A more careful insight of the data reported in Figure 4.25 allowed to obtain some other significant information about the mechanism involved in PC behaviour of these blends. The slope of the "anomalous" linear trends for NPE90 and NPE95 blends, is not constant over the entire range of $E^{1/2}$, which is not the case for the rest of overall NPE series, considered as "regular". For the NPE90 blend (full squares) the linear trend is broken in two not colinear segments, the discontinuity point being found at $E^{1/2} \approx 5.5$ $(V/\mu m)^{1/2}$. Trend for $E^{1/2} < 5.5$ $(V/\mu m)^{1/2}$ is strongly "anomalous", due to the high slope S, while for $E^{1/2} > 5.5$ $(V/\mu m)^{1/2}$, it behaves almost as all other trends referring to "regular" blends. In a similar way, a less sharp

148

discontinuity point appears at $E^{1/2} \approx 7.5$ $(V/\mu m)^{1/2}$ in the trend referring to NPE95 blend. The discontinuity points in such trends mark the values of the applied electric field at which a modification of PC mechanism occurs, as it has been reported in some previous studies[29,58,176,177].

As a last remark on the data represented in Figure 4.25, we can infer some information on the competition existing between the recombination and the dissociation rate of the electron-hole pair formed when the system is optically irradiated and excited. Sect. 1.5 illustrates the mechanism of formation of the photocharges as described by the geminate recombination model in organic materials[58,62]. According to this model, the electron-hole pair obtained in the excited state upon irradiation can recombine to give back the charge-transfer complex or, on the contrary, can dissociate giving origin to free charges, able to migrate by "hopping" mechanism. The balance between those two processes is ruled by the applied electric field E: a threshold value of E exists at which dissociation prevails on recombination. Such a value can be identified for NPE 50 and NPE75 blends in Figure 4.25 as the value of E above which the trend of i_{ph} in semilogarithmic scale becomes linear. It is well evident that threshold value of E is higher for NPE50 (open circles) than for NPE75 (open squares). Threshold for NPE50 and NPE75 is found at $E^{1/2} \approx 5.5$ $(V/\mu m)^{1/2}$ and $E^{1/2} \approx 4.0$ $(V/\mu m)^{1/2}$, respectively. As concerns all other blends (at higher content of NPEMI-E), their trends are linear for all the measured values of applied electric field, starting from the first imposed value of E = 10 V/μm ($E^{1/2} \approx 3.16$ $(V/\mu m)^{1/2}$). Nevertheless, they are expected to have a well lower value of the threshold ($E^{1/2} < 3$ $(V/\mu m)^{1/2}$) although it has not been measured.

The results concerning threshold values of E suggest to assign to NPE50 the lowest value of the photogeneration efficiency η (s. Eq. (1.48), Sect. 1.5); η increases with the increase of NPEMI-E content.
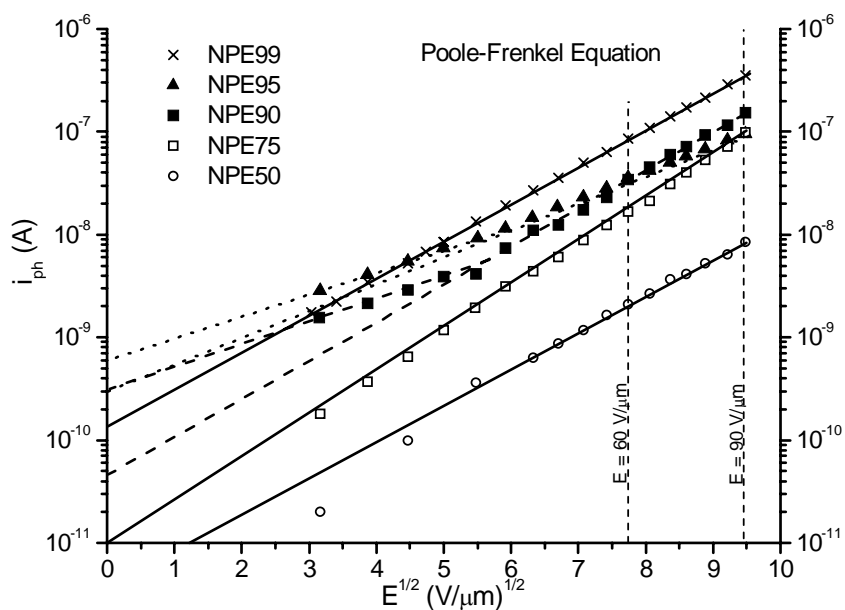
Figure 4.25 Measured photocurrent i_{ph} of NPE blends as a function of the square root of the applied electric field E (Poole-Frenkel-like equation). The meaning of the used symbols is clearly specified in the insert. The results for NPE80 and NPE85 blends have not been reported for clarity of representation but they are not "anomalous", s. text.

4.4.2 PVDMI/NPEMI-A blends (NPA)

Table 4.7 reports the values of the photocurrent i_{ph} as measured at E=50V/μm and E=75V/μm on PVDMI/NPEMI-A blends (NPA blends). The values of the applied electric field E taken as reference for NPA blends differ from those of NPE blends (s. Table 4.6) because measurements on the overall NPA series could not be performed over the same range: some NPA blends, indeed, underwent electrical breakdown for E > 75 V/μm. Figure 4.26 displays the trend of experimental i_{ph} values as a function of relative temperature T_r and of the composition of the blends. Composition of the investigated blends is reported in Table 4.5.

The discussion of the obtained PC measurements results concerning NPA blends could be made on the bases of considerations totally similar to those already made when dealing with NPE blends, s. Sect. 4.4.1.

150

Table 4.7 Photocurrent i_{ph} of the studied NPA blends as measured at two values of the applied electric field, E = 50 V/μm and E = 75 V/μm.

Blend	i_{ph} (E = 50 V/μm) (A)	i_{ph} (E = 75 V/μm) (A)	T_r (°C)
NPA50	8.08 x 10^{-9}	2.92 x 10^{-8}	27.9
NPA70	1.69 x 10^{-8}	6.5 x 10^{-8}	11.1
NPA75	2.11 x 10^{-8}	8.27 x 10^{-8}	7.3
NPA80	2.59 x 10^{-8}	1.06 x 10^{-7}	4.7
NPA85	2.91 x 10^{-8}	1.15 x 10^{-7}	1.9
NPA90	2.72 x 10^{-8}	1.06 x 10^{-7}	0.0
NPA95	3.44 x 10^{-8}	1.45 x 10^{-7}	-2.2
NPA99	5.54 x 10^{-8}	2.4 x 10^{-7}	-3.6

Photocurrents measured in NPA blends are in general larger than those measured in NPE blends at the same NLO molecule content. As concerns NPA50, indeed, its i_{ph} = 8.08 x 10^{-9} A value, measured at E = 50V/μm is well larger than the value reported for NPE50 at E = 60 V/μm (s. Table 4.6). Photocurrent measured in NPA50 is almost identical to that ($i_{ph} \approx 10^{-8}$ A at E = 50 V/μm) found for a blend of PVDMI containing a 30 wt.% of the plasticizer N-methylindole with a comparable value of T_g ($T_g \approx 35°C$)[85], being PVDMI blends taken as reference materials, s. Sect. 4.4.1. Recalling the considerations previously made, it can be inferred that NPEMI-A, is less active than NPEMI-E in disturbing the process of charge migration. Therefore, NPEMI-A, at this 50 wt.% concentration, actually does not act as a heavily screening moiety, leaving almost undisturbed the PC behaviour of PVDMI. As it has already been described for NPEMI-E, indeed, at this relatively low concentration of NPEMI-A , hopping is expected to occur uniquely through PVDMI sites, NPEMI-A molecules being not involved as active sites. Moreover, the lower molecular volume and the reduced steric hindrance with respect to NPEMI-E (lower density) could be also related to a reduced spacing R of hopping sites, this last parameter being a very important one in setting PC properties of a material. On the basis of the GDM treatment[16,58,60-62] the observed behaviour could be explained by assuming a substantial invariance of the width of the DOS: introduction of NPEMI-A does not increase, or very poorly increases energetic disorder of the sites responsible for conductivity and therefore leaves unvaried charge mobility, at least for content up to 50 wt.%.. The increasing content of NPEMI-A causes a corresponding increase in i_{ph}, the largest value being obtained for NPA99. This confirm the evidence for a percolation

mechanism acting in blends, already observed for NPEMI-E: NPEMI-A progressively replaces PVDMI units in their role of charge carriers in the migration through hopping of the photogenerated charges. NPA99, which contains only the lower ip species NPEMI-A, attains therefore the highest value of photocurrent respect to the overall NPA series (s. Table 4.7). Referring now to the trend of i_{ph} values as a function of composition (s. Figure 4.26), as obtained at the two reference E values, a deviation from the linear trend is clearly visible around 90 wt.% content of NPEMI-A. This feature, visualized in both E = 50 and E = 75 V/μm trends, already arose in PC measurements of NPE blends. Nevertheless, some differences have been put in evidence that allow to consider NPA blends separately, its PC behaviour differing from that of NPE blends. First of all, the deviation from linear trend occurs in NPA blends at a slightly larger content of NPEMI-A, namely at $w_1 > 85$ wt. %. Moreover, NPA99 i_{ph} value is found to be in good accordance with the prediction of the linear trend of i_{ph} as a function of composition. On the contrary, i_{ph} measured for NPE99 did not recover linear trend PC behaviour (s. Figure 4.24).

Similarly to NPE series, a relative minimum of NPA trend is found around 90 wt.% of NPEMI-A for both trends reported in Figure 4.26. Nevertheless, the extent of the deviation (the difference between linear trend and experimental value at 90 wt. %) is evidently much less pronounced. The deviation can be explained by means of the same considerations involving GDM and made for NPE blends, s. Sect. 4.4.1: the sudden deviation of photocurrent could be related to a rapid edm increase occurring at a specific composition, as consequence of a supramolecular collaborative effect[136,137], s. Sect. 1.8. Evidently, the reduced extent of i_{ph} deviation in NPA blends should be related to a correspondingly reduced extent of interactions leading to the onset of this supramolecular effect. The reduced extent of this deviation is also ascribable to the higher T_g values of NPA blends (compare data in Table 4.4 and Table 4.5). The good isoorientation of dipolar NLO chromophores was made possible, for NPEMI-E, in the whole range from NPE85 to NPE 99, due to the low Tg and the corresponding large free volume. As concerns NPA, the value of T_g is decisively higher so that the transition from soft to hard blends ($T_r = 0°C$) occurs at 90 wt.% content of NPEMI-A; reduced free volume is therefore available for chromophore reorientation and this could explain a more disordered arrangement with respect to NPEMI-E case. When soft blend regimen is reached (namely for NPA90 and NPA95 blends), the already described collaborative effect leads to a change in edm value of NPEMI-A species in the bulk of the material that is at the origin of the decrease in i_{ph} measured for NPA90 and NPA95. It is important to remark that, due to the higher values of T_g with respect to NPE case, the onset of such collaborative effect is reduced and limited to a narrower range of composition. Energetic

152

and geometric arrangements, indeed, seems to be different in NPE or NPA blends. Once the trend of i_{ph} as a function of the applied electric field is considered, other differences arise. A Poole-Frenkel-like trend is obtained for i_{ph} of each NPA blend, s. Figure 4.27. The trends of NPA80 and NPA85, following the general rules found for all other blends without deviations, have been omitted in order to simplify the figure. From the data reported in Figure 4.27, a slow increase in the slope S for the linear trends when chromophore content increases from NPA50 to NPA99 can be perceived. Such an increase, as already described in Sect. 4.4.1, could be related to an increasing geometrical disorder. The m(0) value (the intercept of the trend at E = 0) seems to be lower than the m(0) value found for NPE blends and also almost constant. A low increase in m(0) indicates a corresponding low increase in energetic order with the progressive replacement of PVDMI by NPEMI-A. This means that DOS for NPA99 is only slightly narrower than DOS for NPA50. Moreover, when Poole-Frenkel-like trends are compared for the two chromophores, namely NPE99 and NPA99 (Figure 4.28), it is evident that $m(0)_{NPA99} < m(0)_{NPE99}$ and $S_{NPA99} > S_{NPE99}$. From these last differences it could be inferred that NPEMI-A molecules are less involved in isoorientation due to supramolecular effects: a broader width of DOS (related to larger m(0)) and an increased topological disorder (high S) account for a more energetically and geometrically disordered system,. Interestingly, these differences between the two chromophores cause the two trends to cross themselves, NPA99 blend having a conductivity value higher than that of NPE99 only at the highest values of applied electric field, viz. $E^{1/2} > 7$ $(V/\mu m)^{1/2}$, s. Figure 4.28.

In addition, no hint of discontinuity points (change in the slope S of the linear trends) has been detected in the trends of the NPA blends, as it was the case for NPE90 and NPE95 blends. This result seems to confirm that in NPA blends the collaborative effect is less effective than in NPE blends.

As a last remark, threshold values (prevailing of dissociation over recombination of photogenerated charges, s. Sect. 4.4.1) for NPA50 and NPA75 blends are found at $E^{1/2} \approx 5.5$ $(V/\mu m)^{1/2}$ and $E^{1/2} \approx 4.0$ $(V/\mu m)^{1/2}$, respectively, while threshold could not be identified for higher content of NPEMI-A due to the low value of E at which it is expected to occur. This behaviour is quite identical to that found for NPE blends. Also in this case photogeneration efficiency η increases with the increase of NPEMI-A content.
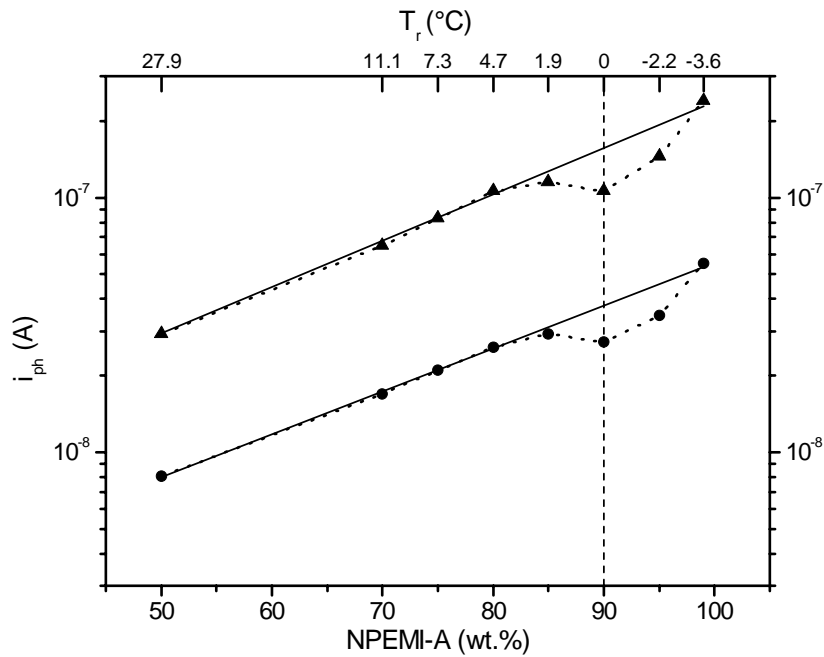
Figure 4.26 Trend of the measured photocurrent i_{ph} in NPA blends as a function of both the composition of the different blends (lower axis) and the reduced temperature $T_r = T_g - T_{rt}$ (upper axis); full circles, values at $E = 50$ V/μm; full triangles, values at $E = 75$ V/μm. Dotted curves are guides for the eye.
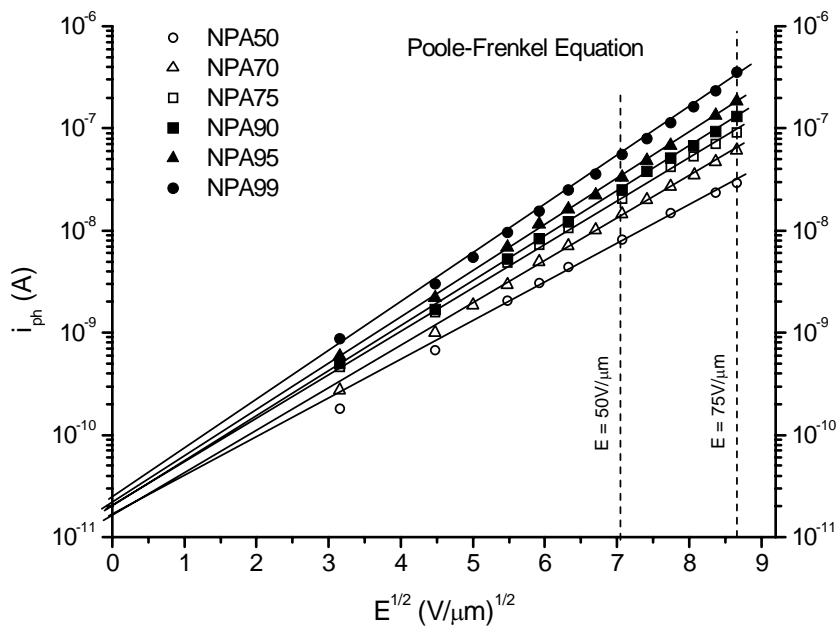

Figure 4.27 Measured photocurrent i_{ph} of NPA blends as a function of the square root of the applied electric field E (Poole-Frenkel-like equation). The meaning of the used symbols is clearly specified in the insert. The results for NPA80 and NPA85 blends have not been reported for clarity of representation.
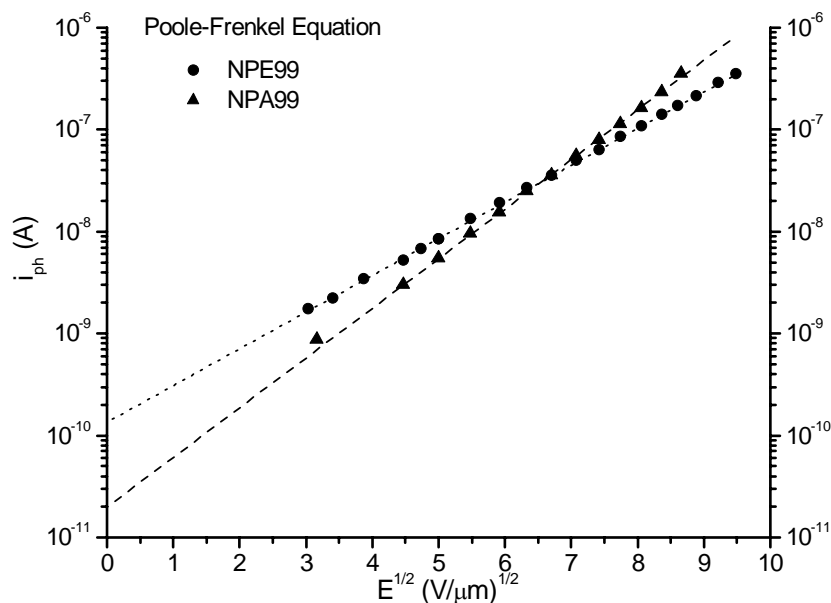
Figure 4.28 Comparison between the trends of i_{ph} as a function of the square root of the applied electric field E (Poole-Frenkel-like equation) for NPE99 and NPA99.

4.5 Photorefractivity measurements

PR behaviour is investigated in this research by means of 2BC technique, whose experimental setup is described in Sect. 3.6. 2BC measurements, performed with the method reported in Sect. 3.7, allowed to obtain the values of PR optical gain Γ_2 (the underscript referring to signal laser beam, named beam 2) for the overall series of NPE and NPA blends, as a function of the applied electric field E. Γ_2 has been considered as the most important PR parameter with which to compare the obtained results with other different PR materials. Moreover, Γ_2 represents for this research the most meaningful parameter because of our particular interest in applications involving light amplification. Indeed, the value of Γ_2 gives a quantitative estimate about the power of the "pump beam" transferred to the "signal beam" (beam 1 and beam 2, respectively, s. Sect. 3.6). The transfer of light power from one laser beam to the second one represents the clearest indicator that we are actually dealing with a real PR material.

Before to report and discuss the obtained PR results we try here to summarize some aspects of the present research, in order to provide the reader with the peculiar point of view in which the results have been discussed. It is important to remark here the original approach of this research, as already depicted in Sect. 2.2. To hit the target of a technically useful and reliable optical PR cell, the different necessary chemical components were selected with the aim of obtaining an efficient supramolecular system. PVDMI was selected as PC polymer due

155

to its already verified good PC properties[82,83,84] and of its compatibility with a dissolved chromophore like DMNPAA[71]. NPEMI-E and NPEMI-A, containing the same indole functionality that is present in PVDMI, were selected as possible good and compatible NLO chromophores, also on the basis of calculations of their relevant electrooptic parameters (s. sect. 2.2 and 4.1) that provided the expectation for a quite large value of Kerr figure of merit, $F^{Kerr} = 0.39 \times 10^{-74} \; C^2 \; V^{-2} \; m^4 \; Kg^{-1}$ mol (s. Sect. 4.1). In so doing, it was decided to develop a research way that is different with respect to that frequently followed in the study of PR organic materials. This last way usually consists in dissolving many different potential chromophores in PVK, with the aim to exploit its good PC, but disregarding the compatibility and the interactions occurring between the two species[2]. The already described problem of phase segregation arises when relatively large amounts of NLO species are introduced in PR blends, their high concentration being desirable to obtain good PR properties (e.g. large values of gain). Moreover, the availability of the chromophore to reorient under the effect of the total poling electric field E_T (made up of the externally applied electric field E and of the resulting inner space charge field E_{SC} , s. Sect. 1.4) is also an extremely important feature. This reorientation depends on the values of the electrooptic parameters -μ, $\Delta\alpha$ and β (which determine the extent of both the "electrooptic contribution" C_{EO} and the "birefringence contribution" C_{BR} to the photorefractivity[27,33,34,178], s. Sect. 1.4)-, these contributions being summarized by F^{Kerr}, Eq. (1.40), and on the values of T_g and free volume, s. Sect. 1.8. A particular care has been devoted to the study of T_g and on the role played by interactions in PR blends, s. Sect. 4.3. It is indeed important to remark that PVDMI acts, chiefly at high wt. % content of the NLO species where the photorefractivity rises to very high values, as a dielectric having a high value of edm. As a consequence, it can efficiently and finely control the intermolecular interactions by placing itself among the NLO molecules. The onset of PR behaviour and the influence of these interactions have been followed step-by-step studying PR at increasing content of NLO chromophores.

With this aim, both NPEMI-A and NPEMI-E based blends with PVDMI have been investigated in the composition range $50 \leq w_1 \leq 100$ wt.%, w_1 being wt. % content of NPEMI-A (or NPEMI-E). Blends at lower NLO species content have not been taken into consideration in PR measurements (as well as in PC ones) because they are not useful for a practical use as PR materials. Indeed, their high values of T_g classify them as "hard-materials", i.e. the materials having their $T_g > T_{rt}$. From the calorimetric considerations previously made, the "free volume" becomes too small to allow some significant molecular reorientation of the chromophore and this results in very poor PR behaviour, uniquely ascribable to electrooptic contribution, C_{EO}, s. Sect. 1.4.

4.5.1 PVDMI/NPEMI-E blends

Composition of the studied blends is given in Table 4.4. Table 4.8 reports the PR optical gain Γ_2 values measured by the 2BC technique[1,71,105] on PVDMI/NPEMI-E blends (NPE blends). Data reported in Figure 4.29 represent the trend of the PR optical gain Γ_2 as a function of both the composition of the blend and the value of T_r. The complete trends of Γ_2 as a function of the applied electric field E, obtained for the overall series of NPE blends, are not reported for conciseness; as an example, $\Gamma_{1,2}$ (both Γ_1 and Γ_2) vs. E trend referring to NPE99 is reported in Figure 4.30 that permits to appreciate the almost symmetric behaviour of the two beams in 2BC experiment: due to the PR effect beam 2 gains in energy ($\Gamma_2 > 0$; gain) at the expense of beam 1 ($\Gamma_1 < 0$; loss).

Starting from NPE50 blend (s. Table 4.8) the value of $T_r = 21.0°C$ ($T_g = 43.0$ °C) places this blend in the class of the so-called "hard-materials". For the already cited reasons, the very small values of $\Gamma_2 = 3.0$ and 10.2 cm^{-1} obtained for NPE50 blend at the two measuring values of E, could approximately be assumed as the values of the "electrooptic contribution" to the photorefractivity, C_{EO}. C_{EO} usually represents the extent of PR in inorganic crystals (Pockels effect) and originates exclusively from the electron system of the chromophore through its electric dipole moment and first hyperpolarizability β: a substantially static contribution.

The subsequent blend in the series, NPE75 blend, is instead classifiable as a "soft" material, having $T_r = -6.6$ °C ($T_g = 15.4$ °C), s. Table 4.8. The transition temperature from hard to soft material, $T_r = 0°C$, corresponds to NPEMI-E content $w_1 \approx 67$ wt.%. The values of PR gain for NPE75 amount to $\Gamma_2 = 63$ and 150 cm^{-1} at E = 60 V/µm and E = 90 V/µm, respectively, confirming a rapid increase with respect to NPE50, s. Table 4.8 and Figure 4.29. An analysis of the trend of Γ_2 reported in Figure 4.29 must imply the consideration of all parameters influencing the PR response of a given material[2]. The first parameter that must be taken into consideration is the photocurrent i_{ph} , s. Sect. 1.5; results and discussion of PC measurements performed on NPE blends are reported in Sect. 4.4.1. PC properties are very important because the migrating charges give origin to the space-charge field E_{SC} responsible for PR effect. E_{SC} is generated by the fraction of the migrating charges that can stay on the so called "traps", local sites inside the material characterized by a sufficiently deep electrical potential (s. sect. 1.5). Under the effect of the optical lattice generated by the two laser beams that interfere inside the material (2BC experiment), setting charges generate an analogous charge lattice that modulates the local value of the refractive index through the electrooptic

effect. The two lattices can be dephased by an angle Θ (s. Eq. (1.10), Sect. 1.1). It can be verified that the following relationship (Eq. 1.13) holds:

$$\Gamma \propto \Delta n \sin \Theta \qquad (4.3)$$

in which Δn is the overall modulation of the refractive index, its extent being related to the value of E_{SC} through Eq. (1.11). On the other hand, under some simplifying assumptions[29] Eq. (1.10) reduces to:

$$\tan \Theta = E_0 / E_q \qquad . \qquad (4.4)$$

E_0 is the projection of the external field E on the lattice wave vector k and E_q is the saturation field (or *trap-limited field)* generated by the traps, whose density N_T is defined from Eq. (1.9)

$$E_q = eN_T / k\varepsilon_r \qquad , \qquad (4.5)$$

where ε_r is the bulk permittivity of the material. The ratio E_0 / E_q of Eq. (4.4) is also present in a possible simplified expression of E_{SC} [29,80], s. Eq. (1.7)

$$|E_{SC}| \approx A \left\{ E_0^2 \Big/ \left[1 + \left(E_0 / E_q \right)^2 \right] \right\}^{1/2} \qquad . \qquad (4.6)$$

A contains parameters referring to the laser irradiation modality and to the transport and recombination mechanism of the photo-charges. It is evident that an increase of E_q, and hence of N_T, can cause an increase of $|E_{SC}|$ with favourable consequences on Δn and Γ_2.

Due to the weak dipole interactions existing inside NPE blends, evidenced by the calorimetric measurements (s. Sect. 4.3.2.1), it is possible to hypothesize a good poling efficiency of NPEMI-E with a corresponding high value of the "birefringence contribution" Δn_{BR} to PR.

On these bases, the values of Γ_2 (s. Table 4.8 and Figure 4.29) can be, at least qualitatively, rationalized. The following discussion deals with trend corresponding to E = 90 V/μm, the trend obtained at E = 60 V/μm being exactly describable by the same argumentations. As NPEMI-E wt.% content increases T_g of NPE blends lowers (s. values of T_r on the upper horizontal axis of Figure 4.29), promoting the mechanism of chromophore

158

reorientation. The birefringence contribution correspondingly increases and Γ_2 should become higher and higher. On the other hand, the progressive onset of a counteracting mechanism becomes more and more important: the decrease in the value of E_q as long as T_g (and T_r) lowers. The reduction of E_q is caused by a progressive reduction of the density of the traps N_T, mainly of the "deep traps" (s. Sect. 1.5). Such deep traps can sustain more permanently the charge lattice that gives origin to E_{SC} [16,29,58,80,135] while the alternative "soft traps" (whose electrical potential is not sufficiently deep), becoming more and more abundant with the lowering of T_g, do not guarantee the temporal stability of the charge lattice. Soft traps are transitory species due to their nature of easily thermally excitable sites. The progressive reduction of E_q -and hence of E_{SC}, s. Eq. (4.6)- causes the increase of Γ_2 to slow down progressively. The balancing of the counteracting mechanisms gives rise to the onset of the maximum in the trend of Γ_2 as a function of composition (s. Figure 4.29). NPE90 blend with its $\Gamma_2 = 2027$ cm^{-1}, marks about the highest value attained (and perhaps the highest value ever obtained for a totally organic PR material), while the true maximum of Γ_2 is actually found at 91.5 wt.% content of NPEMI-E, as shown by a fitting of the obtained trend (dotted line in Figure 4.29). From this maximum on, Γ_2 lowers rapidly down to the still fairly good value $\Gamma_2 = 976$ cm^{-1} measured for NPE99 blend.

The change of the role played by the traps around the critical values of 90 and 95 of the NPEMI-E content, was already evidenced by the PC results reported in Figure 4.24, s. Sect. 4.4. Just only for NPE90 and NPE95, both the slope S and the intercept m(0) at E = 0 of the linear part of the Poole-Frenkel-like trends are distinctly different with respect to the slope and intercept of all other blends. The lower value of S and the higher value of m(0) for these blends have been interpreted as features of a particularly ordered system (s. Sect.4.4). The corresponding small width of the DOS (s. Sect. 1.5) allows the creation of a lower amount of traps, possibly by favouring the most stable ones, namely the "deep traps"[16,58,135]. The observation that almost regular values of S and m(0) are restored for NPE99 blend supports the idea that some peculiar event happens around NPE90 blend. Indeed, maxima positions in Γ_2 trends reported in Figure 4.29 coincide with those of minima of i_{ph} in Figure 4.24; it seems therefore reasonable to hypothesize for PR results an interpretation similar to that already tempted for PC ones. Due to the peculiar interactions among the chromophores occurring around 91.5 wt.% content of NPEMI-E, a rapid change in molecular electrooptic parameters can be expected. Besides the already described variation of edm (s. 4.4.1), a rapid variation of $\Delta\alpha$ and β can also occur; it can be described on the basis of the quanto-mechanical approach developed by Painelli et al.[136,137,174,175], s. Sect. 1.8 and 4.4.1. Such variations could account for an "extra" contribution to PR effect, due to this supramolecular arguments, to be added to

159

the already described electrooptic C_{EO} and birefringence C_{BR} contributions. A similar extra-contribution to the extent of PR was already described from a different but similar point of view by means of the Kirkwood factor g_k[29,179]; it deals with variations of the second order NLO susceptibility due to dipole-dipole interactions. A collaborative contribution C_{COLL} to the electric field induced birefringence Δn_{BR} can therefore be hypothesized to exist. It acts in materials, as the ones object of the present study, in which dipolar interactions among NLO chromophores cannot be neglected; thus, the Oriented Gas Model assumptions depicting the reorientation of NLO chromophores (s. Sects. 1.3 and 1.4), must be, at least partially, modified because they underestimate the role played by the interactions. This collaborative contribution can be seen as a surplus contribution to the usual reorientational Δn_{BR}. In order to estimate the extent of the collaborative contribution, some considerations on the birefringence contribution can be made. It is possible to assume that this usual contribution is proportional to E^2, i. e. $\Delta n_{BR} \propto BE^2$, E being the externally applied electric field acting on PR cell[27,29,178]. B contains the electrooptic parameters edm, $\Delta\alpha$ and β that appear in the Kerr figure of merit, Eq. (1.40). Indeed, the amount of the increase of Γ_2 can be estimated for each NPE blend when E increases from a value of 60 V/μm to 90 V/μm, s. data reported in Table 4.8 and Figure 4.29. In the hypothesis that B remains constant over the series, apart the chromophore concentration, starting from the value Γ_2 measured at E = 60V/μm, its value at E = 90V/μm as expected for reorientational contribution only can be computed for each blend, i.e. $\Gamma_2 \propto E^2$, s. also Eq. (4.3). The computed values for NPE50 and NPE75 almost coincide with the two experimental values of Γ_2 at E = 90 V/μm. The computed values of Γ_2 for blends from NPE80 to NPE99 progressively increase but remain always lower than the experimental ones. The largest difference between experimental values and computed ones corresponds to the maximum of the experimental trend. To give an idea of such differences, for NPEMI-E content of 90wt%, corresponding to the experimental maximum of $\Gamma_2 = 2027$ cm^{-1} a computed value of $\Gamma_2 = 1400$ cm^{-1} has been obtained. The difference $2027 - 1400 = 627$ cm^{-1}, similarly to all other differences observed for each other blend, can be confidently ascribed to the extra collaborative contribution, C_{COLL}. Similar collaborative effects have already been observed in materials having different NLO response[138,180,181,182,183].

As a final remark, PR data obtained for NPE99 revealed the very good PR behaviour of NPEMI-E also when employed as a neat material, with the only addition of a small (1 wt.%) amount of sensitizer TNFM. Its PR properties as LMWG have been therefore successfully verified. Moreover, the large value of $\Gamma_2 = 976$ cm^{-1} measured for NPE99 blend at E =90 V/μm, is possibly a sufficiently good test to exclude that a large part of the NPEMI-

E molecules have the tendency to couple as edm = 0 dimers. The onset of such drawback has instead been observed in some other LMWG PR molecules[33,34,35,102], giving rise to a drastic reduction of PR performances.

Table 4.8 Photorefractive optical gain Γ_2 of the studied NPE blends, as measured at E = 60 V/μm and E = 90 V/μm.

Blend	Γ_2 (E = 60 V/μm) (cm^{-1})	Γ_2 (E = 90 V/μm) (cm^{-1})	T_r (°C)
NPE50	3.0	10.2	21.0
NPE75	63	150	-6.6
NPE80	179	444	-10.2
NPE85	393	1217	-13.8
NPE90	610	2027	-17.4
NPE95	510	1712	-21.5
NPE99	232	976	-24.6
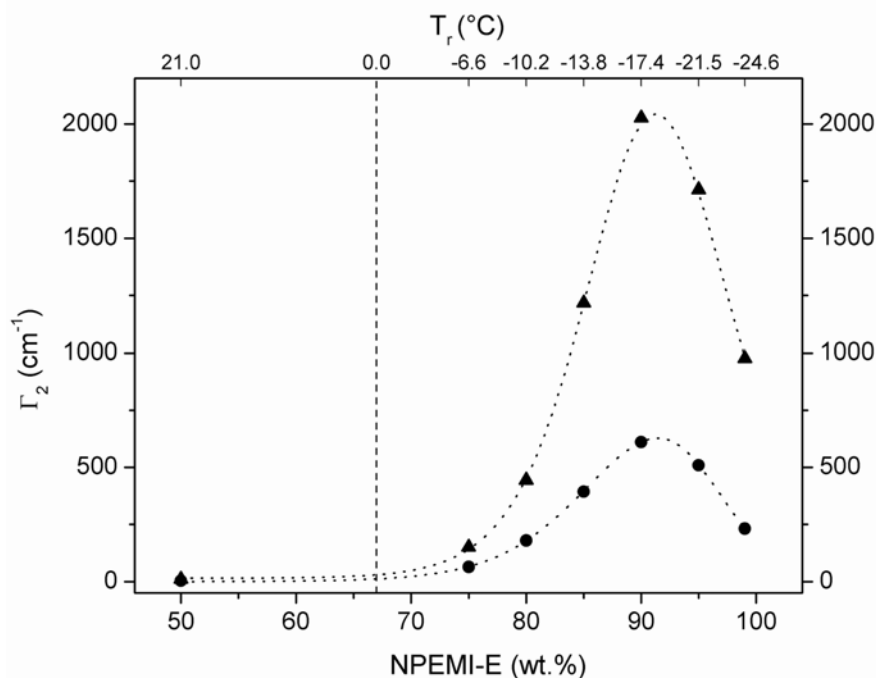
Figure 4.29 The trend of the obtained PR optical gain Γ_2 in NPE blends as a function of both the composition of the different blends (lower axis) and of the reduced temperature T_r = T_g – T_{rt} (upper axis); full circles, values at E = 60 V/μm; full triangles, values at E = 90 V/μm. The maximum of both curves is found at about 91.5 wt.% content of NPEMI-E.
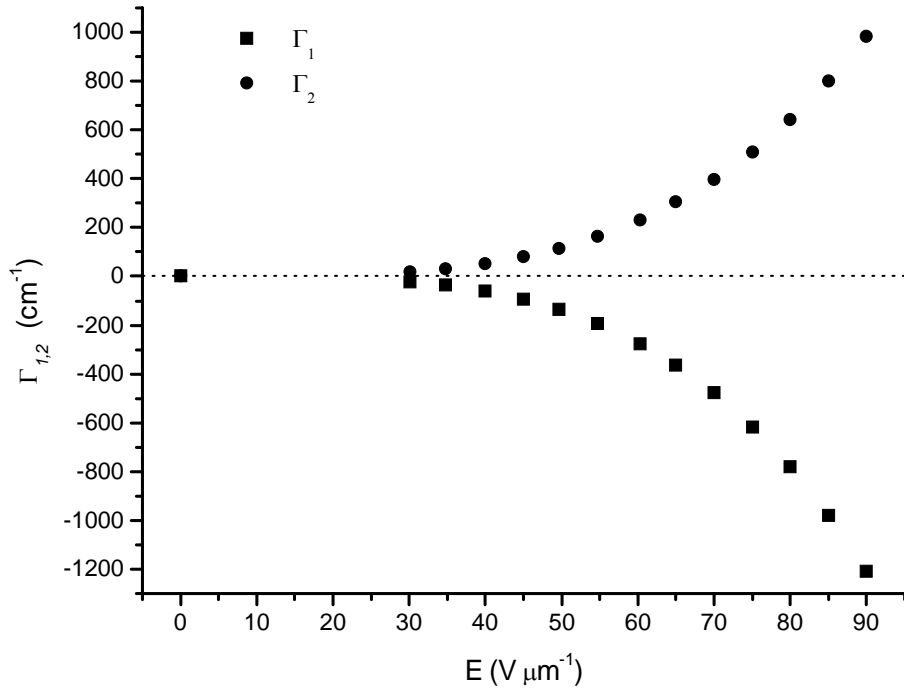
Figure 4.30 Photorefractive optical gain $\Gamma_{1,2}$ measured in a 2BC experiment for beams 1 and 2 as a function of the applied electric field E; NPE99 blend.

4.5.2 PVDMI/NPEMI-A blends

Table 4.9 reports the PR optical gain Γ_2 values measured by the 2BC technique on PVDMI/NPEMI-A blends (NPA blends). Composition of the studied NPA blends is given in Table 4.5. Data reported in Figure 4.31 represent the trends of gain Γ_2, measured at the two values of E = 50 and E = 75 V/µm, as a function of both the composition of the blends and the value of T_r. The complete trends of Γ_2 as a function of the applied electric field E, obtained for the overall series of NPA blends, are not reported for conciseness. Anyway, they are similar to those reported in Figure 4.30 for a NPE99 blend.

Starting from NPA50 blend (s. Table 4.9), its value of T_r = 27.9°C (T_g = 50 °C) places this blend in the class of the so-called "hard-materials". For the already cited reasons, the very small values of Γ_2 = 1.4 and 3.4 cm^{-1} obtained for NPA50 blend at the two measuring values of E, could approximately indentify the values of the "electrooptic contribution" to the photorefractivity, C_{EO}, s. Sect. 1.4. A substantial reduction is found when the values for NPA50 are compared to those obtained for NPE50.

The subsequent blends in the series, NPE70-NPE85 blends, are again classifiable as hard materials, having 11.1 < T_r < 1.9°C, s. Table 4.9. The transition temperature from hard to soft material, T_r = 0°C, corresponds indeed to a NPEMI-A content $w_1 \approx$ 90 wt.%. For 50 − 85

162

wt.% content of NPEMI-A, relatively low Γ_2 values are therefore obtained, the chromophore reorientation being strongly hindered. It is easy to verify that a very slow increase occurs for PR gain with the increase of NPEMI-A content. By comparing the Γ_2 values reported in Table 4.9 for NPA blends with those in Table 4.8 for NPE, it is possible to have an idea of the very different behaviour of the two classes of blends. Both curves reported in Figure 4.31, shows a similar trend: an initial slow continuous increase of Γ_2 with chromophore concentration up to a 90 wt.% content; at this value a clear stop occurs, with a quite plane trend up to 95 wt. %. The curve is then completed by a very steep increase, with NPA99 blend attaining the highest value on the overall series and restoring the trend predictable that could be extrapolated from the values in the range $50 < w_1 < 90$ wt.%. These trends are evidently very different from those reported in Figure 4.29 for NPE blends.

Nevertheless, a discussion of the results could be conducted on the bases of identical considerations. As NPEMI-A wt.% content increases, T_g of NPA blends lowers (s. values of T_r on the upper horizontal axis of Figure 4.31) although the promotion of the mechanism of chromophore reorientation is not really allowed until $T_r < 0$, when NPEMI-A content reaches $w_1 = 90\text{-}95$ wt.%.. The increase in Γ_2 should therefore be ascribable to the increasing concentration of NLO species and to the increase of N_T and, consequently, of E_q. On the other hand, the counteracting mechanism of the decrease in the value of E_q as long as T_g (and T_r) progressively lowers, described for NPEMI-E (s. Sect. 4.5.1), is poorly active in NPA blends until reaching $w_1 = 95$ wt.%, when T_r becomes slightly negative. At this point the collaborative effect can give a contribution to the extent of PR effect. But, being the value of T_g well higher than that of the corresponding NPE blend, this contribution will be of moderate importance, leading to the broad maximum at $w_1 = 90$ wt.%. At $w_1 = 95$ wt.% the blend is going out from the concentration range favourable to the onset of the collaborative effect and Γ_2 tends to assume a lower value. But the value of N_T progressively tends to become larger and larger with the lowering of T_g. For this reason, between $w_1 = 95$ and 99 wt.% the value of Γ_2 rapidly increases again. Here, due to the relatively low value of T_g, a high value of the concentration of the deep traps can be considered to exist. On the contrary, in the case of NPE blends, it was hypothesized that the traps at high content of the NLO chromophore were more and more of the "soft" type (s. Sects.4.5.1 and 1.5)[96] with the recorded decrease of Γ_2 following its maximum. It is also clear that the lowering of T_r towards negative values promotes the reorientational contribution as evidenced in the steep increase of Γ_2 for $95 < w_1 < 99$ wt.%. This improved reorientation leads to the relatively high value attained by NPA99 blend ($\Gamma_2 = 210$ cm^{-1} at $E = 75$V/μm); its $T_g = 18.4$°C permits indeed a more efficient

reorientation of NPEMI-A molecules in the poling field with respect to all other blends in the NPA series.

The fundamental importance of T_g and T_r in setting PR performances has been therefore confirmed. About this feature, it is interesting to compare the obtained results for NPEMI-E and NPEMI-A, as concerns the materials studied as LMWG, that is NPA99 and NPE99. Recalling that their electrooptic parameters have been taken as equal (s. MOPAC calculations, Sect. MOPAC-7 calculations of the relevant electrooptic parameters of the chromophores) and that their PC characterization, although revealing some differences, gave very similar values of i_{ph} (s. for example Figure 4.28), it is remarkable to put in evidence the extremely different PR behaviour in terms of measured Γ_2 values. The markedly larger value of Γ_2 obtained for NPE99 must be ascribed only to the lower value of T_g that is the only real difference between these two molecules.

Table 4.9 Photorefractive optical gain Γ_2 of the studied NPA blends, as measured at E = 50 V/μm and E = 75 V/μm.

Blend	Γ_2 (E = 50 V/μm) (cm^{-1})	Γ_2 (E = 75 V/μm) (cm^{-1})	$T_r = T_g - T_{rt}$ (°C)
NPA50	1.4	3.4	27.9
NPA70	7.1	23.5	11.1
NPA75	13.0	40.2	7.3
NPA80	18.8	59.8	4.7
NPA85	31.0	85.5	1.9
NPA90	41.7	115.4	0.0
NPA95	48.9	120.9	-2.2
NPA99	87.1	210.1	-3.6
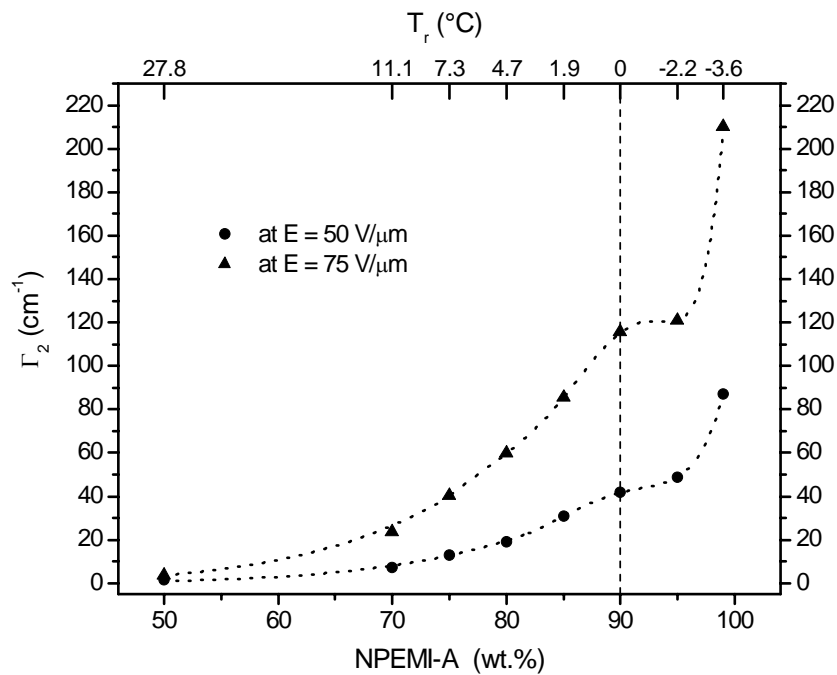
Figure 4.31 The trend of the obtained PR optical gain Γ_2 in NPA blends as a function of both the composition of the different blends (lower axis) and of the reduced temperature $T_r = T_g - T_{rt}$ (upper axis); full circles, values at E = 50 V/μm; full triangles, values at E = 75 V/μm. The drastic change of both curves is found at about 90 wt.% content of NPEMI-A.

4.6 Spectroscopic Ellipsometry measurements

In order to gather further information about the reorientational behaviour of the NPEMI-E chromophore, ellipsometry measurements have been made. Refractive index n and its variation Δn related to the effect of an applied electric field have been investigated on each blend of NPE series. The idea was to follow the effect of composition (and hence the onset of peculiar interactions and supramolecular arrangements, as observed in PC and PR measurements) on refractive index. Spectroscopic Ellipsometry (SE) measurements have been performed on sample cells (namely, the same cells employed in PR measurements) with a particular methodology, expressly planned for these measurements, as described in Sect. 3.10. The results reported here are to be considered as preliminary data, not dealing for example with NPA blends and being obtained only at $T = T_{rt}$; further development of SE measurements has been planned and will be probably object of following researches. Nevertheless, the obtained data have been useful in confirming the peculiar behaviour of NPE blends around 90 wt.% content of NPEMI-E; observed peculiarities are similar to those already discussed in connection with the PC and PR measurements. Figure 4.32 reports the trend of the value of the refractive index n_0 as a function of the composition of the studied blends (right vertical axis, full dots) without an applied static electric field, $E = 0.0$ V/μm. The reported trend shows a clear maximum of n_0 at a NPEMI-E content of $w_1 \approx 90$ wt.%. The change of the value of n_0 is comprised between $n_0 = 1.8$ and $n_0 = 2.0$. When an electric field, $E \neq 0$, is applied on the film, the values of the refractive index change with respect to the values n_0 at $E = 0.0$ V/μm. As an example, the same Figure 4.32 reports the trend of the variation Δn for all the already studied blends, as measured at the reference value $E = 30$ V/μm (open dots). Δn is defined as $\Delta n = n - n_0$, n being the value of the modified refractive index, i.e. the refractive index measured under the application of the electric field $E = 30$ V/μm. Both trends of Figure 4.32 have an evident maximum at $w_1 \approx 90$ wt.% and this occurrence cannot be due to a simple coincidence. It can be said that all physical quantities of the NLO chromophore NPEMI-E, like the refractive indexes n_0 and n depend on the electrooptic parameters[184] that we have already invoked in the previous discussion of the experimental data. The change of the glass transition temperature T_g when the composition of the blend changes, influences the reorientation efficiency with the consequent changes of the electrooptic parameters. When an electric field E is applied, like in the case reported in Figure 4.32, the reorientation efficiency for each blend is modified. In both cases, however, the remarkable maximum, characteristics of both n_0 and n, might be ascribed to the collaborative

166

contribution C_{COLL} (Painelli's effect) that we have previously hypothesized. We are currently analysing the ellipsometric data that demand a more careful and deep examination.
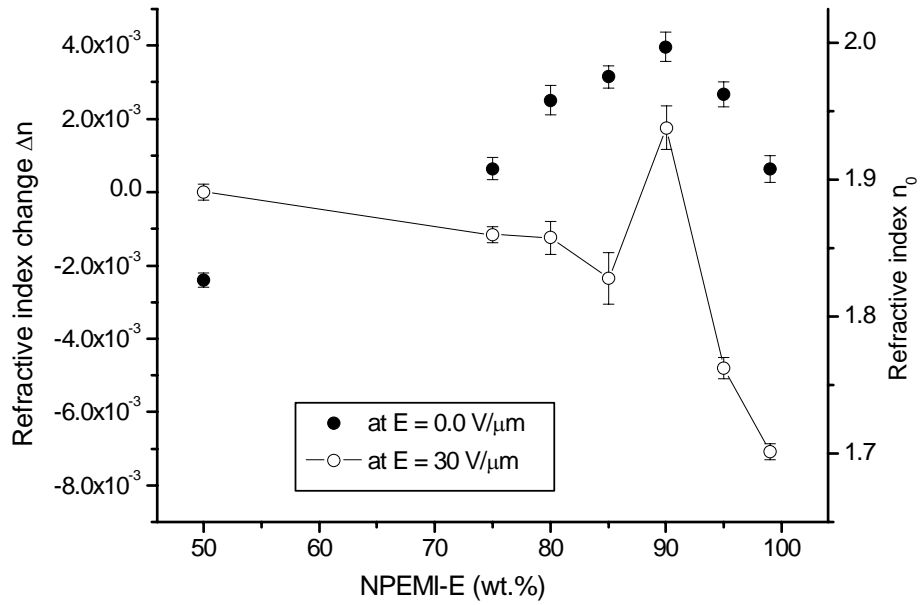

Figure 4.32 Spectroscopic Ellipsometry measurements performed on NPE blends at $\lambda = 685$ nm. Trends of the measured refractive index n_0 (full dots, right vertical axis), at E = 0.0 V/μm, and of the refractive index change Δn (open dots, left vertical axis) under the application of an electric field E = 30 V/μm; each trend is displayed as a function of the composition of NPE blends. The broken line is only an aid for the eyes.

5 Concluding remarks

5.1 Conclusions

This research permitted to get a deeper insight in the complexity of phenomena occurring in photorefractive organic materials. It has been possible to extend the conclusions achieved in previous papers[71,105] concerning PR in blends containing indole-based polymers, to the study of blends designed to behave as efficient supramolecular systems.

First of all, the parameters influencing photorefractive films to give high values of the optical gain Γ_2 and long stability of the material (shelf lifetime) have been considered. The importance of the physico-chemical characteristics of the NLO chromophore and of the polymer substrate has been evidenced in particular as regards the interactions inside the blend and the role played by the glass transition. The selection of the proper combination of NLO chromophore and of its polymer counterpart revealed itself as one of the most important features. The NLO chromophore must have good electrooptic parameters as summarized, for instance, by the Kerr figure of merit F^{Kerr} (s. Sects. 1.4 and 4.1). Suitable electronic properties that prevent the formation of molecular aggregates with edm = 0 and also the recrystallization inside the film are equally important features to obtain unconditionally stable materials. Some preliminary calculations of relevant electrooptic parameters allowed to take into consideration a class of indole derivatives, namely NPEMI, NPEMI-A, NPEMI-E, MeO-NPEI-E, NO$_2$-NPEI-E. These novel species have been synthesized and characterized by common spectroscopic techniques and by a careful calorimetric (DSC) analysis. Charge transfer complexes formation with the photosensitizer agent TNFM has been investigated for the overall series of NLO chromophores by means of UV-Vis absorption spectroscopy. Differences in the spectra have been rationalized on the basis of the calculated values of ip. Photoconductive (PC) and PR behaviour have been investigated for two of these NLO chromophores, namely NPEMI-E and NPEMI-A, when employed both alone (as multifunctional LMWG PR materials) as well as in blends with a PC indolyl polymer, PVDMI, whose good photoconductive behaviour was already established in a previous research.

In order to accomplish PC and PR measurements an electrooptic circuit and a 2BC experiment have been set up. Some attention has been directed to various features of the experimental apparatus affecting the sensitivity of the measurements; the experimental geometry has been selected and optimized in order to settle problems coming out by thermal

or mechanical instabilities. A setup adjustment has been moreover performed together with some preliminary test measurements on samples whose PR behaviour was already known.

The investigation of the series of indole-based materials selected in order to act as novel indole-based NLO chromophores, clearly evidenced the role played in PR organic materials by the glass transition temperature T_g and by the interactions occurring among the molecules. The leading and perhaps most innovative idea was to think out a proper combination of NLO chromophore and PC polymer in order to observe the onset of PR and to evaluate the effect of various contributions to it related to intermolecular interactions. The original point of view is to consider, together with neat NLO chromophores (LMWG approach s. Sect. 1.6.2), blends in which very high concentrations of NLO species can be sustained; the polymer counterpart, PVDMI, can be therefore considered as a screening agent between NLO molecules, separating them and acting as well on the strength of the interactions causing relevant changes in dipoles orientation and molecular parameters responsible for PR properties (Collaborative effect). Moreover, the study on the overall series of unconditionally stable glass blends for increasing content of polymer permitted to follow the onset and the evolution of such interactions. The occurrence and the extent of such interactions have been investigated in NPEMI-E and NPEMI-A blends by careful calorimetric studies that allowed to measure the values of T_g. Data obtained from calorimetric analysis have been compared to numerous theoretical models describing the deviation of T_g trends for different blend compositions and interactions. The existence of weak or moderate specific interactions inside the PR blends under study has been proved. An estimate of some thermodynamic quantities related to such interactions has been evaluated.

Thanks to the unique possibility offered by the studied blends, i.e. their total stability with respect to the composition, the electrostatic interactions have been examined both by their effect on the value of the photorefractive optical gain Γ_2 and on the mechanism of migration of the photogenerated charges. The crucial effect of polymer counterpart has been evidenced: small amounts of polymer PVDMI finely control the electronic and electrostatic interactions among the NLO chromophores at very high concentrations. The onset of drastic changes, never detected before, in PC and PR performances of the studied blends, for concentration of NLO species around 90 wt.%, have been ascribed to the existence of supramolecular collaborative effects acting on clusters of NLO molecules for some specific distances and mutual orientations, as theoretically described by Painelli et al. [136,137,138]. The effect, for the first time detected in PR materials, brings to dipolar species isoorientation, change in edm, α, β of NLO molecules, that in turn modify the PR and PC behaviour. In our opinion, it is this last effect that chiefly allowed to obtain the very good value of $\Gamma_2 = 2027$

170

cm^{-1} for a permanently transparent organic film. In this way, it has been also possible to look for the proper formulation in order to take advantage of such interactions for the achievement of the best PC and PR performances. PC results have been discussed in the frame of GDM and of the deviations of photocurrent i$_{ph}$ from a linear Poole-Frenkel-like behaviour. These deviations have been related to the occurrence of supramolecular arrangements acting on the value of edm. The results of PC, PR and thermal (DSC) analyses of the investigated materials have been discussed jointly, due to the complexity of the many processes occurring simultaneously in organic PR materials. A careful comparison among various and numerous theoretical treatments and experimental data permitted to rationalize the obtained results and to put in evidence the prominent role played by intermolecular interactions.

For instance, to confirm the results of PC and PR measurements, the peculiar reorientational behaviour of the NPEMI-E chromophore has been investigated with ellipsometry (SE) measurements. Refractive index n$_0$ and its variation Δn related to the effect of an applied electric field have been investigated on the overall NPE series. The effect of composition and the onset of peculiar interactions and supramolecular arrangements on refractive index have been estimated. The occurrence of a remarkable maximum of both n$_0$ and Δn, at the same 90 wt.% concentration of NPEMI-E, has been ascribed to the collaborative contribution (Painelli's effect).

As concerns PR, very large values of the photorefractive optical gain Γ have been achieved that classify the organic materials object of this research among the most efficient PR materials to our knowledge. Good PR performances have been demonstrated also for neat NPEMI-A and NPEMI-E molecules. Confirming the formation of CTC, PC and PR measurements permitted to establish the actual multifunctional capabilities of such molecules, able to bear themselves all the necessary properties to act as PR materials. The relevance of the obtained very large values of $\Gamma \approx 2000$ cm^{-1} is clear when they are compared to those reported in literature for similar organic PR materials and for similar conditions (employed laser wavelength, beam ratio, etc.). For instance, in the case of PR polymer blends containing PVK and DMNPAA Γ values up to 220-250 cm^{-1} for E = 90 V/μm were obtained, while values of about 400 cm^{-1} at E = 100 V/μm are reported for PVK blends containing the NLO chromophore DCDHF [2]. This last chromophore, when used alone as a LMWG amorphous PR material, showed PR optical gain $\Gamma \approx 250$ cm^{-1} for E = 40 V/μm[13]. These values are cited with the aim to permit the reader a useful comparison, even if sometimes a comparison between different experimental values is made difficult by the large number of different experimental variables and arrangements employed.

To conclude, it is necessary to remember the importance of the long-term phase stability of these amorphous PR materials, desirable for their practical use in a number of applications. Indefinitely stable PR materials have been obtained. As concerns the capability for a species to form glass phases and the stability of the obtained amorphous material, some evidences have been gathered about the role of a common functional group introduced to favour glass formation. Indeed, we have confirmed that the steric hindrance offered by the 2-ethylhexyl group, frequently exploited with this aim, is not always sufficient to guarantee the formation of an unconditionally stable glass film. The DSC analysis of the derivatives MeO-NPEI-E and NO_2-NPEI-E, both containing this asymmetric alkyl chain on the same nitrogen atom of the indole ring as in NPEMI-E, confirmed that glass phase formation is largely related to electron density on the π-conjugated structure of push-pull molecules and on their value of edm.

5.2 Expected developments

The obtained results suggest that indole-based PR materials, and especially the investigated blends containing NPEMI-E and NPEMI-A, can be considered for a practical use in various applications, especially those related to light amplification: the very large values of PR optical gain Γ found for some blends in this research could be usefully employed in electrooptic apparatuses. The optimization of materials preparation and cells design could allow the development of very efficient devices. As we have evidenced, the remarkable importance of the electrostatic interactions in establishing the final PR and PC performances of the materials paves the way to a novel approach for the design and investigation of PR organic materials. We are confident that a more skilled matching of the characteristics of both the polymer substrate and the chromophore will allow the building of films for photonics applications with improved performances.

Some further developments of the present research could be foreseen. Due to the broad absorption of the induced charge transfer complexes (CTC), irradiation at other wavelengths could be planned. In particular NPEMI-E, due to its CTC absorption centered at $\lambda = 809$ nm and well extending to larger wavelengths, could be suitable for an investigation of its PR behaviour also in the commercially interesting NIR spectral region. The simultaneous use of radiation at various wavelengths could also permit the recording of various interference patterns, responsible for multiple PR gratings in the same volume. Additional SE measurements could be performed in order to complete the study of change in refractive index depending on reorientation behaviour of the studied chromophores, giving a deeper insight in

such mechanisms. The onset of induced birefringence as effect of an applied electric field could be evaluated for all the investigated blends. Moreover, a complete set of PR, PC and SE measurements accomplished at variable temperature could permit a deeper investigation of the role played by T_g and T_r; in such way, the reorientation of the NLO chromophores and the onset of supramolecular arrangements could be varied and checked on the same sample by means of the variation of T_{rt}, spanning over different free-volume states depending on the relative temperature T_r. A correlation temperature/composition could be assessed for the investigated blends.

As concerns quanto-mechanical calculations of the relevant electrooptic parameters, studies on supramolecular systems by using real molecules (as, for instance, those investigated in this research) instead of model dipoles could be useful to obtain a deeper insight in the onset of the collaborative effects that we have shown to be so important in obtaining high values of the photorefractive optical gain.

Further outlook comprehends the development of novel materials on the basis of the obtained results. The addition of small quantities of NPEMI-E to neat NPEMI-A, lowering the T_g of the latter, could permit to appreciate an enhancement of its PR behaviour due to birefringence and/or collaborative contributions without loosing in density of NLO species and also maintaining a good glass-forming capability. A possible alternative outlook for NPEMI-A could be its use in the functionalization of a polysiloxane chain, exploiting the unsaturated allyl group; NPEMI-A could act as a pendant NLO chromophore covalently linked to the macromolecular chain, so realizing a multifunctional PR polymer. The selection of polysiloxane permits indeed to have a polymer material with low T_g ($T_g < T_{rt}$), as confirmed in some previous preliminary researches[85]. In addition, starting from neat NPEMI-A, the allyl functionality could be exploited to induce a controlled crosslinking in the material, possibly through photochemical reactions; in such way, the viscosity of the material could be varied and controlled with important reflections on chromophore reorientation and dielectric rigidity of the obtained films.

The research reported in this thesis has focussed mainly on NPEMI-E and NPEMI-A molecules and on their blends with the PC polymer PVDMI. Anyway, two other novel species MeO-NPEI-E and NO_2-NPEI-E have been also synthesized. The performed DSC analyses, CTC formation studies, quanto-mechanical calculations permit to foresee some possible applications for them. In particular MeO-NPEI-E, due to its low T_g (T_g = -9°C), should be considered for future PR measurements and for the realization of PR blends with PVDMI. In spite of its limited stability in neat glass phase, its blends could be foreseen to be efficiently stable. Moreover, the results of their PR behaviour compared to those obtained for NPEMI-E

could be possibly of great importance in determining the differences in PR for similar molecules depending on edm. As concerns NO_2-NPEI-E its use must be considered for blends only, being the neat material crystalline and hence unserviceable for the construction of electrooptic cells. Nevertheless, in a way similar to what made in the past for DMNPAA, a good compatibility with PVDMI could be expected. The very different edm and ip values of NO_2-NPEI-E, as computed with MOPAC7 calculations (s. Table 4.1) allow to predict a very different PC and PR behaviour. Moreover, the larger extent of dipolar interactions occurring in NO_2-NPEI-E could also give rise to collaborative effects at different (presumably lower) concentration of the active species and for different geometrical arrangements.

By using the MOPAC-7 software, we have also made calculations on the MeO-NPEMI and NO_2-NPEMI molecules having the methyl group in position 2 of the indole ring exactly as in NPEMI-E. As we have verified, s. Table 4.1, the particularly low values of the ionization potential ip (7.35 and 7.29 eV) of the methoxy-substituted molecules are promising for very high values of the photocurrent.

6 Experimental spectra

6.1 ^1H and ^{13}C Nuclear Magnetic Resonance spectroscopy
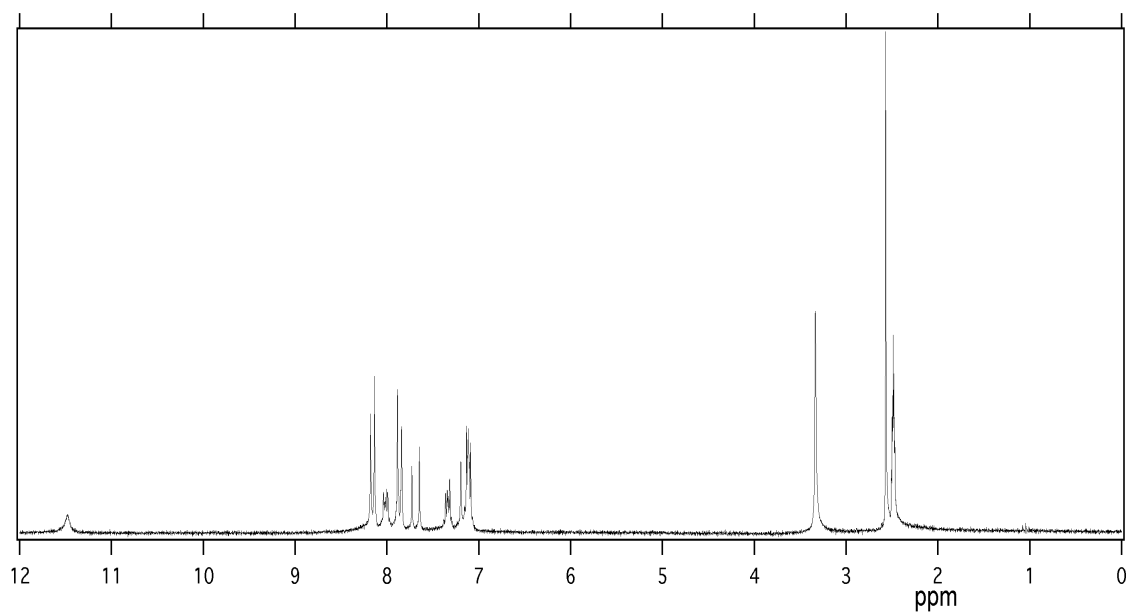
Figure 6.1 ^{1}H-NMR spectrum of 3-[2-(4-nitrophenyl)ethenyl]-2-methylindole (NPEMI) in DMSO-d_6.
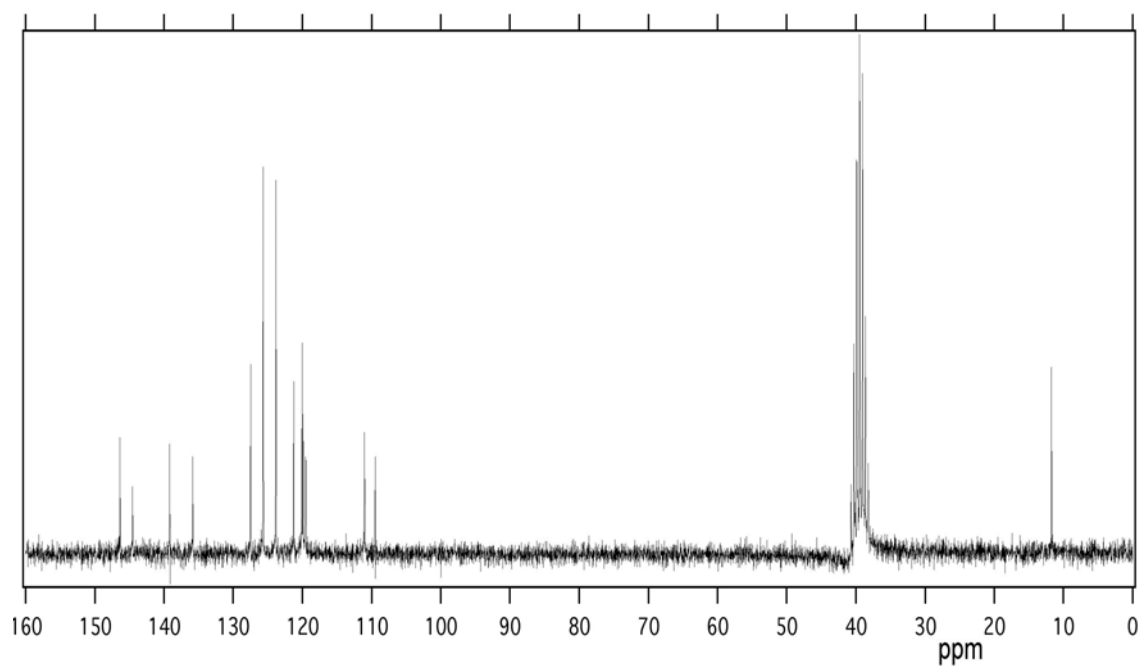
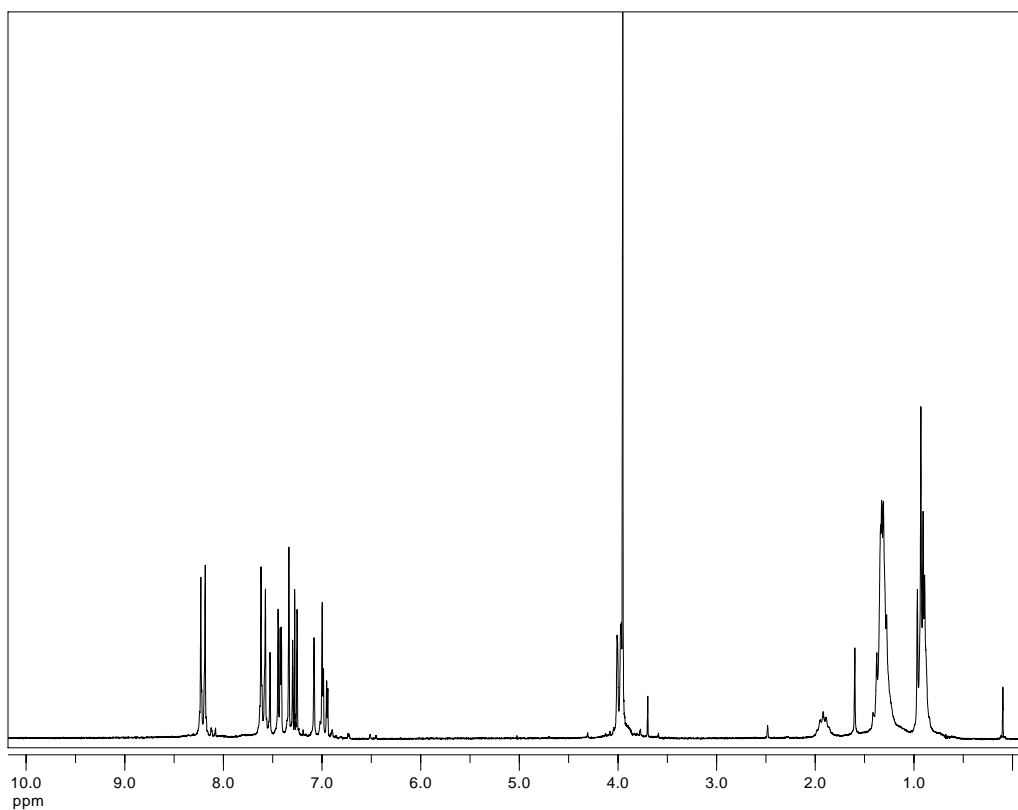Figure 6.2 ^{13}C-NMR spectrum of 3-[2-(4-nitrophenyl)ethenyl]-2-methylindole (NPEMI) in DMSO-d_6.
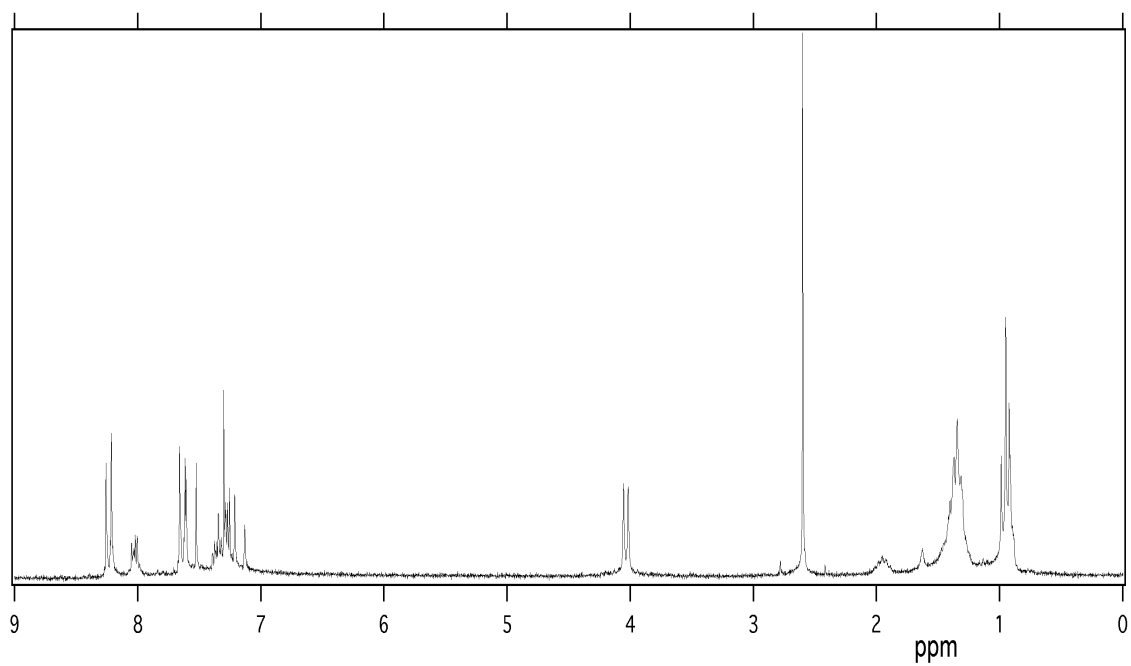
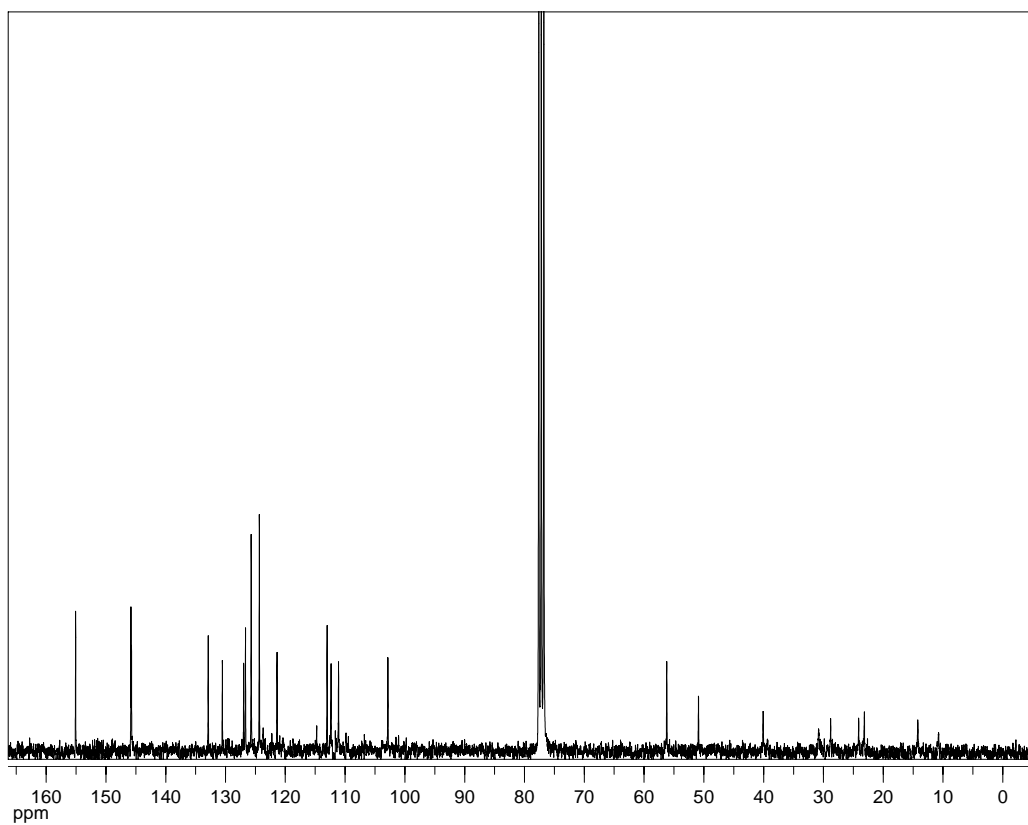Figure 6.3 ^{1}H-NMR spectrum of 3-[2-(4-nitrophenyl)ethenyl]-1-(2-ethylhexyl)-2-methylindole (NPEMI-E) in CDCl$_3$.
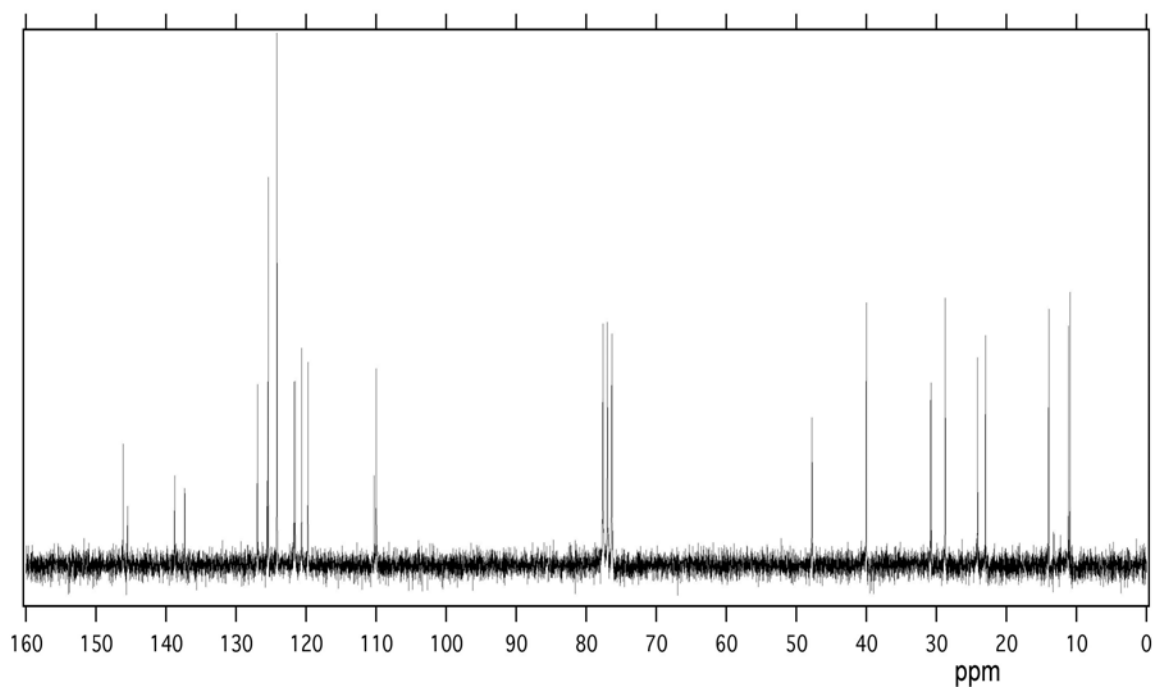
Figure 6.4 ^{13}C-NMR spectrum of 3-[2-(4-nitrophenyl)ethenyl]-1-(2-ethylhexyl)-2-methylindole (NPEMI-E) in CDCl$_3$.

176
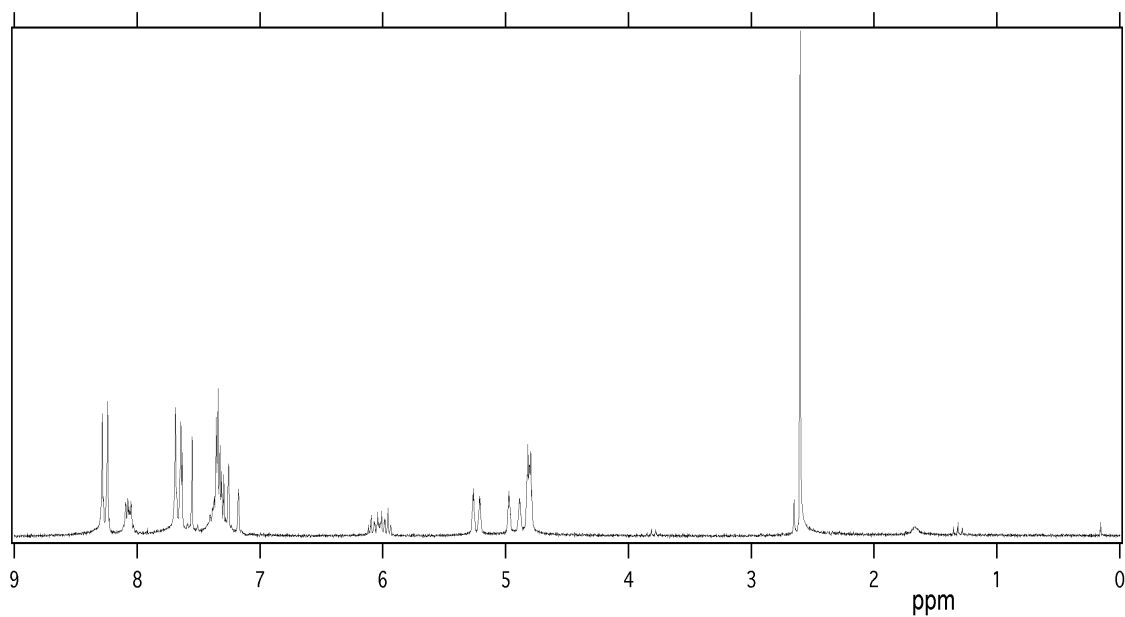
Figure 6.5 ^{1}H-NMR spectrum of 3-[2-(4-nitrophenyl)ethenyl]-1-allyl -2-methylindole (NPEMI-A) in CDCl$_3$.
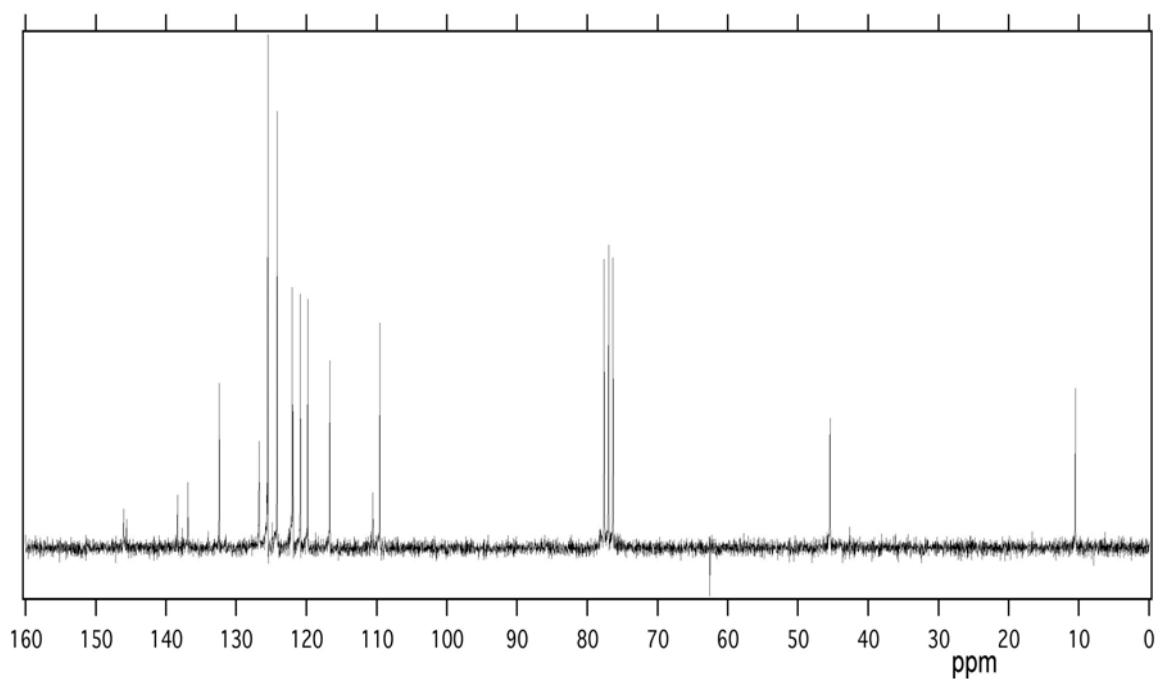
Figure 6.6 ^{13}C-NMR spectrum of 3-[2-(4-nitrophenyl)etheniyl]-1-allyl -2-methylindole (NPEMI-A) in CDCl$_3$.

Figure 6.7 ^{1}H-NMR spectrum of 3-[2-(4-nitrophenyl)ethenyl]-1-(2-ethylhexyl)-5-methoxyindole
(MeO-NPEI-E) in CDCl$_3$.

Figure 6.8 ^{13}C-NMR spectrum of 3-[2-(4-nitrophenyl)ethenyl]-1-(2-ethylhexyl)-5-methoxyindole
(MeO-NPEI-E) in CDCl$_3$.

178
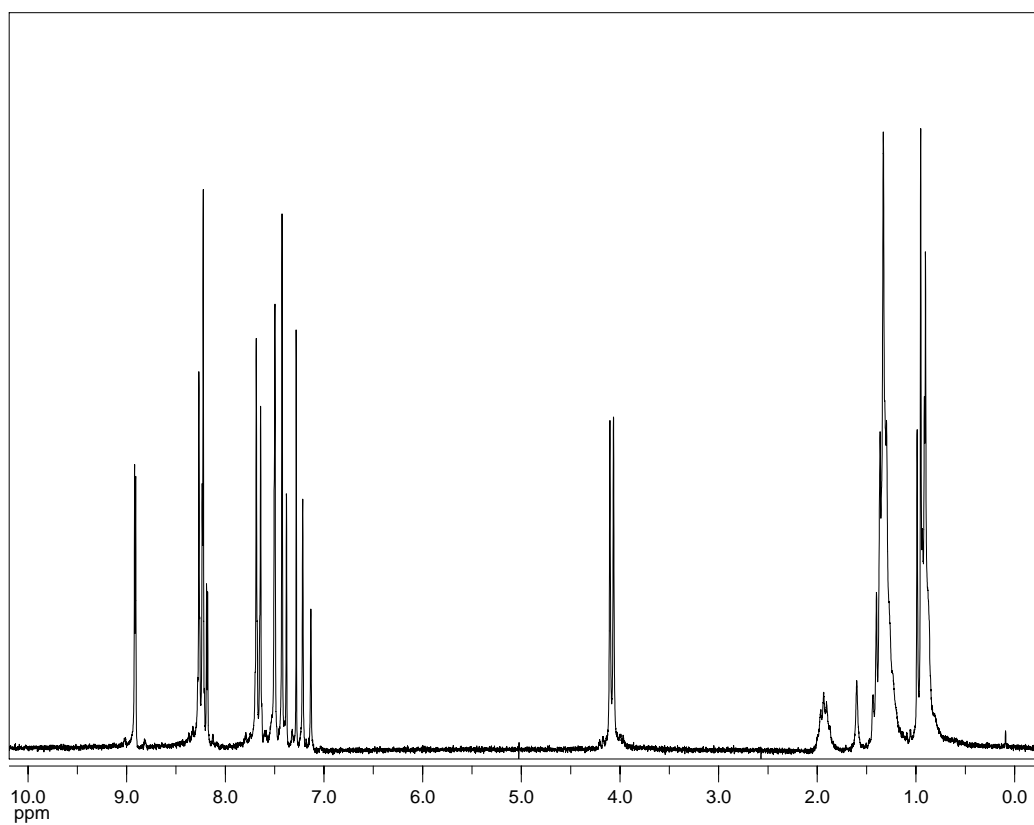
Figure 6.9 ^{1}H-NMR spectrum of 3-[2-(4-nitrophenyl)ethenyl]-1-(2-ethylhexyl)-5-nitroindole (NO$_2$-NPEI-E) in CDCl$_3$.
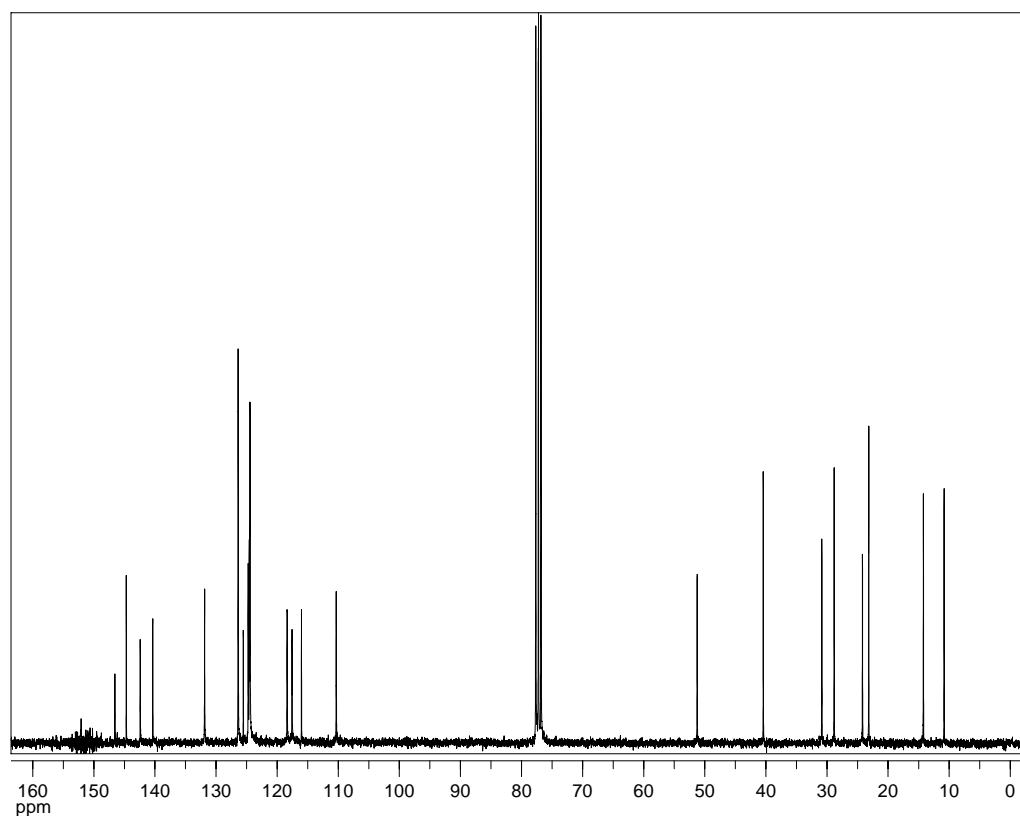
Figure 6.10 ^{13}C-NMR spectrum of 3-[2-(4-nitrophenyl)ethenyl]-1-(2-ethylhexyl)-5-nitroindole (NO$_2$-NPEI-E) in CDCl$_3$.

179

6.2 Infrared spectroscopy
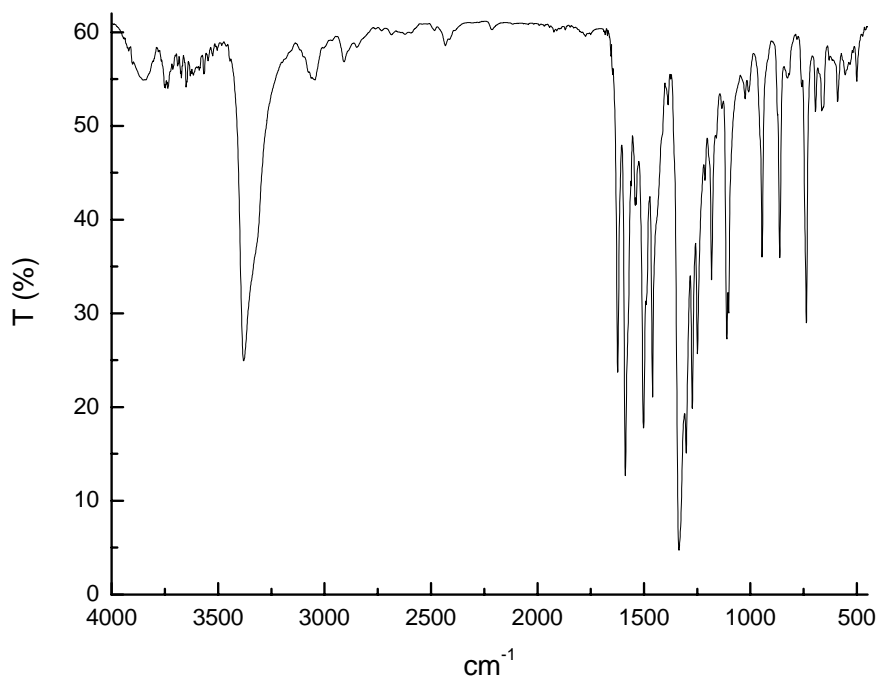
Figure 6.11 FT-IR spectrum of NPEMI in KBr pellet.
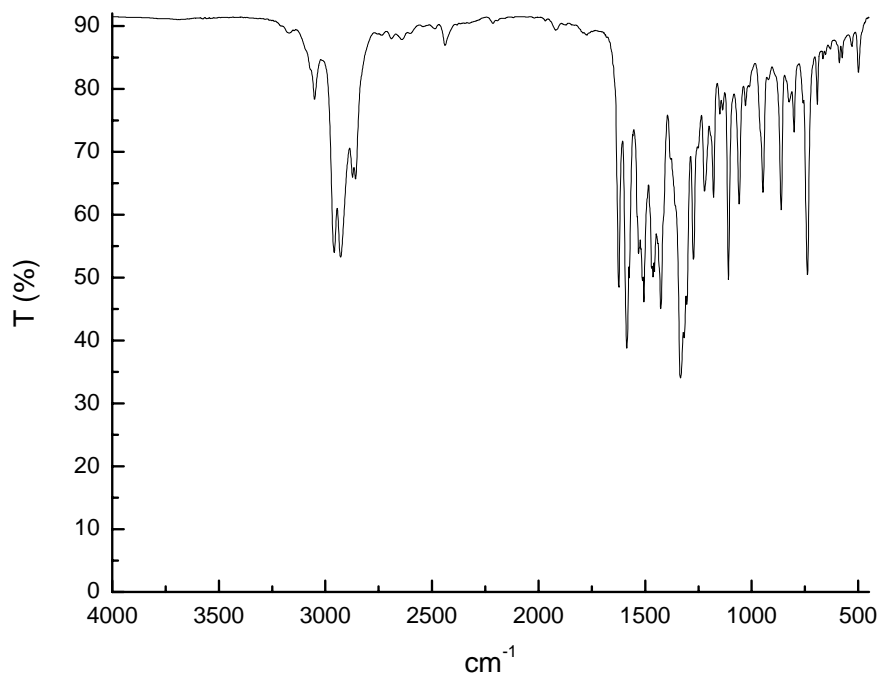
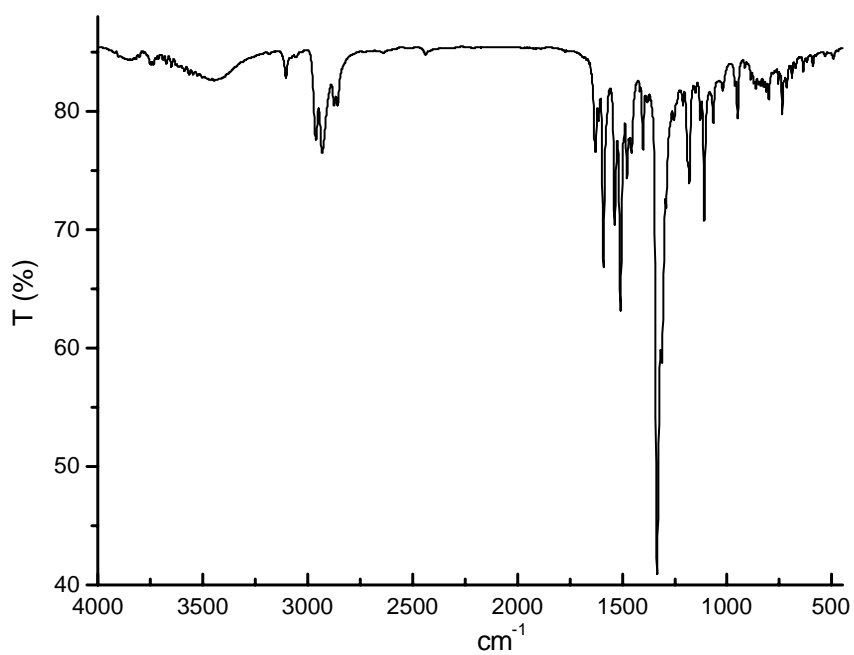Figure 6.12 FT-IR spectrum of NPEMI-E in film between windows of KBr.
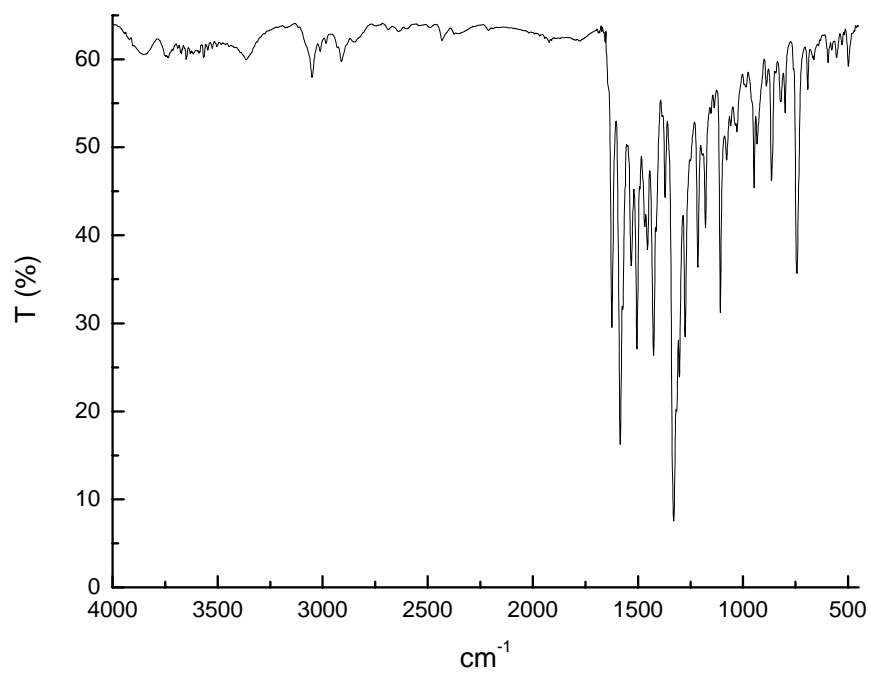
Figure 6.13 FT-IR spectrum of NPEMI-A in KBr pellet.
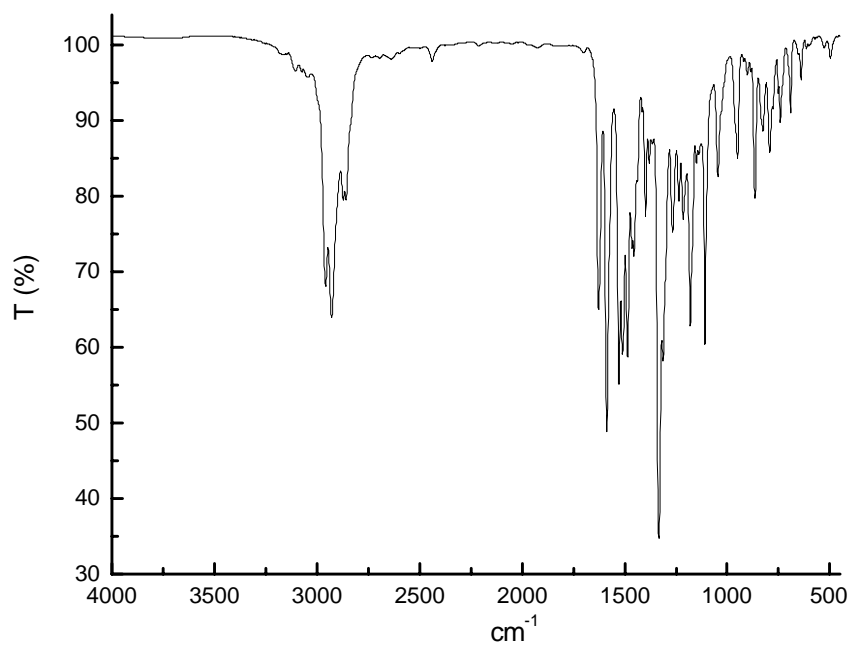
Figure 6.14 FT-IR spectrum of MeO-NPEI-E in film between windows of KBr.

Figure 6.15 FT-IR spectrum of NO$_2$-NPEI-E in film between windows of KBr.
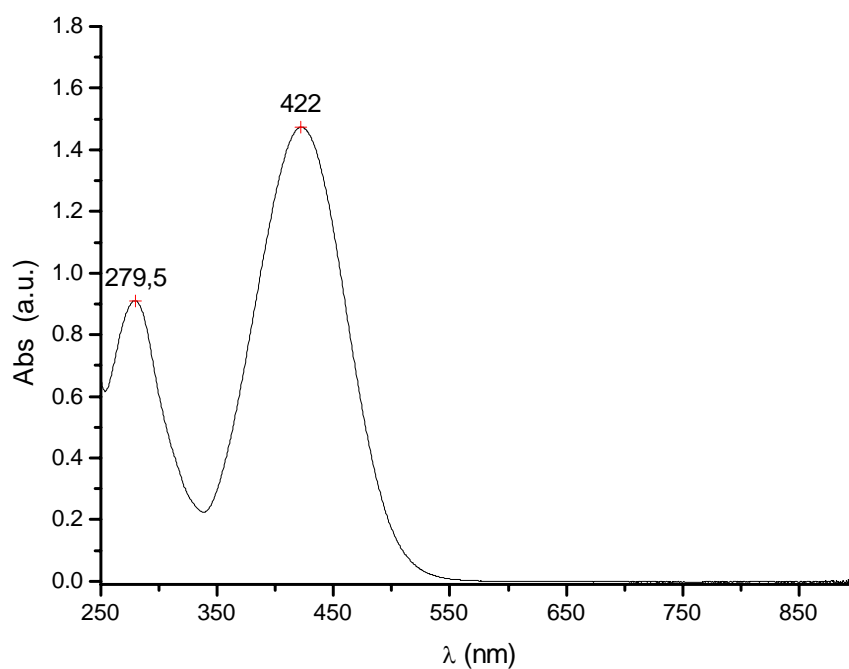
6.3   UltraViolet and Visible spectroscopy

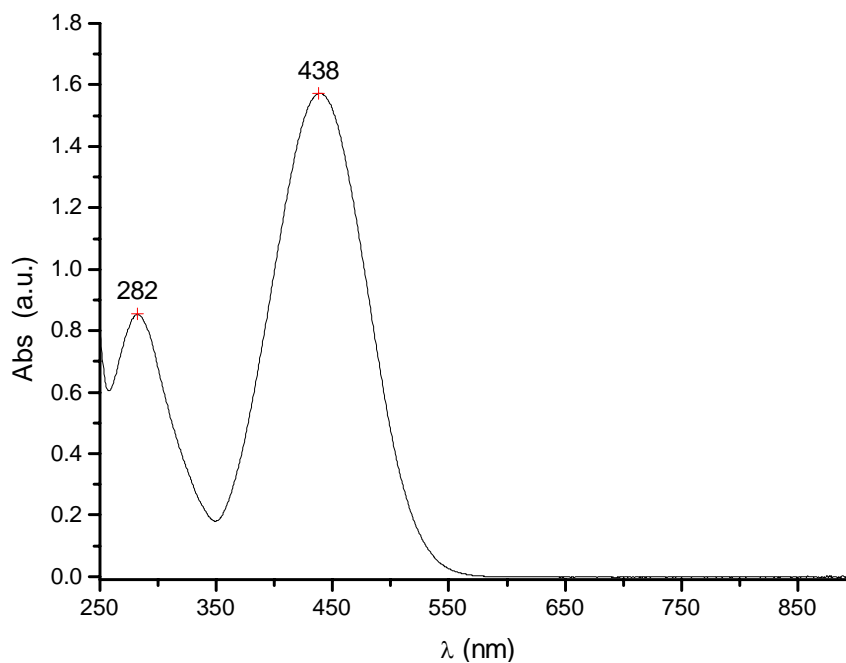Figure 6.16 UV-Vis spectrum of NPEMI in CH_2Cl_2.

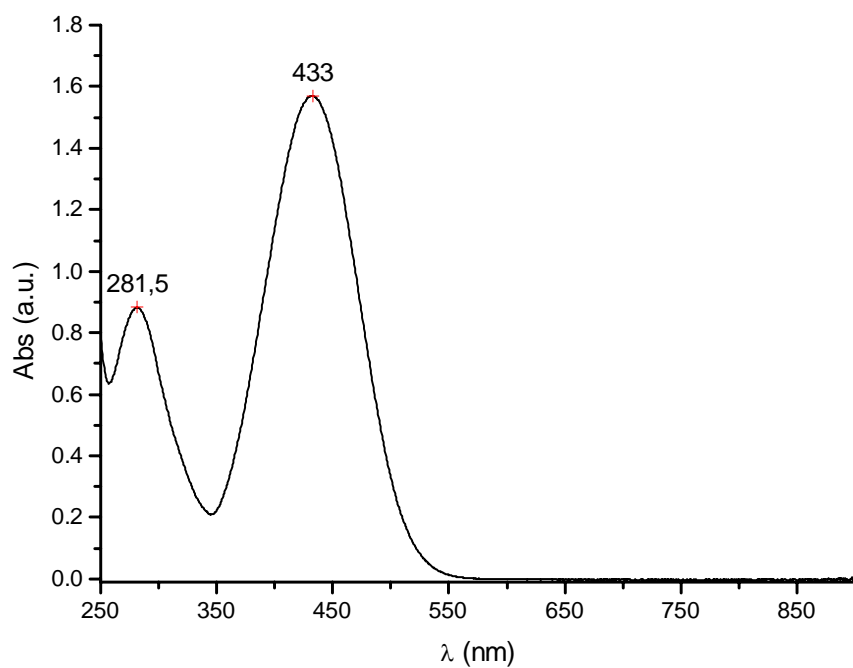Figure 6.17 UV-Vis spectrum of NPEMI-E in CH_2Cl_2.
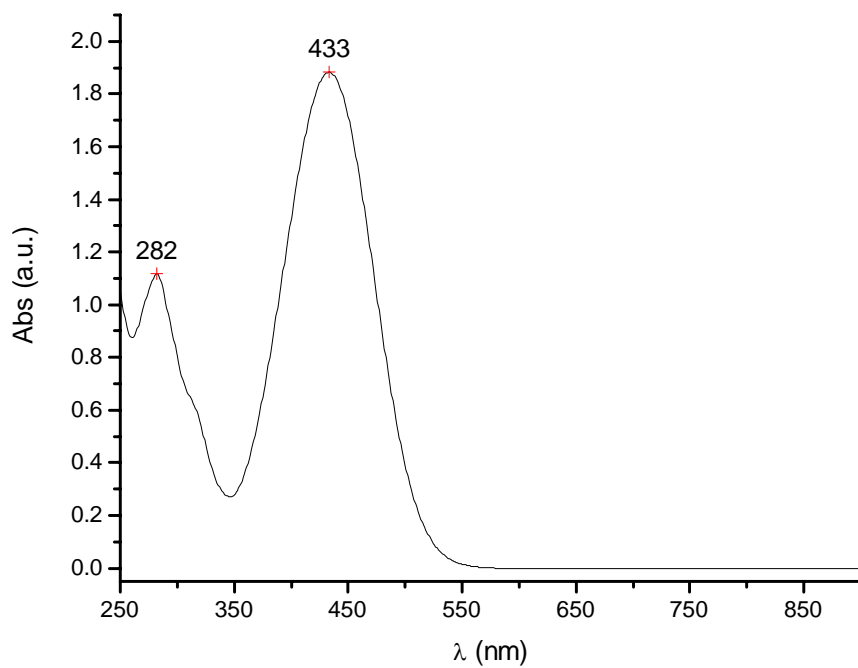
Figure 6.18 UV-Vis spectrum of NPEMI-A in CH_2Cl_2.
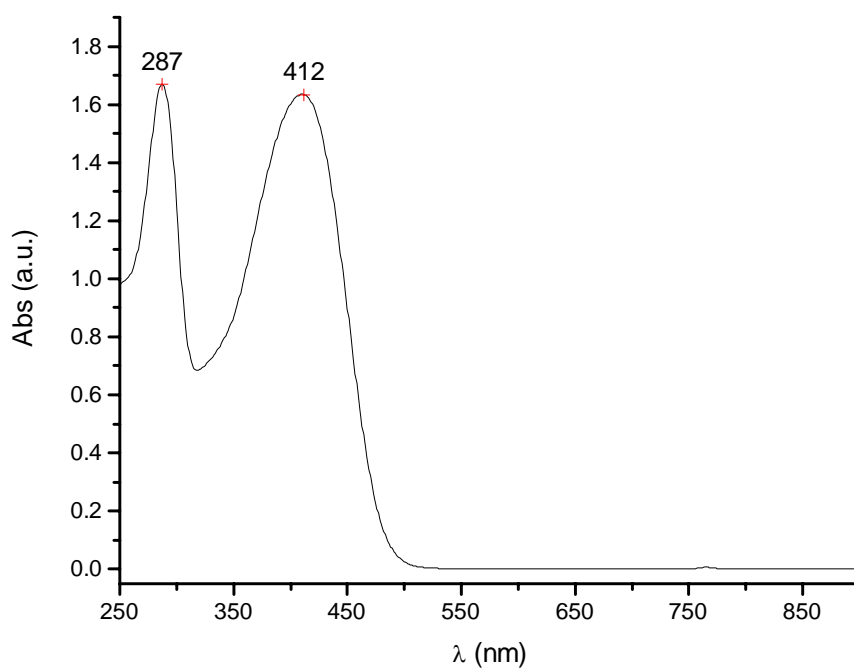

Figure 6.19 UV-Vis spectrum of MeO-NPEI-E in CH_2Cl_2.

Figure 6.20 UV-Vis spectrum of NO_2-NPEI-E in CH_2Cl_2.

Table 6.1 The wavelengths $\lambda_{1\,max}$ and $\lambda_{2\,max}$ corresponding to the maxima of the UV-Vis bands previously reported.

molecule	$\lambda_{1\,max}$ (nm)	$\lambda_{2\,max}$ (nm)
NPEMI	279.5	422.0
NPEMI-E	282.0	438.0
NPEMI-A	281.5	433.0
MeO-NPEI-E	282.0	433.0
NO_2-NPEI-E	287.0	412.0

7 Glossary

7.1 Chemicals

ALD	2-methylindole-3-carboxaldehyde
ALD-E	1-(2-ethylhexyl)-2-methylindole-3-carboxaldehyde
bisA-NPDA	Bisphenol-A diglycidyl ether 4-nitro-1,2-phenylenediamine
CDCl$_3$	Deuterated chloroform
DEH	Diethylaminobenzaldehyde-diphenylhydrazone
DCDHF	Dicyanodihydrofurans (class of NLO chromophores and fluorophores)
DMNPAA	2,5-dimethyl-4-(p-nitrophenylazo)anisole
DMSO	Dimethylsulfoxide
DMSO-d_6	Deuterated dimethylsulfoxide
DMVI	2,3-dimethyl-N-vinylindole
Et$_2$O	Diethyl ether
ITO	Indium Tin Oxide
I	Indole
K	Carbazole
NEI	*N*-ethylindole
NE2MI	*N*-ethyl-2-methylindole
NE3MI	*N*-ethyl-3-methylindole
NE4MI	*N*-ethyl-4-methylindole
NE5MI	*N*-ethyl-5-methylindole
NE6MI	*N*-ethyl-6-methylindole
NE7MI	*N*-ethyl-7-methylindole
NE2,3MI	*N*-ethyl-2,3-dimethylindole
NEK, ECZ	*N*-ethylcarbazole
NPEI	Nitro Phenyl Ethenyl Indoles, class of NLO chromophores
NPEMI	3-[2-(4-nitrophenyl)ethenyl]-2-methylindole
NPEMI-A	3-[2-(4-nitrophenyl)ethenyl]-1-allyl-2-methylindole
NPEMI-E	3-[2-(4-nitrophenyl)ethenyl]-1-(2-ethylhexyl)-2-methylindole
MeO-ALD	5-methoxyindole-3-carboxaldehyde
MeO-ALD-E	1-(2-ethylhexyl)-5-methoxyindole-3-carboxaldehyde
MeO-NPEI-E	3-[2-(4-nitrophenyl)ethenyl]-1-(2-ethylhexyl)-5-methoxyindole
MeO-NPEMI	3-[2-(4-nitrophenyl)ethenyl]-2-methyl-5-methoxyindole
NO$_2$- ALD	5-nitroindole-3-carboxaldehyde
NO$_2$- ALD-E	1-(2-ethylhexyl)-5-nitroindole-3-carboxaldehyde
NO$_2$-NPEI-E	3-[2-(4-nitrophenyl)ethenyl]-1-(2-ethylhexyl)- 5-nitroindole
NO$_2$-NPEMI	3-[2-(4-nitrophenyl)ethenyl]-2-methyl-5-nitroindole
PMMA	Poly-(methyl methacrylate)
PS	Polystyrene
PSX	Poly-(methyl(3-carbazolyl-9-propyl)siloxane)
PPV	Poly-(*p*-phenylenevinylene)
PVDMI	Poly-(*N*-vinyl-2,3-dimethylindole)
PVI	Poly-(*N*-vinylindole)
PVK	Poly-(*N*-vinylcarbazole)
THF	Tetrahydrofuran
TNFM	2,4,7-Trinitrofluorenylidenemalononitrile

7.2 Acronyms and abbreviations

2BC	Asymmetric Two-Beam Coupling
2HG	Second Harmonic Generation
2PA	Two-Photon Absorption
BR	Birefringence
BSC	Brekner-Schneider-Cantow Model
CTC	Charge Transfer Complex
DFWM	Degenerate Four-Wave Mixing
DSC	Differential Scanning Calorimetry
edm	Electric dipole moment
EO	Electro-optic
FWHM	Full Width at Half Maximum
FT-IR	Fourier Transform Infrared Spectroscopy
GDM	Gaussian Disorder Model
GPC	Gel Permeation Chromatography
GT	Gordon Taylor model
HOMO	Highest Occupied Molecular Orbital
HOMO2	Second Highest Occupied Molecular Orbital
ip	Ionization potential
LC	Liquid crystals
LEO	Linear Electro-Optic effect, Pockels effect
LMWG	Low molecular weight organic glass formers
LUMO	Lowest Unoccupied Molecular Orbital
^{1}H-NMR	Proton Nuclear Magnetic Resonance Spectroscopy
^{13}C-NMR	Carbon-13 Nuclear Magnetic Resonance Spectroscopy
NIR	Near Infrared ($750 < \lambda < 14000$ nm)
NLO	Non Linear Optics
PC	Photoconductive, Photoconductivity
PR	Photorefractive, Photorefractivity
SE	Spectroscopic Ellipsometry
SHG	Second Harmonic Generation
THG	Third Harmonic Generation
TLC	Thin Layer Chromatography
TPA	Two-Photon Absorption
UV-Vis	Ultraviolet-Visible Absorption Spectroscopy
WLF	Williams-Landel-Ferry theory

Acknowledgments

References

1. W.E. Moerner, S. Silence, *Chem. Rev.*, **1994**, 94,127.

2. O. Ostroverkhova, W. E. Moerner, *Chem. Rev.*, **2004,** 104, 3267.

3. F.S. Chen, *J. Appl. Phys.*, **1967**, 38, 3418.

4. F. Agullò Lopez, *MRS Bulletin*, **1994**, 19,3.

5. K. Sutter, P. Günter, *J. Opt. Soc. Am.B*, **1990**, 7, 2274.

6. K. Sutter, J. Hulliger, P. Gunter, *Solid State Commun.* **1990**, 74, 867.

7. S. Ducharme, J. C. Scott, R. J. Twieg, W. E. Moerner, *Phys. Rev. Lett.*, **1991**, 66, 1846.

8. W.E. Moerner, *Nature*, **1994**, 371, 475.

9. L.Solymar, D. J. Webb, A. Grunnet-Jepsen, *The Physics and Applications of Photorefractive Materials*, Clarendon Press –Oxford University Press, Oxford, **1996**.

10. A. Grunnet-Jepsen, C. L. Thompson, W. E. Moerner, *Science,* **1997**, 277, 549.

11. A. Goonesekera, D. Wright, W. E. Moerner, *Appl. Phys. Lett.*, **2000**, 76, 3358.

12. E. Hendrickx, D. Van Steenwinckel, A. Persoons, *Appl. Opt.*, **2001**, 40, 1412.

13. U. Gubler, M. He, D. Wright, Y. Roh, R. Twieg, W. E. Moerner, *Adv. Mater.*, **2002**, 14, 313.

14. N.V. Kukhtarev, V.B. Markov, S.G. Odulov, *Opt. Commun.*, **1977**, 23, 338.

15. N. A. Gusak, N. S. Petrov, *Tech. Phys.*, **2001**, 71, 131.

16. D. M. Pai, J. F. Yanus, M. Stolka, *J. Phys. Chem.*, **1984**, 88, 4714.

17. B. Kippelen, N. Peyghambaryan, *Photorefractive Polymers and their Applications*, In: K.-S. Lee (Ed.) *Polymers for Photonics Applications II; Advances in Polymer Science*, Vol. 161; Springer-Verlag, Berlin Heidelberg, **2003**.

18. F. Ghebremichael, M. G. Kuzyk, H. S. Lackritz, *Nonlinear Optics and Polymer Physics,* In: O. Vogl, G. D. Jaycox (Eds.) *Progress in Polymer Science*, Vol. 22, 1147-1201; Elsevier Science Publishers, North-Holland, **1997**.

19. K. Meerholz, B. Kippelen, N. Peyghambarian, *Noncrystalline Organic Photorefractive Materials: Chemistry, Physics, and Applications*, In: D. L. Wise, G. E. Wnek, D. J. Trantolo, T. M. Cooper, J. D. Gresser (Eds.) *Photonic Polymer Systems: Fundamentals, Methods and Applications*, CRC-Press, Boca Raton, **1998**.

20. K. Meerholz, B.L. Volodin, Sandalphon, B. Kippelen, N. Peyghambarian, *Nature*, **1994**, 371, 497.

21. B. Kippelen, K. Meerholz, N. Peyghambarian, In: H.S. Nalwa, S. Miyata, (Eds.) *Nonlinear Optics of Organic Molecules and Polymers*; CRC Press, Boca Raton, **1997**.

22. P. Günter, *Phys. Rep.*, **1982**, 93, 199.

23. D. C. Hanna, M. A. Yuratich, D. Cotter, *Nonlinear Optics of Free Atoms and Molecules. Springer Series in Optical Science*, Springer-Verlag, Berlin Heidelberg, **1979**.

24. P. N. Butcher, D. Cotter, *The elements of Nonlinear Optics. Cambridge Studies in Modern Optics*, Cambridge University Press, Cambridge, **1990**.

25. P. N. Prasad, B. A. Reinhardt, *Chem. Mater.,***1990**, 2, 661.

26. K. Meerholz, R. Bittner, Y. De Nardin, C. Bräuchle, E. Hendrickx, B. L. Volodin, B. Kippelen, N. Peyghambarian, *Adv. Mater.*, **1997**, 9, 1043.

27. W. E. Moerner, S. M. Silence, F. Hache, G. C. Bjorklund, *J. Opt. Soc. Am. B*, **1994**, 11, 320.

28. D. J. Binks, K. Khand, D. P. West, *J. Opt. Soc. Am. B,* **2001**, 3, 306.

29. O. Ostroverkhova, M. He, R. J. Twieg, W. E. Moerner, *CHEMPHYSCHEM*, **2003**, 4, 732.

30. R. Bittner, C. Bräuchle, K. Meerholz, *Appl. Opt.*, **1998**, 37, 2843.

31. R. Wortmann, C. Poga, R. J. Twieg, C. Geletneky, C. R. Moylan, P. M. Lundquist, R. G. De Voe, P. M. Cotts, H. Horn, J. E. Rice, D. M. Burland, *J. Chem. Phys.*, **1996**, 105, 637.

32. B. Kippelen, F. Meyers, N. Peyghambarian, S. R. Marder, *J. Am. Chem. Soc.*, **1997**, 119, 4559.

33. F. Würthner, R. Wortmann, K. Meerholz, *CHEMPHYSCHEM*, **2002**, 3, 17.

34. F. Würthner, S. Yao, J. Schilling, R. Wortmann, M. Redi-Abshiro, E. Mecher, F. Gallego-Gomez, K. Meerholz, *J. Am. Chem. Soc.*, **2001**, 123, 2810.

35. E. Mecher, F. Gallego-Gomez, C. Brauchle, K. Meerholz, R. Wortmann, S. Yao, A. Sautter, F. Würthner, *Proc. SPIE,* **2000**, 4104, 118.

36. K. Meerholz, B. Kippelen, N. Peyghambarian, *Noncrystalline Organic Photorefractive Materials: Chemistry, Physics, and Applications*, In: D. L. Wise, G. E. Wnek, D. J. Trantolo, T. M. Cooper, J. D. Gresser (Ed.) *Photonic Polymer Systems: Fundamentals, Methods, and Applications*, CRC-Press, Boca Raton, **1998**.

37. K. Okamoto, T. Nomura, S. H. Park, K. Ogino, H. Sato, *Chem. Mater.*, **1999**, 11, 3279.

38. J. Sohn, J. Hwang, S. Y. Park, Y. Y. Noh, J. J. Kim, *Appl. Phys. Lett.*, **2002**, 81, 190.

39. L. M. Wang, M. K. Ng, L. P. Yu, *Appl. Phys. Lett*, **2001**, 78, 700.

40. Z. H. Peng, A. R. Gharavi, L. P. Yu, *J. Am. Chem. Soc.*, **1997**, 119, 4622.

41. Q. Wang, L. M. Wang, J. J. Yu, L. P. Yu, *Adv. Mater.*, **2000**, 12, 974.

42. W. You, L. M. Wang, Q. Wang, L. P. Yu, *Macromolecules*, **2002**, 35, 4636.

43. I. Aiello, D. Dattilo, M. Ghedini, A. Bruno, R. Termine, A. Golemme, *Adv. Mater.*, **2002**, 14, 1233.

44. D. J. Suh, O. O. Park, T. Ahn, H. K. Shim, *Opt. Mater.*, **2003**, 21, 365.

45. J. G. Winiarz, L. M. Zhang, M. Lal, C. S. Friend, P. N. Prasad, *Chem. Phys.*, **1999**, 245, 417.

46. J. G. Winiarz, P. Prasad, *Opt. Lett.*, **2002**, 27, 1330.

47. D. J. Binks, D. P. West, S. Norager, P. J. O'Brien, *J. Chem. Phys.*, **2002**, 117, 7335.

48. R. Foster, *Organic charge transfer complexes*, Academic Press, London, **1969**.

49. F. C. Bos, D. M. Burland, *Phys. Rev. Lett.*, **1987**, 58, 152.

50. E. Hendrickx, B. Kippelen, S. Thayumanavan, R.S. Marder, A. Persoons, N. Peyghambarian, *J. Chem. Phys.,* **2000**, 112, 9557.

51. Y. Wang, A. Suna, *J. Phys. Chem. B*, **1997**, 101, 5628.

52. U. Landman, A. Ledwith, D. G. Marsh, D. J. Williams, *Macromolecules*, **1976**, 9, 833.

53. G. Weiser, *Phys. Stat. Sol.(a)*, **1973**, 18, 347.

54. R.A. Marcus, *Annu. Rev. Phys. Chem.*, **1964**, 15, 155.

55. C.A. Walsh, D.M. Burland, *Chem. Phys. Lett.*, **1992**, 195, 309.

56. L. Onsager, *Phys. Rev.*, **1938**, 54, 554.

57. J. Noolandi, K.M. Hong, *J. Chem. Phys.*, **1979**, 70, 3230.

58. H. Bässler, *Adv. Mat.*, **1993**, 5, 662.

59. H. Bässler, G. Schonherr, M. Abkowitz, D. M. Pai, *Phys. Rev. B: Condens. Matter*, **1982**, 26, 3105.

60. R. H. Young, J. A. Sinicropi, J. J. Fitzgerald, *J. Phys. Chem.*, **1995**, 99, 9497.

61. H. Bässler, *Phys. Status Solidi B*, **1993**, 175, 15.

62. R. A. Marcus, P. J. Siders, *J. Phys. Chem.*, **1982**, 86, 622.

63. P. M. Borsenberger, *J. Appl. Phys.*, **1990**, 68, 5188.

64. S. J. Zilker, U. Hofmann, A. Leopold, M. Grasruck, C. Hohle, P. Strohriegl, *Mol. Cryst. Liq. Cryst.*, **2001**, 358, 15.

65. G. G. Malliaras, V. V. Krasnikov, H. J. Bolink, G. Hadziioannou, *Appl. Phys. Lett.*, **1995**, 66, 1038.

66. Y. Zhang, T. Wada, H. Sasabe, *J. Mater. Chem.*, **1998**, 8, 809.

67. S. J. Zilker, *CHEMPHYSCHEM*, **2000**, 1, 72.

68. S. M. Silence, J. C. Scott, J. J. Stankus, W. E. Moerner, C. R. Moylan, G. C. Bjorklund, R. J. Twieg, *J. Phys. Chem*, **1995**, 99, 4096.

69. S. M. Silence, C. A. Walsh, J. C. Scott, W. E. Moerner, *Appl. Phys. Lett.*, **1992**, 61, 2967.

70. M. C. J. M. Donckers, S. M. Silence, C. A. Walsh, F. Haache, D. M. Burland, W. E. Moerner, R. J. Twieg, *Opt. Lett.*, **1993**, 18, 1044.

71. M. Angiuli, F. Ciardelli, A. Colligiani, F. Greco, A. Romano, G. Ruggeri, E. Tombari, *Appl. Opt.*, **2006**, 45, 7928.

72. A. Grunnet-Jepsen, D. Wright, B. Smith, M. S. Bratcher, M. S. DeClue, J. S. Siegel, W. E. Moerner, *Chem. Phys. Lett.*, **1998**, 291, 553.

73. E. Hendrickx, Y. D. Zhang, K. B. Ferrio, J. A. Herlocker, J. Anderson, N. R. Armstrong, E. A. Mash, A. P. Persoons, N. Peyghambarian, B. Kippelen, *J. Mater. Chem.*, **1999**, 9, 2251.

74. J. A. Herlocker, C. Fuentes-Hernandez, K. B. Ferrio, E. Hendrickx, P. A. Blanche, N. Peyghambarian, B. Kippelen, Y. Zhang, J. F. Wang, S. R. Marder, *Appl. Phys. Lett.*, **2000**, 77, 2292.

75. S. Schloter, U. Hoffmann, P. Strohriegl, H. W. Schmidt, D. Haarer, *J. Opt. Soc. Am. B*, **1998**, 15, 2473.

76. H. Chun, I. K. Moon, D. H. Shin, S. Song, N. Kim, *J. Mater. Chem.*, **2002**, 12, 858.

77. E. Mecher, F. Gallego-Gomez, H. Tillmann, H. H. Horhold, J. C. Hummelen, K. Meerholz, *Nature*, **2002**, 418, 959.

78. D. J. Suh, O. O. Park, T. Ahn, H. K. Shim, *Opt. Mater.*, **2003**, 21, 365.

79. D. Wright, M. A. Diaz-Garcia, J. D. Casperson, M. DeClue, W. E. Moerner, R. J. Twieg, *Appl. Phys. Lett.*, **1998**, 73, 1490.

80. R. Bittner, T. K. Daubler, D. Neher, K. Meerholz, *Adv. Mater.*, **1999**, 11, 123.

81. K. Meerholz, R. Bittner, Y. De Nardin, C. Bräuchle, E. Hendrickx, B. L. Volodin, B. Kippelen, N. Peyghambarian, *Adv. Mater.*, **1997**, 9, 1043.

82. A. Colligiani, F. Brustolin, V. Castelvetro, F. Ciardelli, G. Ruggeri, *Proc. SPIE*, **2000**, 4104, 71.

83. F. Brustolin, V. Castelvetro, F. Ciardelli, G. Ruggeri, A. Colligiani, *J. Polym. Sci. A Polym. Chem.*, **2001**, 39, 253.

84. C. Castè, V. Castelvetro, F. Ciardelli, A. Colligiani, A. Mazzotta, D. Michelotti, G. Ruggeri, C. A. Veracini, *Synth. Met.*, **2003**, 138, 341.

85. R. Angelone, C. Castè, V. Castelvetro, F. Ciardelli, A. Colligiani, F. Greco, A. Mazzotta, G. Ruggeri, *e-Polymers,* **2004**, 075.

86. K. Tamura, A. B. Padias, H. K Hall, N. Peyghambarian, *Appl. Phys. Lett.*, **1992**, 60, 1803.

87. L. P. Yu, W. K. Chan, K. Z. Bao, S. Cao, *Macromolecules*, **1993**, 26, 2216.

88. K. D. Belfield, C. Chinna, O. Najjar, *Macromolecules*, **1998**, 31, 2918.

89. E. Heendrickx, D. Van Steenwinckel, A. Persoons, A. Watanabe, *Macromolecules*, **1999**, 32, 2232.

90. S. H. Park, K. Ogino, H. Sata, *Polym. Adv. Technol.*, **2000**, 11, 349.

91. H. Moon, J. Hwang, N. Kim, S. Y. Park, *Macromolecules*, **2000**, 33, 5116.

92. L. Yu, *J. Polym. Sci. A Polym. Chem.*, **2001**, 39, 2557.

93. R. Angelone, F. Ciardelli, A. Colligiani, F. Greco, P. Masi, A. Romano, G Ruggeri, J-L Stehlé, *Appl. Opt.*, **2008**, 47, 6680.

94. Y. Zhang, T. Wada, H. Sasabe, *J. Mater. Chem.*, **1997**, 9, 2798.

95. P. M. Lundquist, R. Wortmann, C. Geletneky, R. J. Twieg, M. Jurich, V. Y. Lee, C. R. Moylan, D. M. Burland, *Science*, **1996**, 274, 1182.

96. O. Ostroverkhova, D. Wright, U. Gubler, W. E. Moerner, M. He, A. Sastre-Santos, R. J. Twieg, *Adv. Funct. Mater.*, **2002**, 12, 621.

97. K. Meerholz, Y. De Nardin, R.Bittner, R. Wortmann, F. Würthner, *Appl. Phys. Lett.*, **1998**, 73, 1.

98. M. He, R. J. Twieg, U. Gubler, D. Wright, W. E. Moerner, *Chem. Mater.*, **2003**, 57, 2771.

99. J. Sohn, J. Hwang, S. Y. Park, G. J. Lee, *Jpn. J. Appl. Phys., Part I* , **2001**, 5A, 3301.

100. H. Chun, N. J. Kim, W. J. Joo, J. W. Han, C. H. Oh, N. Kim, *Synth. Met.*, **2002**, 129, 281.

101. S. Schloter, A. Schreiber, M. Grasruck, A. Leopold, M. Kol'chenko, J. Pan, C. Hohle, P. Strohriegl, S. J. Zilker, D. Haarer, *Appl. Phys. B*, **1999***, 68, 899.

102. F. Würthner, S. Yao, *Angew. Chem. Int. Ed.* , **2000**, 39, 1978.

103. J. Hwang, J. Seo, J. Sohn, S. Y. Park, *Opt. Mater.*, **2003**, 21, 359.

104. R. Wortmann, M. Redi-Abshiro, U. Rosch, S. Yao, F. Wurthner, *Proc. SPIE*, **2002**, 4802, 1.

105. R. Angelone, M. Angiuli, F. Ciardelli, A. Colligiani, F. Greco, A. Romano, G. Ruggeri, E. Tombari, *Proc. SPIE*, **2006**, 6192**,** 61922M-1.

106. G. P. Wiederrecht, *Annu. Rev. Mater. Res.*, **2001**, 31, 139.

107. I. C. Khoo, H. Li, Y. Liang, *Opt. Lett.*, **1994**, 19, 1723.

108. G. P.Wiederrecht, B. A. Yoon, M. R.Wasielewski, *Science*, **1995**, 270, 1794.

109. H. Ono, I. Saito, N. Kawatsuki, *Appl. Phys. Lett.*, **1998**, 72, 1942.

110. S. Bartkiewicz, A. Miniewicz, F. Kajzar, M. Zagorska, *Appl. Opt.*, **1998**, 37, 6871.

111. G. Cipparrone, A. Mazzulla, F. Simoni, *Opt. Lett.*, **1998**, 23, 1505.

112. N. V. Tabiryan, C. Umeton, *J. Opt. Soc. Am. B*, **1998**, 15, 1912.

113. A. Golemme, B. L. Volodin, B. Kippelen, N. Peyghambarian, *Opt. Lett.*, **1997**, 22, 1226.

114. H. Ono, *Opt. Lett.*, **1997**, 22, 1144.

115. P. Wiederrecht, M. R. Wasielewski, *J. Am. Chem. Soc.*, **1998**, 120, 3231.

116. J. Zhang, K. D. Singer, *Appl. Phys. Lett.*, **1998**, 72, 2948.

117. R. Termine, B. De Simone, A. Golemme, *Appl. Phys. Lett.*, **2001**, 78, 688.

118. G. P. Wiederrecht, B. A. Yoon, M. R. Wasielewski, *Adv. Mat.*, **2000**, 12, 1533.

119. T. Sasaki, A. Katsuragi, O. Mochizuki, Y. Nakazawa, *J. Phys. Chem. B*, **2003**, 107, 7659.

120. M. Talarico, R. Termine, G. Barberio, D. Pucci, M. Ghedini, A. Golemme, *Appl. Phys. Lett.*, **2004**, 84, 1034.

121. I. C. Khoo, Y. Ding, Y. Zhang, K. Chen, A. Diaz, *Appl. Phys. Lett.,* **2003**, 82, 3587.

122. H. Ono, N. Kawatsuki, *J. Appl. Phys.,* **1999**, 85, 2482.

123. S. Barktiewicz, K. Matczyszyn, A. Miniewicz, F. Kajzar, *Opt. Commun.*, **2001**, 187, 257.

124. D. Van Steenwinkel, E. Hendrickx, A Persoons, *Chem. Mater.*, **2001**, 13, 1230.

125. H. Ono, H. Shimokawa, A. Emoto, N. Kawatsuki, *J. Appl. Phys.*, **2003**, 94, 23.

126. R.A. Fischer, (Ed.) *Optical Phase Conjugation*, Academic Press, New York, **1983**.

127. J. O. White, M. Cronin-Golomb, B. Fischer, A. Yariv, *Appl. Phys. Lett.*, **1982**, 40, 450.

128. B. L. Volodin, B. Kippelen, K. Meerholz, B. Javidi, N. Peyghambarian, *Nature*, **1996**, 383, 58.

129. C. Halvorson, B. Kraabel, A. J. Heeger, B. L. Volodin, K. Meerholz, Sandalphon, N. Peyghambarian, *Opt. Lett.*, **1995**, 20, 76.

130. P. P. Banerjee, E. Gad, T. Hudson, D. McMillen, H. Abdeldayem, D. Frazier, K. Matsushita, *Appl. Opt.*, **2000**, 39, 5337.

131. H. Ono, T. Kawamura, N. Kawatsuki, H. Norisada, *Appl. Phys. Lett.*, **2001**, 79, 895.

132. B. Kippelen, S. R. Marder, E. Heendrickx, J. L. Maldonado, G. Guillemet, B. Volodin, D. D. Steele, Y. Enami, Sandalphon, Y. J. Yao, J. F. Wang, H. Röckel, L. Erskine, N. Peyghambarian, *Science*, **1998**, 279, 54.

133. D. D. Steele, B. L. Volodin, O. Savina, B. Kippelen, N. Peyghambarian, H. Rockel, S. R. Marder, *Opt. Lett.*, **1998**, 23, 153.

134. J. I. Ostrovskij, *Olografia e sue applicazioni*, Mir, Moscow, **1982**.

135. T. K. Däubler, R. Bittner, K. Meerholz, V. Cimrová, D. Neher, *Phys. Rev. B*, **2000**, 61, 13515.

136. F. Terenziani, A. Painelli, *Phys. Rev. B*, **2003**, 68, 165405.

137. A. Painelli, F. Terenziani, *Synt. Met.*, **2004**, 147, 111.

138. S. J. Chung, K. S. Kim, T. C. Lin, G. S. He, J. Swiatkiewicz, P. N. Prasad, *J. Phys. Chem. B*, **1999**, 103, 10741.

139. D. W. Van Krevelen, *Properties of Polymers*, Elsevier, North Holland, **1997**.

140. T. G. Fox, *Bull. Am. Phys. Soc.*, **1956**, 1, 123.

141. Z. L. Zhow, A. Eisenberg, *J. Polym. Sci. Polym. Lett. Ed.*, **1983**, 21, 233.

142. J. M. Rodriguez-Parada, V. Percec, *Macromolecules*, **1986**, 19, 55.

143. X. Lu, R. A. Weiss, *Macromolecules*, **1991**, 24, 4381.

144. X. Lu, R. A. Weiss, *Macromolecules*, **1992**, 25, 3242.

145. T. K. Kwei, E. M. Pearce, J. R. Pennacchia, M. Charton, *Macromolecules*, **1987**, 20, 1174.

146. P.C. Painter, J. F. Graf, M. M. Coleman, *Macromolecules*, **1991**, 24, 5630.

147. M. Song, D. J. Hourston, H. M. Pollock, A. Hammiche, *Polymer*, **1999**, 40, 4763.

148. M. C. Righetti, G. Ajroldi, G. Pezzin, *Polymer*, **1992**, 33, 4779.

149. M. C. Righetti, G. Ajroldi, G. Marchionni, G. Pezzin, *Polymer*, **1993**, 34, 4307.

150. M. C. Righetti, N. Lotti, A. Munari,G. Pezzin, *Polym. Bull.*, **1999**, 42, 441.

151. R. Simha, R. F. Boyer, *J Chem. Phys.*, **1962**, 37, 1003.

152. M. Gordon, J. S. Taylor, *J. Appl. Chem.*, **1952**, 2, 493.

153. P. R. Couchman, F. R. Karasz, *Macromolecules*, **1978**, 11, 117.

154. M.J. Brekner, H. A. Schneider, H. J. Cantow, *Polymer*, **1988**, 29, 78.

155. P. R. Couchman, *Macromolecules*, **1978**, 11, 1156.

156. P. R. Couchman, *Nature*, **1982**, 298, 729.

157. P. R. Couchman, *Macromolecules*, **1982**, 15, 770.

158. P. R. Couchman, *Macromolecules*, **1987**, 20, 1712.

159. P. R. Couchman, *Macromolecules*, **1991**, 24, 5772.

160. K. K. Chee, *Polymer*, **1995**, 36, 809.

161. P. J. Flory, *Principles of Polymer Chemistry*, Cornell University Press, Ithaca, **1953**.

162. M. Wolf, J. H. Wendorff, *Polym. Commun.*, **1990,** 31, 226.

163. D. R. Lide, *CRC Handbook of Chemistry and Physics. 81st Edition*, CRC Press, Washington DC, **2000**.

164. J. C. Tai, L. Yang, N. L. Allinger, *J. Am. Chem. Soc.,* **1993**, 115, 11906.

165. E. Hendrickx, B. Kippelen, S. Thayumanan, S. R. Marder, A. Persoons, N. Peyghambarian, *J. Chem. Phys.*, **2000**, 112, 9557.

166. W. Reppe, *Ann.*, **1956**, 601,132.

167. C. Castè, *Tesi di Laurea*, Università di Pisa, **2001**.

168. S. M. Silence, M. C. J. M. Donckers, C. A. Walsh, D. M. Burland, W. E. Moerner, *Appl. Phys. Lett.*, **1994**, 64, 712.

169. K. Meerholz, E. Mecher, R. Bittner, Y. De Nardin, *J. Opt. Soc. Am. B*, **1998**, 15, 2114.

170. R. Angelone, private communication, **2006**.

171. B. Saborault, D. Abenhaim, J. Bourdais, *J. Heterocyclic Chem.*, **1976**, 13, 241.

172. H. A. Schneider, *Polymer*, **1989**, 30, 771.

173. D. Van Steenwinckel, E. Hendrickx, A. Persoons, K. Van den Broeck, C. Samyn, *J. Chem. Phys.*, **2000**, 112, 11030.

174. A. Painelli, F. Terenziani, *J. Am. Chem. Soc.*, **2003**, 125, 5624.

175. F. Terenziani, A. Painelli, *J. Lum.*, **2005**, 112, 474.

176. P. M. Borsenberger, L. Pautmeier, H. Bässler, *J. Chem. Phys.*, **1991**, 94, 5447.

177. P. M. Borsenberger, D. S. Weiss, *Organic photoreceptors for xerography, Vol. 59*, Marcel Dekker Inc., **1998**.

178. Sandalphon, B. Kippelen, K. Meerholz, N. Peyghambarian, *Appl. Opt.*, **1996**, 35, 2346.

179. C. H. Wang, *J. Chem. Phys.*, **1993**, 98, 3457.

180. D. Beljonne, W. Wenseleers, E. Zojer, Z. G. Shuai, H. Vogel, S. J. K. Pond, J. W. Perry, S. R. Marder, J. L. Bredas, *Adv. Funct. Mater.*, **2002**, 12, 631.

181. M. Drobizhev, A. Karotki, Y. Dzenis, A. Rebane, Z. Suo, C. W. Spangler, *J. Phys Chem. B*, **2003**, 107, 7540.

182. A. Abbotto, L. Beverina, R. Bozio, A. Facchetti, C. Ferrante, G. A. Pagani, D. Pedron, R. Signorini*, Chem. Commun.*, **2003**, 17, 2144.

183. F. Stellacci, C. A. Bauer, T. Meyer-Friedrichsen, W. Wenseleers, S. R. Marder, J. W. Perry, *J. Am. Chem. Soc.*, **2003**, 125, 328.

184. P. N. Prasad, D. J. Williams, *Introduction to NLO effects in molecules and polymers*, John Wiley, New York, **1991**.

Publications

1. R. Angelone, C. Castè, V. Castelvetro, F. Ciardelli, A. Colligiani, F. Greco, A. Mazzotta, G. Ruggeri, *"Synthesis and electrooptical characterization of polysiloxanes containing indolyl groups acting as photoconductive substrates for photorefractive materials"*, *e-Polymers* **2004**, no. 075.

2. R. Angelone, M. Angiuli, F. Ciardelli, A. Colligiani, F. Greco, A. Romano, G. Ruggeri, E. Tombari, *"An indole-based low molecular weight glass-former giving materials with high cooperative photorefractive optical gain"*, in Organic Optoelectronics and Photonics II, P. L. Heremans, M. Muccini, E. A. Meulenkamp, eds., *Proc. SPIE*, **2006**, 6192**,** 61922M-1.,

3. M. Angiuli, F. Ciardelli, A. Colligiani, F. Greco, A. Romano, G. Ruggeri, E. Tombari, *"The photorefractivity of poly-N-vinylindoles-based materials as compared with that of poly-N-vinylcarbazole based blends"*, *Appl. Opt.* **2006**, 45, 7928.

4. R. Angelone, F. Ciardelli, A. Colligiani, F. Greco, P. Masi, A. Romano, G Ruggeri, J-L Stehlé, *"Unconditionally stable indole-derived glass blends having very high photorefractive gain. The role of intermolecular interactions"*, *Appl. Opt.*, **2008**, 47, 6680.

5. R. Angelone, F. Ciardelli, A. Colligiani, F. Greco, P. Masi, A. Romano, G Ruggeri, *"A confirmation of the importance of the intermolecular interactions on the behaviour of low-T_g photorefractive materials"*, to be sent.

Communications

1. A. Colligiani, F. Ciardelli, F. Greco, G. Ruggeri, E-MRS 2004 Spring Meeting, May 24-28 2004, Strasbourg, France; *"Poly-N-vinylindoles-based photorefractive materials: a favourable comparison with poly-N-vinylcarbazole"*.

2. A. Colligiani, F. Ciardelli, F. Greco, G. Ruggeri, 7th International Conference on Nanostructured Materials, June 20-24 2004, Wiesbaden, Germany; *"Poly-2,3-dimethyl-N-vinylindole as a valid alternative to poly-N-vinylcarbazole in photorefractive materials"*.

3. A. Colligiani, F. Ciardelli, F. Greco, G. Ruggeri, XXXIII Congresso Nazionale Società Chimica Italiana - Divisione di Chimica Fisica, June 21-25 2004, Napoli, Italy; *"Polymer-based photorefractive blends having high optical gain and long shelf-life"*.

4. A.Colligiani, F. Ciardelli, F. Greco, G. Ruggeri, M. Angiuli, E. Tombari, E-MRS 2005 Spring Meeting, May 31 - June 3 2005, Strasbourg, France; *"Very high photorefractive optical gain and cooperative effects of amorphous blends based on poly-N-vinylindoles"*.

5. A. Colligiani, A. Romano, F. Ciardelli, F. Greco, G. Ruggeri, M. Angiuli, E. Tombari, EUROMAT 2005, 5-8 September 2005, Prague, Czech Republic; *"Indole-based low-molecular-weight glass-forming photorefractive materials having a high value of the optical gain"*.

6. A. Colligiani, A. Romano, F. Ciardelli, F. Greco, G. Ruggeri, M. Angiuli, E. Tombari, PHOTONICS Europe – SPIE, 3-7 April 2006, Strasbourg, France; *"Indolyl-based high optical gain photorefractive glass films having indefinitely long shelf-life time"*.

7. A. Colligiani, F. Ciardelli, F. Greco, G. Ruggeri, M. Angiuli, E. Tombari, E-MRS IUMRS ICEM 2006 Spring Meeting, 29 May -3 June 2006, Nice, France; *"Inherently stable and transparent photorefractive films characterized by unusually high values of the optical gain"*.

8. A. Colligiani, R. Angelone, F. Ciardelli, F. Greco, G. Ruggeri, A. Romano, M. Angiuli, E. Tombari, XXII Congresso della Società Chimica Italiana- 35° Congresso Nazionale della Divisione di Chimica Fisica, 10-15 September 2006, Firenze, Italy; *"The intermolecular cooperative effect to obtain glass materials with exceptionally high values of the photorefractivity and shelflife time"*.

9. A. Colligiani, P. Masi, A.Romano, R. Angelone, F. Ciardelli, F. Greco, G. Ruggeri, E-MRS 2007 Spring Meeting, May 28 – June 1 2007, Strasbourg, France; *"The relevance of the intermolecular interactions in obtaining photorefractive materials with very high optical gain Γ and long shelf lifetime"*.

10. A. Colligiani, P. Masi, A. Romano, R. Angelone, F. Ciardelli, F. Greco, G. Ruggeri, EUROMAT 2007, 10-13 September 2007, Nürnberg, Germany; *"The selection of the polymer component in high-gain photorefractive amorphous organic blends by optimization of the intermolecular interactions"*.

11. R. Angelone, F. Ciardelli, A. Colligiani, F. Greco, P. Masi, A. Romano, G. Ruggeri, AIM 2007, XVIII Convegno Nazionale Associazione Italiana Macromolecole, 16-20 September 2007, Catania, Italy; *"The Relevance of the intermolecular interactions to obtain very high photorefractive optical gains in polymer blends"*.

12. A. Colligiani, P. Masi, A.Romano, R. Angelone, F. Ciardelli, F. Greco, G. Ruggeri, J.L. Stehle, E -MRS 2008 Spring Meeting, May 26 – 30 2008, Strasbourg, France; *"The study of the intermolecular interactions in indolyl derivatives characterized by very high values of the photorefractive optical gain"*.

13. A. Colligiani, P. Masi, A.Romano, R. Angelone, F. Ciardelli, F. Greco, G. Ruggeri, J.L. Stehle, E -MRS 2009 Spring Meeting, June 8-12 2009, Strasbourg, France; *"A very efficient and stable supramolecular organic blend having a very high value of the optical gain for photorefractivity applications"* (abstract submitted).